

# C–F Bond Functionalisation using Main Group Reagents

Gregory Coates

Department of Chemistry  
Imperial College London

A Thesis submitted for Doctorate of Philosophy

## **Declaration of Originality**

The work contained within this thesis was performed at Imperial College London between October 2016 and September 2019. Unless otherwise credited, it is entirely my own work and has not been previously submitted for a degree.

## **Statement of Copyright**

The copyright of this thesis rests with the author. Unless otherwise indicated, its contents are licensed under the Creative Commons Attribution Non-Commercial 4.0 International Licence (CC BY-NC).

Under this license you may copy and redistribute the material in any medium or format. You may also create and distribute modified versions of this work. This is on the condition that: you credit the author and do not use it, or any derivative works, for a commercial purpose.

When reusing or sharing this work, ensure you make the license terms clear to others by naming the license and linking to the license text. Where a work has been adapted, you should indicate that the work has been changed and describe those changes.

Please seek permission from the copyright holder for used of this work that are not included in this license or permitted under UK Copyright Law.

# Acknowledgements

It has been a great pleasure to be a part of the Crimmin group over the last three years and an experience I will never forget. I extend my deepest gratitude to Dr. Mark Crimmin for his unwavering support, time, and patience over this period of my studies. Mark has been and endless source of great ideas and helpful discussion to guide my project to success. I could not have hoped for better supervision during my PhD. Mark's work ethic and enthusiasm has been inspiring and has maintained my focus towards my own project and chemistry in general. Particular thanks are required for the final months of this PhD programme where a lot of time has been dedicated towards reading and correcting this thesis.

I would like to thank all members of the Crimmin group, past and present, for the amazing experience these three years have been. It would not have been as enjoyable or as easy without a great group of friends and colleagues to spend breaks, lunches and Friday evenings at the pub with! I appreciate all of the help and guidance from the analytical staff at Imperial, with particular thanks to Andrew White and Pete Haycock for all of their characterisation assistance.

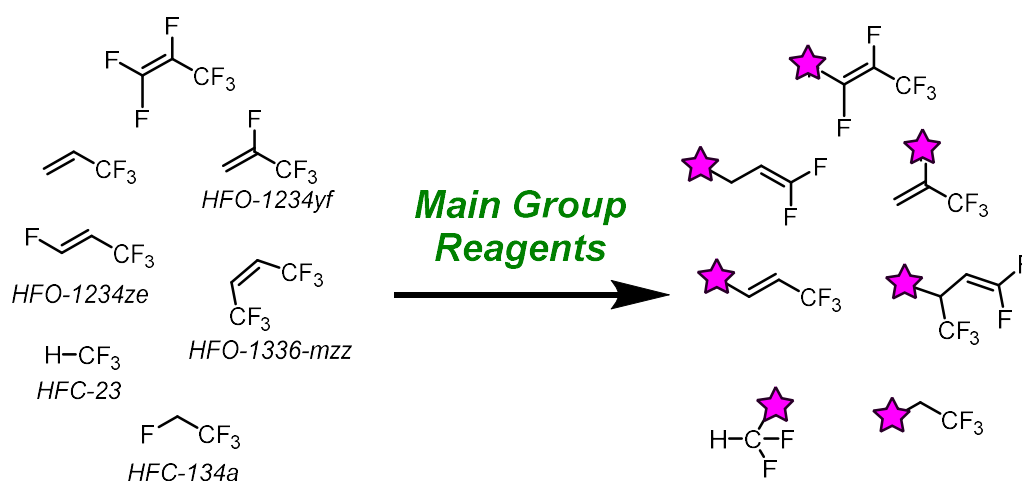
I would like to thank my parents, not just for support during this PhD but the constant help and guidance throughout all of my education and whole life in general. I am very appreciative of all of my family. You have provided much the needed time out from my PhD studies, whether it has been meals out, drinks at the pub or just non-chemistry related conversation! A special thanks goes to Antonia, my auntie that happily provided me a place to live during my final year at Imperial.

Last but in no way least, Kseniya I would like to thank you for your never-ending confidence and support during my PhD and before. You have always brought positivity and provided the bigger picture view when necessary. I appreciate all the help you have given me over the years. You have been my pillar of support and I would not have been able to do this without you.

# Thesis Abstract

Fluorinated compounds have greatly increased our quality of life. They have found application in nearly every industry. Among their many uses they find applications as aerosols, in polymeric materials, as solvents and surfactants whilst they are particularly relied upon for refrigeration purposes. However, the fluorine industry is not currently sustainable. Most organofluorine compounds can be considered 'single-use' and the majority are lost into the atmosphere as fluorinated gases such as hydrofluorocarbons.

The desirable characteristics of organofluorine compounds are also their detriment. They are particularly inert to decomposition and are therefore persistent in the environment. The emission of fluorocarbons into the atmosphere is a significant contributor to climate change and environmental pollution. The recycling of fluorinated compounds therefore represents a timely challenge to synthetic chemists. Due to the increasing incorporation of fluorine into complex molecules such as pharmaceuticals and agrochemicals, the upgrading of fluorine-dense hydrofluorocarbons and hydrofluoroolefins (HFOs and HFCs) to fluorine containing reactive building blocks is an attractive method to close the fluorine cycle.



In this context, we demonstrate methods to selectively activate  $sp^2$  and  $sp^3$ C–F bonds in fluorocarbons using main group compounds. We have developed efficient methods to chemically upgrade industrially relevant HFOs and HFCs to simple-bench stable silicon compounds. Furthermore, we have advanced the understanding of how to activate strong C–F bonds, by interrogating the reaction mechanisms using computational calculations (DFT).



# Table of Contents

|   |    |
|---|----|
| Chapter 1 – Introduction .....  | 11 |
| 1.1 Properties of Fluorine .....  | 11 |
| 1.2 Industrial Applications of Fluorinated Chemicals (Properties) .....     | 13 |
| 1.2.1 Perfluorinated compounds .....  | 13 |
| 1.2.2 Refrigerants .....  | 14 |
| 1.2.3 Pharmaceutical Chemistry .....  | 19 |
| 1.2.4 Nuclear Medicine .....  | 20 |
| 1.2.5 Agrochemicals .....   | 21 |
| 1.3 Origin of Fluorine and How to Introduce it into Organic Compounds ..... | 23 |
| 1.3.1 Industrial Fluorination using HF .....                                | 23 |
| 1.3.2 Elemental Fluorine .....  | 25 |
| 1.3.3 Introducing Fluorine in the Life Sciences .....                       | 26 |
| 1.4 Sustainability of Fluorine .....  | 29 |
| 1.5 Aims .....  | 32 |
| 1.6 References .....  | 33 |
| Chapter 2 – $sp^3C-F$ Activation of Fluorocarbons .....                     | 35 |
| 2.1 Introduction .....  | 35 |
| 2.1.1 Transition–Metal Catalysed Defluoroaromatisation .....                | 36 |
| 2.1.2 Transition–Metal Catalysed Hydrodefluorination .....                  | 37 |
| 2.1.3 Hydrodefluorination using Lewis Acids .....                           | 38 |
| 2.1.4 Oxidative Addition at a Transition–Metal .....                        | 41 |
| 2.1.5 Oxidative Addition to Main Group Reagents .....                       | 42 |
| 2.1.6 Nucleophilic Substitution Reactions of Fluoroalkanes .....            | 44 |
| 2.2 C–F Activation of Fluoroalkanes .....                                   | 47 |
| 2.2.1 Synthesis of Magnesium(I) Complexes .....                             | 47 |
| 2.2.2 Initial Experiments with 1-Fluorohexane .....                         | 48 |
| 2.2.3 Scope in Fluorocarbon with Mg–Mg Bonds .....                          | 50 |
| 2.2.3.1 Synthesis of New Fluorocarbons .....                                | 50 |
| 2.2.3.2 $sp^3C-F$ Activation Results .....                                  | 52 |
| 2.2.3.3 Unsuccessful Substrates for C–F Activation .....                    | 54 |
| 2.2.4 Synthesis of Pure Samples of Mg–Alkyl Species .....                   | 54 |

|   |     |
|---|-----|
| 2.2.5 Transfer of Alkyl Group from C–F Activated Products .....   | 55  |
| 2.2.5.1 Reaction with Boron Reagents.....   | 55  |
| 2.2.5.2 Reaction with other Main Group Electrophiles .....  | 62  |
| 2.2.6 Coupling to sp <sup>2</sup> C–F bonds of Perfluoroarenes .....  | 63  |
| 2.2.6.1 Independent Synthesis of n-Hexyl Substituted Fluoroarenes .....   | 63  |
| 2.2.6.2 One-pot Coupling of sp <sup>3</sup> C–F and sp <sup>2</sup> C–F Bonds.....  | 64  |
| 2.2.6.2 Reaction of Independently Synthesised Mg–n-Hexyl.THF with Perfluoroarenes.....                                      | 65  |
| 2.2.6.3 Reaction with Partially Fluorinated Arenes .....  | 66  |
| 2.2.7 Competition Experiments .....   | 67  |
| 2.2.7.1 Primary vs. Secondary sp <sup>3</sup> C–F Bonds .....   | 67  |
| 2.2.7.2 sp <sup>2</sup> C–F vs. sp <sup>3</sup> C–F Bonds .....   | 68  |
| 2.2.7.3 sp <sup>3</sup> C–X vs. sp <sup>3</sup> C–F Bonds.....  | 68  |
| 2.2.8 Functional Group Tolerances (External ‘Poisons’) .....  | 70  |
| 2.2.9 Mechanistic Probe Reactions.....  | 71  |
| 2.2.10 Computational Calculations.....  | 73  |
| 2.2.10.1 sp <sup>3</sup> C–F Activation at Mg–Mg .....  | 73  |
| 2.2.10.2 C–C Bond Formation through sp <sup>2</sup> C–F Cleavage .....  | 76  |
| 2.3 Experimental.....   | 78  |
| 2.3.1 Preparation of Starting Materials .....   | 80  |
| 2.3.2. Oxidative Addition of sp <sup>3</sup> C–F Bonds to Mg–Mg Bonds .....   | 87  |
| 2.3.3 sp <sup>3</sup> C–F activation in the presence of external ‘poisons’ .....  | 96  |
| 2.3.4. sp <sup>3</sup> C–F to sp <sup>3</sup> C–B, sp <sup>3</sup> C–Si, and sp <sup>3</sup> C–Sn Bond Transformations..... | 97  |
| 2.3.5. Magnesium-mediated Intramolecular Coupling of sp <sup>3</sup> C–F and sp <sup>3</sup> C–X Bonds.....                 | 102 |
| 2.3.6. Magnesium-mediated Intermolecular Coupling of sp <sup>3</sup> C–F and sp <sup>2</sup> C–F Bonds.....                 | 103 |
| 2.3.7 Assessment of Computational Methodology .....   | 109 |
| 2.4 References.....   | 110 |
| Chapter 3 –Defluorosilylation of Fluoroalkenes and Industrially Relevant HFOs.....  | 114 |
| 3.1 Introduction.....   | 114 |
| 3.1.1 Unselective hydrodefluorination .....   | 114 |
| 3.1.2 Transition Metal Catalysed Partial Hydrodefluorination .....  | 116 |
| 3.1.3 Main Group Mediated Partial Hydrodefluorination .....   | 117 |
| 3.1.4 Hydrodefluorination with C–Element Bond Formation.....  | 119 |
| 3.1.5 Mono Defluoroborylation and Defluorosilylation .....  | 121 |
| 3.1.6 C–F Aluminatation of Fluoroolefins.....   | 125 |

|   |     |
|---|-----|
| 3.1.7 Reaction with Oxygen Nucleophiles .....   | 126 |
| 3.1.8 Defluorosilylation With s-Block Anions.....   | 127 |
| 3.2 Defluorosilylation of Industrially Relevant Fluoroolefins .....   | 132 |
| 3.2.1 Synthesis of Magnesium and Lithium Silyl Compounds .....  | 132 |
| 3.2.2 Defluorosilylation with Magnesium Silyl Compounds .....   | 137 |
| 3.2.3 Defluorosilylation with Lithium Silyl Compounds.....  | 140 |
| 3.2.3.1 Reactions with PhMe <sub>2</sub> SiLi.TMEDA & PhMe <sub>2</sub> SiLi.PMDETA .....   | 143 |
| 3.2.4 Multiple Silylation Reactions.....  | 145 |
| 3.2.5 Reactivity of Fluorosilicon Products towards Electrophiles.....   | 147 |
| 3.2.6 Computational Studies.....  | 150 |
| 3.2.6.1 Nucleophilic Vinylic Substitution Calculations .....  | 150 |
| 3.2.6.2 Nucleophilic Conjugate Substitution Calculations .....  | 151 |
| 3.3 Experimental.....   | 155 |
| 3.3.1 General Experimental .....  | 155 |
| 3.3.2 Preparation of Magnesium Reagents .....   | 157 |
| 3.3.4 Preparation of Lithium Reagents .....   | 163 |
| 3.3.5 Preparation of Silicon Products Through sp <sup>2</sup> and sp <sup>3</sup> C–F Activation.....                             | 165 |
| 3.3.6 Multiple Silylation Reactions.....  | 171 |
| 3.3.7 Low Temperature reactions with PhMe <sub>2</sub> SiLi.TMEDA and PhMe <sub>2</sub> SiLi.PMDETA .....                         | 173 |
| 3.3.8 Fluoroalkene Addition to 2-Naphthaldehyde .....   | 174 |
| 3.4 References.....   | 175 |
| Chapter 4 – Defluorosilylation of Trifluoromethane and HFCs .....   | 179 |
| 4.1 Introduction.....   | 179 |
| 4.1.1 Difluoromethylation of Alcohols and Thiols using Trifluoromethane .....   | 180 |
| 4.1.2 Reactions of Lithium Enolates with Trifluoromethane .....   | 180 |
| 4.1.3 α-Difluoromethylation of Nitriles and sp, sp <sup>2</sup> and sp <sup>3</sup> Carbon Centres using<br>Trifluoromethane..... | 183 |
| 4.1.4 C–F Borylation of Trifluoromethane using a Nucleophilic Boron Reagent .....   | 185 |
| 4.1.5 Difluoromethylation Reactions using Trifluoromethane under Continuous Flow .....  | 187 |
| 4.2 C–F Silylation of Trifluoromethane .....  | 190 |
| 4.2.1 Silyl Lithium Reagent Comparisons – Ligand Effects.....   | 190 |
| 4.2.2 Solvent Screen.....   | 191 |
| 4.2.3 Temperature Screen .....  | 193 |
| 4.2.4 Carbene Trap Experiments.....   | 194 |

|  |     |
|--|-----|
| 4.2.5 Silyl Lithium Concentration Studies .....  | 195 |
| 4.2.6 Large Scale Defluorosilylation of Trifluoromethane .....                               | 197 |
| 4.2.7 C–F Silylation of Other CF <sub>3</sub> Containing Species .....                       | 198 |
| 4.2.8 Use of C–F Activated Product as Fluorinated Building Block.....                        | 200 |
| 4.2.9 Preliminary Computational Calculations .....   | 201 |
| 4.3 Experimental.....  | 205 |
| 4.3.1 General procedure for NMR scale reactions with fluorinated gases.....                  | 206 |
| 4.3.2 General procedure for NMR scale reactions with fluorinated liquids.....                | 206 |
| 4.3.3 General procedure for large scale reaction with TMS–CF <sub>3</sub> .....              | 206 |
| 4.3.4 Large scale synthesis of silyl lithium reagent.....                                    | 207 |
| 4.3.5 Preparation of fluorosilicon compounds: .....  | 208 |
| 4.4 References.....  | 209 |
| Chapter 5. Future Work .....   | 211 |
| 5.1 Stereochemistry of sp <sup>3</sup> C–F Bond Cleavage.....                                | 211 |
| 5.2 Scale-Up and Application of Fluorinated Organosilicon Compounds .....                    | 212 |
| 5.3 Development of sp <sup>3</sup> C–F Activation of HFCs and Mechanistic Understanding..... | 214 |
| 5.4 References.....  | 215 |
| 6. Appendix.....   | 216 |
| 6.1 X-Ray Diffraction Data .....   | 216 |
| 6.2 Crystal Structures Absent from Main Text.....  | 219 |

# List of Abbreviations

|       |   |   |
|-------|---|---|
| 9-BBN | – | 9-Borabicyclo(3.3.1)nonane              |
| Ac    | – | Acetyl                                  |
| Adam  | – | Adamantyl                               |
| aHF   | – | Anhydrous Hydrofluoric Acid             |
| API   | – | Active Pharmaceutical Agent             |
| BCF   | – | Tris(pentafluorophenyl)borane           |
| BDE   | – | Bond Dissociation Enthalpy              |
| BDI   | – | $\beta$ -Diketiminato                   |
| cat   | – | Catechol                                |
| CFC   | – | Chlorofluorocarbon                      |
| COD   | – | 1,5-Cyclooctadiene                      |
| Cp    | – | Cyclopentadiene                         |
| Cp'   | – | 1,2,4-Tri-tert-butylcyclopentadiene     |
| Cp*   | – | Pentamethylcyclopentadiene              |
| Cy    | – | Cyclohexyl                              |
| DFT   | – | Density Functional Theory               |
| DIBAL | – | Di-iso-butylaluminium hydride           |
| Dipp  | – | 2,6-di-iso-propylphenyl                 |
| DMA   | – | <i>N,N</i> -Dimethylacetamide           |
| DMAP  | – | <i>N,N</i> -Dimethylaminopyridine       |
| DME   | – | Dimethoxyethane                         |
| DMF   | – | <i>N,N</i> -Dimethylformamide           |
| dmpe  | – | 1,2-Bis(dimethylphosphino)ethane        |
| E1    | – | Unimolecular Electrophilic Substitution |
| E2    | – | Bimolecular Electrophilic Substitution  |
| EDG   | – | Electron Donating Group                 |
| EWG   | – | Electron Withdrawing Group              |
| FGI   | – | Functional Group Interconversion        |
| FLP   | – | Frustrated Lewis Pair                   |
| GC    | – | Gas Chromatography                      |

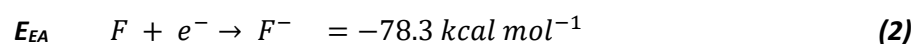
|           |   |  |
|-----------|---|--|
| GWP       | – | Global Warming Potential                           |
| HCFC      | – | Hydrochlorofluorocarbon                            |
| HDF       | – | Hydrodefluorination                                |
| HFC       | – | Hydrofluorocarbon                                  |
| HFO       | – | Hydrofluoroolefin                                  |
| HMDS      | – | Hexamethyldisilazane                               |
| IPr       | – | 1,3-Bis(2,6-di-iso-propylphenyl)imidazol-2-ylidene |
| Mes       | – | 2,4,6-Trimethylphenyl                              |
| mmol      | – | Millimoles   |
| <i>mw</i> | – | Molecular Weight                                   |
| NBS       | – | <i>N</i> -Bromo-succinimide                        |
| nep       | – | Neopentyl  |
| NHC       | – | <i>N</i> -Heterocyclic Carbene                     |
| NMR       | – | Nuclear Magnetic Resonance                         |
| ODP       | – | Ozone Depleting Potential                          |
| PE        | – | Polyethylene                                       |
| PET       | – | Positron Emission Tomography                       |
| PFC       | – | Perfluorocarbon                                    |
| phen      | – | 1,10-Phenanthroline                                |
| pin       | – | Pinacol  |
| PTFE      | – | Polytetrafluoroethylene                            |
| SMD       | – | Solvation Model based on Density                   |
| $S_N1$    | – | Unimolecular Nucleophilic Substitution             |
| $S_N2$    | – | Bimolecular Nucleophilic Substitution              |
| $S_N2'$   | – | Nucleophilic Conjugate Substitution                |
| $S_NAr$   | – | Nucleophilic Aromatic Substitution                 |
| $S_NV$    | – | Nucleophilic Vinylic Substitution                  |
| TBAF      | – | Tetrabutylammonium Fluoride                        |
| Tf        | – | Triflate   |
| TMS       | – | Trimethylsilyl                                     |
| TON       | – | Turn-over Number                                   |
| TS        | – | Transition State                                   |



## Chapter 1 – Introduction

### 1.1 Properties of Fluorine

Fluorine is the 9<sup>th</sup> element on the periodic table. It has an electronic configuration of  $1s^2 2s^2 2p^5$ . It is the most electronegative element with a value of  $\chi^p = 4.0$  on the Pauling scale, compared to that of H  $\chi^p = 2.2$ , C  $\chi^p = 2.6$  and O  $\chi^p = 3.5$ .<sup>[1]</sup> Fluorine has a large 1<sup>st</sup> ionisation energy ( $IE_1 = +401.2 \text{ kcal mol}^{-1}$ ) meaning it is extremely difficult to remove an electron from the 2p shell as they are held very close to the core.<sup>[2]</sup> Fluorine also has a high electron affinity ( $E_{EA} = -78.3 \text{ kcal mol}^{-1}$ ), releasing energy upon the addition of one electron to atomic F.



Fluorine has the lowest van der Waals' atomic radius of the period 2 elements at  $r_{vdW} = 1.47 \text{ \AA}$  (*c.f.* hydrogen  $r_{vdW} = 1.20 \text{ \AA}$ ). This contraction is a result of fluorine's high nuclear charge. The small atomic radius of fluorine makes it a good candidate for the direct substitution of hydrogen in molecules. This will alter the electronic properties whilst maintaining a similar steric environment. This substitution has been exploited in medicinal chemistry and will be discussed later.<sup>[3]</sup>

Fluorine forms the strongest single bond to carbon. This can generate remarkable properties in fluoroorganic compounds. The C–F bond is stronger than the corresponding C–H bonds in hydrocarbons (*See Table 1.1*). Due to these high bond strengths, it is no surprise that carbon–fluorine bonds are particularly challenging to break. The C–F bond is highly polarised and the bond strength can be rationalised by its large ionic character (43 %) which is based on the electronegativity difference of the atoms ( $\Delta\chi^p = 1.5$ ).<sup>[4]</sup>

| Compound                   | CH <sub>3</sub> F | CH <sub>4</sub> | Ph–F     | Ph–H      | C <sub>2</sub> H <sub>3</sub> F | C <sub>2</sub> H <sub>4</sub> |
|----------------------------|-------------------|-----------------|----------|-----------|---------------------------------|-------------------------------|
| BDE kcal mol <sup>-1</sup> | 115±4             | 104.9±0.1       | 98.7±0.7 | 112.9±0.1 | 123.3±0.8                       | 110.7±0.7                     |

Table 1.1 Bond Dissociation Enthalpies of select C–F bonds in fluorocarbons vs the corresponding C–H bonds<sup>[5]</sup>

This large electronegativity difference results expectedly in a large dipole ( $\mu$ ). For example fluoromethane has  $\mu = 1.85$  Debye (D) which increases to  $\mu = 1.97$  D in difluoromethane.<sup>[2]</sup> The high strength of C–F bonds is also attributed to the favourable overlap of 2s and 2p orbitals.<sup>[6]</sup>

The bond dissociation enthalpy (BDE) for the C–F bond in CH<sub>3</sub>F is  $115\pm 4.0 \text{ kcal mol}^{-1}$ .<sup>[5]</sup> This compares to weaker C–X (where X = halogen) bonds as you move down the group to heavier halogen atoms



(BDE's =  $\text{H}_3\text{C}-\text{Cl}$   $83.7 \pm 0.1$ ,  $\text{H}_3\text{C}-\text{Br}$   $72.1 \pm 0.3$  and  $\text{H}_3\text{C}-\text{I}$   $57.6 \pm 0.4$  kcal mol<sup>-1</sup>). Although the C–F bond is highly polarised, the large bond strength makes fluorine a poor leaving group. Halogen leaving group abilities display the inverse trend to their bond strengths ( $\text{I}^- > \text{Br}^- > \text{Cl}^- > \text{F}^-$ ).

| Compound                   | CF <sub>4</sub> | CH <sub>3</sub> F | CH <sub>3</sub> Cl | CH <sub>3</sub> Br | CH <sub>3</sub> I |
|----------------------------|-----------------|-------------------|--------------------|--------------------|-------------------|
| BDE kcal mol <sup>-1</sup> | 130             | 115±4             | 83.7±0.1           | 72.1±0.3           | 57.6±0.4          |

Table 1.2 Bond Dissociation Enthalpies of C–X bond in select organohalides<sup>[5]</sup>

Sequential substitution of hydrogen for fluorine atoms in methane results in increasing C–F bond strengths, with the maximum C–F bond strength being achieved in tetrafluoromethane (BDE for CF<sub>4</sub> = 130 kcal mol<sup>-1</sup>).<sup>[7]</sup> This is a product of the increasing ionic character of the C–F bonds upon higher  $\alpha$ -fluorine content. This is an anomalous property of fluorine, with the trend reversing for the other halogens. Due to this  $\alpha$ -fluorine effect, –CF<sub>3</sub> and CF<sub>2</sub>H functional groups are some of the most inert groups and have found widespread application where this is desirable – such as for use in harsh conditions.

Though the C–F bond is extremely strong, fluorine can form stronger bonds with other elements, notably silicon, hydrogen and boron (BDE = 135, 136 and 159 kcal mol<sup>-1</sup> respectively).<sup>[8]</sup> The formation of these bonds can be exploited as driving forces in C–F bond breaking processes. The formation of alkali metal fluorides are also favourable over C–F bonds. Crystal lattice energies of alkali metal fluorides are larger than the bond dissociation enthalpies of C–F bonds. These lattice energies decrease down the group with LiF exhibiting the highest energy of 251 kcal mol<sup>-1</sup>.<sup>[4]</sup>

| Compound               | CsF | KF  | NaF | LiF | <i>c.f.</i> CH <sub>3</sub> F |
|------------------------|-----|-----|-----|-----|-------------------------------|
| Lattice Energy         | 177 | 198 | 222 | 251 | 115±4                         |
| kcal mol <sup>-1</sup> |     |     |     |     | (BDE)                         |

Table 1.3 Lattice enthalpies of group 1 fluorides compared to the BDE of fluoromethane

Fluorine has three lone pairs. They are held tightly to its core and are rendered reasonably non-polarisable.<sup>[2]</sup> The C–F bond also largely refuses to take part in hydrogen bonding processes. Due to their lack of polarisability and weak intermolecular interactions their surface energies are typically low. As a result of their low surface energies, fluorocarbons tend to have low boiling points in comparison to their hydrocarbon or alkyl halide analogues.<sup>[6]</sup> For example the boiling point of perfluoro-n-hexane is 57 °C, which is 12 °C lower than that of n-hexane (69 °C) even though the molecular weight is nearly four times greater ( $m_w = 338.04$  and  $86.18$  respectively).

## 1.2 Industrial Applications of Fluorinated Chemicals (Properties)

Fluorinated compounds have greatly improved our quality of life over the last century. They are ubiquitous in the developed world and their use spans nearly all industrial sectors. They have found application as refrigerants, propellants, fire suppressants and as specialist solvents, polymers and surfactants. More recently there is a growing adoption of fluorine in pharmaceutical and agrochemical products. This phenomenon is due to the unique set of properties bestowed on the fluorine atom which translates to the unique characteristics of fluorinated compounds.

The first widely implemented industrial applications of organofluorine chemistry began in the late 1920's when Henne and Midgely discovered that chlorofluorocarbons (CFCs) made excellent refrigerant gases thanks to their low flammability, low toxicity, thermal and chemical stability and high volatility.<sup>[9]</sup> These properties are attributed largely to their low reactivity due to high C–F bond strengths.

### 1.2.1 Perfluorinated compounds

Polytetrafluoroethane (PTFE), a linear polymer with repeating  $\text{CF}_2$  units, was discovered serendipitously in 1938 during research into CFC refrigerants and quickly began to be commercialised as Teflon on large scales, due to its advantageous thermal and chemical inertness.<sup>[6]</sup> This inertness is in part due to the increased C–C bond strengths of the PTFE polymer (by approximately  $8 \text{ kcal mol}^{-1}$ ) compared to its non-fluorinated analogue polyethylene (PE).<sup>[10]</sup>

Perfluorocarbons, compounds containing only carbon and fluorine atoms, are important chemicals for a wide range of industries, from heat and chemical resistant containment, as specialist solvents to blood substitutes. They exhibit high chemical inertness, high thermal stability, have low surface energies, high dielectric strength and are known for their 'slippery-ness'.

PTFE or Teflon® is the basis for coatings on frying pans and other cookware. It has the lowest friction coefficient of any material which gives its non-stick properties, whilst the high chemical and thermal resistance means that it will not melt or interact with the food.<sup>[11]</sup> The high hydrophobicity of perfluorocarbons also means PTFE finds applications in clothing. Gore-Tex® is a patented brand that utilises PTFE membranes and is arguably the world leader in waterproof clothing technology.

Alkanes and their perfluorinated analogues are both non-polar and do not mix with water, yet they are largely immiscible between themselves. This is a result of their low surface energies and is a defining reason why fluorocarbons have found application as effective textile finishers, as they exhibit both water and oil repellence. This property of fluoro- and perfluorocarbons (low surface energies) is a contributing factor in many of their industrial applications. For example they make excellent fire

extinguishers as they will form a layer over burning hydrocarbons cutting off the fuel (oxygen) to the fire, whilst they themselves are highly inflammable (high thermal stability).<sup>[7]</sup>

Due to the weak intermolecular forces between fluorocarbon molecules, perfluorocarbon liquids have a large degree of interstitial space and therefore can be compressed quite significantly. This property spurred research into the ability of perfluorocarbons, notably perfluorodecalin, to be used as synthetic blood. They were shown to exhibit very high oxygen solubility whilst remaining biologically inactive.<sup>[12-14]</sup> Perfluorocarbons have been considered “orthogonal to life” meaning they are not recognised as foreign to the body. They trigger little or no biological response which allows their application *in vivo* with minimal risk.

### 1.2.2 Refrigerants

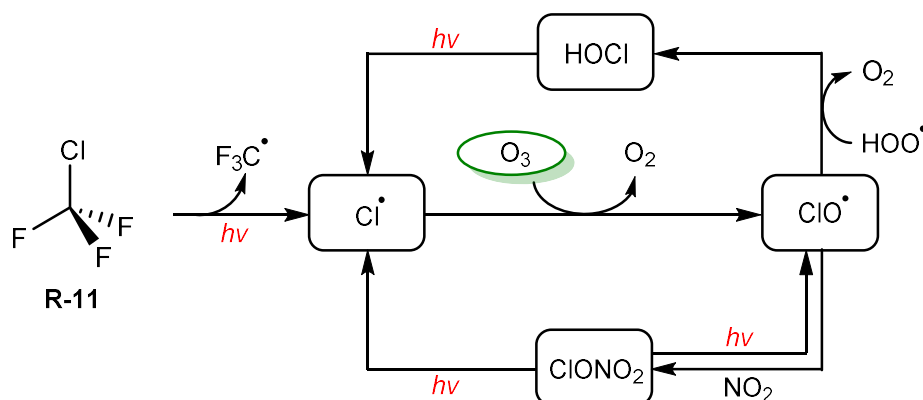
As previously mentioned, the first industrial application of organofluorine chemistry came with the discovery of chlorofluorocarbons, CFCs or Freons, in 1928. These are a class of gases containing only carbon, chlorine and fluorine atoms and possessed a unique set of properties that made them desirable for a wide range of industrial applications. They were highly volatile yet chemically inert. They are non-flammable and also non-toxic.<sup>[6]</sup> Their first wide-scale use was for refrigeration processes, but they also later became main components of aerosol propellants and blowing agents.

The concept of refrigeration had existed for centuries before the discovery of CFCs, with the first patents in this area submitted in the early 19<sup>th</sup> Century. The use of volatile fluids for refrigeration was suggested by Evans in 1805. By 1834 Jacob Perkins invented a machine for vapour-compression where he describes “...volatile fluid for the purpose of producing the cooling and freezing...”. Perkins is now famously known as the father of the refrigerator.<sup>[15]</sup> In the early years, any compounds that worked as refrigerants were used, such as propane or ammonia. These were often non-ideal and led to accidents due to their inherent flammability or toxicity.

The first CFCs to be put into industrial production were chlorotrifluoromethane (CFC<sub>3</sub>, R-11) and dichlorodifluoromethane (Cl<sub>2</sub>CF<sub>2</sub>, R-12) in the early 1930's. These, and variants thereof, were the primary refrigerants alongside hydrochlorofluorocarbons (HCFCs) until the late 1980s.

The production and application of CFCs and HCFCs grew right up until their phasing out in the Montreal Protocol (1987), with peak production hitting approximately one million tonnes per annum. The Montreal Protocol was an internationally agreed treaty aiming to completely phase out the use of chemicals that would damage the ozone layer, namely chlorofluorocarbons.<sup>[16]</sup>

Ultraviolet (UV) radiation in the higher stratosphere was found to homolytically cleave the C–Cl bonds of CFCs generating chlorine radicals. It is the formation of these radicals that make CFCs so damaging to the ozone layer. The chlorine radicals will react with ozone ( $O_3$ ) to generate oxygen ( $O_2$ ) and chloroxide radicals, then regenerating Cl radicals which will propagate the cycle.<sup>[6]</sup> A metric was developed to measure this damaging effect, called the Ozone Depletion Potential (ODP) that took  $ClCF_3$  as the standard, pegged at 1.0 units.<sup>[17]</sup> Larger numbers signify a higher level of ozone depleting ability. The ODP values for HCFCs are lower than those of CFCs.

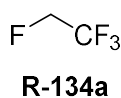


*Scheme 1.1 Simplified schematic showing the destruction of ozone by chlorine radicals*

Post Montreal Protocol, there was a rapid push to find CFC replacements that could be used directly in the machines that required them. Bromofluorocarbons exhibited similar ozone-depleting properties and were also included in the phase-out. However, compounds made entirely of carbon, hydrogen and fluorine (HFCs) were discovered to be ideal replacements as fluorine radicals do not significantly deplete ozone – their ODP value is 0. HFCs have similar chemical and thermal properties to CFCs that make them ideal refrigerants and are now regarded as the ‘Third Generation’ of refrigerants.<sup>[16]</sup> Approximately 80 % of HFC consumption is from refrigeration purposes, with the other 20 % representing foaming agents, aerosols and fire suppressants.

One of the most widely used HFC refrigerants is 1,1,1,2-tetrafluoroethane, R-134a.

**Common uses of R-134a:**



1. Domestic Refrigeration
2. Commercial Refrigeration
3. Commercial Refrigeration: Plug-ins & Vending Machines
4. Industrial Refrigeration
5. Transport Refrigeration
6. Mobile Air Conditioning (cars etc.)
7. Industrial / Commercial Air Conditioning DX Chillers

## 8. Industrial / Commercial Centrifugal Compressors

As well as being used on its own directly, R-134a also makes up a component of many commercially available refrigerant blends, such as R-449a branded as Opteon XP40 by Du Pont (1:1:1:1 composition by % wt = R-32 : R-125 : R-1234yf : R-134a). Refrigerant blends can be beneficial as they allow for the fine tuning of thermophysical properties towards the specific application, as well as keeping emission metrics down (GWPs, average atmospheric lifetimes) upon the inclusion of greener refrigerants.

| Refrigerant/<br>Formula                             | Atmospheric<br>Lifetime (years) | Main<br>Uses                       | Ozone<br>Depleting<br>Potential (ODP) | Global Warming<br>Potential<br>( <sup>100</sup> GDP) |
|---|---------------------------------|------------------------------------|---------------------------------------|--|
| R-11, Cl <sub>3</sub> CF                            | 45                              | Refrigerant                        | 1.0                                   | 4660   |
| R-12, Cl <sub>2</sub> CF <sub>2</sub>               | 102                             | Refrigerant                        | 1.0                                   | 10200  |
| R-115, C <sub>2</sub> CF <sub>5</sub> Cl            | 1700                            | Refrigerant                        | 0.6                                   | 10300  |
| R-13, CF <sub>3</sub> Cl                            | 640                             | Foam blowing                       | 1.0                                   | 14000  |
| R-13B1, BrCF <sub>3</sub>                           | 69                              | Fire suppression                   | 10.0                                  | 6900   |
| R-23, HCF <sub>3</sub>                              | 264                             | Refrigerant/industry<br>by-product | 0                                     | 14800  |
| R-134a,<br>H <sub>2</sub> FCCF <sub>3</sub>         | 14                              | Refrigerant                        | 0                                     | 1600   |
| R-1234yf,<br>H <sub>2</sub> C=CFCF <sub>3</sub>     | 10 days                         | Refrigerant, replace<br>R-134a     | 0                                     | 4  |
| R-1234ze,<br>(E)-HFC=CHCF <sub>3</sub>              | 18 days                         | Refrigerant                        | 0                                     | <1   |
| R-1336-mzz,<br>F <sub>3</sub> CCH=CHCF <sub>3</sub> | 22 days                         | High temp<br>refrigerant           | 0                                     | 2  |

Table 1.4 Examples of CFC, HCFC, BrFC, HFC and HFO refrigerants, their uses and environmental metrics<sup>[6][18]</sup>

Though the problem of ozone depletion was seemingly ‘fixed’, there was a new issue raised through the use of fluorocarbons – the ‘Greenhouse Effect’. Fluorocarbons exhibit infrared stretches in the transparent region (1000 – 1400 cm<sup>-1</sup>) and therefore have high Global Warming Potentials (GWPs). This is a metric which, simplified, is a measure of how much heat a gas will trap in the atmosphere relative to carbon dioxide (pegged at 1.0 units) and is sometimes represented as 100-year potentials (<sup>100</sup>GWP). Most HFCs have GWPs over 1000 and are therefore extremely potent greenhouse gases (See Table 1.4). The use of R-134a gas is preferred over other HFCs due to its significantly lower atmospheric lifetime and GWP value.

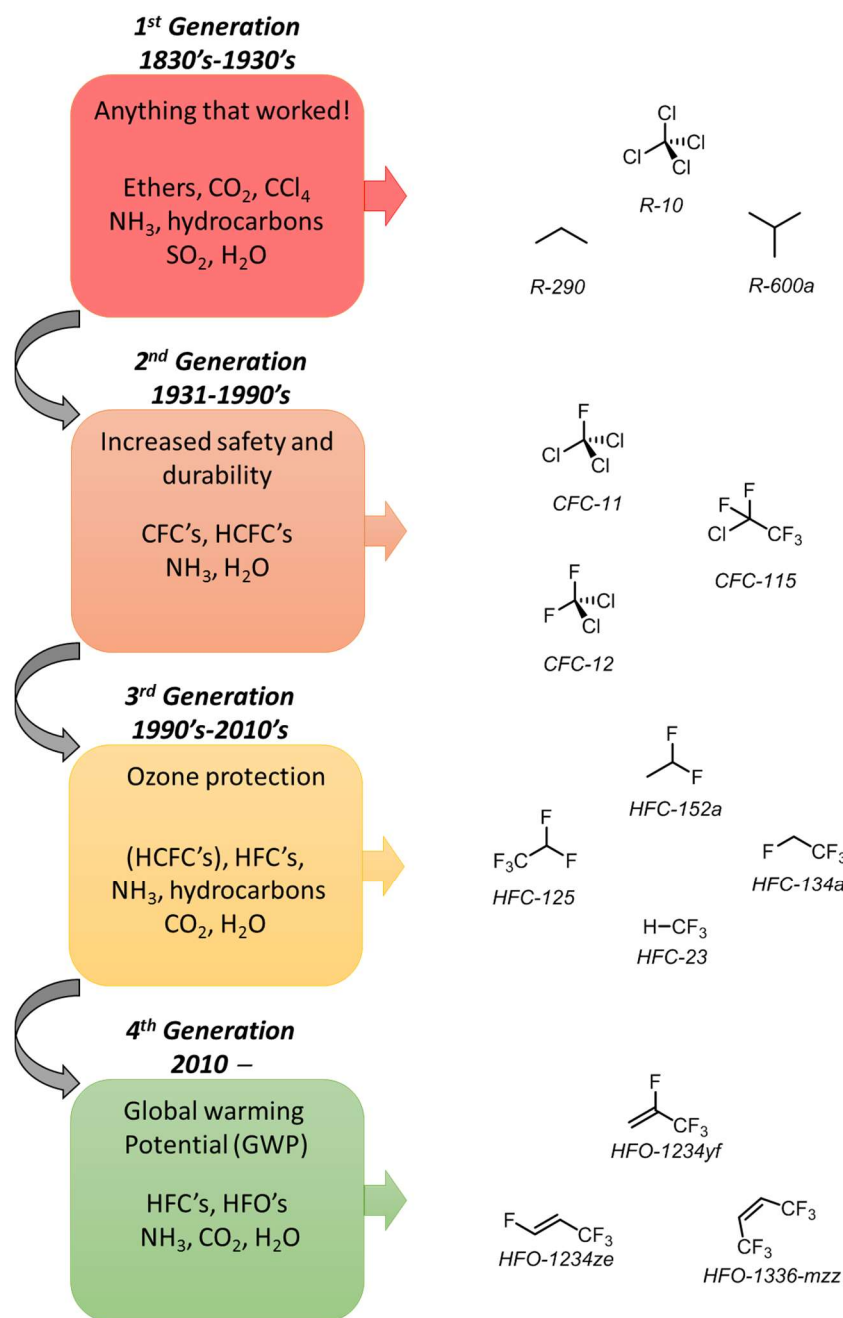


Figure 1.1 The evolution of refrigerant chemicals. Time periods, what their desirable attributes are and examples of those used

In 1997 a new international climate treaty, the Kyoto Protocol, was signed as a follow up to the hugely important Montreal Protocol a decade before. This legislation committed signatories to reduce greenhouse gas emissions on the basis of two statements; firstly that global warming is occurring and secondly that it is likely that man-made CO<sub>2</sub> and CO<sub>2</sub> equivalent emissions are the driving factor. Legislation focused on the reduction and replacement of six groups of gases, including HFCs and perfluorocarbons (PFCs). Unfortunately, the Kyoto Protocol faced criticism due to the limited effectiveness as it predominantly focused on developed countries and had a narrow time period.<sup>[56]</sup>

More recently, the agreements made as part of the original Montreal Protocol have been developed to accelerate phase-outs and work harder on tackling issues surrounding HFCs. In 2016 the Kigali Amendment was signed by over 150 countries, marking the beginning of the end for hydrofluorocarbon (HFC) refrigerants.<sup>[19]</sup>

For this to be effective and to meet the targets set by the treaty, new chemicals or technologies were required to replace HFC refrigerants.

Companies such as Honeywell and Chemours had long predicted this demand, investing heavily in the development of ultra-low GWP refrigerants – the so called ‘Fourth Generation’ of refrigerants.

Hydrofluoroolefins (HFOs) containing only C, H and F atoms with at least one C=C bond proved suitable. One such example is 2,3,3,3-tetrafluoropropene (R-1234yf), marketed as a direct replacement for the widely used R-134a. R-1234yf has an extremely low GWP of just 4, similar thermophysical properties and is suitably stable.<sup>[15]</sup> (*E*)-1,3,3,3-Tetrafluoropropene (R-1234ze) is another hydrofluoroolefin that is in an advanced stage of production for HFC replacements, whilst 1,1,1,4,4,4-hexafluorobut-2-ene (R-1336mzz) is a more recent development with potential applications in high-temperature heat pumps.

The inclusion of C=C double bonds brings both advantages and disadvantages. They are more reactive than their HFC counterparts therefore they typically have lower atmospheric lifetimes and lower GWPs, though they exhibit decreased stabilities and higher toxicities.<sup>[15]</sup> Those with very low global warming potentials (~ 1) will decompose much closer to the source of emission. That brings a potential to contribute to local pollution in the form of smog, or to decompose to other chemicals that could have higher GWPs (indirect GWP).

When designing new refrigerants, there are a variety of considerations to be made. Availability, can the replacements be produced in the quantities required? Will they perform as well? Are they as safe (toxicity, flammability etc.)? Can they become economical? Can the required applications accept the replacements directly? Similarly to when HFCs replaced CFCs, a major design feature was the ability to directly replace one with the other, without the need of retro-fitting or replacing the equipment. As with all new chemicals, the long-term environmental impact of their release or loss into the atmosphere is a difficult to establish, yet an important consideration.

### 1.2.3 Pharmaceutical Chemistry

The advantages fluorinated compounds have for society are not confined to bulk gases and polymers. The incorporation of fluorine is also an increasingly common technique by chemists in the

pharmaceutical and agrochemical sectors to increase the quality of our medicine and strengthen the security of food supplies.<sup>[20]</sup> These classes of compounds are typically more complex, higher molecular weight substances that are produced on smaller scales with high purity. The use of fluorine in pharmaceuticals is a product of the many unique aspects of the C–F bond that have been described in section 1.1.

In the context of medicinal chemistry, the addition of a well-placed C–F bond can often result in remarkable therapeutic and metabolic properties.<sup>[21]</sup> Fluorine can enhance the metabolic stability of a drug. In turn, this will increase its persistency *in vivo* and could allow for lower or less frequent dosing. This ability stems from the high C–F bond strength. C–F bonds typically resist the oxidation processes of P450 enzymes.<sup>[21]</sup> Fluorine incorporation can also increase the lipophilicity of drugs. The drug then exhibits a higher bioavailability and makes the crossing of cell-membranes more facile.<sup>[20]</sup>

Due to the relatively small size of the fluorine atom (atomic radius 1.47 Å), a C–F bond can act as an isostere for the hydrogen atom (atomic radius 1.20 Å). Due to the bond polarisation, they can also mimic the hydroxyl group. Therefore these are two of the most common pharmaceutical modifications.

C–F bonds and fluoroorganic compounds are almost entirely absent in nature and to date, no biological processes have been identified that require fluorinated metabolites.<sup>[6]</sup> Up until the 1950's, there were no drugs on the market that contained fluorine as traditional medicines (pre 1970's) were based heavily on naturally occurring compounds. The first breakthrough in organofluorine pharmaceuticals was the synthesis of Fludrocortisone, installing a fluorine atom on cortisol and greatly improving its anti-inflammatory abilities.<sup>[22]</sup> This was shortly followed by the synthesis of 5-fluorouracil, a drug with anti-cancer properties still used to this day.<sup>[23]</sup>

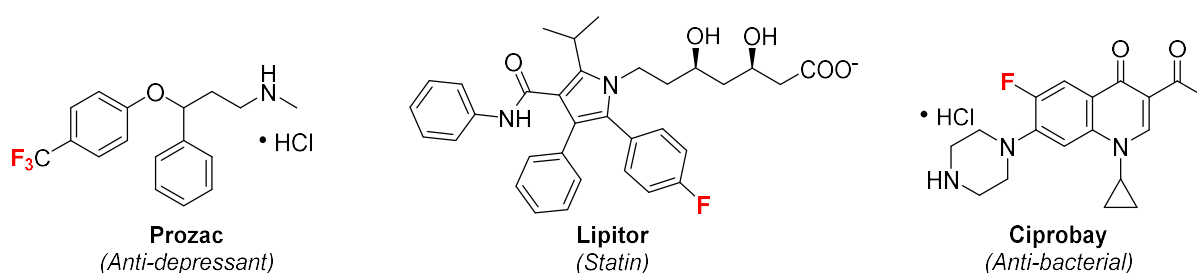


Figure 1.2 Examples of fluorinated blockbuster drugs

Within just 50 years of their seminal discovery, fluorinated compounds now make up over 20 % of pharmaceuticals.<sup>[24]</sup> When considering just blockbuster drugs, those with sales over \$1bn per year, the proportion containing at least one fluorine atom now rises to 50 %.<sup>[22,25]</sup> Notable fluorinated



blockbuster drugs are the anti-depressant Prozac, Ciprobay an anti-bacterial drug and Lipitor, a statin which is also the highest grossing drug to date with lifetime sales exceeding \$150bn!

Fluorinated compounds have also found medical uses as anaesthetics. These compounds resemble the gases used in the refrigeration industry. They are non-flammable and show minimal side-effects, due to their relative inertness. Common fluorinated anaesthetics such as Isoflurane ( $C_3H_2ClF_5O$ ) and Halothane ( $C_2HBrClF_3$ ) therefore became the preferred agents over the previous state-of-the-art anaesthetic, diethyl ether.<sup>[26]</sup>

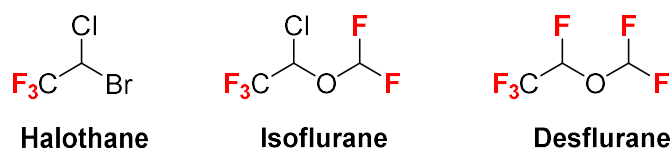
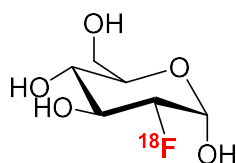


Figure 1.3 Examples of fluorinated anaesthetics

#### 1.2.4 Nuclear Medicine

Fluorine has also found application in the growing specialist field of nuclear medicine. This exploits the radioactive  $^{18}F$  isotope and is monitored by positron emission tomography (PET) imaging.<sup>[27]</sup>  $^{18}F$  is particularly useful in this field as a result of its long half-life ( $^{18}F$ ,  $t_{1/2} = 110$  min) compared to other isotopes ( $^{11}C$ ,  $t_{1/2} = 20$  min,  $^{13}N$ ,  $t_{1/2} = 10$  min and  $^{15}O$ ,  $t_{1/2} = 2$  min). These radionuclides are generated in a cyclotron and incorporated into a compound very close to the time of ingestion by a patient. The most common radiopharmaceutical is a simple glucose analogue and is innocuous in the body.



**2-Deoxy-2-[ $^{18}F$ ]-fluoro-D-glucose**

Figure 14 Structure of the most prevalent  $^{18}F$  radiotracer, 2-deoxy-2-[ $^{18}F$ ]-fluoro-D-glucose

Furthermore, due to the ubiquitous nature of fluorine in pharmaceuticals,  $^{18}F$  radiotracers can be installed in place of standard  $^{19}F$  atoms in fluorinated drugs by late stage methods. The drug action can then be monitored directly *in vivo*. This can provide vital information such as its uptake, whether it crosses blood-brain boundaries or how specifically it targets the desired organs.<sup>[27]</sup>

#### 1.2.5 Agrochemicals

With an increasing world population and improving living standards, the importance of efficiently producing and protecting crops for human and livestock consumption is growing. This is described as food security. Agricultural chemicals (agrochemicals) are used in farming industries to achieve this. They mostly comprise of chemicals to protect crops such as herbicides, insecticides and fungicides as well as growth agents and fertilisers.

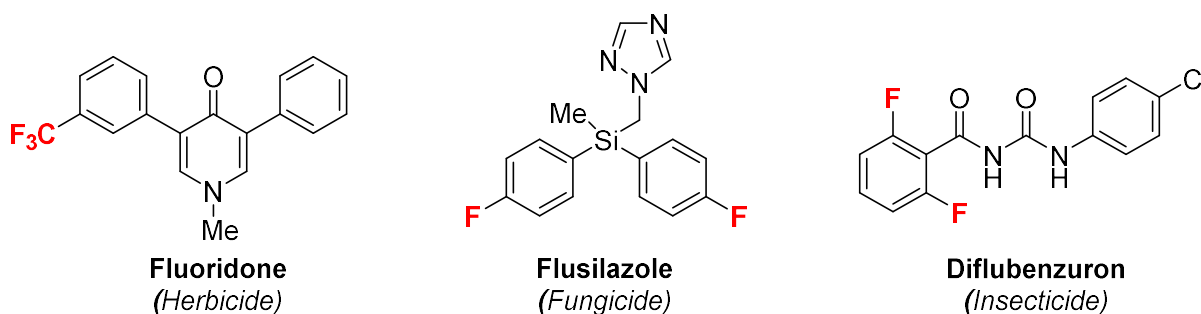


Figure 1.5 Examples of fluorine containing pesticides

Much like pharmaceuticals, the incorporation of fluorine to this class of chemicals has seen a surge in the last three decades.<sup>[6,28,29]</sup> From 1988 to 1999 the quantity of fluorine containing compounds for pesticide applications rose from 9 to 17 %. For insecticides and herbicides specifically, the amount is approximately 40 %. The most common modifications are the addition of aromatic C–F bonds, aromatic trifluoromethyl (CF<sub>3</sub>) and aromatic trifluoromethoxy (OCF<sub>3</sub>) groups. One of the major factors behind this drive has been their increased activity over the non-fluorinated counterparts, often more than an order of magnitude more effective.<sup>[30]</sup> Although fluorinated chemicals are typically more expensive weight-for-weight, the increased activity and persistency can cancel this out. From an environmental standpoint, the use of lower quantities of product can result in reduced chemical contamination.

The impact a fluorine modification can make to the efficacy of an agrochemical can be profound. Many of these benefits can be attributed to the high electronegativity of the fluorine atom.

The benefits gained upon incorporating fluorine into agrochemicals are similar to those previously described for pharmaceuticals, such as enhanced lipophilicity, bioavailability and metabolic stability.<sup>[20,21,28]</sup> Many agrochemicals take advantage of the trifluoromethyl group. These can result in changes to the compound's polarity and will induce or modify dipoles. This can adjust the conformation of the agrochemical which has potential for enhancing target binding. The acidity of neighbouring functional groups (notably OH) can be altered due to fluorine's electron withdrawing effects. Again due to the relatively the small size of fluorine, being similar to hydrogen, the steric environment of the compound remains largely unchanged when making a C–H to C–F modification.

### 1.3 Origin of Fluorine and How to Introduce it into Organic Compounds

Naturally, fluorine exists almost exclusively in mineral forms. It is the thirteenth most common element in the earth's crust. The most abundant of these fluoride ores (in decreasing abundance) are fluorite or fluorspar ( $\text{CaF}_2$ ), fluoroapatite commonly known as phosphate rock ( $\text{Ca}_5(\text{PO}_4)_3\text{F}$ ) and cryolite ( $\text{Na}_3\text{AlF}_6$ ).<sup>[31,32]</sup> Fluorite, once mined, requires upgrading either to Metspar-grade for metallurgy applications, or to Acid-grade for the production of HF.<sup>[11]</sup>

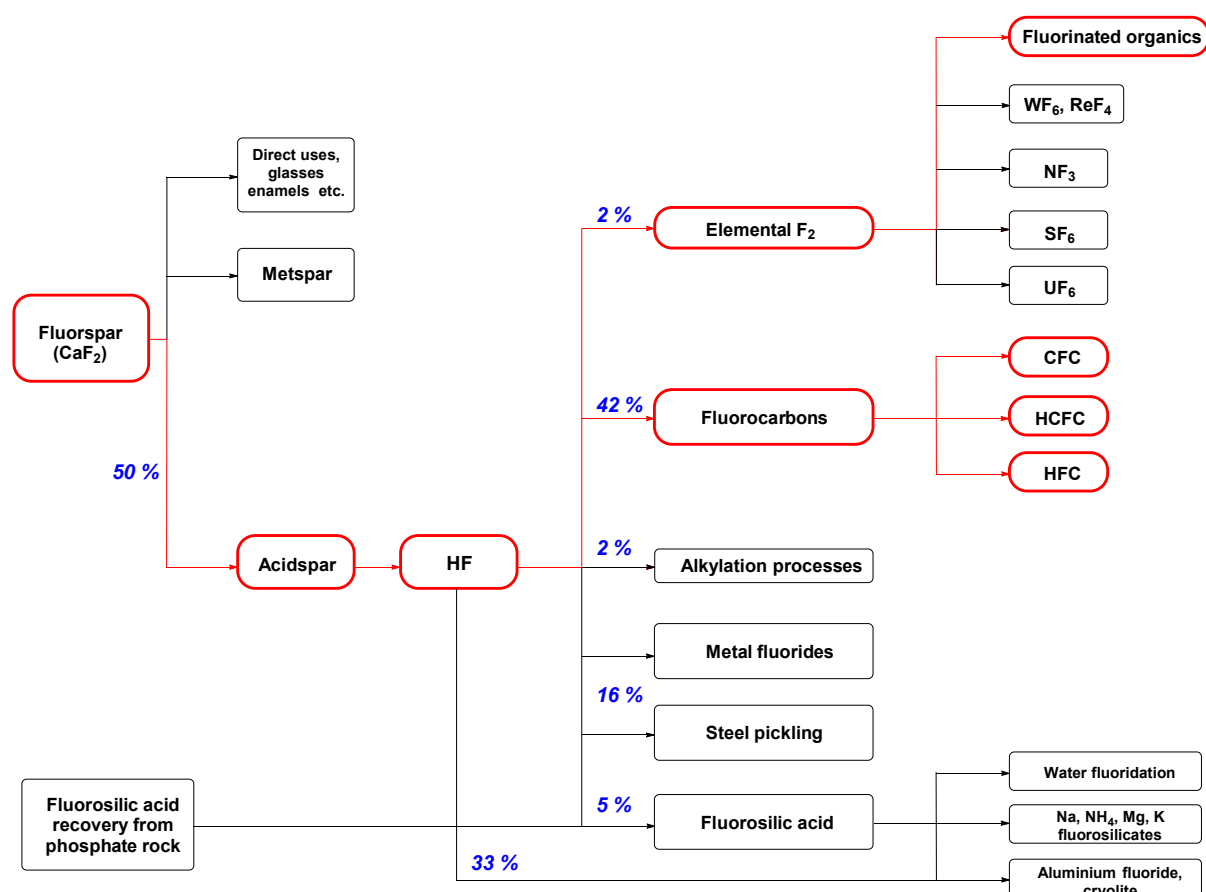
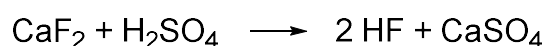


Figure 1.6 The destination of fluorine from its major source, Fluorspar rock ( $\text{CaF}_2$ ) highlighting the routes to organofluorine compounds and approximate proportions<sup>[11]</sup>

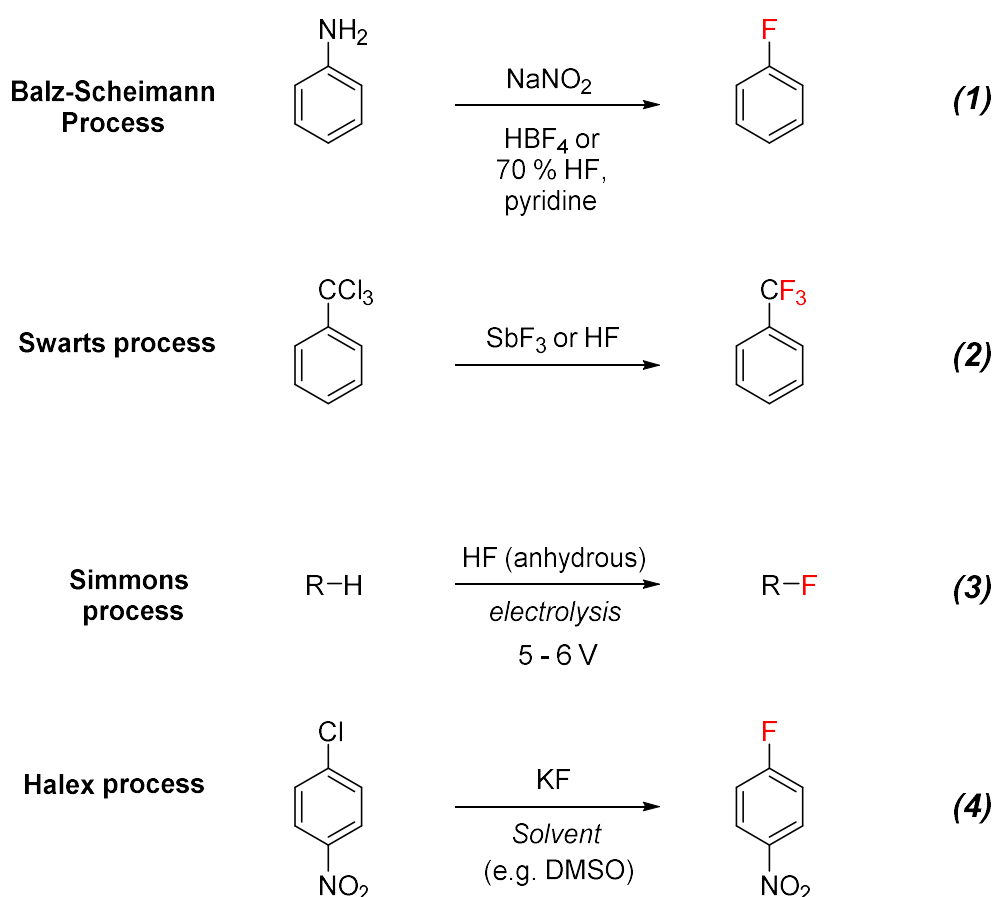
#### 1.3.1 Industrial Fluorination using HF

The majority of fluorine in fluorochemicals stems from hydrofluoric acid (HF) (See fluorine diagram, Figure 1.6). Hydrofluoric acid is obtained in aqueous form through reaction of fluorite ( $\text{CaF}_2$ ) with sulfuric acid ( $\text{H}_2\text{SO}_4$ ).<sup>[6]</sup>



Antimony trifluoride,  $\text{SbF}_3$ , was known to react with chlorinated compounds, converting them to the corresponding fluorinated ones. In 1930s, Swarts found that HF could be used as the fluoride source utilising  $\text{SbF}_3$  catalytically or as a direct alternative – the so named Swarts reaction. This technique was used for the industrial production of refrigerant CFCs such as trifluorochloromethane (R-11) and other related species.

The majority of simple fluorinated aromatics are synthesised through the Balz-Schiemann process. Established in the 1920's, it represents one of the most general methods for introducing fluorine into aromatic compounds.<sup>[33]</sup> In the presence of  $\text{HBF}_4$  (produced from HF) and nitric acid ( $\text{HNO}_3$ ) anilines are converted into the corresponding diazonium tetrafluoroborates. These reactive intermediates then decompose through thermal or photolytic methods to generate the corresponding fluoroarene.



*Scheme 1.2 Methods for the bulk fluorination of organic compounds*

Anhydrous hydrofluoric acid can also be used as a fluorinating agent in an electrochemical reaction, called the Simmons process, to generate aliphatic C–F bonds from C–H bonds.<sup>[34]</sup>

Another method for the bulk synthesis of fluorinated compounds is *via* the Halex reaction.<sup>[35]</sup> This process involves the nucleophilic aromatic substitution ( $\text{S}_{\text{N}}\text{Ar}$ ) of fluoride ion for chloride or bromide, typically in electron-poor aromatic systems.

HF is a particularly toxic compound and its uses are therefore limited to large scale production at industrial plants and largely avoided for research purposes.

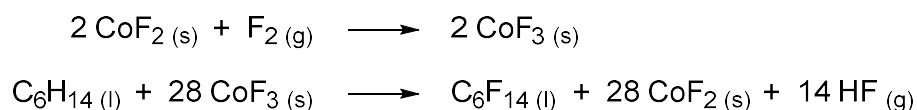
### 1.3.2 Elemental Fluorine

HF is used as a precursor in the synthesis of elemental fluorine ( $F_2$ ). This is an extremely oxidising gas ( $E^\circ = + 2.87 \text{ V}$ )<sup>[36]</sup> and will undergo facile homolytic cleavage into F radicals (BDE of F–F = 37.8 kcal mol<sup>-1</sup>).  $F_2$  will react with virtually anything. However, elemental fluorine can be tamed to be used in the synthesis of fluorocarbons.

The synthesis of elemental fluorine ( $F_2$ ) was first achieved by Moissan in 1886 upon the electrolysis of anhydrous solution of potassium fluoride (KF) and hydrogen fluoride. The basis of his electrolysis technique is still used to this day to produce industrial quantities of  $F_2$ .

Elemental carbon (C) will react directly with elemental fluorine to form the incredibly inert gas carbon tetrafluoride ( $CF_4$ ). A highly destructive process will take place upon direct combination with hydrocarbons. For example a methane-fluorine mixture will explode and C–C bonds can get severed in longer alkane chains.<sup>[37]</sup> For this reason, the fluorination of organic molecules with  $F_2$  gas is typically performed as a low concentration mixture with inert gases such as nitrogen or argon ( $N_2$  and Ar). It is also difficult to control the level of fluorination, with the most common outcome being the perfluorination of the organic substrate – replacing all C–H bonds with C–F bonds.<sup>[32]</sup> The reaction of  $F_2$  with dihydrogen ( $H_2$ ) is highly exergonic leading to the formation of HF. Likewise, the reaction with water ( $H_2O$ ), leads to HF and  $H_2O_2$ .<sup>[32]</sup>

In the 1940's, elemental fluorine was harnessed for the industrial manufacture of perfluorocarbons, in a procedure known as the Fowler Process.<sup>[38,39]</sup> This process has two main steps. The fluorination of cobalt difluoride ( $CoF_2$ ) by  $F_2$  to generate cobalt trifluoride ( $CoF_3$ ), which is then heated with a hydrocarbon substrate to perform the perfluorination. The  $CoF_2$  by-product can then be used again in the cycle. The development of this process allowed for the large scale production of perfluorocarbons, which in turn strengthened research into their potential applications.



*Scheme 1.3 Example of two-step Fowler Process for the generation of perfluorohexane*

Research into the use of  $F_2$  vastly accelerated during the years of the Manhattan Project (1939 – 1947). Large quantities of elemental fluorine were required for the enrichment of uranium whilst specialist

materials, coolants and lubricants were needed for the separation and containment of isotopes and fluorocarbons were found to be particularly suited to these roles.

### 1.3.3 Fluorine in the Life Sciences

The main route to selective fluorination in the life-sciences sector are *via* the Swarts halogen exchange process and the Balz-Schiemann process. These focus on fluoroaromatics and trifluoromethyl aromatics respectively and both use anhydrous HF as the fluorinating agent.<sup>[40]</sup> HF is particularly toxic. It can easily pass through the skin barrier and has an anaesthetic effect meaning that contact is not quickly detected. It has the ability to dissolve bone and also interrupts the function of  $\text{Ca}^{2+}$  ions that are vital for metabolic processes. HF is also extremely reactive which can lead to limited selectivity and substrate scope. These fundamental problems with traditional fluorination methods opened the door for a new area of fluorine chemistry – easy-to-use fluorinating agents.

The growth in the discovery rate of new fluorinated pharmaceuticals is undoubtedly due in part to the development and availability of commercial fluorinating agents that can be obtained by researchers in academia or industry. There are many such agents on the market. They can be split into subcategories such as electrophilic<sup>[41]</sup> or nucleophilic fluorinating agents, deoxy-fluorinating agents or trifluoromethylating agents among some others.<sup>[42–44]</sup> They are milder, more selective reagents for the installation of fluorine allowing for easier and more widespread application. These can be referred to as ‘Late Stage Reagents’ allowing the fluorine to be installed towards the end of the product synthesis rather than requiring its presence in the initial building blocks. These specialised fluorinating agents are designed to be highly specific, targeting the fluorination of certain functional groups, or positions in a molecule allowing more complexity to be present beforehand.

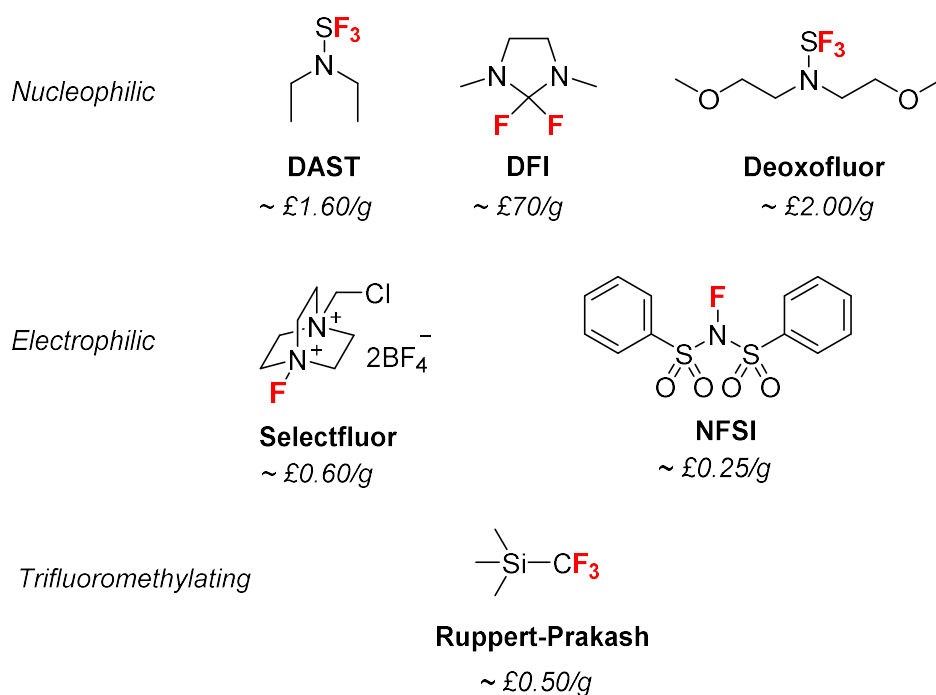


Figure 1.7 Examples of common nucleophilic, electrophilic and trifluoromethylating agents, plus cheapest available prices per gram of reagents (Apollo Scientific catalogue, September 2019)

They are excellent reagents for simplifying and accelerating the discovery process of active pharmaceutical agents (APIs). Their use allows the fluorination of many similar compounds on smaller scales, all of which can then be screened for pharmaceutical activity. They are “user-friendly” fluorinating agents and the desired fluorinated products can be accessed without the necessity of being trained specifically in (often dangerous) traditional fluorine chemistry methods. Unfortunately, once the drug makes it past the initial screening, these reagents are typically too expensive to be used on larger plant scales – where the use of more fundamental fluorination techniques take place.

One such example is Selectfluor. This was developed as a source of electrophilic fluorine in the early 1990’s and was quickly commercialised (now sold by Air Products and Chemicals) for use in organofluorine chemistry.<sup>[41,45]</sup> It is an ‘N-F’ reagent, an *N*-fluoroammonium salt and has become one of the most accessible sources of ‘F<sup>+</sup>’. There are huge benefits of using reagents such as those in Fig. 1.7 over F<sub>2</sub>. They are non-gaseous, less toxic, less reactive and non-explosive whilst also being relatively inexpensive (from a research tool point-of-view).

Approximately 25 tonnes of Selectfluor are sold each year for over \$7.5m, which make it the world’s bestselling electrophilic fluorinating agent.<sup>[46]</sup> There are over 130 reported citations for the use of Selectfluor in pharmaceutical patents with approximately 80 % of all fluorinated steroids using Selectfluor in their synthesis. For example, fluticasone propionate is a multimillion dollar-per-year generic drug sold around the world, used to treat asthma, which uses Selectfluor in its synthesis.<sup>[47]</sup>

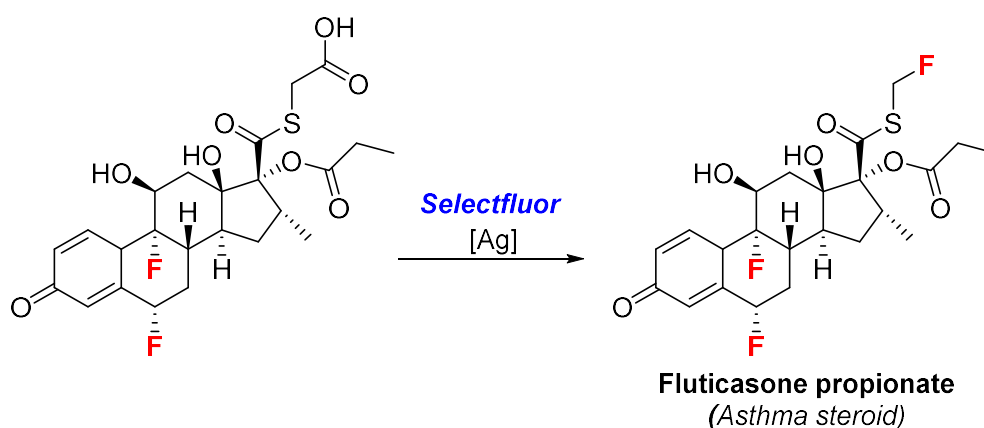


Figure 1.8 Steroid drug produced worldwide and synthesised using Selectfluor reagent<sup>[47]</sup>

Another such fluorinating agent is trifluoromethyltrimethylsilane or the Ruppert-Prakash reagent, developed by its name bearers in the 1980's. This will deliver a trifluoromethyl group ( $\text{CF}_3$ ). The simplest nucleophilic trifluoromethyl agent that may be imagined would be lithium or magnesium trifluoromethyl. These have proved experimentally impractical however due to their problematic synthesis and the ease of  $\alpha$ -fluorine elimination which results in highly reactive difluoromethylcarbene species.<sup>[48]</sup> With the development of the Ruppert-Prakash reagent, the  $\text{CF}_3$  synthon became stable, bottleable, easy to handle and reasonably cost effective due to its simplicity.<sup>[49]</sup> This reagent can be considered as a 'fluorinated building-block' – a compound that will install a  $\text{CF}_3$  moiety on demand (under the correct reaction conditions). This particular class of organofluorine reagents is growing in interest as the demand for more complex, specialist or selective fluorinated groups are required.

The development of new fluorinating agents goes hand-in-hand with the discovery of new pharmaceuticals and agrochemicals. To date, the majority of agents delivered a single fluorine atom or  $\text{CF}_3$  group. This translates (though not the only factor) to the ubiquitous presence of these moieties in pharmaceutical and agrochemical products.

Recently, more complex and intricate fluorine modifications are being proposed to generate desirable properties in APIs, such as the difluoromethyl, trifluoroethyl, perfluoroalkyl or fluoroalkenyl groups.



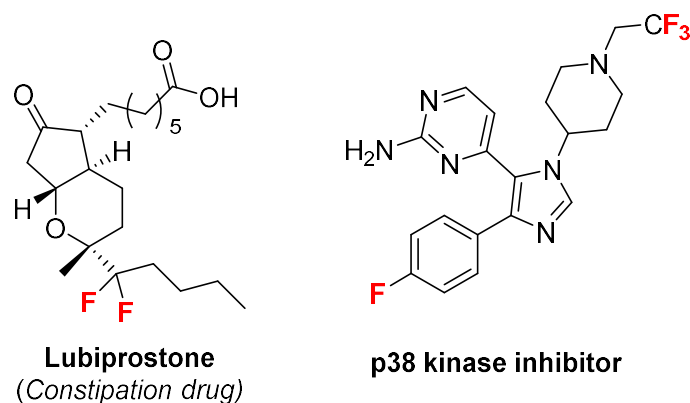


Figure 1.9 Examples of difluoromethylene<sup>[50]</sup> and trifluoroethyl<sup>[51]</sup> drugs

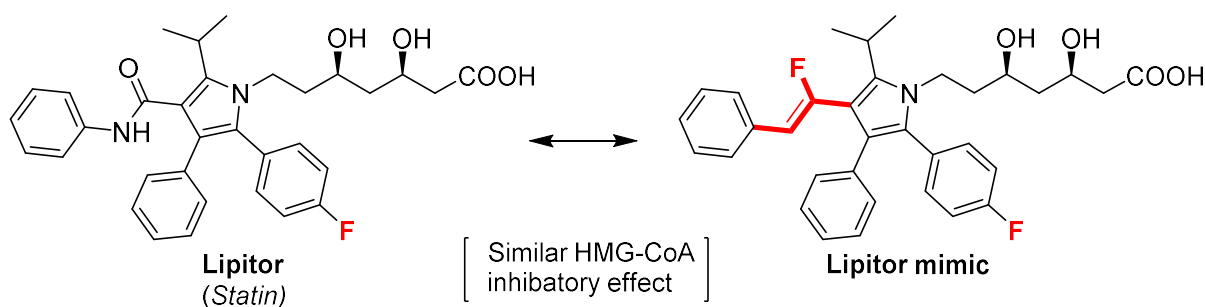


Figure 1.10 Use of fluoroalkene moiety as amide mimic<sup>[52]</sup>

For example, fluoroalkene moieties are gaining interest for their ability to mimic amide bonds.<sup>[53,54]</sup> Fundamentally, for new fluorinated groups to gain the attention of industry, there need to be effective and “user-friendly” methods to install them. The development of new fluorinated building blocks has the potential to achieve this goal.

## 1.4 Sustainability of Fluorine

Despite the clear importance in modern society, the fluorine and fluorochemicals industry is not currently sustainable. At the moment, negligible amounts of the fluorine used in industry is recycled or reclaimed. At first glance, this may not worry many as fluorine is the 13<sup>th</sup> most abundant element in the earth’s crust and there are arguably greater supply threats to other strategic elements.

Fluorine is ultimately a finite source. Although fluorine is a component in many rocks and ores, only three general types allow for commercial extraction. One of these, cryolite (Na<sub>3</sub>AlF<sub>6</sub>), is all but exhausted. Phosphate rock which contains fluoroapatite is abundant in places such as the US, however it is used primarily in the fertiliser industry and barely as a fluorine source as it contains only a small amount of fluorine by mass (Ca<sub>5</sub>(PO<sub>4</sub>)<sub>3</sub>F). The main source of fluorine is fluorspar (CaF<sub>2</sub>). Half of this CaF<sub>2</sub> is used directly in metallurgy processes, altering metallic properties during smelting largely in the iron and steel industries. The remainder is used to generate anhydrous hydrofluoric acid (aHF), the

origin of most fluorochemicals. In 2007 it was suggested that there was approximately a 100 year supply remaining of fluor spar rock if use continued at the current rate.<sup>[11]</sup> Global use is approximately 6.7 million tonnes per annum, with 500 million tonnes in global reserves. New sources are likely to be found over the next century, but the consumption of fluorine is also likely to grow in the developing world as living standards increase, with the potential to outstrip the supply from new discoveries.<sup>[40]</sup>

The majority of fluorine is lost into the atmosphere as fluorinated gases such as HFCs, or discarded as a mixture of solid wastes from industrial processes, notably from fertiliser and metal manufacturing. The release of these fluorinated gases is also problematic from an environmental standpoint. HFCs have high GWPs and are a significant contributor to climate change. The growth of production and consumption of HFCs have been growing rapidly since the phase-out of CFCs and HCFCs, particularly in the developing world, due to increased living standards and the desire for more commercial and domestic refrigeration. For example, the annual growth rate of HFC emissions from China between 2005-2009 was 40 %.<sup>[55]</sup>

To manage our unsustainable use of fluorine, new sources need to be discovered or better recycling methods put in place. Re-purposing the fluorine in current waste streams could be ideal. For example, large quantities of fluorine is in permanent storage in the form of UF<sub>6</sub> and fluorosilic acid (H<sub>2</sub>Si<sub>2</sub>F<sub>6</sub>), a waste from the fertiliser industry, is not currently recycled.

Another such example would be the capturing and re-use of fluorine in fluorinated gases. They have a high density of fluorine by mass and are widespread throughout the world. They already exist as organofluorines so harsh processing techniques may not be required. Current methods for preventing the emission into the atmosphere of refrigerant gases are limited to; direct re-sale or re-use, safe storage or destruction.

***Typical destruction methods of HFCs:***

- Liquid injection incineration
- Reactor cracking
- Gaseous/fume oxidation
- Rotary kiln incineration
- Cement kiln
- Radio frequency plasma

With regards to the storage or destruction methods, significant costs are likely to be incurred through energy or space demands. Direct re-sale and re-use can be limited by changes in composition of the

gases (or mixtures) after usage which affects their thermal properties. These problems with current procedures creates a demand for methods that have more utility and versatility, or can add value.

As we have seen, the use of fluorinating agents and fluorinated building blocks is a major driving force for the discovery of new pharmaceuticals and agrochemicals which have a marked impact on quality of life. Can fluorinated gases become be a part of this fluorine cycle?

## 1.5 Aims

The aim of this PhD programme was to advance state-of-the-art methodology towards recycling and upgrading fluorinated gases *via* chemical methods. More specifically, the aim was to develop processes that exploit main group reagents to activate the very strong carbon–fluorine bonds in hydrofluoroolefins and hydrofluorocarbons (HFOs and HFCs) to generate new, reactive fluorinated building blocks. It was our ambition to generate fluorinated compounds that can be used in further synthesis, such as for the construction of higher value compounds like pharmaceuticals or agrochemicals.

The project could be broken down into three main stages. The first was to understand the underlying fundamentals surrounding  $sp^3C-F$  bond cleavage processes at main group metal reagents. This was an extension of the work that had previously been undertaken in the group prior to this project. It was our goal to evaluate the scope and limitations of a low oxidation state, nucleophilic magnesium reagent towards activating the C–F bonds in aliphatic fluorocarbons. This first venture yielded important information, such as the necessity of potent nucleophiles that contain a fluoride acceptor. The fluoride acceptor was shown to provide a thermodynamic driving force for the reaction.

The next aim was to broaden the substrate scope to HFOs that are currently used as industrial refrigerants. We built upon our knowledge by synthesising novel compounds that were suitable for the selective activation of the C–F bonds in HFOs *via* two defined reaction pathways, whilst also generating synthetically useful building blocks. These building blocks were shown in preliminary studies to efficiently transfer polyfluoropropyl groups to organic electrophiles.

Finally, we addressed the most difficult target of this PhD programme, the C–F functionalisation of HFC gases. The chemical reactivity of these compounds are limited, with sparse examples in the literature. Very pleasingly we made good progress, particularly with trifluoromethane (R-23), transforming it into a simple bench-stable difluoromethyl containing silicon compound that can be used to efficiently deliver the  $CF_2H$  moiety to carbonyl compounds. The preliminary reactivity with other HFC gases appeared promising and this project will continue within the group.

## 1.6 References

- [1] L. Pauling, *J. Am. Chem. Soc.*, **1932**, *54*, 3570–3582.
- [2] D. O'Hagan, *Chem. Soc. Rev.*, **2008**, *37*, 308–19.
- [3] E. P. Gillis, K. J. Eastman, M. D. Hill, D. J. Donnelly, N. A. Meanwell, *J. Med. Chem.* **2015**, *58*, 8315–8359.
- [4] B. E. Smart, *The Chemistry of Functional Groups, Supplement D*, Wiley, New York, **1983**.
- [5] S. J. Blanksby, G. B. Ellison, *Acc. Chem. Res.* **2003**, *36*, 255–263.
- [6] P. Kirsch, *Modern Fluoroorganic Chemistry: Synthesis, Reactivity, Applications*, Wiley, New York, **2005**.
- [7] D. M. Lemal, *J. Org. Chem.* **2004**, *69*, 1–11.
- [8] Y. R. Luo, *Comprehensive Handbook of Chemical Bond Energies*, CRC Press, **2007**.
- [9] A. J. Elliott, in *Organofluor. Chem. Princ. Commer. Appl.* (Eds.: R.E. Banks, B.E. Smart, J.C. Tatlow), Plenum Press, New York, **1994**, pp. 145–157.
- [10] W. E-Chung, A. S. Rodgers, *J. Am. Chem. Soc.*, **1976**, *98*, 6112–6115.
- [11] G. Villalba, R. U. Ayres, H. Schroder, *J. Ind. Ecol.* **2007**, *11*, 85–101.
- [12] M. A. Hamza, G. Serratrice, M. J. Stébé, J. J. Delpuech, *J. Am. Chem. Soc.*, **1981**, *103*, 3733–3738.
- [13] R. K. Spence, E. D. Norcross, J. Costabile, S. McCoy, A. C. Cernaianu, J. B. Alexander, M. J. Pello, U. Atabek, R. C. Camishion, *Artif. Cells, Blood Substitutes, Biotechnol.* **1994**, *22*, 955–963.
- [14] I. T. Horváth, *Acc. Chem. Res.* **1998**, *31*, 641–650.
- [15] J. M. Calm, *Int. J. Refrig.* **2008**, *31*, 1123–1133.
- [16] L. E. Manzer, *Science*, **1990**, *249*, 31–35.
- [17] A. McCulloch, *J. Fluor. Chem.* **1999**, *100*, 163–173.
- [18] [https://ec.europa.eu/clima/policies/f-gas/alternatives\\_en](https://ec.europa.eu/clima/policies/f-gas/alternatives_en), (accessed 23<sup>rd</sup> Septemrber 2019).
- [19] M. P. Bailey, *Chem. Eng. (United States)* **2017**, *124*.
- [20] K. Muller, C. Faeh, F. Diederich, *Science*, **2007**, *317*, 1881–1886.
- [21] B. K. Park, N. R. Kitteringham, P. M. O'Neill, *Annu. Rev. Pharmacol. Toxicol.*, **2001**, *41*, 443–470.
- [22] D. O'Hagan, *J. Fluor. Chem.* **2010**, *131*, 1071–1081.
- [23] C. Heidelberger, N. K. Chaudhuri, P. Danneberg, D. Mooren, L. Griesbach, R. Duschinsky, R. J. Schnitzer, E. Plevén, J. Scheiner, *Nature* **1957**, *179*, 663–666.
- [24] K. L. Kirk, *J. Fluor. Chem.* **2006**, *127*, 1013–1029.
- [25] H. Mei, J. Han, S. Fustero, M. Medio-Simon, D. M. Sedgwick, C. Santi, R. Ruzziconi, V. A. Soloshonok, *Chem. – A Eur. J.* **2019**, *25*, 11797–11819.
- [26] D. Halpern, *J. Fluor. Chem.* **2002**, *118*, 47–53.

- [27] S. Purser, P. R. Moore, S. Swallow, V. Gouverneur, *Chem. Soc. Rev.*, **2008**, *1*, 320–330.
- [28] T. Fujiwara, D. O'Hagan, *J. Fluor. Chem.* **2014**, *167*, 16–29.
- [29] C. Isanbor, D. O'Hagan, *J. Fluor. Chem.* **2006**, *127*, 303–319.
- [30] D. Cartwright, in *Organofluor. Chem.*, **1994**, pp. 237–262.
- [31] L. Pelham, *J. Fluor. Chem.* **1985**, *30*, 1–17.
- [32] E. Lück, G. von R. Lipinski, *Ullmann's Encycl. Ind. Chem.* **2012**, *10*, 671–692.
- [33] G. Balz, G. Schiemann, *Berichte der Dtsch. Chem. Gesellschaft A B Ser.* **1927**, *60*, 1186–1190.
- [34] J. H. Simons, *J. Electrochem. Soc.* **1949**, 47–52.
- [35] G. C. Finger, C. W. Kruse, *J. Am. Chem. Soc.*, **1956**, *78*, 6034–6037.
- [36] G. Milazzo, *J. Electrochem. Soc.* **1978**, *125*, 261C.
- [37] C. Seeger, G. Rotzoll, A. Lübbert, K. Schügerl, *Int. J. Chem. Kinet.* **1981**, *13*, 39–58.
- [38] R. Benner, A. Benning, F. Downing, C. Irwin, K. Johnson, A. Linch, H. Parmelee, W. Wirth, *Ind. Eng. Chem.*, **1947**, *39*, 329.
- [39] R. Fowler, W. Buford III, J. Hamilton, Jr., R. Sweet, C. Weber, J. Kasper, I. Litant, *Ind. Eng. Chem.* **1947**, *39*, 292–298.
- [40] A. Harsanyi, G. Sandford, *Green Chem.* **2015**, *17*, 2081–2086.
- [41] R. E. Banks, S. N. Mohialdin-Khaffaf, G. S. Lal, I. Sharif, R. G. Syvret, *J. Chem. Soc. Chem. Commun.* **1992**, 595–596.
- [42] P. Tang, W. Wang, T. Ritter, *J. Am. Chem. Soc.*, **2011**, *133*, 11482–11484.
- [43] C. N. Neumann, T. Ritter, *Angew. Chem. Int. Ed.*, **2015**, *54*, 3216–3221.
- [44] G. K. S. Prakash, A. K. Yudin, *Chem. Rev.*, **1997**, *97*, 757–786.
- [45] R. E. Banks, *J. Fluor. Chem.* **1998**, *87*, 1–17.
- [46] <https://www.chemistry.manchester.ac.uk/research/impact/safer-cheaper-fluorination/> (accessed 9th June 2019)
- [47] J. Zhou, C. Jin, W. Su, *Org. Process Res. Dev.* **2014**, *18*, 928–933.
- [48] D. L. S. Brahms, W. P. Dailey, *Chem. Rev.*, **1996**, *96*, 1585–1632.
- [49] G. K. S. Prakash, M. Mandal, *J. Fluor. Chem.* **2001**, *112*, 123–131.
- [50] D. O'Hagan, Y. Wang, M. Skibinski, A. M. Z. Slawin, *Pure Appl. Chem.* **2012**, *84*, 1587–1595.
- [51] K. G. Andrews, R. Faizova, R. M. Denton, *Nat. Commun.* **2017**, *8*, 15913.
- [52] H. Sakaguchi, Y. Uetake, M. Ohashi, T. Niwa, S. Ogoshi, T. Hosoya, *J. Am. Chem. Soc.*, **2017**, *139*, 12855–12862.
- [53] E. Villiers, S. Couve-Bonnaire, D. Cahard, X. Pannecoucke, *Tetrahedron* **2015**, *71*, 7054–7062.
- [54] N. A. Meanwell, *J. Med. Chem.* **2018**, *61*, 5822–5880.
- [55] J. Zhang, C. Wang, *Nat. Clim. Chang.* **2014**, *4*, 943–945.

- [56] G. J. M. Velders, A. R. Ravishankara, M. K. Miller, M. J. Molina, J. Alcamo, J. S. Daniel, D. W. Fahey, S. A. Montzka, S. Reimann, *Science*, **2012**, 335, 922–923.

## Chapter 2 – $sp^3C-F$ Activation of Fluorocarbons

Results from this chapter have been published by Wiley in Chemistry – A European Journal.

G. Coates, B. J. Ward, C. Bakewell, A. J. P. White, M. R. Crimmin, *Chem. Eur. J.* **2018**, 54, 16282-16286.

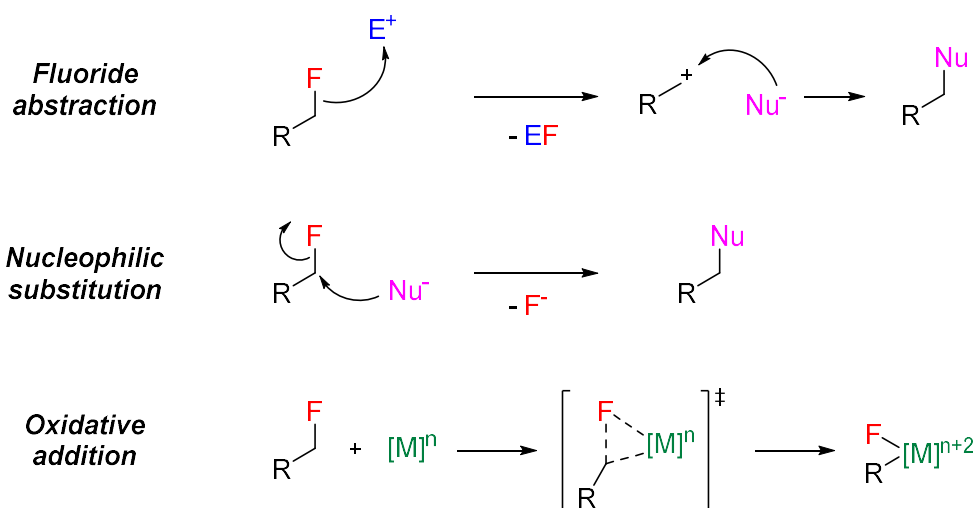
### 2.1 Introduction

The activation and functionalisation of  $sp^3C-F$  bonds of fluoroalkanes represents an important but largely unsolved challenge. The reactivity of aliphatic  $C-X$  bonds (where  $X = Cl, Br, I$ ) has been studied in great detail over the last half century and exploited for many synthetically useful transformations such as  $C-C$  and  $C$ -element bond forming reactions.<sup>[1-3]</sup> Unfortunately, this methodology cannot typically be applied in the same manner to  $sp^3C-F$  bonds.

Whilst there are abundant examples of oxidative addition processes for fluoroarenes,<sup>[4-6]</sup> the addition of  $sp^3C-F$  bonds to transition metals is problematic. The high  $sp^3C-F$  bond dissociation energy (BDE for  $CH_3F = 115 \pm 4.0 \text{ kcal mol}^{-1}$ )<sup>[7]</sup> along with the lack of charge stabilisation in the transition state for bond breaking means that defined oxidative addition reactions are incredibly scarce. When considering reaction processes at transition metals, the resulting metal-alkyl bonds can be unstable with respect to  $\beta$ -hydride elimination, a process which is abetted by the availability of metal  $d$  orbitals and agostic interactions.<sup>[8,9]</sup>

Due to these challenges, the field of  $sp^3C-F$  activation is still in its infancy. Over recent years however, progress has been accelerating and we will explore in this chapter the various techniques that have been implemented to overcome the inherent difficulties presented by aliphatic  $C-F$  bonds. The use of transition metal complexes, highly electrophilic or nucleophilic reagents will be examined, activating  $sp^3C-F$  bonds *via* processes such as fluoride abstraction, nucleophilic substitution, electron transfer and oxidative addition.

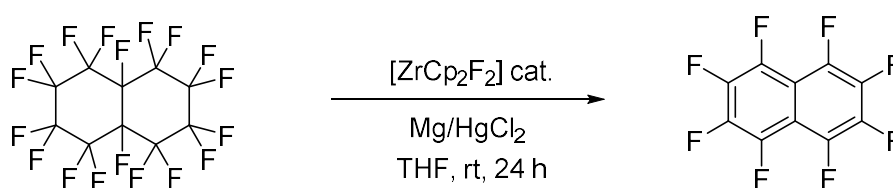




Scheme 2.1 Three simplified techniques to break  $sp^3C-F$  bonds

### 2.1.1 Transition–Metal Catalysed Defluoroaromatisation

In 1996, Kiplinger reported the synthesis of fluoroaromatics *via* a selective defluorination and aromatisation process of perfluorodecalin and related compounds.<sup>[10]</sup> They exploited group IV metallocenes ( $M = Ti, Zn$ ) to facilitate electron transfer from reductants such as magnesium or aluminium metal to the perfluorocarbon substrate. A catalytic turnover number (TON) of  $>100$  was achieved, representing the number of fluorides removed per metal centre. A low-valent metal centre (“ $ZrCp_2$ ”) (where Cp = cyclopentadiene) was postulated as the active species in the defluorination process. Independently synthesised  $[ZrCp_2]$  and  $[TiCp_2]$  were shown to similarly transform perfluorodecalin to perfluoronaphthalene, thus supporting their hypothesis.



Scheme 2.2 Defluorination and aromatisation of perfluorodecalin mediated by a zirconocene catalyst

The authors attempted the defluoroaromatisation of perfluorocyclohexane under their reaction conditions hoping to form hexafluorobenzene. However, the formation of 1,2,4,5-tetrafluorobenzene was observed. Deuterium was incorporated into the substrate when repeating the reaction in  $THF-d_8$ . This result represented an early example of hydrodefluorination (HDF), but whether it took place directly from the  $sp^3C-F$  bond or from the  $sp^2C-F$  bond of hexafluorobenzene was unclear. It is likely to occur from  $C_6F_6$  based upon established literature however.<sup>[11]</sup>

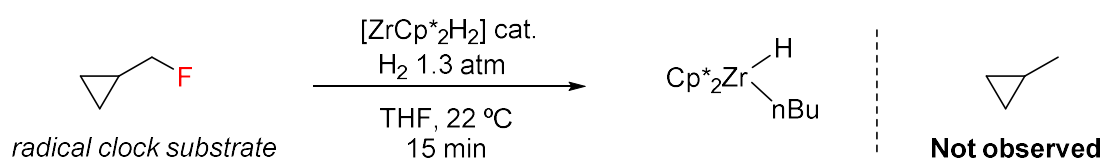
### 2.1.2 Transition–Metal Catalysed Hydrodefluorination

Many of the early examples of  $sp^3C-F$  activation were limited to HDF processes. A zirconocene system similar to Kiplinger's was employed by Jones *et al.* to perform the hydrodefluorination of aliphatic fluorides.<sup>[12–14]</sup> Under an atmosphere of  $H_2$ , a stoichiometric quantity of  $[ZrCp^*_2H_2]$  (where  $Cp^*$  = pentamethylcyclopentadiene) would quantitatively convert 1-fluorohexane to n-hexane within two days. Secondary and tertiary fluorides would also react, though more forcing conditions of  $>100\text{ }^\circ\text{C}$  for multiple days were required (competition reactions show decreasing rate for  $1^\circ > 2^\circ > 3^\circ$  fluorocarbons). Some CFCs, fluoroalkenes and fluoroaromatics also participated in the defluorination process.

Initially, a  $\sigma$ -bond metathesis pathway was speculated as radical trap experiments did not alter the results significantly. However upon further studies, a radical pathway was in fact concluded to be operative.<sup>[13]</sup>

Upon using an alternative batch of zirconium reagent, the speed of reaction was found to be different. This gave the authors their first evidence for a radical process, suggesting that a small impurity in the batch could have been acting as an initiator.

Repeating the hydrodefluorination reactions of aliphatic compounds in the presence of radical inhibitors, compounds with weak homolytic C–H bonds such as 9,10-dihydroanthracene, led to large reductions in activity.  $^1H$  NMR spectroscopic studies upon  $[ZrCp^*_2H_2]$  in the presence of radical initiators such as  $TiCl_3$  or  $Na/naphthalene$  showed severe broadening of the spectrum which indicated the presence of paramagnetic  $Zr^{III}$  species being generated *in situ*. These initiators also sped up the reaction by an order of three. Further evidence was provided when the hydrodefluorination reaction was performed on cyclopropylcarbonyl fluoride – a radical clock substrate.<sup>[15]</sup> If a radical process was operating, a radical would be formed on the exocyclic carbon. This intermediate will undergo a facile ring-opening process to relieve the ring strain to yield a but-2-ene radical. Upon conducting this experiment, a zirconium–butyl species was observed with no evidence for methyl cyclopropane, which provided evidence for the radical pathway.

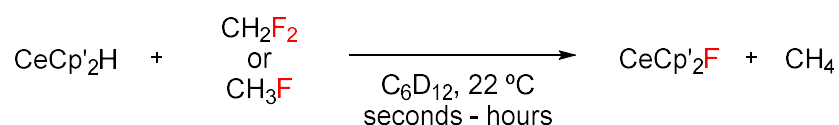


Scheme 2.3 Evidence for a radical hydrodefluorination process mediated by a Zr catalyst

A slight anomaly was detected when the HDF of 1-fluoronaphthalene was performed. The addition of 9,10-dihydroanthracene showed no reaction inhibition, whilst the addition of  $Na/naphthalene$  did

not increase the reaction rate. These results seem to suggest that a radical pathway was not proceeding for this substrate.

Andersen *et al.* reported the hydrodefluorination of fluoromethane (CH<sub>3</sub>F, CH<sub>2</sub>F<sub>2</sub> and CHF<sub>3</sub>) substrates using a cerium hydride species [CeCp'<sub>2</sub>H] (where Cp' = η<sup>5</sup>-1,2,4-(Me<sub>3</sub>C)<sub>3</sub>C<sub>5</sub>H<sub>2</sub>).<sup>[16]</sup> The hydrodefluorination reactions decreased in speed upon higher fluorine incorporation (CH<sub>3</sub>F, CH<sub>2</sub>F<sub>2</sub> and CHF<sub>3</sub>, seconds, hours and weeks respectively), consistent with the increasing C–F bond strengths. CF<sub>4</sub> did not participate in the H/F exchange reaction even after prolonged periods of time.



Scheme 2.4 Hydrodefluorination of difluoro- and fluoromethane using a cerium hydride complex

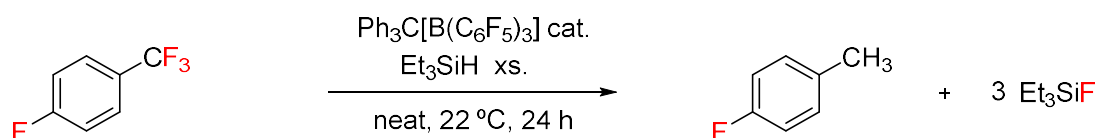
Based upon <sup>1</sup>H NMR spectrum data, it was speculated that reaction with trifluoromethane was not occurring through the same hydrodefluorination pathway as for difluoro- or fluoromethane. The observation of dihydrogen in the reaction mixture indicated that deprotonation of trifluoromethane was occurring, which would form [CeCp'<sub>2</sub>CF<sub>3</sub>]. This could be expected due to the weakened C–H bond in trifluoromethane.

However, after undertaking computational calculations on their system it was believed that C–H bond activation was occurring as the first step with all substrates. The determining factor to reactivity was generation of a carbene from [CeCp'<sub>2</sub>CH<sub>3-x</sub>F<sub>x</sub>] and subsequent trapping by H<sub>2</sub>. The rates of carbene recombination with H<sub>2</sub> were of the order CH<sub>2</sub>>CHF>>CF<sub>2</sub>. Therefore, H<sub>2</sub> acts as the carbene trap in the case of reaction with CF<sub>2</sub>H<sub>2</sub> and CH<sub>3</sub>F because the reaction occurs within the coordination sphere. This reaction pathway contrasts the radical process observed with zirconocene complexes.

### 2.1.3 Hydrodefluorination using Lewis Acids

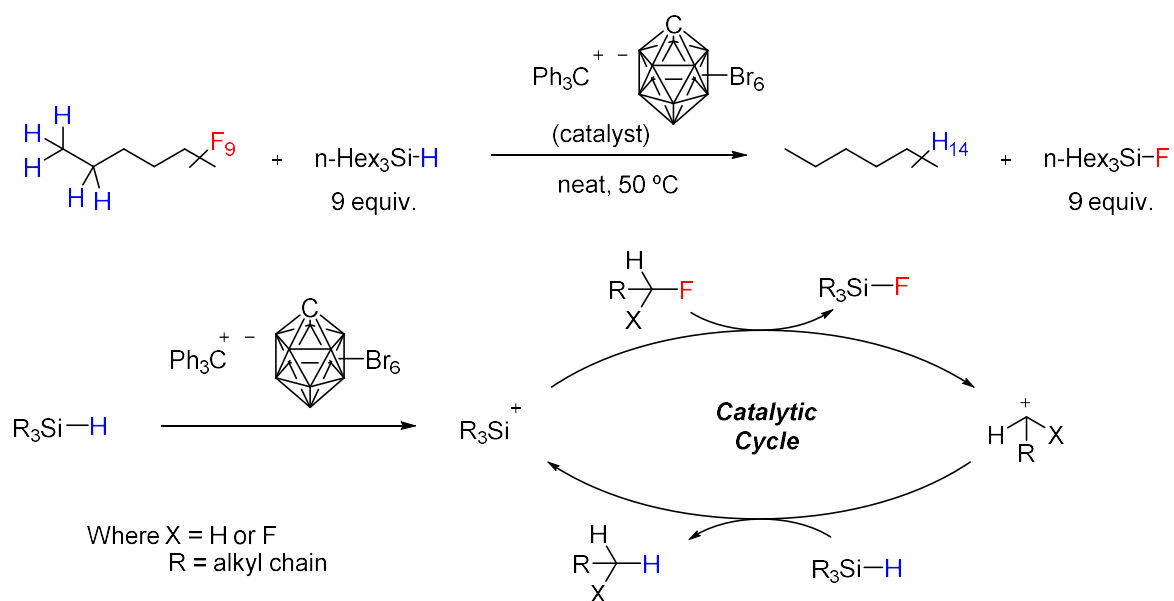
Since the start of the 21<sup>st</sup> century, highly reactive cationic and Lewis acidic species have proven to be particularly efficient in the field of aliphatic hydrodefluorination.<sup>[17–20]</sup> Ozerov was a pioneer in this discipline and proposed that a strong Lewis acid with high F<sup>-</sup> affinity, such as a silylium ion (R<sub>3</sub>Si<sup>+</sup>), should be an ideal reagent.<sup>[21]</sup> A masked source of Si<sup>+</sup> could be used directly as the catalyst in the form of Et<sub>3</sub>Si[B(C<sub>6</sub>F<sub>5</sub>)<sub>4</sub>], exploiting the weakly coordinating boron anion. They were also able to generate the same species *in situ* upon the addition of a trityl salt, Ph<sub>3</sub>C[B(C<sub>6</sub>F<sub>5</sub>)<sub>4</sub>] to a sample of Et<sub>3</sub>SiH. This reaction generates Et<sub>3</sub>Si[B(C<sub>6</sub>F<sub>5</sub>)<sub>4</sub>] and Ph<sub>3</sub>CH. Turnover is achieved after the first fluoride abstraction, when the substrate cation abstracts a proton from the excess Et<sub>3</sub>SiH, regenerating the active catalyst Et<sub>3</sub>Si[B(C<sub>6</sub>F<sub>5</sub>)<sub>4</sub>].

A range of trifluoromethyl arenes were shown to effectively partake in the HDF process, as well as aliphatic primary C–F containing substrates. Perfluorinated substrates such as perfluoromethylcyclohexane were left intact under this system. This system also shows orthogonal selectivity compared to many transition metal mediated HDF reactions, whereby  $sp^3C-F$  bonds react preferentially. Under these reaction conditions, aryl  $sp^2C-X$  (where  $X = F, Cl, Br$ ) bonds remain intact. This is likely a result of the extremely unstable nature of aryl cations.



Scheme 2.5  $sp^3$  hydrodefluorination of 1-fluoro-4-trifluoromethylbenzene using *in situ* generated silylium ions.

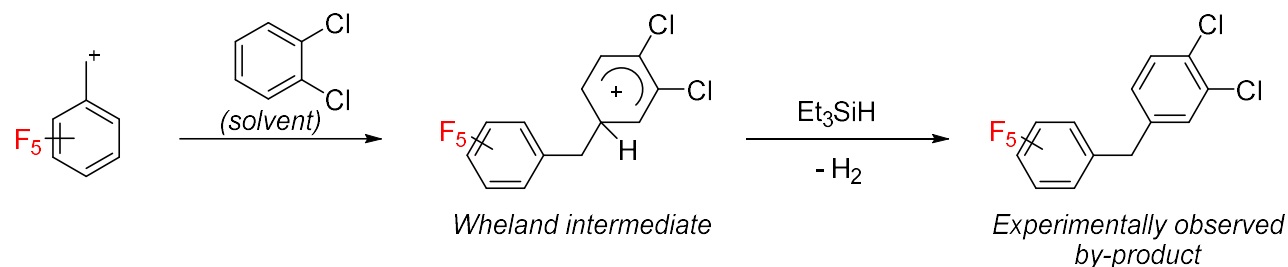
Ozerov later showed that complete hydrodefluorination of perfluoroalkyl chains could be achieved upon exposure to cationic silylium species.<sup>[17]</sup> These were generated *in situ* by a trityl carborane catalyst and stoichiometric quantity of silane (n-Hex<sub>3</sub>SiH). The trityl cation initially abstracts the hydride from n-Hex<sub>3</sub>SiH to form a highly reactive silylium species. This will then proceed to abstract a fluoride from the substrate and generate another reactive species, a carbocation of the substrate. The process then perpetuates until all C–F bonds have been cleaved or all silane is consumed (Scheme 2.6).



Scheme 2.6 Hydrodefluorination of perfluoroalkyl chains using highly reactive silylium species

In these two examples by Ozerov, highly polar haloarene solvents were shown to be necessary, with 1,2-dichlorobenzene proving optimum. Unfortunately, in the carborane catalysed example, there was a significant side reaction that consumed the fluoroarene by an undesired Friedel-Crafts alkylation

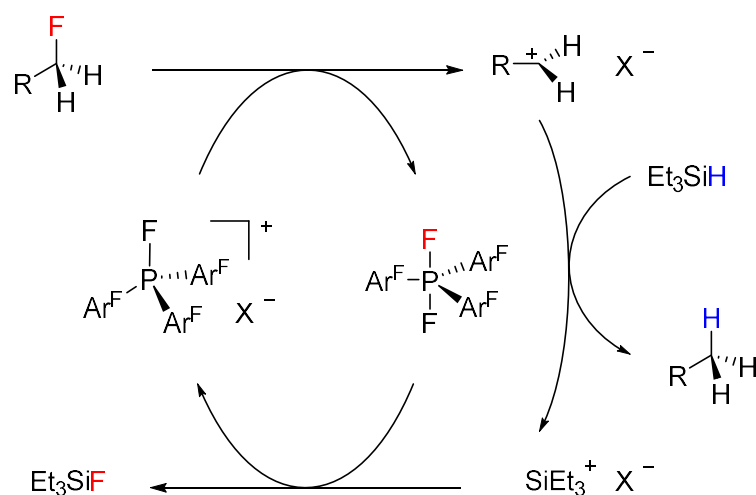
process. This would have been a disadvantage to this process had the reaction not been possible in neat fluoroarene substrate.



*Scheme 2.7 Proposed mechanism of formation of the Friedel-Crafts products upon reaction with solvent*

This method was extended a year later to include a process to completely defluoromethylate trifluoromethyl groups using  $\text{AlMe}_3$ , in place of  $\text{Et}_3\text{SiH}$ , by generating alumenium ( $\text{Me}_2\text{Al}^+$ ) cations.<sup>[22]</sup> Whilst this offers a new mode of reactivity, the synthetic utility of these two methods is limited with the resulting products rendered significantly inert to further synthesis.

Phosphonium salts were shown to act in a similar fashion to silylium ions and could be used to efficiently hydrodefluorinate a range of fluoroarenes and fluorocarbons.<sup>[23]</sup> Phosphorus(III) compounds have been exploited extensively as Lewis base ligands in transition metal based chemistry. This study investigated a previously unexplored field of highly Lewis acidic phosphonium salts. Upon addition of  $\text{XeF}_2$  to  $(\text{C}_6\text{F}_5)_3\text{P}$  the quantitative formation of P(V) compound  $(\text{C}_6\text{F}_5)_3\text{PF}_2$  was achieved. Fluorine abstraction from this species was not possible upon addition of  $\text{B}(\text{C}_6\text{F}_5)_3$  or  $\text{Me}_3\text{SiOTf}$  (where  $\text{Tf} = \text{SO}_2\text{CF}_3$ ). This predicts that the expected phosphonium cation  $(\text{C}_6\text{F}_5)_3\text{PF}^+$  should be a stronger Lewis acid than both  $\text{Me}_3\text{Si}^+$  and  $\text{B}(\text{C}_6\text{F}_5)_3$ . F<sup>-</sup> abstraction from  $(\text{C}_6\text{F}_5)_3\text{PF}_2$  could be achieved using  $\text{Al}(\text{C}_6\text{F}_5)_3$  or  $[\text{Et}_3\text{Si}][\text{B}(\text{C}_6\text{F}_5)_4]$  to generate the corresponding phosphonium salt. This species was able to abstract fluorine from trityl fluoride ( $\text{Ph}_3\text{CF}$ ), yielding  $\text{Ph}_3\text{C}[\text{B}(\text{C}_6\text{F}_5)_4]$  plus the P(V) difluoride starting material. This reactivity was extended to aliphatic and trifluoromethyl substrates with the resulting cations forming unidentified products with  $\text{B}(\text{C}_6\text{F}_5)_4^-$ . In the presence of  $\text{Et}_3\text{SiH}$  however, a catalytic HDF system was established.



Where  $X^- = B(C_6F_5)_4^-$ ,  $Ar^F = C_6F_5$

Scheme 2.8 Catalytic cycle for hydrodefluorination of fluoroalkanes using Lewis acidic phosphonium salts in the presence of  $Et_3SiH$

Mechanistic experiments and DFT calculations support the notion that the phosphonium species was the active catalyst and not just an initiator to generate  $Et_3Si^+$ , which in itself could then perform catalytic HDF as shown previously by Ozerov and others.<sup>[17,21]</sup> The silylium ion was shown to abstract  $F^-$  from  $(C_6F_5)_3PF_2$  preferentially over the fluorocarbon, whilst  $(C_6F_5)_3PF^+$  would not abstract  $H^-$  from triethyl silane.

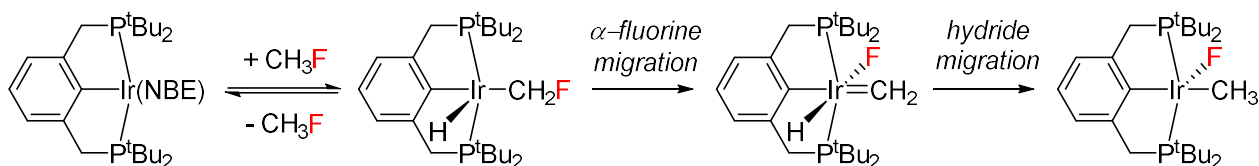
Gabbai and co-workers reported a related system.<sup>[24]</sup> In their example, a stibonium cation  $Ar_4Sb^+$  (where  $Ar = C_6F_5$ ) was shown to hydrodefluorinate 1-fluorooctane and  $\alpha,\alpha,\alpha$ -trifluorotoluene. It was shown to be a particularly potent Lewis acid. Fluoride abstraction from salts of  $[B(C_6F_5)_3F]^-$  and  $[SbF_6]^-$  was observed upon addition of  $[Sb(C_6F_5)_4][B(C_6F_5)_4]$ . This suggests the Lewis acidity of the stibonium cation is higher than that of both  $B(C_6F_5)_3$  and  $SbF_5$ .

In 2011, Stephan reported an elegant technique to hydrodefluorinate alkyl fluorides using a frustrated Lewis pair (FLP).<sup>[18]</sup> The system utilised commercially available reagents, a highly Lewis acidic boron species  $B(C_6F_5)_3$  (BCF) and simple phosphine  $tBu_3P$  and was effective on primary, secondary and tertiary  $sp^3C-F$  bonds under mild conditions, whilst  $CF_3$  groups were left intact. Again, whilst it is advantageous to evolve current state-of-the-art methodology, these techniques offer little value from a synthetic point of view.

#### 2.1.4 Oxidative Addition at a Transition–Metal

Although there are inherent difficulties when considering transition metal mediated  $sp^3C-F$  activation processes, it is not completely without precedent. For example, when no  $\beta$ -hydrogens are present the

formation of transition metal alkyl species becomes simpler. One such example was reported in 2011. Fluoromethane ( $\text{CH}_3\text{F}$ ) was shown to undergo a formal oxidative addition to an iridium complex, *via* an initial C–H activation process.<sup>[25]</sup> Addition of fluoromethane to a pincer ligated iridium complex,  $[\text{Ir}(\text{PCP})]$  (where  $\text{PCP} = \kappa^3\text{-C}_6\text{H}_3\text{-2,6,-}[\text{CH}_2\text{P}(t\text{-Bu})_2]_2$ ) resulted in quantitative conversion to a single product. After extensive analysis of the multinuclear NMR spectra, a 5-coordinate iridium methyl fluoride product  $[\text{Ir}(\text{PCP})(\text{CH}_3)\text{F}]$  was elucidated. DFT calculations were performed to explore the reaction mechanism. The direct oxidative addition of the C–F of fluoromethane to  $[\text{Ir}(\text{PCP})]$  was calculated to proceed by a high energy transition state ( $\Delta G^\ddagger_{298\text{K}} = + 37.5 \text{ kcal mol}^{-1}$ ). Ultimately, a more complex model was proposed which begins with an oxidative addition of a C–H bond of fluoromethane to  $[\text{Ir}(\text{PCP})]$  to form  $[\text{Ir}(\text{PCP})(\text{CH}_2\text{F})\text{H}]$ . The  $\alpha$ -fluorine then migrates from carbon to iridium to form an iridium methylidene as the rate limiting step ( $\Delta G^\ddagger_{298\text{K}} = + 22.9 \text{ kcal mol}^{-1}$ ), followed by hydride migration from iridium to the  $\text{CH}_2$  unit, generating the experimentally observed product.



Where NBE = norbornene

*Scheme 2.9 C–F activation of fluoromethane by an iridium pincer complex, proceeding through initial C–H activation*

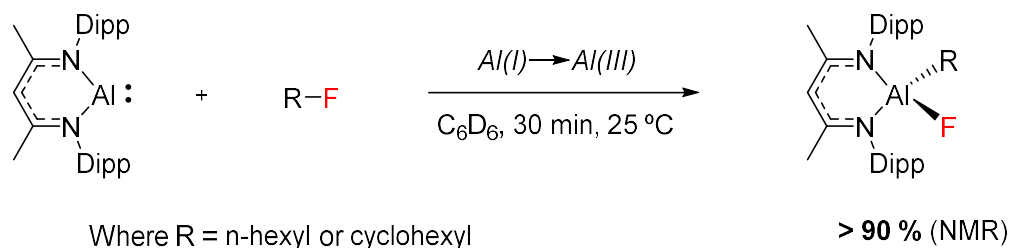
Larger fluoroalkanes that possess  $\beta$ -hydrogens such as fluoroethane also react with  $[\text{Ir}(\text{PCP})]$ , however they result in the formation of  $[\text{Ir}(\text{PCP})(\text{F})(\text{H})]$  as a result of  $\beta$ -hydride decomposition. An iridium ethene complex was also characterised, which was consistent with this degradation pathway.

### 2.1.5 Oxidative Addition to Main Group Reagents

Methods to functionalise  $\text{sp}^3\text{C–F}$  bonds in fluoroalkanes are limited, yet the frequency of such reports are increasing. Specialist main group reagents, such as those that are low-valent<sup>[26–28]</sup> or nucleophilic<sup>[29]</sup> are showing success in this area. Low-valent main group reagents have been shown to mimic the chemistry of transition metals, particularly with respect to the invaluable oxidative addition step.<sup>[30]</sup> Counter to transition metals the resulting metal–alkyl species exhibit higher stabilities to decomposition pathways, such as facile  $\beta$ -fluoride elimination. The use of main group metals on the whole is preferable to transition metals as they tend to be more abundant, cheaper and less toxic.

Low oxidation state aluminium(I) and magnesium(I) species, reported by Roesky and Jones respectively, have shown widespread application in small molecule activation processes and as specialist reducing agents.<sup>[31,32]</sup>

In 2015 our group reported that primary and secondary C–F bonds of fluoroalkanes could undergo oxidative addition to a low valent aluminium(I) reagent, this was shortly followed by a similar report by Nikonov *et al.*<sup>[26,33,34]</sup> 1-Fluorohexane and cyclohexane were shown to react with the  $\beta$ -diketiminato Al(I) species within 30 minutes under ambient conditions achieving high yields (>90 % upon interpretation of the multinuclear NMR spectra), to generate new Al(III) alkyl/fluoride compounds. This work represented an example of fluorocarbon upgrading, producing a more reactive building block *via* C–F activation.



*Scheme 2.10*  $sp^3C-F$  activation of primary and secondary fluorocarbons using a low valent aluminium species

Unfortunately, no further reactivity has been demonstrated with these reagents and they are highly susceptible to degradation upon contact with moisture or air.

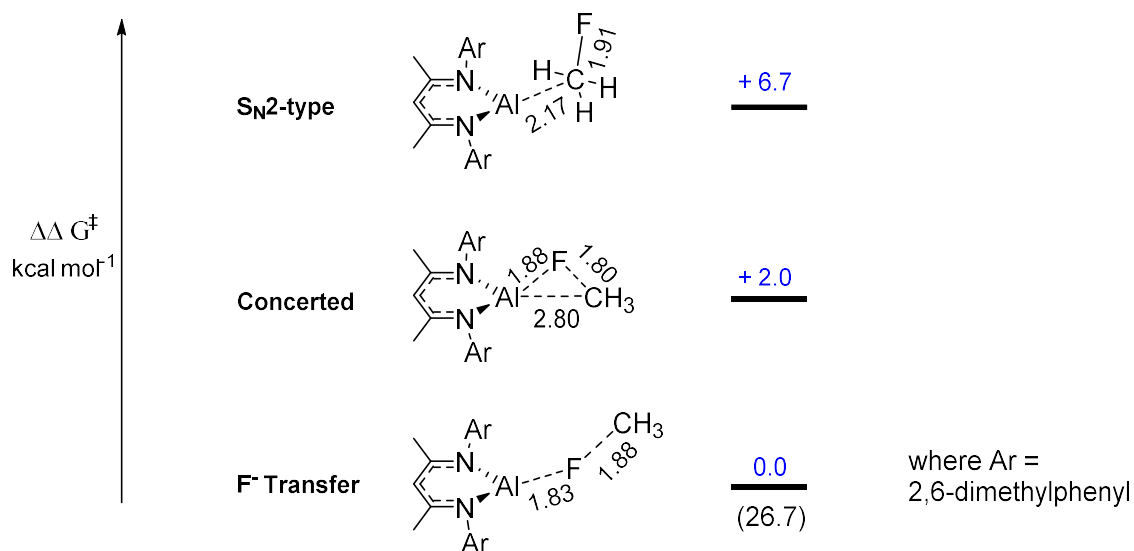
The mechanisms of both  $sp^2$  and  $sp^3$  C–F activation were probed computationally in later publications by the groups of Hwang and Wang.<sup>[35,36]</sup> The group of Huang used the B3LYP functional without considering solvation effects whilst Wang *et al.* opted for the B3LYP-D3 functional, including the SMD solvation model.

A concerted mechanism was shown to be favoured for fluoroarenes in both cases much resembling a  $S_NAr$  (nucleophilic aromatic substitution) process. Upon investigation of fluorocarbon substrates however, differing conclusions were drawn. Hwang studied the C–F activation of fluoromethane, 1-fluoropentane and fluorocyclohexane with three Al(I) species (differing in  $\beta$ -diketiminato ligands). Transition states for the concerted oxidative addition to  $sp^3C-F$  bonds were located, though alternative pathways were not considered. Values fell in the range of 25 to 35 kcal mol<sup>-1</sup>, increasing in energy from fluoromethane to fluorocyclohexane and upon increasing steric bulk on the aryl groups of the  $\beta$ -diketiminato ligand. The subsequent publication by Wang considered other methods for  $sp^3C-F$  activation, such as  $S_N2$  type reactivity, or a step-wise F<sup>-</sup> abstraction process.

The model investigated the reaction of fluoromethane with a simplified aluminium complex, incorporating 2,3-dimethylphenyl groups rather than 2,6-di-iso-propylphenyl which were used experimentally. Surprisingly, the lowest barrier to activation was located for the fluoride abstraction and cation recombination process ( $\Delta G^\ddagger_{298K} = 26.7$  kcal mol<sup>-1</sup>). The concerted oxidative addition



pathway was slightly higher ( $\Delta\Delta G^\ddagger_{298K} = +2.0 \text{ kcal mol}^{-1}$ ), whilst the highest energy process was located for the  $S_N2$ -type reactivity ( $\Delta\Delta G^\ddagger_{298K} = +6.7 \text{ kcal mol}^{-1}$ ).



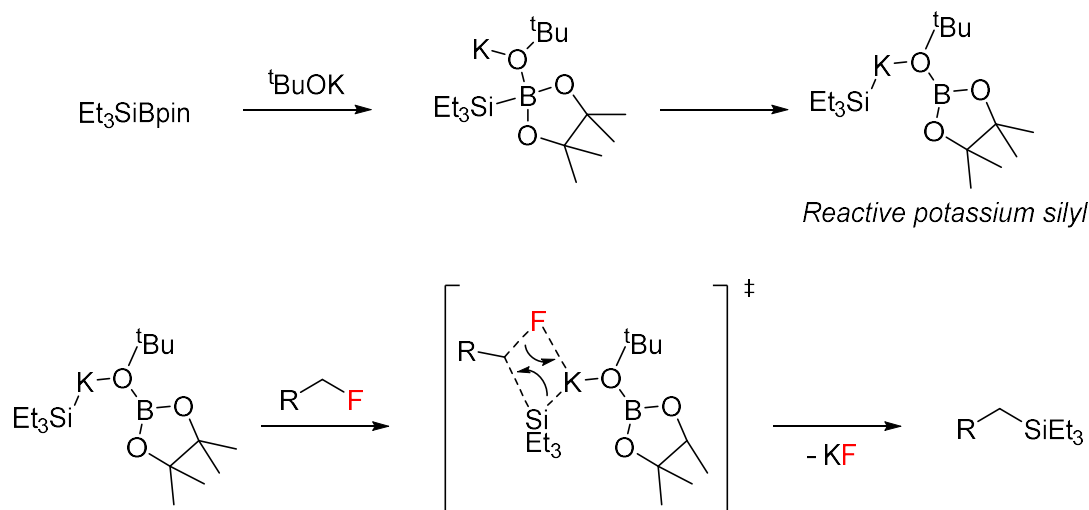
Scheme 2.11 Three plausible mechanisms for C–F activation of fluoromethane by Al(I) species as calculated by DFT. B3LYP-D3/6-31G(d,p) with single point solvation effects, SMD benzene.<sup>[36]</sup>

No such fluoride transfer mechanism had been shown before by experiment or computation and represented an interesting alternative. However, this loses credence due to simplifying the model substrate to fluoromethane and using a much less sterically hindered ligand, which could affect the overall relative values. The first publication by Hwang is more thorough in this context as they consider the experimentally tested reagents, however they use a lower level of computational theory by not including solvent and dispersion considerations.

### 2.1.6 Nucleophilic Substitution Reactions of Fluoroalkanes

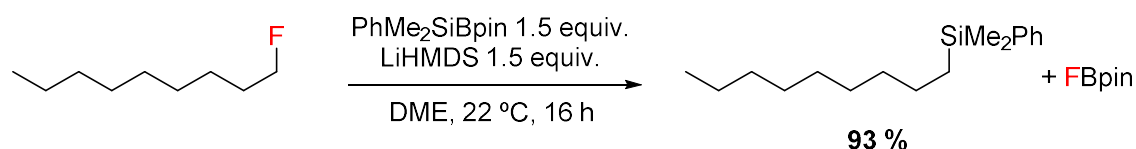
Sources of nucleophilic silicon have recently prevailed as simple reagents for C–F silylation transformations of fluoroarenes and fluoroalkanes.<sup>[37–39]</sup>

As part of a study on nickel catalysed defluorosilylation of fluoroarenes, Shibata and co-workers found a simple process for  $sp^3C-F$  silylation. Their method required only a simple silyl boronate ester ( $Et_3SiBpin$ ) and potassium *tert*-butoxide. They discovered that the nickel catalyst used in the activation of fluoroarenes was not required.<sup>[39]</sup> A reactive potassium silyl species, generated *in situ*, provided a source of nucleophilic silicon with the potassium acting as a fluoride acceptor.



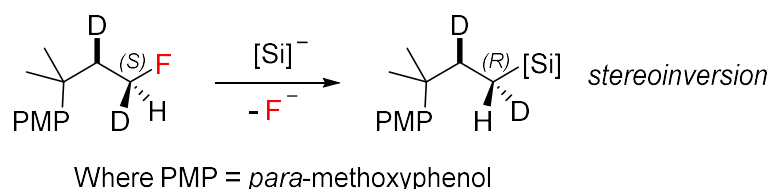
Scheme 2.12 Defluorosilylation of  $sp^3C-F$  bonds using nucleophilic silicon

In related studies, Martin showed that a lithium base was also an effective promoter for C-F silylation.<sup>[37]</sup> Combining  $Et_3SiBpin$  (or  $PhMe_2SiBpin$ ) with LiHMDS, a wide range of fluoroarenes and primary fluoroalkanes could be defluorosilylated under mild conditions. This reaction was found to be highly solvent dependant however. After an initial solvent screen, dimethoxyethane (DME) was shown to be the only one that allowed for the reaction to occur with good yields. Furthermore, the use of lithium as the counter ion was also found to be important. When substituting for heavier group 1 metals, such as Na and K, the yields were significantly dampened.



Scheme 2.13 Defluorosilylation of 1-fluorononane exploiting an *in situ* generated lithium silyl species

Martin *et al.* described an elegant method for determining the  $S_N2$  inversion process occurring at the  $sp^3C-F$  bond. They synthesised primary fluorocarbons that had one  $\alpha$  and one  $\beta$  deuterium atom. Upon reaction with a silicon nucleophile, they determined that inversion of the stereocentre had occurred after analysis of the  $^1H$  NMR spectra.



Scheme 2.14 Literature method to determine  $S_N2$  inversion at primary fluorocarbons<sup>[37]</sup>

Overall, these methods represent rare examples of  $S_N2$  reactivity at fluoroalkanes. The high  $sp^3C-F$  bond strength typically resists this mode of reactivity. Furthermore, the reactions are conceptually simple, cost effective and avoid toxic transition metals.

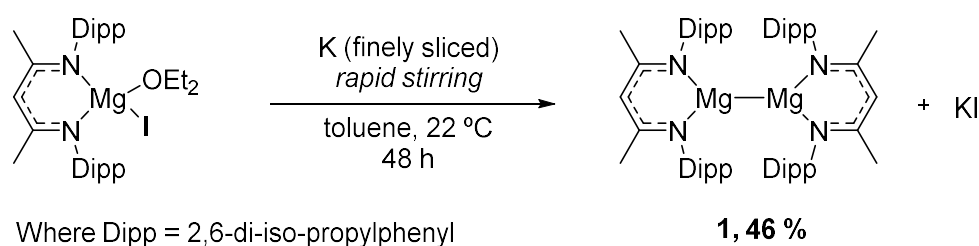
## 2.2 C–F Activation of Fluoroalkanes

### 2.2.1 Synthesis of Magnesium(I) Complexes

The Crimmin group reported the C–F activation of fluoroarenes to a low oxidation state magnesium(I) compound in 2016.<sup>[40]</sup> This methodology was considered analogous to the formation of Grignard reagents occurring in homogeneous solutions. We were interested whether this technique could be extended to the  $sp^3C-F$  bonds of fluorocarbons. Although alkyl halides (when halide = Cl, Br, I) react with magnesium metal to form Grignard reagents, fluorocarbons are typically considered inert towards this process (barring a few early accounts that require suitable initiators or Rieke magnesium).<sup>[41–43]</sup>

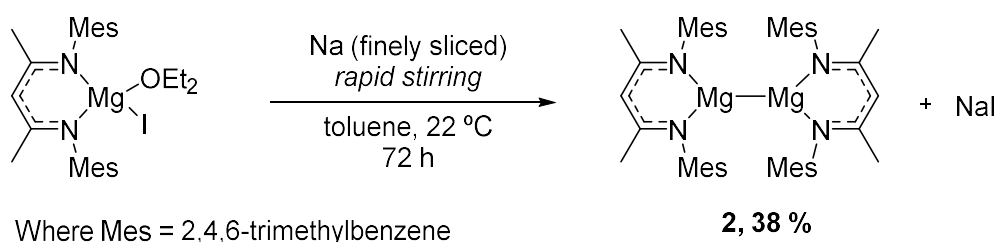
The activation of simple fluoroalkanes represented an important step towards understanding and tackling the C–F activation of environmentally damaging fluorocarbons that are used in the refrigeration industry, such as 1,1,1,2-tetrafluoroethane (R-134a), which represented one of the key aims of this PhD project.

The synthesis of the magnesium(I) compounds supported by  $\beta$ -diketiminato ligands (BDI) were first reported by Jones and co-workers in 2007 and have been used extensively for small molecule activations and as specialist reductants.<sup>[27,31,44]</sup> The analogue with 2,6-di-isopropylphenyl (Dipp) groups could be synthesised from the parent  $[^{Dipp}(BDI)MgI.OEt_2]$  complex upon reduction by potassium metal. The authors report the use of a potassium mirror, however it was found that simplification of this procedure could be achieved using finely sliced potassium metal, with comparable results.



Scheme 2.15 Synthesis of  $[^{Dipp}(BDI)Mg]_2$ , compound **1**

A similar compound featuring less bulky 2,4,6-trimethylphenyl (Mesityl, Mes) groups could be synthesised upon reduction by sodium metal from the parent magnesium iodide.



Scheme 2.16 Synthesis of  $[\text{Mes}(\text{BDI})\text{Mg}]_2$ , compound **2**

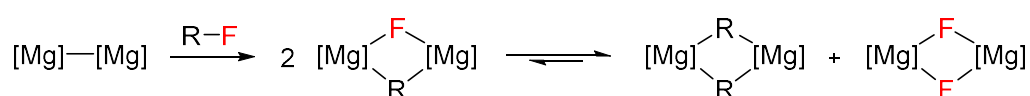
Compounds **1** and **2** could be isolated as yellow crystalline solids with high purity (in some schemes their structure will be simplified to  $[\text{Mg}]$ – $[\text{Mg}]$  with their corresponding compound number **1** or **2**).

### 2.2.2 Initial Experiments with 1-Fluorohexane

With prior understanding of the possibilities and limitations of  $\text{sp}^2\text{C}$ –F bond activation of fluoroarenes with **1** we set out to investigate the reactivity towards fluorocarbons.<sup>[40]</sup> 1-Fluorohexane was selected as a model substrate for the initial experiments due to commercial availability and the presence of only one C–F bond.

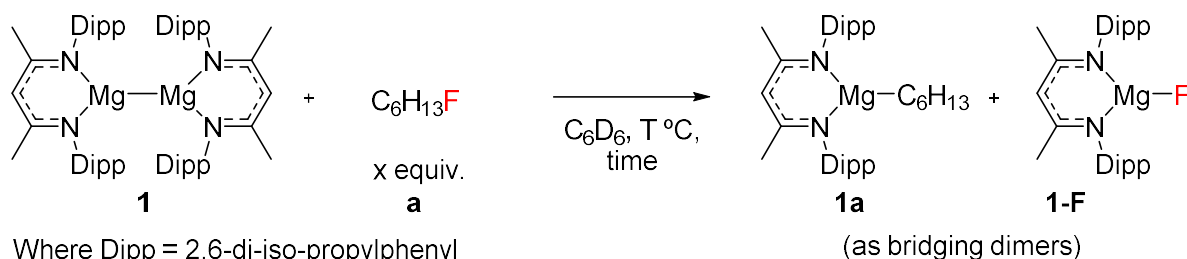
A tenfold excess of 1-fluorohexane was added to 0.02 M benzene- $\text{d}_6$  solution of **1** at 22 °C and the reaction progression was monitored by  $^1\text{H}$  and  $^{19}\text{F}$  NMR spectroscopy. To our satisfaction C–F activation was observed, confirmed by the formation of  $[\text{Dipp}(\text{BDI})\text{Mg}(\mu\text{-F})]_2$  (**1-F**) indicated by the singlet resonance at  $\delta = -187$  ppm in the  $^{19}\text{F}$  NMR spectrum. Consumption of **1** was occurring alongside the formation of three new singlet methine resonances in the  $^1\text{H}$  NMR spectrum between  $\delta = 4.80$  and 4.95 ppm, indicating three new  $\beta$ -diketiminate ligated species.

The formation of an intermediate species was determined by the decrease in intensity of one methine resonance at  $\delta = 4.82$  in the  $^1\text{H}$  NMR spectrum, whilst the other two resonances  $\delta = 4.85$  and  $\delta = 4.95$  were still increasing relative to the internal standard. The intermediate structure was hypothesised to be an unsymmetrical species,  $[\text{Dipp}(\text{BDI})\text{Mg}_2(\mu\text{-F})(\mu\text{-C}_6\text{H}_{13})]$ , the direct result of the bond breaking process before undergoing equilibration to the two homodimers,  $[\text{Dipp}(\text{BDI})\text{Mg}(\mu\text{-F})]_2$  **1-F** and  $[\text{Dipp}(\text{BDI})\text{Mg}(\mu\text{-C}_6\text{H}_{13})]_2$  **1a**. The formation of **1a** could easily be identified upon the formation of an up-field triplet resonance in the  $^1\text{H}$  NMR spectrum ( $\delta = -0.23$  ppm,  $^3J_{\text{HH}} = 7.9$  Hz). (It is known that three coordinate magnesium compounds can exist in a monomer/dimer equilibrium. For the purpose of this work, they will be displayed as the monomer species in the reaction schemes.)



Scheme 2.17 Simplified model for the formation of homodimer products from unsymmetrical magnesium  $(\mu\text{-F})(\mu\text{-R})$  species

The formation of an intermediate species was further supported after analysis of the products upon full consumption of **1**. The two final products were quantified in an unequal ratio (22 % : 166 %, **1a** : **1-F**), based upon analysis of the <sup>1</sup>H NMR spectroscopy compared to the internal standard (ferrocene, δ = 4.00 ppm) (**Entry 1, Table 2.1**). Yields are calculated in millimoles (mmol) from **1** allowing, theoretically, a maximum yield of 200 % of the combined products.

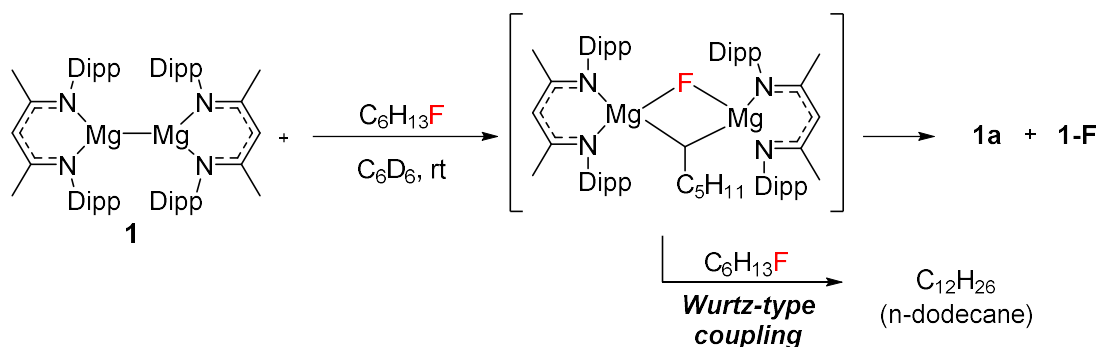


| Entry          | Fluorocarbon<br>equivalents | Temperature<br>(°C) | Time<br>(h) | 1a yield<br>% | 1-F yield<br>%   | Ratio<br>(1a : 1-F) |
|----------------|-----------------------------|---------------------|-------------|---------------|------------------|---------------------|
| 1              | 10                          | 22                  | 4.5         | 22            | 166 <sup>a</sup> | 1.0 : 7.5           |
| 2 <sup>b</sup> | 1                           | 22                  | 24          | 26            | 100              | 1.0 : 3.8           |
| 3              | 1                           | 80                  | 0.75        | 74            | 94               | 1.0 : 1.3           |
| 4              | 2                           | 80                  | 1           | 88            | 94               | 1.0 : 1.1           |

Table 2.1 Initial C–F activation screening of 1-fluorohexane <sup>a</sup>based on mmol from **1**, results from further reactivity with 1-fluorohexane <sup>b</sup>Reaction not to completion

The reaction was repeated using stoichiometric 1-fluorohexane. The reaction was significantly slower with full consumption of **1** not achieved after 24 hours. Analysis of the <sup>1</sup>H NMR spectrum revealed a similar scenario to the previous reaction, whereby there was an unequal product distribution (26 % : 100 %, **1a** : **1-F**) though less pronounced (**Entry 2, Table 2.1**).

A Wurtz-type side reaction was postulated. Due to the similarity to Grignard reagents, the postulated intermediate could react with excess 1-fluorohexane to produce n-dodecane *via* a second C–F cleavage reaction. This would account for production of **1-F** in greater than 100 % conversion (**Scheme 2.18**). n-Dodecane could also be generated directly from **1** through a radical pathway, though no experimental evidence supports the presence of radical species.



Scheme 2.18 Proposed intermediate and cause of unequal product ratios observed experimentally

The formation of n-dodecane was confirmed upon analysis of the reaction mixture by gas-chromatography (GC), comparing the retention times to a commercial sample of n-dodecane.

The stoichiometric reaction of 1-fluorohexane was investigated at an elevated temperature (80 °C) and the reaction monitored by  $^1\text{H}$  and  $^{19}\text{F}$  NMR spectroscopy. Full consumption of **1** was achieved within 1 hour. Analysis of the  $^1\text{H}$  NMR spectrum at regular time intervals (~15 min) revealed only trace quantities of the intermediate species. The product ratio from this reaction was much closer and represented the best result to date (74 % : 94 % , **1a** : **1-F**) (**Entry 3, Table 2.1**). Further optimisation of the reaction conditions (2 equivalents, 80 °C, 1 hour) achieved a high yield for **1a** (88 %) (**Entry 4, Table 2.1**).

To identify the reactive magnesium species in the Wurtz-type coupling 1-fluorohexane was added to a benzene- $d_6$  solution of **1a** and **1-F** and the concentration of **1a** was monitored by  $^1\text{H}$  NMR spectroscopy over time at 22 °C. No significant decrease was observed, indicating that the intermediate complex is likely the source of undesired reactivity towards 1-fluorohexane. Suppression of the side reaction was achieved by elevating the temperature, due to this intermediate's shorter life-span under these conditions.

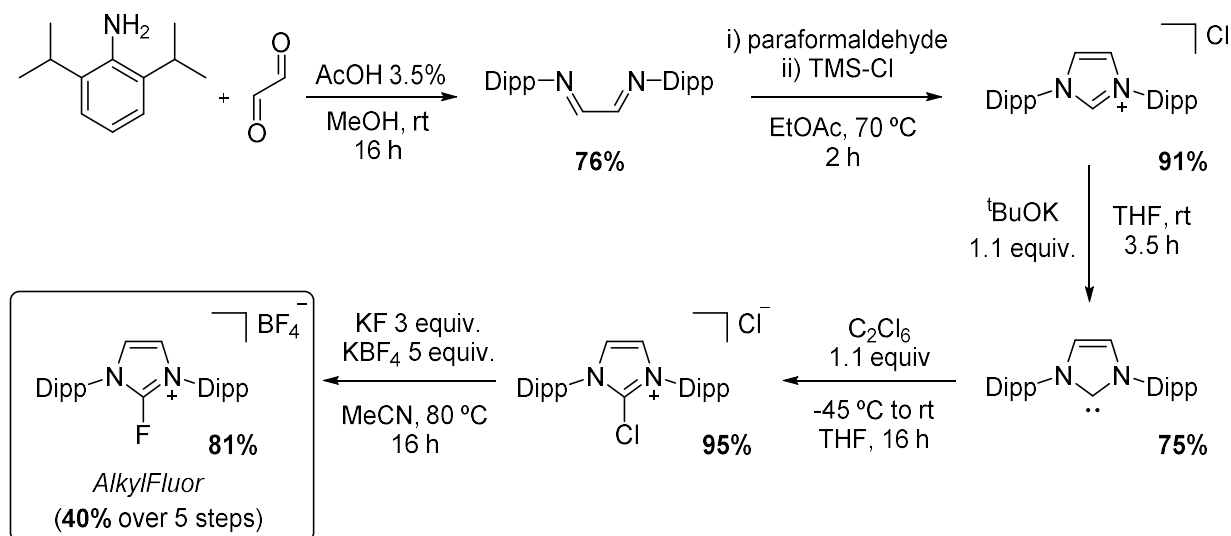
### 2.2.3 Scope in Fluorocarbon with Mg–Mg Bonds

We aimed to demonstrate a wide scope in fluorocarbon, encompassing primary, secondary and tertiary  $\text{sp}^3\text{C-F}$  bonds as well as cyclic, linear and branched species. Unfortunately, there was a distinct lack of commercially available mono- fluorocarbons with only 1-fluorohexane, fluorocyclohexane and 1-fluoroadamantane being immediately available.

#### 2.2.3.1 Synthesis of New Fluorocarbons

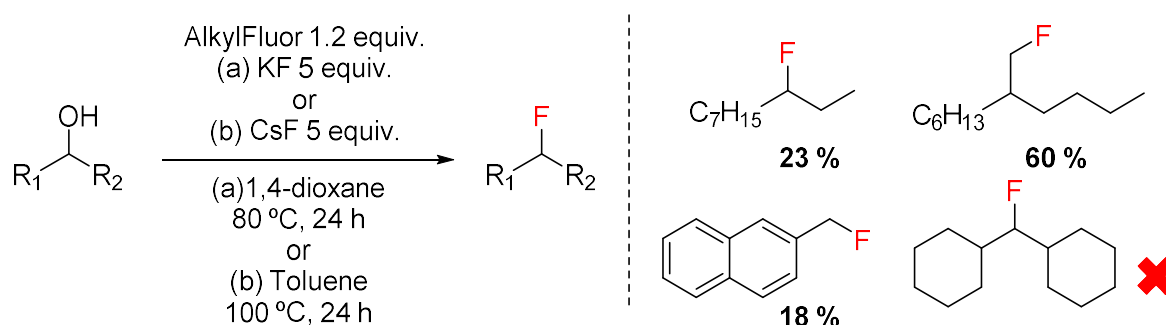
The synthesis of a variety of fluorocarbons was undertaken. A deoxyfluorination process reported by Ritter *et al.* represented a convenient method to access aliphatic fluorocarbons from alcohols.<sup>[45]</sup> The

method utilised a stoichiometric N-heterocyclic based nucleophilic fluorinating agent (AlkylFluor). This could be synthesised in 5 steps on large scales from the parent 2,6-di-iso-propylaniline and glyoxal ( $C_2O_2H_2$ ).



Scheme 2.19 Synthesis of deoxyfluorinating agent – AlkylFluor

AlkylFluor, in combination with KF or CsF, was heated (80 – 100 °C) with the alcohol substrates to generate the desired fluoroalkanes in modest yields. The synthesis of 2-butyl-1-fluorooctane, 3-fluorodecane and 2-fluoromethylnaphthalene was achieved. The fluorination of dicyclohexylmethanol could not be achieved under the reaction conditions.



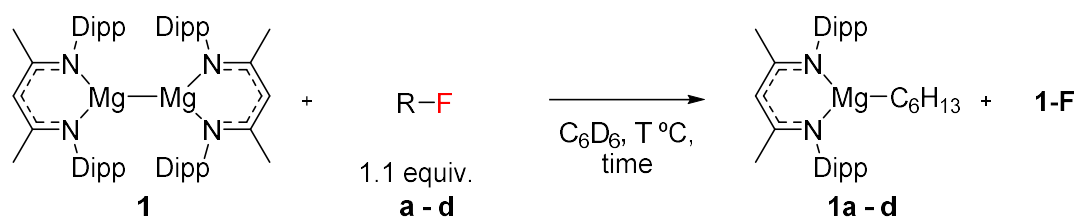
Scheme 2.20 General procedure for the deoxyfluorination of alcohols using AlkylFluor reagent

Unfortunately, 2-fluoromethylnaphthalene turned from a colourless oil to a yellow solid after a few days in the glovebox. Due to this compound's low solubility in organic media, it could not be identified by NMR spectroscopy however, benzyl fluorides are known to undergo self-polymerisation reactions.<sup>[46–48]</sup> The deoxyfluorination of secondary alcohol 3-fluorodecane was achieved in a low yield (23 %) due in part to the competitive formation of dec-2-ene and dec-3-ene through an elimination pathway. These species had to be removed upon work-up *via* a hydroboration (with  $BH_3 \cdot THF$ ) and filtration process. 2-Butyl-1-fluorooctane could be isolated in a satisfactory yield (60 %).

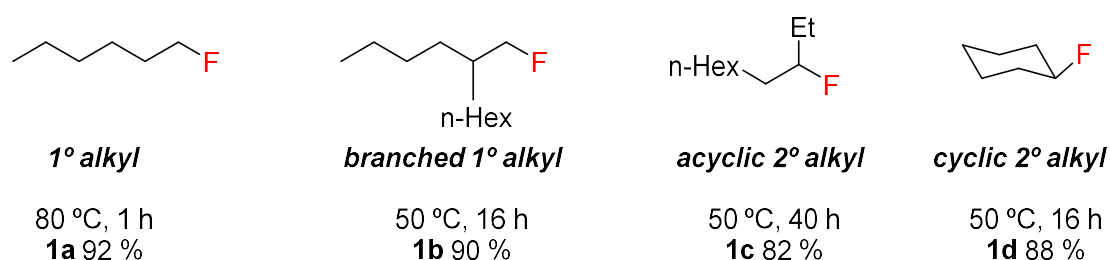


### 2.2.3.2 $sp^3C-F$ Activation Results

C–F activation of the new substrates was performed. Fluorocarbon (1.1 equivalents) was added to a benzene- $d_6$  solution of **1** and heated at 50 – 80 °C, while the reaction was monitored by  $^1H$  and  $^{19}F$  NMR spectroscopy. It was found that the best results for secondary fluoroalkanes were achieved when performed at 50 °C. The products **1c** and **1d** were prone to  $\beta$ -hydride elimination at higher temperatures which dampened the *in situ* yield. This decomposition was identified upon observation of a triplet resonance corresponding to cyclohexene in the  $^1H$  NMR spectrum ( $\delta = 5.70$  ppm). Cyclohexene could also be generated *via* an  $E1_{CB}$  or  $E2$  pathway directly from **1** and fluorocyclohexane and both pathways could be operating simultaneously. A benzene- $d_6$  solution of **1d** when heated at 80 °C will slowly produce cyclohexene.



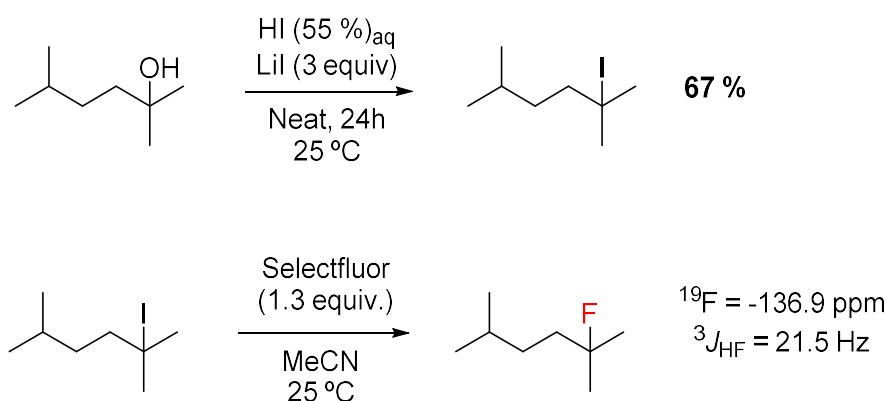
Where Dipp = 2,6-di-iso-propylphenyl



Scheme 2.21 Results of C–F activation of 1° and 2° fluorocarbons with **1**. Yields determined *in situ* against an internal standard (ferrocene,  $\delta = 4.00$  ppm)

1-Fluoroadamantane was subject to the reaction conditions with **1**, however no significant reaction was observed after extended periods of time (there were trace quantities of **1-F** but no identifiable magnesium–alkyl species). We hypothesised that 1-fluoroadamantane may be too sterically demanding to efficiently access the reactive Mg–Mg bond of **1**.

Several attempts were made at synthesising a tertiary fluorocarbon with less steric bulk. This was targeted through an alternative method to that previously described.<sup>[49]</sup> 2,5-Dimethylhexan-2-ol was converted to the corresponding alkyl iodide upon reaction with hydroiodic acid (HI 55 %) and lithium iodide (LiI). The product could be isolated as a colourless oil, however it would degrade to form an orange oil after a few hours. 2-Iodo-2,5-dimethylhexane was determined to be a light sensitive compound. It could be stored in a freezer (-20 °C) in the dark for long periods of time however.

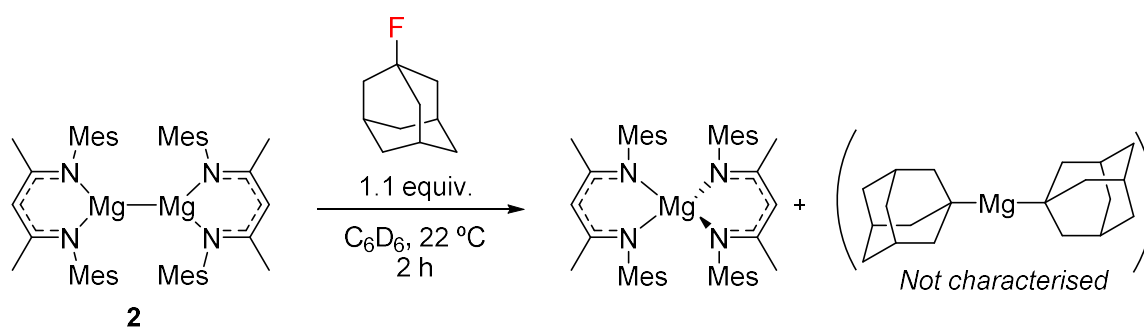


Scheme 2.22 Attempted synthesis of 2-fluoro-2,5-dimethylhexane

Attempts to convert 2-iodo-2,5-dimethylhexane into 2-fluoro-2,5-dimethylhexane upon reaction with Selectfluor in acetonitrile were partially successful. Analysis of the crude product by  $^1\text{H}$  and  $^{19}\text{F}$  NMR spectroscopy indicated the formation of a  $3^{\circ}\text{ sp}^3\text{C-F}$  bond ( $\delta = -136.9\text{ ppm}$ ,  $^3J_{\text{HF}} = 21.5\text{ Hz}$ ).<sup>[50]</sup> Upon purification through silica gel and further analysis by  $^1\text{H}$  and  $^{19}\text{F}$  NMR spectroscopy, the impurities were found to be amplified and a degradation process was suspected. Due to these difficulties, the synthesis of tertiary fluorocarbons was put on hold at this stage.

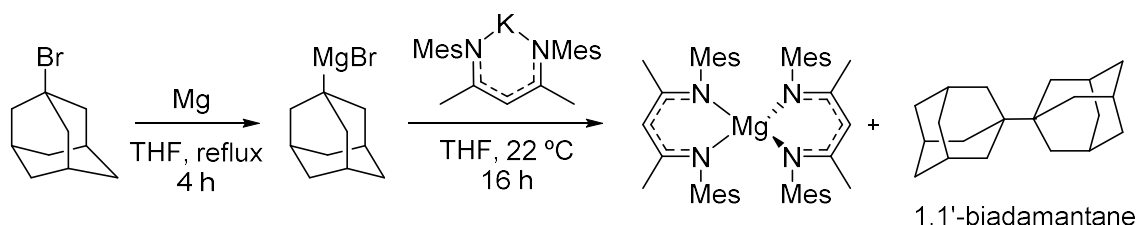
Turning attention back to 1-fluoroadamantane, it was speculated that the decreased steric environment around the Mg–Mg bond of **2** may allow for C–F activation to occur.

1-Fluoroadamantane was added to a 0.02 M benzene- $d_6$  solution of **2** and the reaction monitored by  $^1\text{H}$  and  $^{19}\text{F}$  NMR spectroscopy. After one hour, two new species were determined upon formation of two new singlet resonances in the  $^1\text{H}$  NMR spectrum ( $\delta = 4.88$  and  $4.95\text{ ppm}$ ) corresponding to the methine proton of the  $\beta$ -diketiminato ligand. Full consumption of **2** was achieved within 2 hours. The product [ $^{\text{mes}}(\text{BDI})\text{Mg}(1\text{-adam})$ ] (**2e**) was determined to be unstable with respect to Schlenk equilibria. The compound exhibiting the singlet resonance in the  $^1\text{H}$  NMR spectrum at  $\delta = 4.95\text{ ppm}$  was identified as [ $^{\text{mes}}(\text{BDI})_2\text{Mg}$ ] upon consultation with the literature.<sup>[51]</sup>



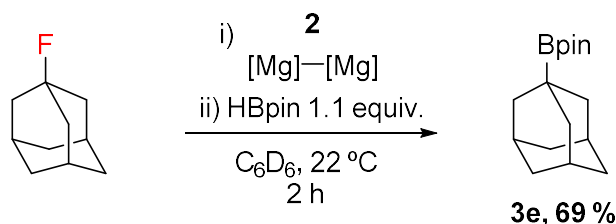
Scheme 2.23 Reaction of 1-fluoroadamantane with **2**, revealing a bis-ligated Mg species [ $^{\text{mes}}(\text{BDI})_2\text{Mg}$ ]

This suggested the magnesium–alkyl species existed as  $\text{Mg}(\text{1-adam})_2$ . This equilibrium was further confirmed upon attempted synthesis of **2e** by route of salt metathesis between  $[\text{mes}(\text{BDI})\text{K}]$  and 1-MgBr-adamantane, which yielded  $[\text{mes}(\text{BDI})_2\text{Mg}]$  and 1,1'-biadamantane. The C–C cross coupled product could conceivably be generated upon reaction of  $\text{Mg}(\text{1-adam})_2$  with residual 1-bromo-adamantane.



*Scheme 2.24 Attempted independent synthesis of **2e** by salt metathesis. Identification of undesired products  $[\text{mes}(\text{BDI})_2\text{Mg}]$  and 1,1'-biadamantane as determined by  $^1\text{H}$  NMR spectroscopy and single crystal X-ray diffraction respectively*

The alkyl moiety (1-adam) could be trapped upon addition of HBpin to yield 1-Bpin-adamantane 69 % yield over a two-step process. The target product was confirmed by singlet resonances at  $\delta = 1.05$  ppm and  $\delta = 33.9$  ppm in the in the  $^1\text{H}$  and  $^{11}\text{B}$  NMR spectra respectively, which were in accordance with the literature.<sup>[52]</sup>



*Scheme 2.25 C–F activation and borylation of 1-fluoroadamantane*

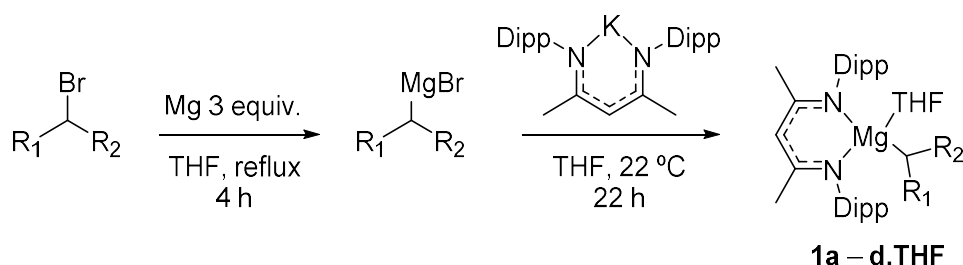
Overall, the activation of  $1^\circ$ ,  $2^\circ$  and  $3^\circ$   $\text{sp}^3\text{C–F}$  bonds using either reagents **1** or **2** could be achieved in high yields.

### 2.2.3.3 Unsuccessful Substrates for C–F Activation

The reaction of **1** with perfluorohexane and  $\alpha,\alpha,\alpha$ -trifluorotoluene was probed. Heating the solutions ( $80^\circ\text{C}$ ) for extended periods (weeks) resulted in negligible reactivity. The very slow formation of **1–F** was observed however, as evidenced by the singlet resonance in the  $^{19}\text{F}$  NMR spectrum ( $\delta = -187$  ppm). No magnesium–alkyl species were detected, with only **1** and **1–F** identified upon analysis of the methine region in the  $^1\text{H}$  NMR spectrum.

## 2.2.4 Synthesis of Pure Samples of Mg–Alkyl Species

The products of C–F activation (**1a – d**) were unambiguously confirmed and characterised upon the synthesis of pure compounds *via* an alternative pathway. A metathesis reaction between [<sup>Dipp</sup>(BDI)K] and the corresponding alkyl Grignard reagents in THF yielded compounds **1a – d.THF**.



Scheme 2.26 The synthesis of pure samples of compounds **1a – d.THF**

Addition of THF to *in situ* generated compounds **1a – d** also yielded **1a – 1d.THF**. The <sup>1</sup>H NMR spectra could be directly compared to the pure samples that were synthesised according to the metathesis reaction described above. The results were all in concordance of those expected.

## 2.2.5 Transfer of Alkyl Group from C–F Activated Products

In the context of our aim to upgrade fluorocarbons to reactive building blocks, we embarked on a series of alkyl transfer reactions from compounds **1a – d**. It was envisaged that the magnesium–alkyl species would participate in  $\sigma$ –bond metathesis reactions and addition to electrophiles, due to their similarity to Grignard reagents. We were particularly interested in the borylation of the alkyl moiety due to the extensive library of well understood organoboron chemistry, which could be exploited for further derivatisation.

### 2.2.5.1 Reaction with Boron Reagents

Five boron reagents were investigated, B<sub>2</sub>pin<sub>2</sub> (bis(pinacolato)diboron), B<sub>2</sub>nep<sub>2</sub> (bis(neopentyl glycolato)diboron), HBcat (catecholborane), HBpin (Pinacolborane) and 9-BBN (9-borabicyclo[3.3.1]nonane). The reaction between HBpin and magnesium alkyl complexes has been previously reported,<sup>[53]</sup> so we were confident the approach would be successful.

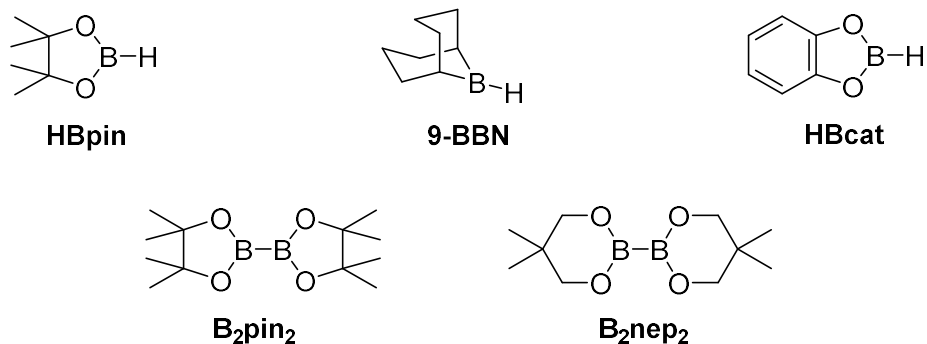
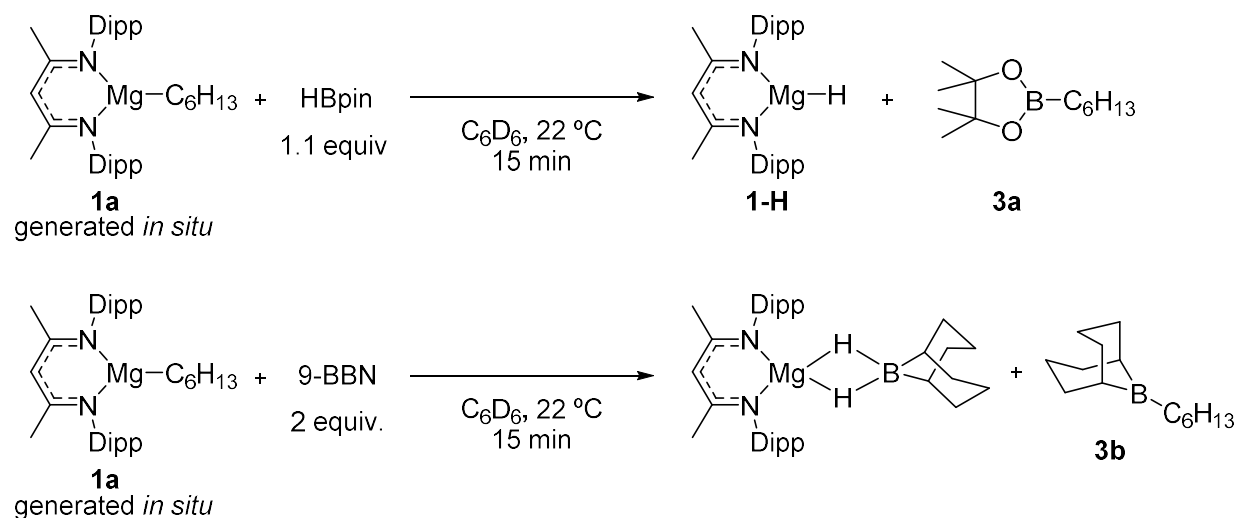


Figure 2.1 The five boron reagents investigated in alkyl transfer reactions with **1a**

Addition of HBpin and 9-BBN (1.1 equiv.) to separate samples of **1a** generated *in situ* from **1** and 1-fluorohexane led to the formation of  $[\text{Dipp}(\text{BDI})\text{Mg}(\mu\text{-H})_2]$  **1-H** as evidenced by a singlet resonance in the  $^1\text{H}$  NMR spectrum ( $\delta = 4.03$  ppm), plus the corresponding alkyl boron compound.<sup>[51,54]</sup> These reactions were clean, resulting in quantitative conversion from **1a** with minimal side reaction. The formation of n-hexylBpin (**3a**) was unambiguously confirmed upon  $^1\text{H}$  and  $^{11}\text{B}$ NMR spectra comparison to a commercial sample. The generation of n-hexyl 9-BBN derivative (**3b**) was determined upon  $^{11}\text{B}$  NMR analysis and comparison to the literature ( $\delta = 88.00$  ppm).<sup>[55]</sup> Addition of 2 equivalents 9-BBN to a benzene- $\text{d}_6$  solution of **1a** led also to the formation of an asymmetrical bridging magnesium hydride species, as characterised *in situ* by  $^1\text{H}$  and  $^{11}\text{B}$  NMR ( $\delta = -18.09$  ppm) and previously characterised by Hill and co-workers.<sup>[56]</sup>

Addition of two equivalents HBcat to a 0.038 M benzene- $\text{d}_6$  solution of **1a** led to the immediate formation of a precipitate. Inspection of the  $^1\text{H}$  NMR spectrum revealed the presence of a complex mixture of products. The loss of methine proton resonances was observed, alongside messy alkyl/aryl regions. This led us to believe significant side reactions were occurring, possibly at the nucleophilic backbone of the ligand or the aromatic moiety of the borane.

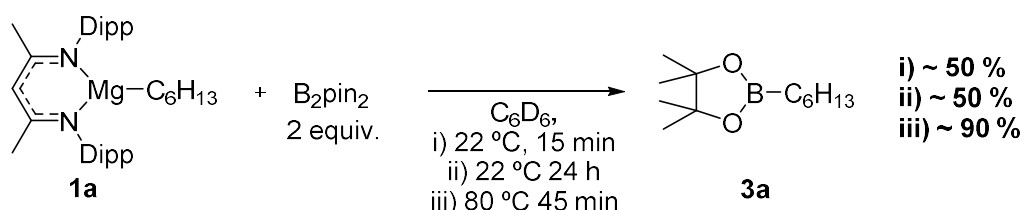


Scheme 2.27 Alkylation of hydridoboranes upon  $\sigma$ -bond metathesis with **1a**

These were promising results and represented one of the first examples of a one-pot procedure to convert  $sp^3C-F$  bonds to  $sp^3C-B$  bonds.

We next investigated the diboron reagents. If a simple  $\sigma$ -bond metathesis process is underway, there was potential for the formation of magnesium-boryl species which could feature atypical nucleophilic boron character (based upon the bond polarisation).

Two equivalents  $B_2pin_2$  were added to a 0.038 M benzene- $d_6$  solution of **1a** and the reaction monitored at regular time intervals by  $^1H$  and  $^{11}B$  NMR spectroscopy. Within 15 minutes **1a** had been fully consumed, identified by the complete loss of the triplet at  $\delta = -0.23$  ppm in the  $^1H$  NMR spectrum attributed to the  $Mg-CH_2-$  unit. However, only  $\sim 50\%$  n-hexylBpin (**3a**) had been generated as determined by integration of the singlet resonance at  $\delta = 1.07$  ppm in the  $^1H$  NMR spectrum, which corresponds to the methyl groups of n-hexylBpin. This was further confirmed by spiking the reaction with a commercial sample. The reaction solution was left at 22 °C for 24 hours with no further reaction occurring, based upon  $^1H$  NMR spectrum analysis.



Scheme 2.28 Reaction of **1a** and  $B_2pin_2$

The solution was heated to 80 °C and a  $^1H$  NMR spectrum recorded after 45 minutes. Gratifyingly, over 90% of the desired product (**3a**) was achieved, as determined by  $^1H$  NMR spectroscopy. This was a somewhat intriguing result that half of the product would be generated rapidly, yet the solution required heating to achieve the formation of greater than 50 %.

We postulated the formation of an intermediate complex. This was supported experimentally by the full consumption of **1a** within the first 15 minutes. To identify this intermediate, the reaction was repeated on a larger scale with no heating undertaken. After 30 minutes, the solvent was removed and the contents crystallised from n-hexane at -35 °C, affording material suitable for single crystal X-ray diffraction.

Two distinct molecules (**4** and **5**) had co-crystallised, providing insight into the reaction process (**Scheme 2.29**). It can be noted from the X-ray data that B-O bond lengths are non-equivalent.  $B^{90}-O^{91}$  is 0.068(4) Å longer than  $B^{90}-O^{94}$ , whilst  $B^{99}-O^{100}$  is 0.126(4) Å longer than  $B^{99}-O^{103}$ , possibly as a result

of oxygen coordination to magnesium. Furthermore, B–O bonds at the 4 coordinate boron are at least 0.1 Å longer than those at the 3 coordinate unit.

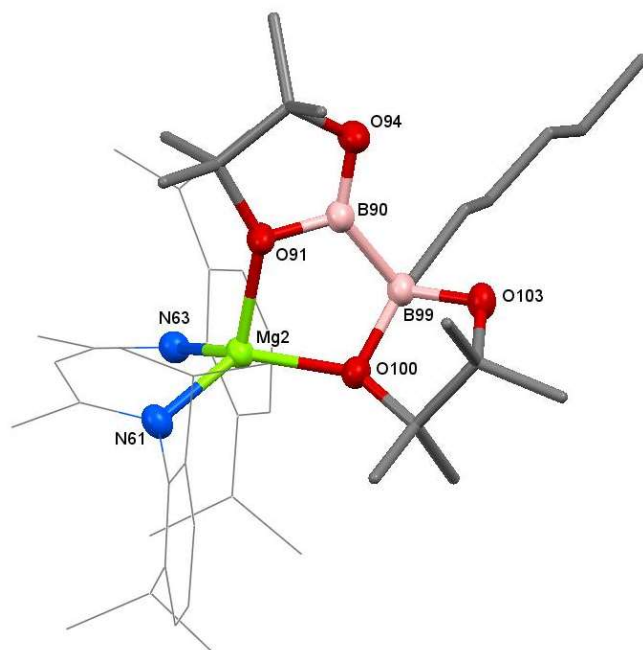


Figure 2.2 X-ray structure of compound **4**, formed upon reaction of **1a** and  $B_2pin_2$  and co-crystallised with **5** (50 % probability ellipsoids). Selected bond lengths (Å); Mg(2)-O(100) = 1.9434(12), Mg(2)-O(91) = 2.0651(12), B(90)-O(94) = 1.358(2), B(90)-O(91) = 1.426(2), B(90)-B(99) = 1.754(3), B(99)-O(103) = 1.474(2), B(99)-O(100) = 1.600(2), B(99)-C(108) = 1.609(3)

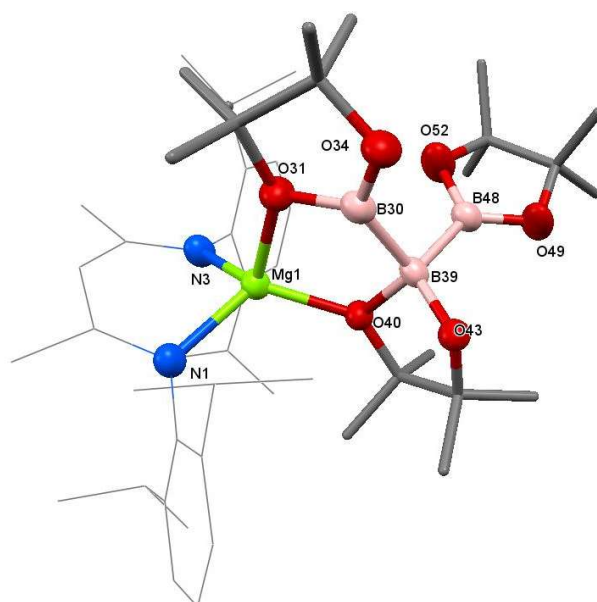
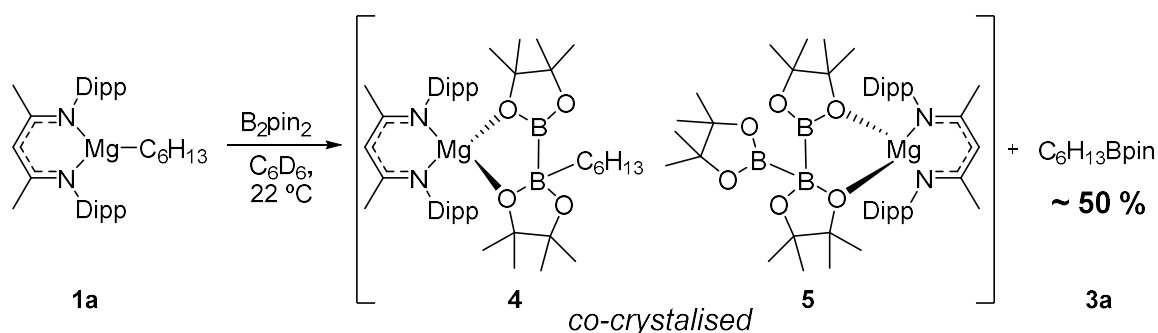
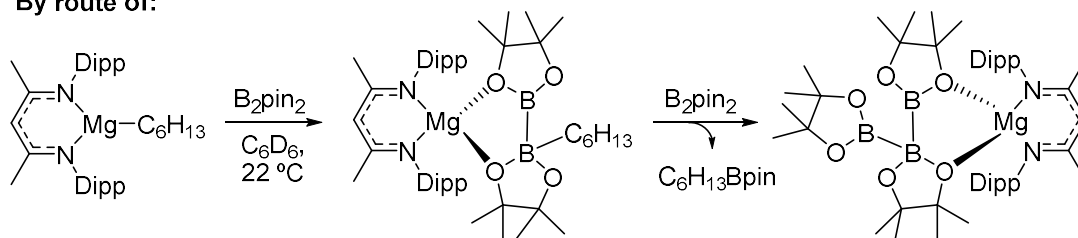


Figure 2.3 X-ray structure of compound **5**, formed upon reaction of **1a** and  $B_2pin_2$  and co-crystallised with **4** (50 % probability ellipsoids). Selected bond lengths (Å); Mg(1)-O(40) = 1.9329(13), Mg(1)-O(31) = 2.0857(13), B(30)-O(34) = 1.358(2), B(30)-O(31) = 1.423(2), B(30)-B(39) = 1.726(3), B(39)-O(43) = 1.458(2), B(39)-O(40) = 1.566(2), B(39)-B(48) = 1.747(3), B(48)-O(52) = 1.366(3), B(48)-O(49) = 1.376(3)



**By route of:**

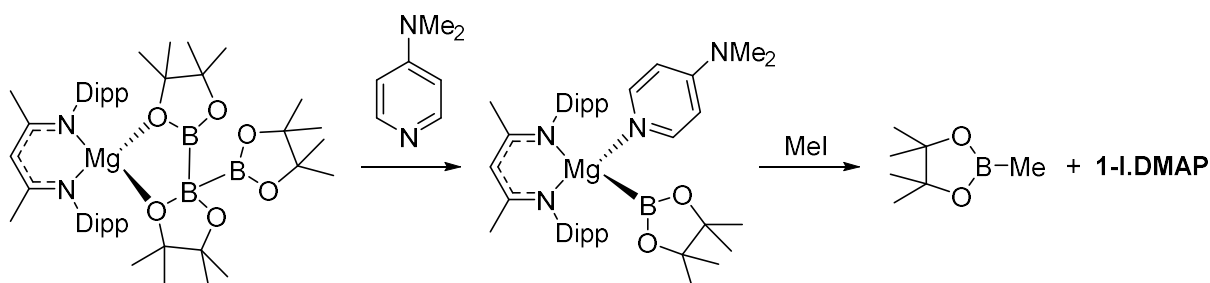


*Scheme 2.29 Reaction of 1a with B<sub>2</sub>pin<sub>2</sub> revealing the identity and source of intermediate complexes*

Compound **4** is the result of one equivalent B<sub>2</sub>pin<sub>2</sub> inserting into the Mg–C bond. The n-hexyl moiety is transferred to one boron atom, whilst the B<sub>2</sub>pin<sub>2</sub> structure is bound to magnesium through the oxygen atoms.

**5** exhibits a triboron unit. It is hypothesised that this is generated through a further insertion of B<sub>2</sub>pin<sub>2</sub> one n-hexylBpin molecule. This model does not however account for the observation of only 50 % of **3a**, as two equivalents of B<sub>2</sub>pin<sub>2</sub> should be sufficient to completely convert **4** to **5**.

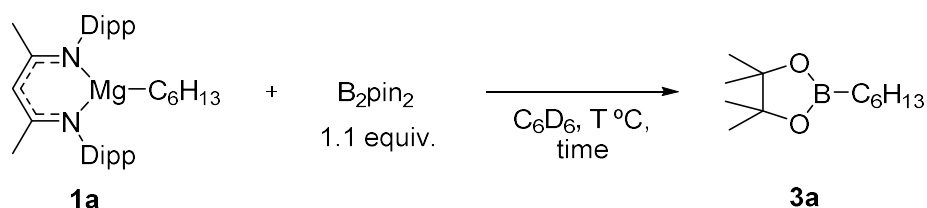
Similar reactivity was reported by the Hill group as part of the successful development of a nucleophilic boron reagent.<sup>[57]</sup> They found upon addition of *N,N*-dimethylpyridin-4-amine (DMAP) to compound **4** or **5**, a new Mg–B bond is formed of which boron is the more electronegative atom. This nucleophilic character was demonstrated upon addition of electrophiles such as methyl iodide (MeI). The boron moiety would attack the electropositive carbon to generate methylBpin plus the magnesium iodide derivative [<sup>Dipp</sup>(BDI)MgI.DMAP] (**1-I.DMAP**).



*Scheme 2.30 Formation of Mg–B bond upon addition of DMAP to 5 and demonstration of boron nucleophilicity<sup>[57]</sup>*



The borylation of **1a** with B<sub>2</sub>pin<sub>2</sub> was performed at a range of temperatures and the conversion to **3a** monitored by <sup>1</sup>H NMR spectrum analysis. It was found that the equivalents of B<sub>2</sub>pin<sub>2</sub> could be decreased to 1.1 and at a temperature of > 40 °C full conversion to **3a** could be achieved. (**Table 2.2**).



| Entry | B <sub>2</sub> pin <sub>2</sub><br>equivalents | Temperature<br>(°C) | Time<br>(h) | Boronate ester <b>3a</b><br>yield (%) <sup>a</sup> |
|-------|--|---------------------|-------------|--|
| 1     | 2  | 22                  | 0.25        | 50   |
| 2     | 1.1  | 22                  | 24          | 53   |
| 3     | 1.1  | 80                  | 1           | >90  |
| 4     | 1.1  | 50                  | 1           | >90  |
| 5     | 1.1  | 40                  | 1           | >90  |

Table 2.2 Results of the borylation reactions of **1a** with B<sub>2</sub>pin<sub>2</sub> at a range of temperatures <sup>a</sup>Yields determined in situ upon comparison to an internal standard (ferrocene, δ = 4.00 ppm)

A similar result was observed upon reaction of **1a** with B<sub>2</sub>nep<sub>2</sub>. Addition of 1.1 equivalents B<sub>2</sub>nep<sub>2</sub> to a benzene-d<sub>6</sub> solution of **1a** led to the complete consumption of **1a** in 15 minutes at 22 °C. The desired product n-hexylBnep (**3c**) was not observed and analysis of the <sup>1</sup>H NMR spectrum indicated the formation of a single species. This suggested a similar intermediate complex from the diboron insertion into the Mg–C bond had been formed.

The intermediate species was crystallised from *n*-hexane at -35 °C, providing material suitable for single crystal X-ray analysis. This elucidated complex **6**, analogous to that of complex **4** (**Scheme 2.31**).

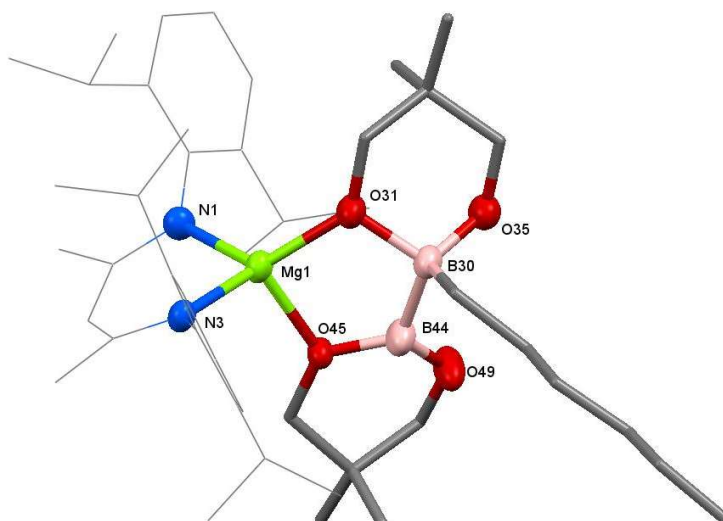
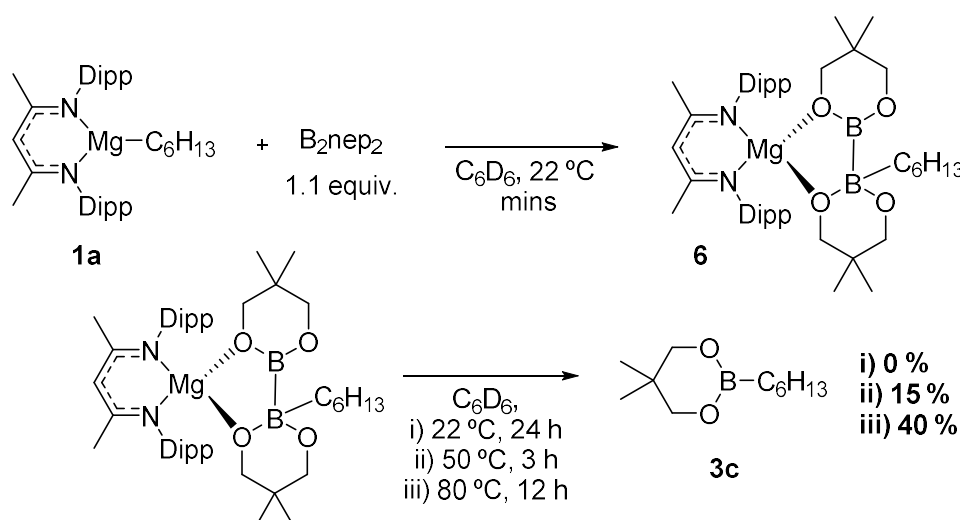


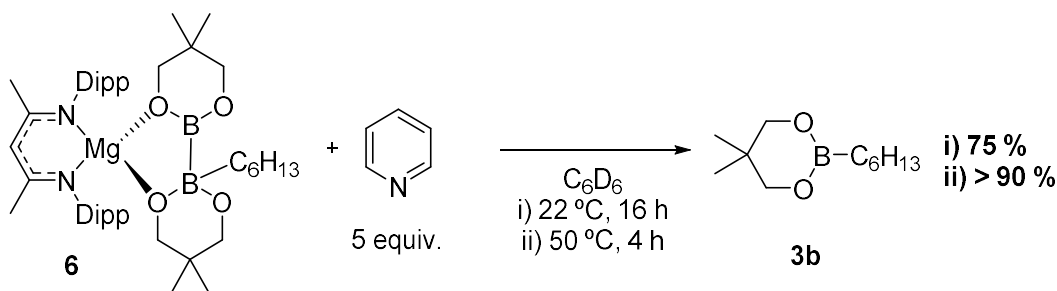
Figure 2.4 X-ray structure of compound **6**, formed upon reaction of **1a** and  $B_2nep_2$  (50 % probability ellipsoids). Selected bond lengths ( $\text{\AA}$ );  $Mg(1)-O(31) = 1.9111(17)$ ,  $Mg(1)-O(45) = 2.028(8)$ ,  $B(30)-O(31) = 1.587(3)$ ,  $B(44)-O(45) = 1.409(7)$ ,  $B(30)-O(35) = 1.467(3)$ ,  $B(44)-O(49) = 1.393(4)$ ,  $B(30)-B(44) = 1.728(4)$



Scheme 2.31 Intermediate complex formed upon reaction of **1a** and  $B_2nep_2$

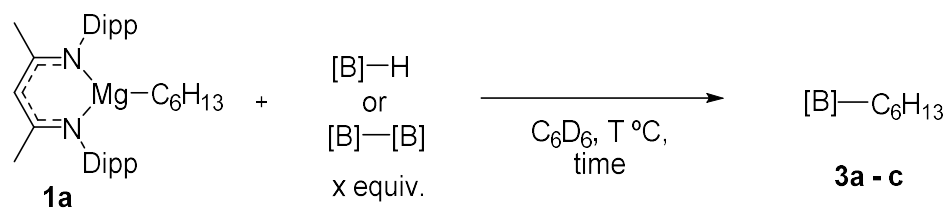
Compound **6** was heated at 50 – 80 °C and the slow formation of **2c** was observed. This result suggests **6** has a higher stability than **4**. This increased stability is speculated to be a result of the decreased strain exhibited in the 6-membered  $B_2nep_2$  ring.

Addition of a Lewis base was postulated to enhance the formation of **3c** from **6**. The addition of pyridine to a pure sample of **6** in benzene- $d_6$  led to the formation of **3c** in 75 % yield after 16 hours at 22 °C, as determined by  $^1H$  NMR spectroscopy. Raising the reaction temperature to 50 °C over 4 hours led to a further enhanced yield (**Scheme 2.32**).



Scheme 2.32 Reaction of compound **6** with pyridine

Due to the limitations with diboron reagents, the boranes HBpin and 9-BBN were deemed to be the best compounds for alkyl transfer.



| Entry          | Boron reagent                   | Equivalents | Temperature (°C) | Time     | Yield of <b>3</b> (%) <sup>a</sup> |
|----------------|---------------------------------|-------------|------------------|----------|------------------------------------|
| 1              | HBpin                           | 1.1         | 22               | <15 mins | >90                                |
| 2              | 9-BBN                           | 1.1         | 22               | <15 mins | >90                                |
| 3              | HBcat                           | 2           | 22               | <15 mins | 0                                  |
| 4              | B <sub>2</sub> pin <sub>2</sub> | 1.1         | 40               | 1 h      | >90                                |
| 5              | B <sub>2</sub> nep <sub>2</sub> | 1.1         | 80               | 12 h     | 40                                 |
| 6 <sup>b</sup> | B <sub>2</sub> nep <sub>2</sub> | -           | 50               | 4        | >90                                |

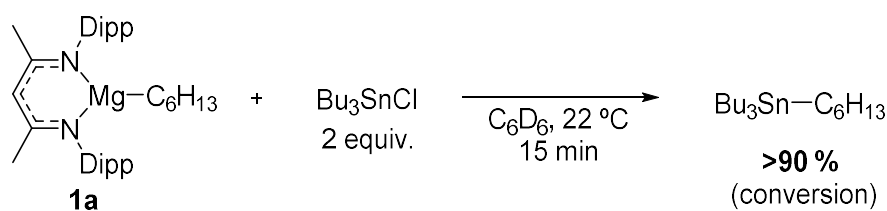
Table 2.3 Summary of borylation reaction with **1a** <sup>a</sup>Yield determined *in situ* on comparison to an internal standard

<sup>b</sup> Upon addition of 5 equivalents pyridine to the isolated intermediate complex **5** after 16 hours at 22 °C

### 2.2.5.2 Reaction with other Main Group Electrophiles

The alkyl moiety of **1a** was also shown to transfer to tin and silicon compounds under mild conditions. Organotin and organosilicon compounds are versatile reagents in cross-coupling reactions and demonstrate a degree of orthogonality to organoboron species.

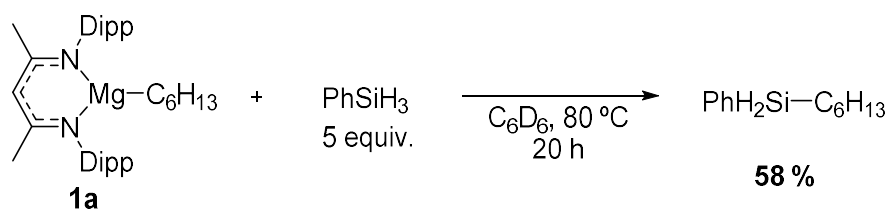
Bu<sub>3</sub>SnCl was added to a 0.02 M benzene-d<sub>6</sub> solution of **1a** generated *in situ* from **1** and 1-fluorohexane. Within 15 minutes at 22 °C full conversion of **1a** was realised, indicated by the loss of triplet resonance ( $\delta = -0.22$  ppm) in the <sup>1</sup>H NMR spectrum, corresponding to the methylene adjacent to magnesium. The product, tributyl(n-hexyl)stannane was confirmed (>90 % conversion) by a singlet resonance ( $\delta = -13.96$ ) in the <sup>119</sup>Sn{<sup>1</sup>H} NMR spectrum which was in accordance with analogous tetrabutyltin compounds from the literature.<sup>[58]</sup>



Scheme 2.33 Reaction of **1a** with  $\text{Bu}_3\text{SnCl}$

The reaction was repeated with  $\text{Bu}_3\text{SnH}$ . Forcing conditions were required but after 6 days at  $80\text{ }^\circ\text{C}$ , the complete conversion to tributyl(*n*-hexyl)stannane was achieved (>90 % conversion).

Phenylsilane was added to a benzene- $\text{d}_6$  solution of **1a** generated *in situ* from **1** and the reaction heated ( $80\text{ }^\circ\text{C}$ ) for 20 hours. Upon analysis of the  $^1\text{H}$  NMR spectrum full conversion of **1a** was realised, indicated by the loss of the triplet resonance at ( $\delta = -0.22\text{ ppm}$ ). The desired product, 1-hexyl(phenyl)silane was confirmed (58% yield) upon comparison of the  $^1\text{H}$  NMR spectrum to the literature data.<sup>[59]</sup>



Scheme 2.34 Reaction of **1a** with phenylsilane

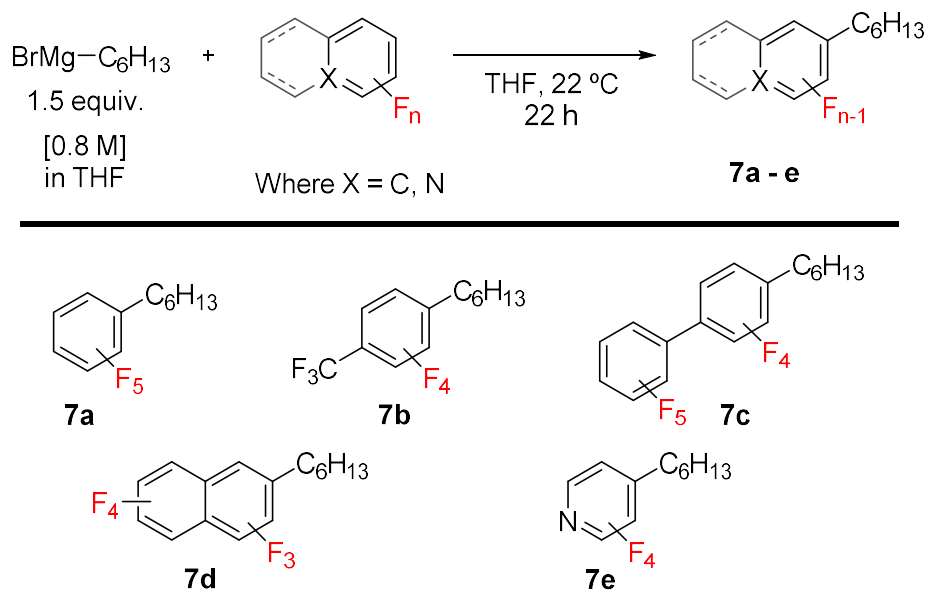
### 2.2.6 Coupling to $\text{sp}^2\text{C}-\text{F}$ bonds of Perfluoroarenes

Encouraged by the ease of nucleophilic addition to main group electrophiles, we aimed to expand this investigation to the construction of  $\text{C}-\text{C}$  bonds. We targeted the alkylation of perfluoroarenes, hoping the fluorophilicity of magnesium would provide a key driving force in the  $\text{sp}^2\text{C}-\text{F}$  bond cleavage step. This process represented the first example of a transition-metal free  $\text{C}-\text{C}$  coupling reaction from two  $\text{C}-\text{F}$  bonds and could be performed in 'one-pot'.

We investigated the reactivity of **1a**, generated *in situ* from **1**, with a range of perfluoroarenes (hexafluorobenzene, octafluorotoluene, decafluorobiphenyl, octafluoronaphthalene and pentafluoropyridine).

#### 2.2.6.1 Independent Synthesis of *n*-Hexyl Substituted Fluoroarenes

To confirm the assignment of desired products, generated from the addition of **1a** to fluoroarenes, were correct we undertook the independent synthesis of *n*-hexyl fluoroarene derivatives **7a** – **7e**. This was achieved upon addition of *n*-hexyl magnesium bromide to the corresponding perfluoroarene.<sup>[60]</sup>



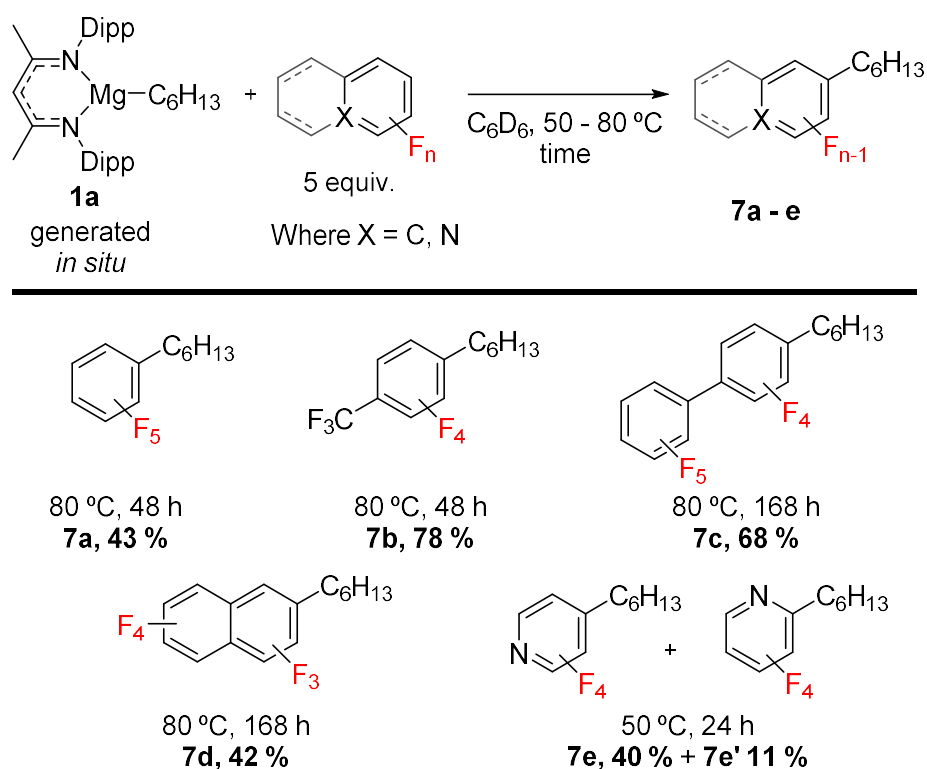
Scheme 2.35 Independent synthesis of *n*-hexyl derivatives of perfluoroarenes

The products generated upon reaction of **1a** and perfluoroarenes could then be determined and quantified easily *in situ* upon analysis of the  $^1\text{H}$  and  $^{19}\text{F}$  NMR spectra.

#### 2.2.6.2 One-pot Coupling of $\text{sp}^3\text{C-F}$ and $\text{sp}^2\text{C-F}$ Bonds

The reactions were performed as a one-pot, two-step process. **1a** was consistently generated in ~ 90 % yield from **1** and 1-fluorohexane. The yields were determined upon *in situ*  $^1\text{H}$  NMR spectrum comparison to an internal standard (ferrocene,  $\delta = 4.00$  ppm). The products were confirmed upon comparison of the  $^{19}\text{F}$  NMR spectrum resonances to the independently synthesised compounds (*vide supra*).

Addition of  $\text{C}_6\text{F}_6$  to a benzene- $\text{d}_6$  solution of **1a** and subsequent heating (80 °C) led to the formation of 6-hexyl-pentafluorobenzene (**7a**) as determined by the formation of a triplet resonance in the  $^1\text{H}$  NMR spectrum corresponding to the methylene protons adjacent to the aromatic ring ( $\delta = 2.29$  ppm,  $^3J_{\text{HH}} = 7.7$  Hz) plus five new resonances in the  $^{19}\text{F}$  NMR spectrum. Full consumption of **1a** was achieved after 48 h at 80 °C with a modest yield for **7a** (single C–C step = 43 %, overall from **1** = 38 %).



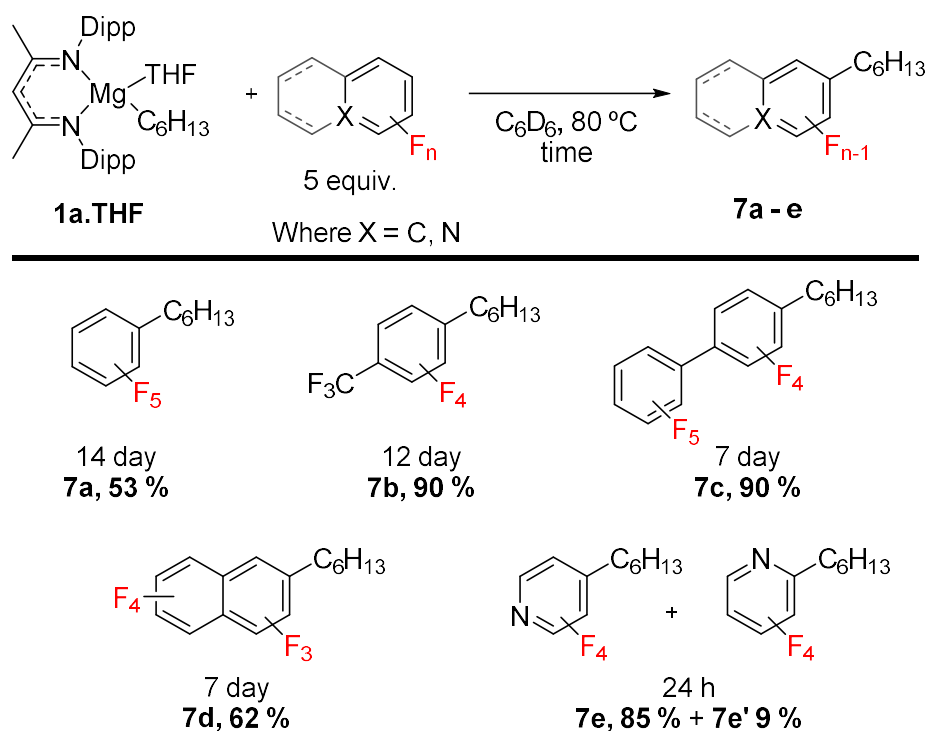
Scheme 2.36 Results for single C–C coupling step between **1a** and perfluoroarenes

Higher yields were achieved for more electron rich fluoroarenes, octafluorotoluene (single C–C step = 78 %, overall from **1** = 72 %) and decafluorobiphenyl (single C–C step = 68 %, overall from **1** = 60 %). 7-Hexyl-heptafluoronaphthalene was generated in modest yield after an extended period of heating (single C–C step = 40 %, overall from **1** = 34 %).

Upon addition of pentafluoropyridine to a benzene- $d_6$  solution of **1a**, two fluorinated products were formed as determined by  $^{19}F$  NMR spectroscopy. The major component was the desired product **7e**, confirmed upon comparison to the independently synthesised compound (1 step = 40 %, 2 step = 35 %). The other species exhibited four distinct resonances in the  $^{19}F$  NMR spectrum ( $\delta$  = - 85.0, - 141.3, - 148.4 and - 161.6 ppm), suggesting C–C coupling had occurred at the 2- position of the heterocycle. This was strongly supported by comparison of the  $^{19}F$  NMR spectrum data to a related compound reported in the literature, 6-methyl-tetrafluoropyridine ( $\delta$  = - 85.3, - 141.5, - 146.6 and - 161.7 ppm).<sup>[61]</sup>

#### 2.2.6.2 Reaction of Independently Synthesised Mg–n-Hexyl.THF with Perfluoroarenes

The alkylation of perfluoroarenes was also performed using isolated samples of **1a.THF**, to check the robustness of the method.



Scheme 2.37 Results for C–C coupling step between **1a.THF** and perfluoroarenes

The reactions were slower in all cases, requiring up to 2 weeks to observe full consumption of **1a.THF**. This is consistent with THF inhibiting the reaction due to coordination to Mg. The yields for the alkylated perfluoroarenes were higher in this scenario when compared to the reactions from *in situ* generated **1a**. **1a.THF** was found to be more stable in solution at 80 °C than **1a**, therefore the decomposition (into products unknown) of the magnesium compound is suppressed upon THF coordination.

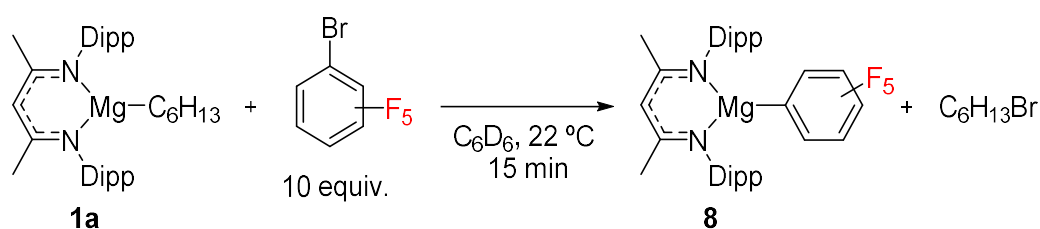
A marked improvement to product yield (compared to reaction with **1a** generated *in situ*) was achieved upon reaction with pentafluoropyridine. The *para* : *ortho* selectivity was also enhanced, possibly due to the disfavoured coordination to the Mg centre through nitrogen, due to competition with THF.

### 2.2.6.3 Reaction with Partially Fluorinated Arenes

The C–C coupling reactions of **1a** with perfluoroarene substrates were shown to be reasonably efficient and selective at one position. Extending this reactivity to partially fluorinated arenes was the next logical step.

We investigated the reaction of **1a** with 1-bromo-pentafluorobenzene ( $\text{C}_6\text{F}_5\text{Br}$ ), expecting the formation of **7a** plus  $[\text{Dipp}(\text{BDI})\text{Mg}(\mu\text{-Br})_2]$  (**1-Br**). Full consumption of **1a** was achieved within 15 minutes after fluoroarene addition as evidenced by  $^1\text{H}$  NMR spectroscopy. The formation of **7a** was

not achieved however. Further analysis of the  $^1\text{H}$  NMR spectrum identified the formation of 1-bromohexane with a characteristic triplet resonance ( $\delta = 2.92$  ppm). Consultation of the  $^{19}\text{F}$  NMR spectrum revealed the formation of magnesium–fluoroarene derivative [ $^{\text{Dipp}}(\text{BDI})\text{Mg}(\text{C}_6\text{F}_5)$ ] (**8**) and upon addition of THF, the  $^{19}\text{F}$  NMR resonances could be matched to those of the literature reported compound **8.THF** ( $\delta = -113.0, -158.0$  and  $-161.9$  ppm).<sup>[40]</sup> This reaction can be considered as a metal–halogen exchange process. It is similar to the reaction of n-butyl lithium with bromobenzenes and the reaction is proposed to occur through an  $\text{S}_{\text{N}}2\text{X}$  pathway in which nucleophilic attack occurs at the halogen atom.<sup>[62]</sup>



Scheme 2.38 Reaction of **1a** with 1-bromopentafluorobenzene

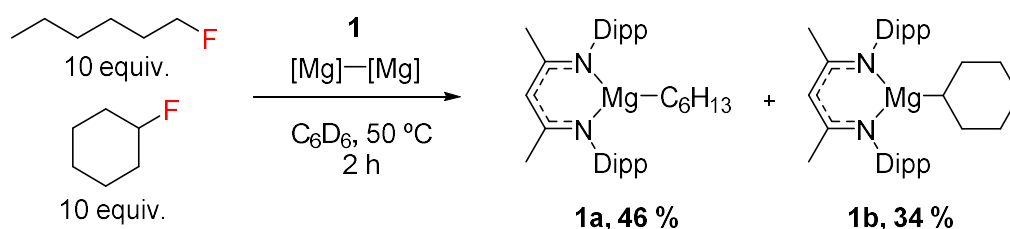
Repeating this reaction with pentafluorobenzene gave a similar outcome. In this scenario the alkyl moiety can be considered as a base, deprotonating pentafluorobenzene to generate n-hexane and **8**.

### 2.2.7 Competition Experiments

A series of competition reactions were undertaken to determine the relative rates of reaction of **1** between substrates. The study included  $\text{sp}^3\text{C}-\text{F}$  vs.  $\text{sp}^2\text{C}-\text{F}$  bonds,  $1^\circ$  vs.  $2^\circ$   $\text{sp}^3\text{C}-\text{F}$  bonds and  $\text{sp}^3\text{C}-\text{F}$  vs.  $\text{sp}^3\text{C}-\text{X}$  bonds (where  $\text{X} = \text{Cl}, \text{Br}$  and  $\text{I}$ ).

#### 2.2.7.1 Primary vs. Secondary $\text{sp}^3\text{C}-\text{F}$ Bonds

The reaction of **1** with 1-fluorohexane and fluorocyclohexane ( $1^\circ$  vs.  $2^\circ$ ) was investigated under pseudo first-order conditions. A tenfold excess of 1-fluorohexane and fluorocyclohexane were added simultaneously to a benzene- $\text{d}_6$  solution of **1** and the reaction heated at  $50^\circ\text{C}$ , monitoring the reaction by  $^1\text{H}$  and  $^{19}\text{F}$  NMR spectroscopy.



Scheme 2.39 Competition reaction of **1** between 1-fluorohexane and fluorocyclohexane

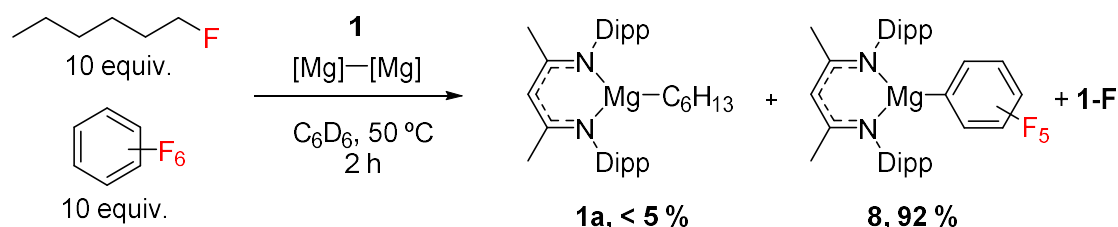


Upon full consumption of **1**, the formation of **1a** and **1b** was determined in 46 % and 34 % yield (1.3 : 1.0) respectively. This result indicates the C–F activation of primary C–F bonds is slightly favoured (at 50 °C) over secondary ones. One origin of this selectivity could be the decreased steric hindrance of the C–F bond in 1-fluorohexane compared to its cyclic analogue. However, due to only the slight preference for 1° C–F bonds the reaction rates are likely to be very similar.

### 2.2.7.2 $sp^2C-F$ vs. $sp^3C-F$ Bonds

The reaction **1** with fluoroarenes was previously reported to occur at 22 °C, typically within 1 hour to achieve full consumption of **1** (when the arene is perfluorinated or has at least five fluorine atoms on the ring that is undergoing reaction).<sup>[40]</sup> It was expected therefore that  $sp^2C-F$  bonds on these substrates would undergo C–F activation by **1** preferentially to  $sp^3C-F$  bonds in fluorocarbons.

The competition between hexafluorobenzene and 1-fluorohexane was undertaken. The substrates, in a ten-fold excess, were added simultaneously to a benzene- $d_6$  solution of **1** and the  $t=1$   $^1H$  and  $^{19}F$  NMR spectra recorded within 15 minutes. The full consumption of **1** was confirmed upon  $^1H$  NMR spectrum analysis plus the generation of  $[^{Dipp}(BDI)Mg(C_6F_5)]$  (**8**, 92 %) and **1a** (< 5 %). (It should be noted that this reaction considered the absolute concentration of the substrate and did not take into account the total number of  $sp^2C-F$  bonds vs.  $sp^3C-F$  bonds (6 : 1), therefore this result could be considered not an exact comparison.)



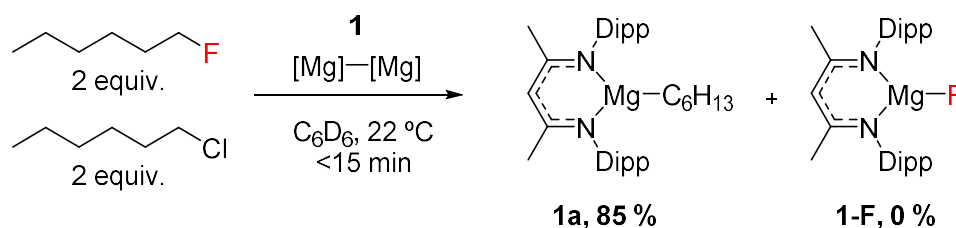
Scheme 2.40 Competition reaction of **1** between 1-fluorohexane and hexafluorobenzene

### 2.2.7.3 $sp^3C-X$ vs. $sp^3C-F$ Bonds

It was predicted that the activation of C–X (where X = Cl, Br and I) bonds would occur preferentially over C–F bonds due to the relative bond strengths (BDE's =  $FCH_3$   $115 \pm 4.0$ ,  $ClCH_3$   $83.7 \pm 0.1$ ,  $BrCH_3$   $72.1 \pm 0.3$  and  $ICH_3$   $57.6 \pm 0.4$  kcal mol $^{-1}$ ).<sup>[7]</sup>

A benzene- $d_6$  solution of 1-fluorohexane and 1-chlorohexane were added to a solution of **1**, an immediate colour change from pale yellow to colourless was observed. The reaction was analysed by  $^1H$  and  $^{19}F$  NMR spectroscopy. **1a** was generated in 85 % yield based upon comparison to an internal standard (ferrocene,  $\delta = 4.00$  ppm). **1-F** was not present in the solution, determined by lack of a singlet

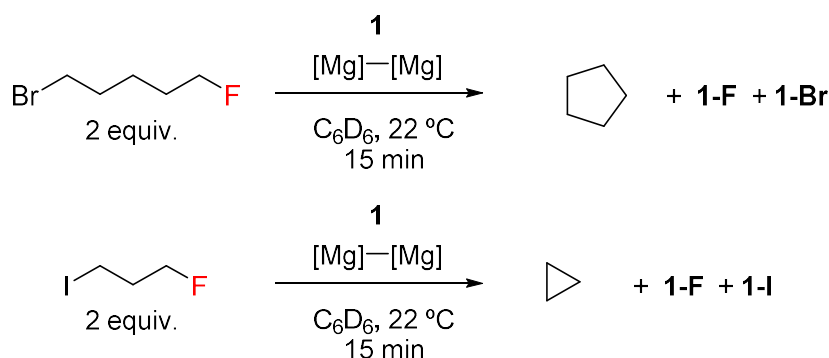
resonance in the  $^{19}\text{F}$  NMR spectrum ( $\delta = -187$  ppm), which indicated the formation of **1a** was due to the reaction with 1-chlorohexane rather than 1-fluorohexane. This result confirmed the original hypothesis.



Scheme 2.41 Competition reaction between 1-fluorohexane and 1-chlorohexane with **1**

Additional competition reactions between the activation of C–F and C–X bonds (where X = Br and I) were undertaken internally on the same substrate (*i.e.* reaction of **1** with 1-bromo-5-fluoropentane and 1-iodo-3-fluoropropane). In both cases, an immediate colour change and the complete consumption of **1** was realised within 15 minutes of addition of the substrate as determined by  $^1\text{H}$  NMR spectroscopy. This led to the assumption that the C–X bond had undergone facile cleavage by **1**, to form magnesium–fluoroalkane compounds [ $^{\text{dipp}}(\text{BDI})\text{Mg}(n\text{-C}_3\text{H}_6\text{F})$ ] and [ $^{\text{dipp}}(\text{BDI})\text{Mg}(n\text{-C}_5\text{H}_{10}\text{F})$ ]. However, investigation of the  $^{19}\text{F}$  NMR spectrum revealed the formation of **1-F** in both cases, as indicated by a singlet resonance ( $\delta = -187$  ppm). Furthermore, there was no evidence for the presence of a methylene carbon bound to magnesium ( $\text{Mg}-\text{CH}_2-$ ) as determined by analysis of the  $^1\text{H}$  NMR spectrum.

A cyclisation reaction was confirmed upon analysis of the volatile compounds in the solution following separation by trap-to-trap distillation.  $^1\text{H}$  NMR spectroscopy identified the formation of cyclopentane and cyclopropane (singlet resonances at  $\delta = 1.46$  and  $\delta = 0.14$  ppm respectively).



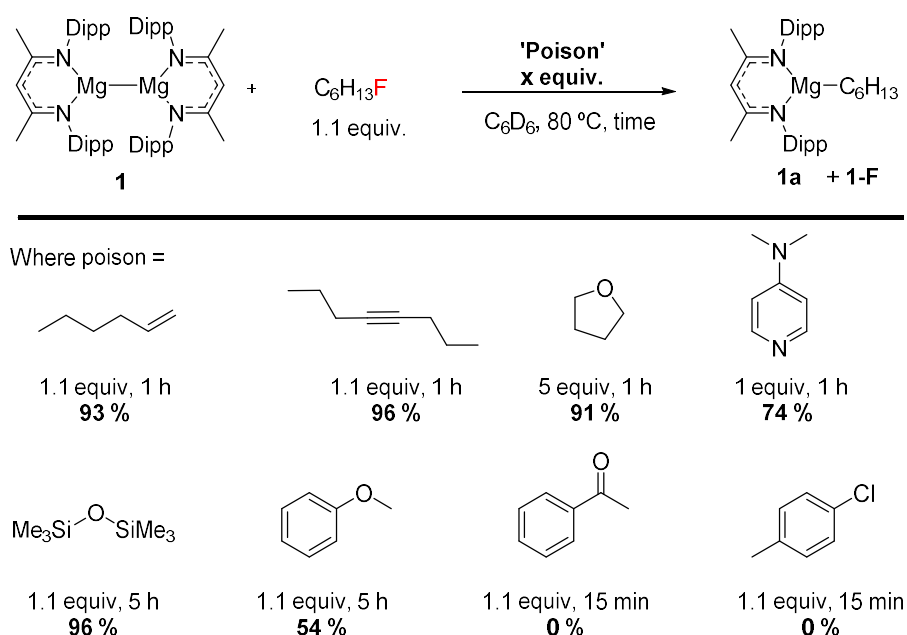
It was hypothesised that this procedure occurs *via* a rapid C–X bond activation by **1**, which is followed by C–C bond formation upon bond metathesis between Mg–C and C–F bonds. These results support the previous observation of C–C coupling between **1a** and 1-fluorohexane. The C–C cyclisation

reactions (5-*exo-tet* and 3-*exo-tet*) in these cases occur faster, presumably due to the C–F bonds existing in close proximity to the Mg–C bonds.

## 2.2.8 Functional Group Tolerances (External ‘Poisons’)

Attempts to probe the functional group tolerances of the C–F activation process were undertaken. Due to the lack of commercial availability and difficulty synthesising  $sp^3C-F$  containing compounds, the C–F activation of 1-fluorohexane by **1** was undertaken in the presence of external ‘poisons’ (compounds containing different functional groups, not present on the fluorocarbon substrate). The limitations to this approach are worth mentioning. Coordination to compound **1** may be favoured or disfavoured to the fluorocarbon which could alter the reactivity rates. Furthermore, the hypothetical products (from intramolecular C–F activation) would express the functional group which may go on to react further (*i.e.* cyclisation reactions), whereas **1a** does not exhibit any other functionality.

1-Fluorohexane and the functional group containing reagent were added simultaneously in equimolar amounts to a benzene- $d_6$  sample of **1** and the reaction heated to 80 °C for 1 hour (optimised conditions for C–F activation). The reactions were monitored by  $^1H$  and  $^{19}F$  NMR spectroscopy and the yields of **1a** determined upon comparison to an internal standard (ferrocene,  $\delta = 4.00$  ppm).



Scheme 2.42 Results of functional group tolerance reactions. C–F activation of 1-fluorohexane by **1** in the presence of external ‘poisons’

The C–F activation step was shown to tolerate terminal alkenes, internal alkynes, furans, tertiary amines and siloxane with **1a** being generated in high yields in the presence of these functional groups (> 90 %). Anisole, exhibiting an aryl ether functional group, hindered the reaction slightly with **1a**

generated in 54 % yield which suggested a competitive pathway was occurring and plausibly coordination through the oxygen atom to the magnesium atoms suppressing reactivity.

Carbonyls and aryl halides were shown to completely suppress C–F reactivity, with no **1a** generated in the presence of acetophenone or 4-chlorotoluene.

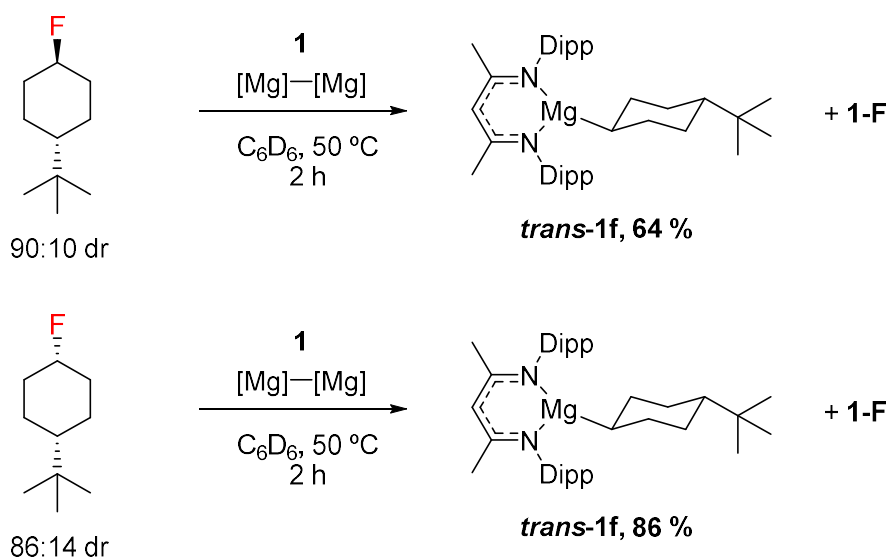
### 2.2.9 Mechanistic Probe Reactions

With the possibilities and limitations of  $sp^3C-F$  activation fully investigated, we aimed to elucidate the reaction mechanism. It was shown that a concerted nucleophilic aromatic substitution ( $S_NAr$ ) process takes place during the  $sp^2C-F$  activation of fluoroarenes with **1**, therefore we hypothesised that a concerted  $S_N2$ -like process may be operating with fluorocarbon substrates.<sup>[63]</sup> We should note that, from the perspective of the Mg–Mg reagent both these processes involve oxidative addition of the substrate to **1**.

This could be probed using fluorocarbon substrates that contain stereochemical information. As an initial approach to understanding the stereochemistry of this reaction, two diastereoisomers were synthesised, *cis*- and *trans*-4-*tert*-butyl-fluorocyclohexane. These were derived from their parent alcohols upon reaction with AlkylFluor, the fluorination procedure described previously (Section 2.2.3).

If an  $S_N2$  process was occurring, inversion of the stereocentre should be expected resulting in two distinct magnesium–alkyl species [<sup>di</sup>pp(*BDI*)Mg(*cis*-4-*tBu*-Cy)] and [<sup>di</sup>pp(*BDI*)Mg(*trans*-4-*tBu*-Cy)] (***cis*-1f** and ***trans*-1f** respectively).

Addition of *cis*- or *trans*-4-*tert*-butyl-fluorocyclohexane to a 0.02 M benzene- $d_6$  solution of **1** and subsequent heating (50 °C) led in both cases to the formation of the same products, as evidenced by a triplet resonance ( $\delta = 0.09$  ppm,  $^3J_{HH} = 13.4$  Hz and  $^3J_{HH} = 2.9$  Hz) in the  $^1H$  NMR spectrum. Full conversion of **1** occurred after 40 + hours.  $^1H$  NMR spectrum analysis at regular time intervals revealed only the presence of one magnesium–alkyl species. Interpreting the  $^3J_{HH}$  coupling constants using the Karplus equation (the correlation between  $^3J_{HH}$  coupling constants and dihedral torsion angles) suggested the formation of ***trans*-1f** as the major product with both substrates, plus **1-F**. The process was therefore stereoconvergent.



Scheme 2.43 Reaction of *cis*- and *trans*-4-*tert*-butyl-fluorocyclohexane with **1** in a stereoconvergent process

Unfortunately these reactions could not illuminate the plausible reaction pathway. Facile isomerisation to **trans-1f** from **cis-1f** could be occurring after the initial C–F activation. The experimentally observed product is thermodynamically favoured over the *cis* analogue ( $\Delta\Delta G_{298\text{K}} = 5.4 \text{ kcal mol}^{-1}$ ) according to computational calculation (B3PW91, 6-31G(d,p)/SDDAll accounting for dispersion, GD3 and solvent effects, pcm=benzene). Further investigation employing enantiomerically pure fluorocarbons is required to fully determine the stereoselectivity of this reaction. Even then, isomerisation at the Mg–C bond cannot be ruled out.

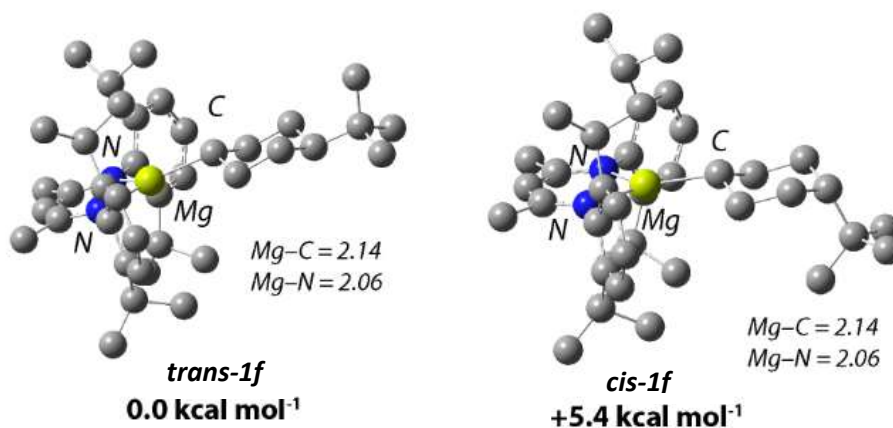


Figure 2.5 Structures of **trans-1f** and **cis-1f** as calculated by DFT, showing relative Gibbs energies in kcal mol<sup>-1</sup> (B3PW91/GD3 + PCM benzene)

Martin *et al.* described an elegant method for determining the  $\text{S}_{\text{N}}2$  inversion process occurring at  $\text{sp}^3\text{C–F}$  bonds of fluoroalkanes upon reaction with silicon nucleophiles (see section 2.1.6).<sup>[37]</sup> This technique could be effective for investigating the stereo-specificity of the reaction of fluorocarbons with **1**.

Performing the C–F bond activation of 1-fluorohexane in the presence of a radical trap substrate, 9,10-dihydroanthracene, had no negative effect on the formation of **1a** from **1**. This does not categorically rule out the involvement of radicals, but does not suggest any are generated.

## 2.2.10 Computational Calculations

A series of calculations were undertaken on the reaction of **1** with 1-fluoropropane to try and gain a deeper understanding of the C–F bond breaking process that is occurring. The B3PW91 functional and a hybrid basis set (6-31G(d,p)/SDDAll) was used, as well as incorporating single point energy corrections for solvent effects (pcm, benzene) and dispersion (GD3). These methods have been previously benchmarked in the group against experimentally determined parameters in C–F bond activation reactions.<sup>[63]</sup>

### 2.2.10.1 $sp^3$ C–F Activation at Mg–Mg

*(The majority of the calculations described in this section (2.2.10.1) were performed by Dr. Bryan Ward)*

The  $sp^3$ C–F activation of model substrate 1-fluoropropane with **1** begins with the coordination at one Mg centre through the fluorine atom. This is reminiscent of the ‘harpoon’ mechanism and analogous to the  $sp^2$ C–F activation of hexafluorobenzene with **2** (where Mg---F interaction = 2.67 Å).<sup>[63]</sup> The coordination of fluorocarbon is enthalpically favoured but entropically disfavoured resulting in an overall endergonic process (**Int-1**,  $\Delta G_{298K} = + 3.4 \text{ kcal mol}^{-1}$ ). Upon coordination, the  $\beta$ -diketiminato ligands become co-planar relative to one another, whereas their preferred orientation is perpendicular.

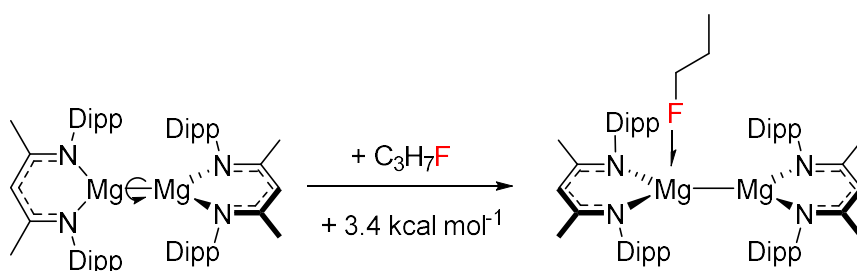


Figure 2.6 Endergonic coordination of 1-fluoropropane to **1** as calculated by DFT

Migration of the fluorocarbon from one Mg atom to the centre of the Mg–Mg bond leads to **TS-1** ( $\Delta G_{298K}^\ddagger = 23.6 \text{ kcal mol}^{-1}$ ). In **TS-1** the  $\alpha$ -carbon is situated above the fluorine. This transition state geometry is reminiscent of  $S_N1$ -type reactivity and the fluoride abstraction process described by Pitsch and Wang for the C–F activation of fluoromethane by Al(I) compounds.<sup>[36]</sup> However, in this scenario the electron-flow is reversed and fluoride abstraction (to form a carbocation) is not occurring.

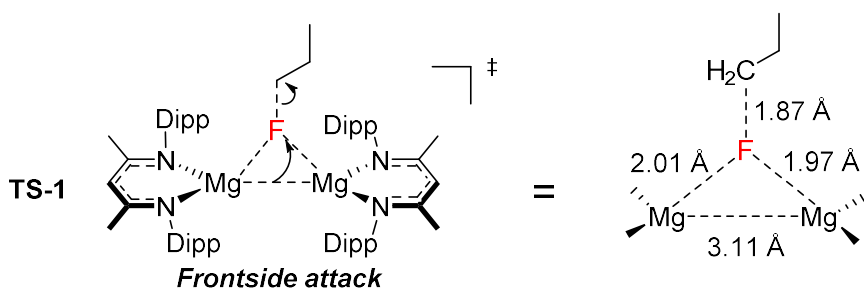


Figure 2.7 **TS-1** geometry and key interaction distances

The C–F bond stretches from 1.39 Å to 1.87 Å and both Mg–F distances are short ( $\sim 2.0$  Å), whilst Mg–C bonds remain long ( $> 3.6$  Å). This is a peculiar transition state which resembles a front-side nucleophilic attack.<sup>[64–66]</sup> In this scenario, the alkyl moiety becomes the leaving group exhibiting carbanion character (as determined by NPA charges compared to those at **Int-1**) and the electron-pair situated between the Mg–Mg atoms of **1** act as the nucleophile. This reactivity could be regarded as an  $S_N2X$  reaction, similar to that recently reported by Zhang and co-workers upon reaction of tertiary bromides with sulphur based nucleophiles, but never reported for C–F bonds.<sup>[67]</sup> Second-order perturbation calculation on **TS-1** reveal donor-acceptor interactions from the  $\sigma$ -bond between **1** and the low lying  $\sigma^*(\text{C–F})$  orbital on 1-fluoropropane (37 kcal mol<sup>-1</sup>). There is also an interaction between the filled F  $\pi$ -orbitals and the empty  $\sigma^*(\text{Mg–Mg})$  orbitals (7 kcal mol<sup>-1</sup>). This interaction can aid the stabilisation of the unusual transition state geometry by locking in place the orientation of the C–F bond.

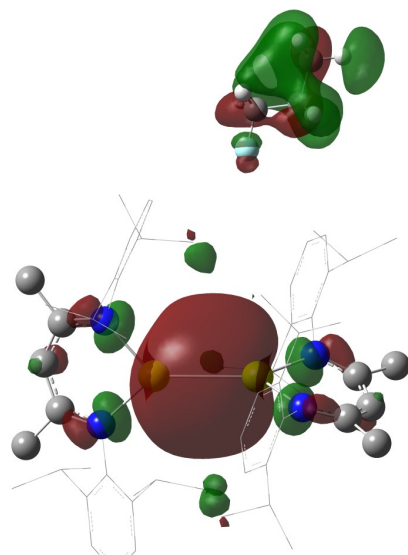


Figure 2.8 HOMO of **1** and LUMO of 1-fluoropropane. Ligand hydrogens omitted for clarity

More typical transition-state geometries were anticipated, such as the side-on and  $S_NAr$  processes determined for the reaction of **1** with  $\text{CO}_2$  and  $\text{C}_6\text{F}_6$  respectively.<sup>[63,68]</sup> However this could not be located

after multiple attempts of re-orientating the fluorocarbon substrate, always favouring the end-on approach.

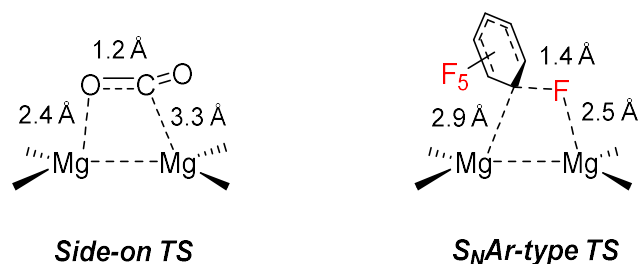


Figure 2.9 Side on and S<sub>N</sub>Ar-type TS geometry for the activation of CO<sub>2</sub> and C<sub>6</sub>F<sub>6</sub> with **1** respectively

Following the potential energy surface from **TS-1** leads directly to C–F activated product **Int-2/3** ( $\Delta G_{298K} = 72.7 \text{ kcal mol}^{-1}$ ). This intermediate was shown experimentally to undergo Schlenk redistribution to form the two homodimers **1a** and **1-F**. Rearrangement of **Int-2/3** to **Int-2<sub>2</sub>** and **Int-3<sub>2</sub>** can occur *via* the dissociation into the relevant monomers **Int-2** and **Int-3** and then recombination. Overall this is a thermoneutral process but the separation into monomers is endergonic ( $\Delta G_{298K} = 25.3 \text{ kcal mol}^{-1}$ ). This value represents the complete dissociation and is therefore the upper limit of the process (see figure 2.12)

Similar transition states for C–F cleavage were also located for 2-fluoropropane (**TS-2**,  $\Delta G_{298K}^{\ddagger} = 24.8 \text{ kcal mol}^{-1}$ ) and *tert*-butyl-fluoride (2-methyl-2-fluoropropane) (**TS-3**,  $\Delta G_{298K}^{\ddagger} = 28.7 \text{ kcal mol}^{-1}$ ).

| Substrate                            | TS ( $\Delta G_{298K}^{\ddagger} \text{ kcal mol}^{-1}$ ) | TS ( $\Delta\Delta G \text{ kcal mol}^{-1}$ ) |
|--------------------------------------|---|---|
| <b>1-fluoropropane (1°)</b>          | 23.6  | 0.0   |
| <b>2-fluoropropane (2°)</b>          | 24.8  | + 1.2   |
| <b>2-methyl-2-fluoropropane (3°)</b> | 28.7  | + 5.1   |

Table 2.4 Comparison of transition state energies for sp<sup>3</sup>C–F activation of 1°, 2° and 3° fluorocarbons

The relative energies of the C–F activation barriers are in line with what was expected based upon experimental observations. The competition reaction between 1-fluorohexane and fluorocyclohexane (1° and 2°) with **1** revealed that activation of the primary fluorocarbon was favoured. Furthermore, the activation of tertiary C–F bond containing 1-fluoroadamantane was not achievable with **1**. The latter substrate is slightly less sterically demanding than *tert*-butyl-fluoride therefore the transition state barrier would be expected to be lower (*i.e.*  $24.8 < \text{but} < 28.7 \text{ kcal mol}^{-1}$ ). In all cases, the transition state geometry was one resembling a ‘front-side attack’.



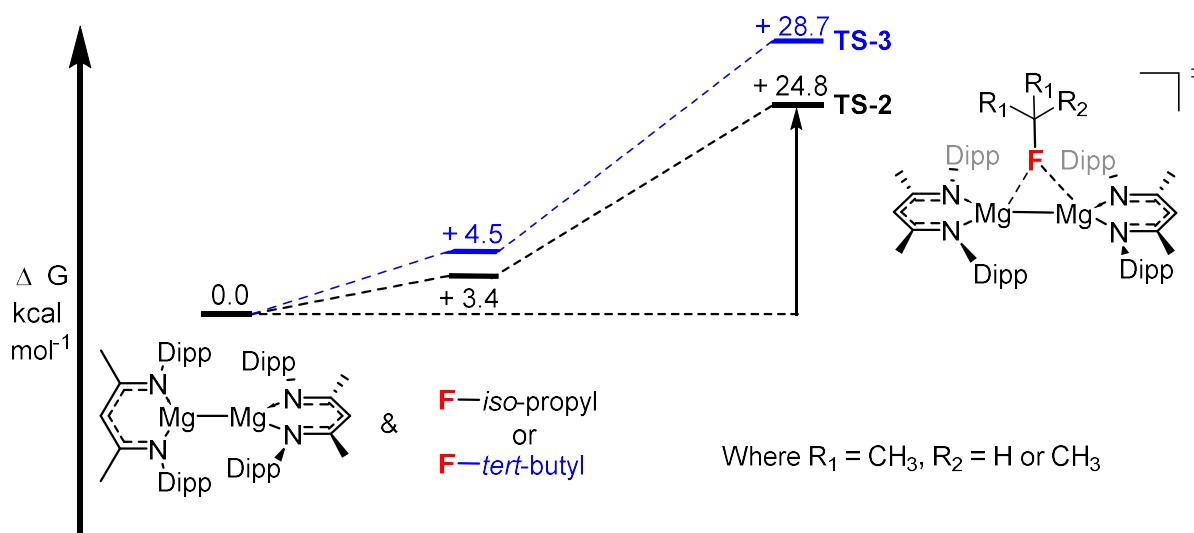


Figure 2.10 Potential energy surface for the C–F activation of 2-fluoropropane and tert-butyl fluoride by **1**

For secondary and tertiary magnesium–alkyl derivatives of **1**, it was determined computationally that the 3-coordinate monomer species is thermodynamically favoured. This is likely a factor of the increasing steric repulsion between the alkyl branches and the 2,6-di-iso-propylphenyl aromatic rings on the ligand.

#### 2.2.10.2 C–C Bond Formation through $sp^2C$ –F Cleavage

We extended our computational investigation to the second C–F bond cleavage step at magnesium, probing the addition of the n-propyl moiety to hexafluorobenzene.

Beginning from **Int-2<sub>2</sub>** and **Int-3<sub>2</sub>**, established through the Schlenk-like redistribution of two equivalents of **Int-2/3**, monomerisation of the alkyl species occurs to access the reactive compound (2 x **Int-2** plus **Int-3<sub>2</sub>**). The carbon–carbon bond forming step occurs through nucleophilic attack of the electron deficient fluoroarene *via* a high energy  $S_NAr$  transition state (**TS-4**,  $\Delta G^\ddagger_{298K} = 26.1$  kcal mol<sup>-1</sup>).

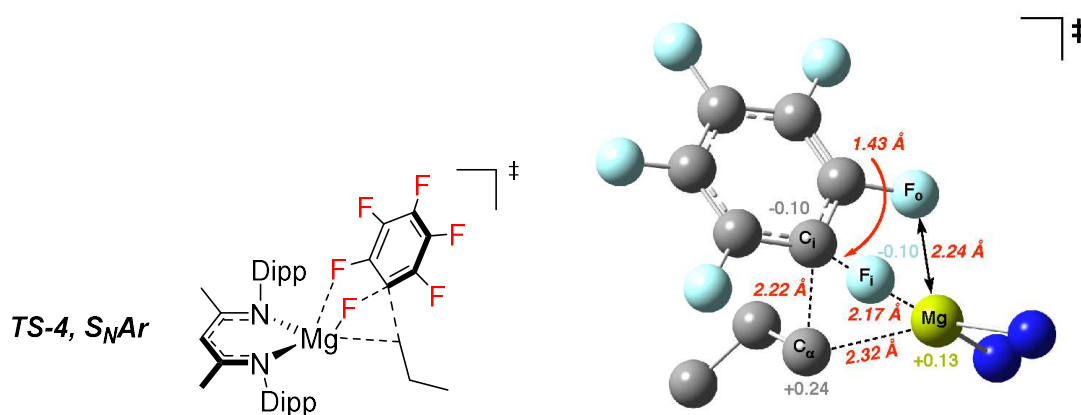


Figure 2.11 **TS-4** geometry for C–C bond forming reaction, key bond lengths and NPA charges

The transition state geometry is stabilised by an *ortho*-fluorine interaction between the fluoroarene and magnesium. An alternative, higher energy pathway for C–C coupling through a  $\sigma$ -bond metathesis pathway was also located whereby there were no *ortho*-fluorine interactions with the metal centre (**TS-4'**,  $\Delta G^\ddagger_{298\text{K}} = 30.9 \text{ kcal mol}^{-1}$ ,  $\Delta\Delta G_{298\text{K}} = + 4.8 \text{ kcal mol}^{-1}$ ).

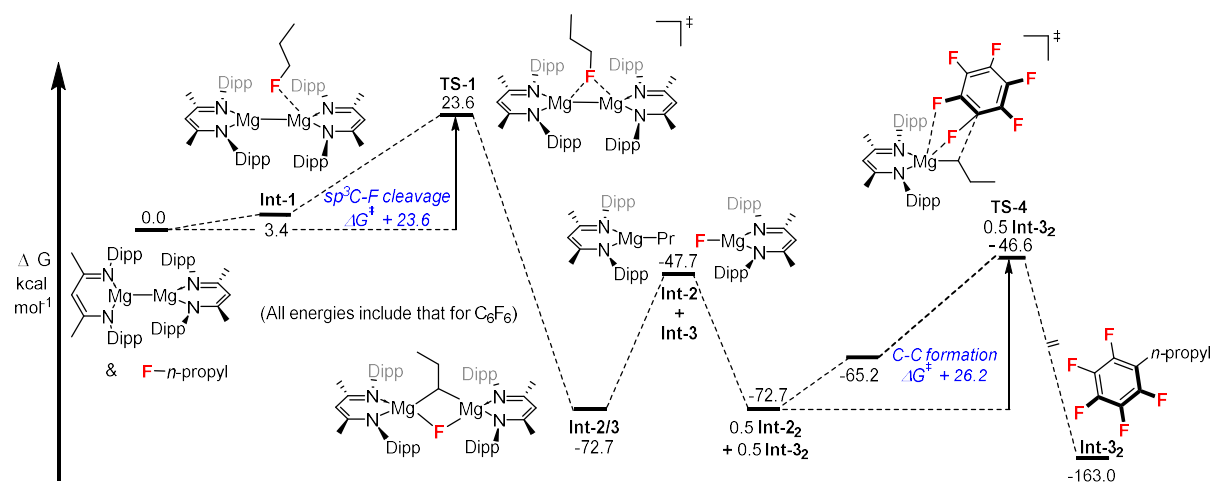


Figure 2.12 Calculated potential energy surface for the sequential reaction of **1** with 1-fluoropropane and  $\text{C}_6\text{F}_6$

Overall, we have elucidated using computational methods the  $\text{sp}^3\text{C-F}$  activation process for fluorocarbons that appears to occur through a remarkable front-side nucleophilic attack of the C–F bond. We have further extended the investigation to reveal the  $\text{S}_{\text{N}}\text{Ar}$  process to form new C–C bonds through the subsequent reaction with perfluoroarene substrates.

## 2.3 Experimental

Standard Schlenk line and glovebox techniques were used for all manipulations under an inert atmosphere of dinitrogen or argon unless otherwise stated. NMR scale reactions were performed in J. Young's tap NMR tubes equipped with internal standard capillaries of ferrocene ( $^1\text{H}$  NMR) or 1-trifluoromethylnaphthalene ( $^{19}\text{F}$  NMR) and prepared in a glovebox. An MBraun Labmaster glovebox was used, operating at  $<0.1$  ppm  $\text{H}_2\text{O}$  and  $<0.1$  ppm  $\text{O}_2$ .  $^1\text{H}$ ,  $^{13}\text{C}$ ,  $^{11}\text{B}$ ,  $^{19}\text{F}$  NMR and  $^{119}\text{Sn}$  spectra were recorded on BRUKER 400 MHz or 500 MHz machines. Data were processed using the MestReNova software. Coupling constants ( $J$ ) are quoted in Hz.

Solvents were dried over activated alumina from a solvent purification system (SPS) based upon the Grubbs design and de-gassed before use. Glassware was dried for  $>6$  h prior to use at  $120$  °C. Benzene- $d^6$  was stored over  $3\text{\AA}$  molecular sieves, distilled and de-gassed before use. All heating mentioned was done using silicone oil baths.

All reagents were acquired from VWR, Apollo Scientific, Sigma Aldrich, Honeywell or Fluorochem and used without further purification unless specified. Where liquids at  $25$  °C, reagents were dried over activated  $3\text{\AA}$  molecular sieves and freeze-pump-thaw degassed prior to use.  $[\text{Mes}(\text{BDI})\text{Mg}]_2$  (**2**),  $[\text{Dipp}(\text{BDI})\text{K}]$ ,  $[\text{Mes}(\text{BDI})\text{K}]$ , and Alkylfluor reagent were prepared by the literature procedures ( $\text{MesBDI} = \{2,4,6\text{-Me}_3\text{C}_6\text{H}_3\text{NC}(\text{Me})\}_2\text{CH}$ ,  $\text{DippBDI} = \{2,6\text{-}^i\text{Pr}_2\text{C}_6\text{H}_3\text{NC}(\text{Me})\}_2\text{CH}$ ).<sup>[69],[70],[45]</sup> 4-*tert*-Butylcyclohexanol (*trans* and *cis*) were synthesised according to the literature procedure.<sup>[71]</sup>

Single crystal X-Ray data were obtained on Agilent Diffraction Xcalibur PX Ultra A and Xcalibur diffractometers. The structures were refined using the SHELXTL, SHELX-97 and SHELX-2013 program systems. Gas chromatography (GC) analyses were performed using an Agilent Technologies 7820A GC using a HP-5 column with FID detector. The carrier gas was helium (at a flow rate of  $25$  mL/min). CHN analysis was run by Stephen Boyer of London Metropolitan University.

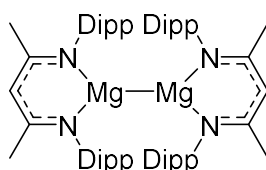
DFT calculations were run using Gaussian 09 (Revision D.01)<sup>[72]</sup> using the B3PW91 density functional.<sup>[73–77]</sup> Mg centres were described with Stuttgart SDDAll RECPs and associated basis sets whereas 6-31G\*\* basis sets was used for all other atoms.<sup>[78–80]</sup>

Geometry optimisation calculations were performed without symmetry constraints. The Gaussian 09 default optimisation criteria were tightened to  $10^{-9}$  on the density matrix and  $10^{-7}$  on the energy matrix. The default numerical integration grid was also improved using a pruned grid with 99 radial

shells and 590 angular points per shell. Frequency analyses for all stationary points were performed using the enhanced criteria to confirm the nature of the structures as either minima (no imaginary frequency) or transition states (only one imaginary frequency). Intrinsic reaction coordinate (IRC) calculations followed by full geometry optimisations on final points were used to connect transition states and minima located on the potential energy surface allowing a full energy profile (calculated at 298.15 K, 1 atm) of the reaction to be constructed.<sup>[81,82]</sup> Free energies reported within the main text are corrected for the effects of benzene solvent ( $\epsilon=2.2706$ ) using the polarizable continuum model (PCM).<sup>[83]</sup> In addition, single point dispersion corrections were applied to the B3PW91 optimised geometries employing Grimme's D3 correction.<sup>[84]</sup>

The graphical user interface used to visualise the various properties of the intermediates and transition states was GaussView 5.0.9.<sup>[85]</sup> Natural Bond Orbital analysis was carried out using NBO 6.0.<sup>[86]</sup> The topology of the electron density for selected systems within the QTAIM framework was carried out using the AIMALL software.<sup>[87-89]</sup>

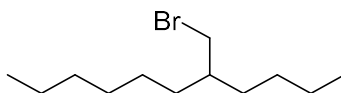
### 2.3.1 Preparation of Starting Materials



**Synthesis of compound 1:** Following a modified procedure,<sup>[45]</sup> in a glovebox [<sup>Dipp</sup>(BDI)MgI.OEt<sub>2</sub>] (2.57 g, 4.00 mmol) was added to a Schlenk flask and dissolved in toluene (~40 mL), then finely sliced potassium (1.60 g, 41.00 mmol) added. The mixture was allowed to stir in the glovebox for two days then the solution transferred to a separate Schlenk via cannula filtration. The resulting orange solution was concentrated under reduced pressure until a precipitate was observed. The crude product was recrystallised from toluene at -35 °C, forming yellow crystals. The product was isolated by cannula filtration and dried *in vacuo*, yielding bright yellow crystals of **1** (801 mg, 0.89 mmol, 46 %).

$\delta_{\text{H}}$  (400 MHz, C<sub>6</sub>D<sub>6</sub>, 298K): 7.06 (t, 12H, ArH), 4.81 (s, 2H, C(CH<sub>3</sub>)CH(CH<sub>3</sub>)C), 3.12 – 3.02 (sept, 8H, <sup>3</sup>J<sub>HH</sub> = 6.8 Hz, CH(CH<sub>3</sub>)<sub>2</sub>), 1.53 (s, 12H, CHC(CH<sub>3</sub>)) 1.16 (d, 24H, <sup>3</sup>J<sub>HH</sub> = 6.8 Hz, CH(CH<sub>3</sub>)<sub>2</sub>) 0.98 (d, 24H, <sup>3</sup>J<sub>HH</sub> = 6.8 Hz, CH(CH<sub>3</sub>)<sub>2</sub>).

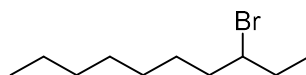
$\delta_{\text{C}}$  (100 MHz, C<sub>6</sub>D<sub>6</sub>, 298K): 167.7 (s, 4C, CHC(CH<sub>3</sub>)), 145.9 (s, 4C, *ipso*-C<sup>IV</sup>), 142.1 (s, 8C, *o*-C<sup>IV</sup>), 125.3 (s, 4C, *p*-CH), 123.9 (s, 8C, *m*-CH), 96.2 (s, 2C, C(CH<sub>3</sub>)CH(CH<sub>3</sub>)C), 28.6 (s, 8C, CH(CH<sub>3</sub>)<sub>2</sub>), 25.3 (s, 8C, CH(CH<sub>3</sub>)<sub>2</sub>), 24.4 (s, 4C, C<sup>IV</sup>CH<sub>3</sub>), 24.0 (s, 8C, CH(CH<sub>3</sub>)<sub>2</sub>).



**Synthesis of 2-butyl-bromooctane:** In a three-neck flask under argon atmosphere, triphenylphosphine ( $\text{PPh}_3$ ) (13.12 g, 50 mmol) was dissolved in dichloromethane (100 mL). The solution was stirred for 15 minutes then cooled to 0 °C. Bromine ( $\text{Br}_2$ ) (3.59 mL, 70 mmol) was added dropwise to the solution, a colour change to orange was observed along with a precipitate. 2-Butyl-1-octanol (9.32 mL, 42 mmol) was added dropwise over 30 minutes to the suspension using a dropping funnel, the reaction mixture was then allowed to warm to room temperature (22 °C) and stirred for 20 hours, the precipitate re-dissolved over this time period. The reaction mixture was concentrated under reduced pressure and the product extracted into n-hexane (100 mL), and washed with brine. The organic layers were combined and dried with  $\text{MgSO}_4$ . The solution was concentrated under reduced pressure to yield a colourless oil. The product was purified by column chromatography (eluent : n-hexane) yielding 2-butyl-bromooctane as a colourless oil (8.93 g,  $d = 1.039 \text{ g/mL}$ , 85 %).

$\delta_{\text{H}}$  (400 MHz,  $\text{CDCl}_3$ , 298K): 3.45 (d, 2H,  $^3J_{\text{HH}} = 4.8 \text{ Hz}$ ,  $\text{CH}_2\text{Br}$ ), 1.59 (m, 1H,  $\text{CH}(\text{CH}_2)_3$ ), 1.44 – 1.20 (br m, 16H,  $(\text{CH}_2)_8$ ), 0.92 – 0.87 (m, 6H,  $(\text{CH}_3)_2$ ).

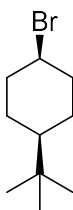
$\delta_{\text{C}}$  (100 MHz,  $\text{CDCl}_3$ , 298K): 39.7 (s, 1C,  $\text{CH}_2\text{I}$ ), 39.5 (s, 1C,  $\text{CH}(\text{CH}_2\text{I})$ ), 32.6 (s, 1C,  $\text{CH}_2$ ), 32.3 (s, 1C,  $\text{CH}_2$ ), 31.8 (s, 1C,  $\text{CH}_2$ ), 29.5 (s, 1C,  $\text{CH}_2$ ), 28.8 (s, 1C,  $\text{CH}_2$ ), 26.6 (s, 1C,  $\text{CH}_2$ ), 22.9 (s, 1C,  $\text{CH}_2$ ), 22.7 (s, 1C,  $\text{CH}_2$ ), 14.11 (s, 1C,  $\text{CH}_3$ ), 14.08 (s, 1C,  $\text{CH}_3$ ).



**Synthesis of 3-bromodecane:** In a three-neck flask under argon atmosphere, triphenylphosphine ( $\text{PPh}_3$ ) (2.75 g, 10.5 mmol) was dissolved in dichloromethane (25 mL). The solution was stirred for 15 minutes and then cooled to 0 °C. Bromine ( $\text{Br}_2$ ) (748  $\mu\text{L}$ , 14.6 mmol) was added dropwise to the solution, observing a colour change to orange was observed along with a precipitate. 3-Decanol (1.50 mL, 7.8 mmol) was added dropwise over 30 minutes to the suspension using a dropping funnel. The reaction mixture was allowed to warm to room temperature (22 °C) and stirred for 20 hours, the precipitate re-dissolved over this time period. The reaction mixture was concentrated under reduced pressure and the product extracted into n-hexane (50 mL), and washed with brine. The organic layers were combined and dried with  $\text{MgSO}_4$ . The solution was concentrated under reduced pressure to yield a colourless oil. The product was purified by column chromatography (eluent : n-hexane) yielding the target compound as a colourless oil (1.18 g,  $d = 1.09 \text{ g/mL}$ , 68 %)

$\delta_{\text{H}}$  (400 MHz,  $\text{CDCl}_3$ , 298K): 4.01 – 3.95 (m, 1H,  $\text{CHBr}$ ), 1.91 – 1.74 (m, 4H,  $(\text{CH}_2)_2\text{CHBr}$ ), 1.46 (dm, 2H,  $\text{CHBr}(\text{CH}_2)\text{CH}_2$ ), 1.36 – 1.22 (br m, 8H,  $(\text{CH}_2)_4$ ), 1.04 (t, 3H,  $^3J_{\text{HH}} = 7.3 \text{ Hz}$ ,  $\text{CHBr}(\text{CH}_2)\text{CH}_3$ ), 0.88 (t, 3H,  $(\text{CH}_2)_6\text{CH}_3$ ).

$\delta_{\text{C}}$  (100 MHz,  $\text{CDCl}_3$ , 298K): 60.7 (s, 1C,  $\text{CHBr}$ ), 38.8, 32.2, 29.2, 29.1, 27.6, 22.7, 14.1 (s, 1C,  $\text{CH}_3$ ), 12.1 (s, 1C,  $\text{CH}_3$ ).

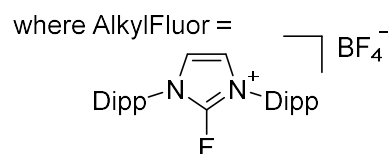
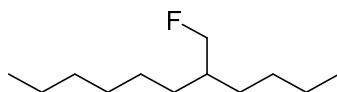


**Synthesis of cis-1-bromo-4-(tert-butyl)cyclohexane:** In a 250 mL three-neck flask under an argon atmosphere, triphenylphosphine (6.11 g, 23.3 mmol) was dissolved in dichloromethane (40 mL), cooled to 0 °C and stirred for 15 minutes. Bromine (1.38 mL, 26.9 mmol) was added dropwise to the solution observing the formation of a precipitate and the solution stirred for 20 minutes. A solution of *trans*-4-(tert-butyl)cyclohexan-1-ol (2.80 g, 17.9 mmol) in dichloromethane (10 mL) was added dropwise over a 20 minute period. The solution allowed to warm to room temperature and the solution stirred for 24 hours. The reaction was quenched upon the addition of water (30 mL) and sodium thiosulfate (10.0 g) and the solution stirred for 15 minutes. The dichloromethane was removed on a rotary evaporator and the product extracted into n-hexane (3 x 40mL) washing with brine. The fractions were combined and concentrated *in vacuo* yielding white crystals and a colourless oil. The product was suction filtered, washing with portions of n-hexane (~40 mL). A crude <sup>1</sup>H NMR spectrum was recorded, identifying the desired product and 4-(tert-butyl)-cyclohex-1-ene among other impurities. BH<sub>3</sub>.THF (2.00 mL, 2.0 mmol) was added forming hydroboration products which were removed by filtering through a pad of silica and washing with n-hexane. The solution was concentrated *in vacuo* and the product purified by vacuum distillation, a mixture of diastereomers (91:9, *cis:trans*) as a colourless oil (630 mg, 16 %, d = 1.23 g mL<sup>-1</sup>).

$\delta_{\text{H}}$  (400 MHz, CDCl<sub>3</sub>, 298K): 4.68 (t, 1H, <sup>3</sup>J<sub>HH</sub> = 2.9 Hz, CHBr), 2.14 (dm, 2H, <sup>3</sup>J<sub>HH</sub> = 14.9 Hz, ax(CH)<sub>2</sub>CHBr), 1.82 – 1.70 (m, 2H, eq(CH)<sub>2</sub>CHBr), 1.65 – 1.52 (m, 4H, (CH)<sub>2</sub>CHC<sup>IV</sup>), 1.07 – 0.99 (m, 1H, CHC<sup>IV</sup>), 0.88 (s, 9H, C<sup>IV</sup>(CH)<sub>3</sub>).

$\delta_{\text{C}}$  (100 MHz, CDCl<sub>3</sub>, 298K): 55.5 (s, 1C, CHBR), 48.0 (s, 1C, CHC<sup>IV</sup>), 35.5 (s, 2C, (CH)<sub>2</sub>CHBr), 32.8 (s, 1C, C<sup>IV</sup>(CH)<sub>3</sub>), 27.6 (s, 2C, (CH)<sub>2</sub>CHC<sup>IV</sup>), 21.9 (s, 2C, (CH)<sub>2</sub>CHC<sup>IV</sup>)





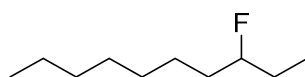
**Synthesis of 2-Butyl-1-fluorooctane:** Following a modified procedure,<sup>[45]</sup> potassium fluoride (1.50 g, 25.8 mmol) and AlkylFluor reagent (3.03 g, 6.1 mmol) were dried at 100 °C under vacuum for 1 hour in a Schlenk flask. 2-Butyl-1-octanol (820  $\mu$ L, 3.7 mmol) and dry THF (80 mL) were added and the reaction heated at 50 °C for 4 days. The mixture was cooled to room temperature then suction filtered, washing with *n*-hexane then concentrated *in vacuo* to yield an orange powder. The crude was triturated with *n*-hexane (40 mL) for 1 hour, then the insoluble material removed again via suction filtration. The filtrate was concentrated *in vacuo* forming a pale yellow liquid and a colourless precipitate. *n*-Hexane (10 mL) was added and the resultant solution filtered twice, through separate pads of silica (w x h = 2 cm x 4 cm). The colourless solution was concentrated *in vacuo* yielding 2-butyl-1-fluorooctane as a colourless liquid (0.48 mL, 60 %, d = 0.860 g mL<sup>-1</sup>).

$\delta_{\text{H}}$  (400 MHz, CDCl<sub>3</sub>, 298K): 4.33 (dd, 2H, <sup>2</sup>J<sub>HF</sub> = 47.7, <sup>3</sup>J<sub>HH</sub> = 5.3, CH<sub>2</sub>F), 1.68 – 1.56 (br m, 1H, (CH<sub>2</sub>)<sub>3</sub>CH), 1.37 – 1.24 (br m, 16H, (CH<sub>2</sub>)<sub>8</sub>), 0.93 – 0.86 (m, 6H, (CH<sub>3</sub>)<sub>2</sub>).

$\delta_{\text{C}}$  (100 MHz, CDCl<sub>3</sub>, 298K): 85.7 (d, 1C, <sup>1</sup>J<sub>CF</sub> = 170.0 Hz, CH<sub>2</sub>F), 39.0 (d, 1C, <sup>2</sup>J<sub>CF</sub> = 17.8 Hz, CH-CH<sub>2</sub>F), 31.8 (s, 1C, CH<sub>2</sub>), 30.6 (d, 1C, <sup>3</sup>J<sub>CF</sub> = 5.1 Hz, CH-CH<sub>2</sub>), 30.3 (d, 1C, <sup>3</sup>J<sub>CF</sub> = 5.1 Hz, CH-CH<sub>2</sub>), 29.7 (s, 1C, CH<sub>2</sub>), 29.0 (s, 1C, CH<sub>2</sub>), 26.8 (s, 1C, CH<sub>2</sub>), 23.0 (s, 1C, CH<sub>2</sub>), 22.7 (s, 1C, CH<sub>2</sub>), 14.0 (s, 1C, CH<sub>3</sub>), 13.09 (s, 1C, CH<sub>3</sub>).

$\delta_{\text{F}}$  (376 MHz, CDCl<sub>3</sub>, 298K): -224.9 – -225.2 (td, 1F, <sup>2</sup>J<sub>HF</sub> = 47.7, <sup>3</sup>J<sub>HF</sub> = 23.6, CH<sub>2</sub>F).

Mass spec. (EI, +ve) 168 ([M-HF]<sup>+</sup>, 50 %), 155, 111, 99; High-resolution mass spec. calc. for C<sub>12</sub>H<sub>24</sub> ([M-HF]<sup>+</sup>) 168.1878, found 168.1880.



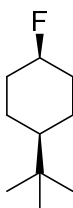
**Synthesis of 3-fluorodecane:** Following a modified procedure,<sup>[45]</sup> potassium fluoride (1.50 g, 25.8 mmol) and AlkylFluor reagent (3.70 g, 7.5 mmol) were dried at 100 °C under vacuum for 1 hour in a Schlenk flask. 3-Decanol (950  $\mu$ L, 5.0 mmol) and dry THF (80 mL) were added and the reaction heated at 50 °C for 3 days. The mixture was cooled to room temperature then suction filtrated, washing with *n*-hexane then concentrated *in vacuo* to yield an orange powder. The material was triturated with *n*-hexane (40 mL) for 1 hour then the insoluble material removed via suction filtration. The filtrate was concentrated *in vacuo* forming a pale yellow liquid and a colourless precipitate. *n*-Hexane (10 mL) was added and filtered through two pads of silica (w x h = 2 cm x 4 cm) yielding a colourless solution. Analysis by NMR spectroscopy showed a mixture including the alkyl fluoride plus dec-2-ene and dec-3-ene as elimination products. A sub stoichiometric quantity of BH<sub>3</sub>.THF (0.5 mL) was added to the crude reaction mixture and stirred for 1 hour at 22 °C forming hydroboration products. *n*-Hexane (10 mL) was added to the mixture which was then filtered through a pad of silica (w x h = 2 cm x 4 cm) and concentrated *in vacuo* giving 3-fluorodecane as a colourless liquid (0.25 mL, 26 %, d = 0.840 g mL<sup>-1</sup>).

$\delta_{\text{H}}$  (400 MHz, C<sub>6</sub>D<sub>6</sub>, 298K): 4.21 (dm, 1H, <sup>2</sup>J<sub>HF</sub> = 49.2 Hz, CHF), 1.58 – 1.14 (br m, 14H, (CH<sub>2</sub>)<sub>7</sub>), 0.90 (t, 3H, CH<sub>3</sub>), 0.88 (t, 3H, <sup>3</sup>J<sub>HH</sub> = 7.5 Hz, CH<sub>3</sub>).

$\delta_{\text{C}}$  (100 MHz, C<sub>6</sub>D<sub>6</sub>, 298K): 94.8 (d, 1C, <sup>1</sup>J<sub>CF</sub> = 168.7 Hz, CF), 34.8 (d, 1C, <sup>2</sup>J<sub>CF</sub> = 21.0 Hz, (CF)CH<sub>2</sub>), 31.8 (s, 1C, CH<sub>2</sub>), 29.5 (s, 1C, CH<sub>2</sub>), 29.3 (s, 1C, CH<sub>2</sub>), 28.1 (d, 1C, <sup>2</sup>J<sub>CF</sub> = 21.5 Hz, (CF)CH<sub>2</sub>), 25.2 (d, 1C, <sup>3</sup>J<sub>CF</sub> = 4.1 Hz, CH<sub>2</sub>), 22.7 (s, 1C, CH<sub>2</sub>), 14.0, (s, 1C, CH<sub>2</sub>), 9.3 (d, 1C, <sup>3</sup>J<sub>CF</sub> = 5.4 Hz, CF(CH<sub>2</sub>)CH<sub>3</sub>).

$\delta_{\text{F}}$  (376 MHz, C<sub>6</sub>D<sub>6</sub>, 298K): -181.2 – -182.6 (m, 1F, CHF).

Mass spec. (EI, +ve) 140 ([M-HF]<sup>+</sup>, 40 %), 111, 97; High-resolution mass spec. calc. for C<sub>10</sub>H<sub>20</sub> ([M-HF]<sup>+</sup>) 140.1565, found 140.1560.



**Synthesis of *cis*-1-fluoro-4-(*tert*-butyl)cyclohexane:** Following a modified procedure,<sup>[45]</sup> potassium fluoride (1.86 g, 32.0 mmol), caesium fluoride (4.86 g, 32.0 mmol) and AlkylFluor reagent (6.33 g, 12.8 mmol) were dried at 100 °C under vacuum for 1 hour in a Schlenk flask. 4-(*tert*-butyl)cyclohexan-1-ol (6.00 g, 6.4 mmol) (91:9, *trans*:*cis*) and dry 1,4-dioxane (100 mL) were added and the reaction heated at 80 °C for 2 days. The mixture was cooled to room temperature then suction filtered, washing with *n*-hexane then concentrated *in vacuo* to yield an orange powder. The material was triturated with *n*-hexane (40 mL) for 1 hour then the insoluble material removed via suction filtration. The filtrate was concentrated *in vacuo* forming a pale yellow liquid and a colourless precipitate. *n*-Hexane (10 mL) was added and filtered through two pads of silica (w x h = 2 cm x 4 cm) yielding a colourless solution. Analysis by NMR spectroscopy showed a mixture including the alkyl fluoride plus 4-(*tert*-butyl)cyclohex-1-ene as an elimination product. A sub stoichiometric quantity of BH<sub>3</sub>.THF (0.8 mL) was added to the crude reaction mixture and stirred for 1 hour at 22 °C forming hydroborated products. *n*-Hexane (10 mL) was added to the mixture which was then filtered through a pad of silica (w x h = 2 cm x 4 cm) and concentrated *in vacuo* giving the target compound (86:14, *cis*:*trans*) as a colourless liquid (210 mg, 21 %, d = 0.920 g mL<sup>-1</sup>).

$\delta_{\text{H}}$  (400 MHz, CDCl<sub>3</sub>, 298K): 4.81 (dm, 1H, <sup>2</sup>J<sub>HF</sub> = 48.8 Hz, CHF), 2.16 – 2.00 (m, 2H, axCH<sub>2</sub>CHF), 1.68 – 1.23 (m, 6H, eqCH<sub>2</sub>/(CH<sub>2</sub>)<sub>2</sub>CH), 1.07 – 0.98 (m, 1H, CHC<sup>IV</sup>), 0.86 (s, 9H, C<sup>IV</sup>(CH<sub>3</sub>)<sub>3</sub>)

$\delta_{\text{C}}$  (100 MHz, CDCl<sub>3</sub>, 298K): 88.9 (d, 1C, <sup>1</sup>J<sub>CF</sub> = 166.4 Hz, CHF), 47.6 (s, 1C, CHC<sup>IV</sup>), 32.7 (s, 1C, C<sup>IV</sup>(CH<sub>3</sub>)<sub>3</sub>), 31.6 (d, 2C, <sup>2</sup>J<sub>CF</sub> = 21.3 Hz, (CH<sub>2</sub>)CHF), 27.6 (s, 3C, C<sup>IV</sup>(CH<sub>3</sub>)<sub>3</sub>), 21.4 (s, 2C, (CH<sub>2</sub>)<sub>2</sub>CHC<sup>IV</sup>)

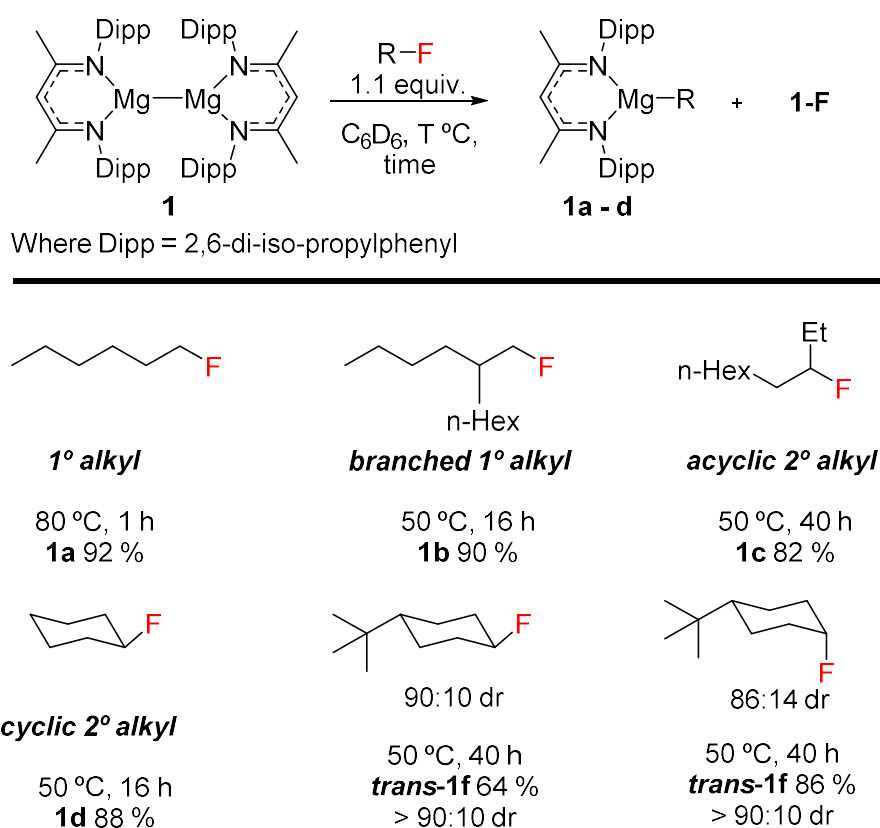
$\delta_{\text{F}}$  (376 MHz, CDCl<sub>3</sub>, 298K): -184.7 – -185.3 (m, 1F, CHF)

Mass spec. (EI, +ve) 139 ([M-HF]<sup>+</sup>, 70 %), High-resolution mass spec. calc. for C<sub>10</sub>H<sub>19</sub> ([M-HF]<sup>+</sup>) 139.1487, found 139.1491.

***trans*-1-fluoro-4-(*tert*-butyl)cyclohexane:** Synthesised using the same procedure as *cis*-1-fluoro-4-(*tert*-butyl)cyclohexane starting from 4-(*tert*-butyl)cyclohexan-1-ol (91:9, *cis*:*trans*). The product could not be purified completely. The C–F activation was performed with the crude mixture and proceeded effectively.

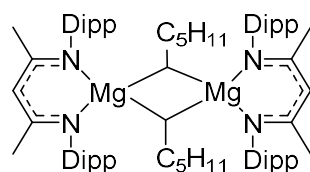
### 2.3.2. Oxidative Addition of $sp^3C-F$ Bonds to Mg–Mg Bonds

**General Procedure for Oxidative Addition of C–F bonds to Mg–Mg bonds:** **1** (10.2 mg, 0.012 mmol) or **2** (8.2 mg, 0.012 mmol) was dissolved in  $C_6D_6$  and added to a J. Young NMR tube equipped with a ferrocene capillary insert and a  $t=0$   $^1H$  NMR spectrum was recorded. Fluorocarbon (1.1 – 10 equiv.) was added and the reaction monitored over time intervals by relevant  $^1H$  and  $^{19}F$  NMR spectroscopy. Yields were recorded against an internal standard and are presented in **Scheme 2.44**. The products were confirmed by either preparative scale synthesis or independent synthesis (details below).



*Scheme 2.44 Summary of the addition of  $sp^3C-F$  bonds to Mg–Mg bonds of **1**. Yields measured by  $^1H$  NMR spectroscopy by comparison against an internal standard.*

**Note:** CHN microanalysis has been attempted for all magnesium–alkyl species, however the results have been quite a way off on every occasion. This has been noted in our group before with similar Mg–R species and may be amplified upon coordination of a labile THF molecule

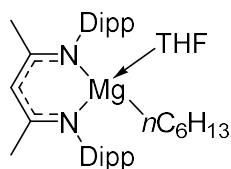


**Synthesis of 1a from C–F activation:**  $[\text{Dipp}(\text{BDI})\text{Mg}]_2$  (**1**) (200 mg, 0.22 mmol) was dissolved in toluene (10 mL) and 1-fluorohexane (35.0 mL, 0.27 mmol) was added. The reaction was heated at 80 °C for 1 hour, after which time the solvent was removed *in vacuo*. The product, **1a**, was extracted into *n*-hexane (3 mL),  $[\text{Dipp}(\text{BDI})\text{Mg}(\mu\text{-F})]_2$  (**1-F**) remained largely insoluble. The *n*-hexane fraction was transferred to the freezer and crystals of the desired product were isolated after storage of the solution at –35 °C overnight (80 mg, 0.15 mmol, 67 %).

**Independent Synthesis of 1a:** Magnesium turnings (69 mg, 2.85 mmol) were dried under reduced pressure in an ampoule. Diethyl ether (10 mL) was added, followed by 1-bromohexane (307  $\mu\text{L}$ , 2.19 mmol) and the solution heated to reflux for 3 hours. The newly formed Grignard was filtered into a solution of  $[\text{Dipp}(\text{BDI})\text{K}]$  (1.00 g, 2.19 mmol) in diethyl ether (30 mL) and left to react at 25 °C overnight, observing a colour change to pale yellow and a white precipitate. The diethyl ether was removed *in vacuo* yielding a yellow residue, which was then transferred to a glovebox. *n*-Hexane (15 mL) and a few drops of toluene were added, forming a colourless precipitate. The crude reaction mixture was transferred to a Teflon centrifuge tube and separated by centrifugation into a pale yellow liquid and white precipitate. The liquid was filtered through a glass filter and stored at –35 °C in *n*-hexane yielding the product as a pale yellow powder (629 mg, 1.19 mmol, 55 %).

$\delta_{\text{H}}$  (400 MHz,  $\text{C}_6\text{D}_6$ , 298K): 7.11 (s, 6H, ArH), 4.94 (s, 1H,  $\text{C}(\text{CH}_3)\text{CH}(\text{CH}_3)\text{C}$ ), 3.21 – 3.15 (m, 4H,  $^3J_{\text{HH}} = 6.9$  Hz,  $\text{CH}(\text{CH}_3)_2$ ), 1.67 (s, 6H,  $\text{CHC}(\text{CH}_3)_2$ ), 1.36 (sept, 2H,  $^3J_{\text{HH}} = 7.6$  Hz,  $(\text{CH}_2)_4$ ), 1.28 (d, 12H,  $^3J_{\text{HH}} = 6.9$  Hz,  $\text{CH}(\text{CH}_3)_2$ ), 1.18 (br m, 4H,  $(\text{CH}_2)_4$ ), 1.16 (d, 12H,  $^3J_{\text{HH}} = 6.9$  Hz,  $\text{CH}(\text{CH}_3)_2$ ), 1.01 (br m, 2H,  $(\text{CH}_2)_4$ ), 0.87 (t, 3H,  $(\text{CH}_2)_5\text{CH}_3$ ), –0.22 (t, 2H,  $^3J_{\text{HH}} = 7.9$  Hz  $\text{MgCH}_2$ ).

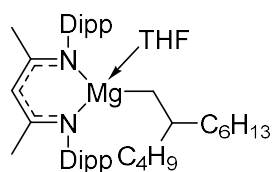
$\delta_{\text{C}}$  (100 MHz,  $\text{C}_6\text{D}_6$ , 298K): 169.3 (s, 2C,  $\text{CHC}(\text{CH}_3)_2$ ), 143.9 (s, 2C, *ipso*– $\text{C}^{\text{IV}}$ ), 141.9 (s, 2C, *o*– $\text{C}^{\text{IV}}$ ), 126.0 (s, 4C, *p*–CH), 124.1 (s, 4C, *m*–CH), 95.4 (s, 1C,  $\text{C}(\text{CH}_3)\text{CH}(\text{CH}_3)\text{C}$ ), 38.1 (s, 1C,  $\text{CH}_2$ ), 32.4 (s, 1C,  $\text{CH}_2$ ), 28.8 (s, 1C,  $\text{CH}_2$ ), 28.7 ( $\text{CH}(\text{CH}_3)_2$ ), 24.7 ( $\text{C}(\text{CH}_3)$ ), 23.6 (s, 1C,  $\text{CH}_2$ ), 23.5 ( $\text{CH}(\text{CH}_3)_2$ ), 23.2 (s, 1C,  $\text{CH}_2$ ), 14.6 (s, 1C,  $(\text{CH}_2)_5\text{CH}_3$ ), 5.9 ( $\text{MgCH}_2$ ).



**Independent Synthesis of 1a.THF:** Magnesium turnings (69 mg, 2.85 mmol) were dried under reduced pressure in an ampoule. THF (10 mL) was added, followed by 1-bromohexane (307  $\mu$ L, 2.19 mmol) and the solution heated to reflux for 3 hours. The newly formed Grignard was filtered into a solution of [Dipp(BDI)K] (1.00 g, 2.19 mmol) in THF (30 mL) and left to react at 22 °C for 22 hours, a colour change to pale yellow was observed and a white precipitate formed. The solvent was removed *in vacuo* yielding a yellow residue. n-Hexane (20 mL) was added and the mixture stirred for 4 hours. The solution was filtered by cannula, concentrated *in vacuo* and the product crystallised over 24 hours at -35 °C yielding colourless crystals of **1a.THF** (856 mg, 65 %).

$\delta_{\text{H}}$  (400 MHz,  $\text{C}_6\text{D}_6$ , 298K): 4.81 (s, 1H,  $\text{C}(\text{CH}_3)\text{CH}(\text{CH}_3)\text{C}$ ), 3.68 (br t, 4H,  $\text{O}(\text{CH}_2)_2$ ), 3.35 – 3.25 (m, 4H,  $\text{CH}(\text{CH}_3)_2$ ), 1.66 (s, 6H,  $\text{CHC}(\text{CH}_3)_2$ ), 1.55 – 1.48 (m, 2H,  $\text{CH}_2$ ), 1.37 – 1.17 (br m, 10H,  $(\text{CH}_2)_5$ ), 1.31 (d, 12H,  $^3J_{\text{HH}} = 6.7$  Hz,  $\text{CH}(\text{CH}_3)_2$ ), 1.24 (d, 12H,  $^3J_{\text{HH}} = 6.8$  Hz,  $\text{CH}(\text{CH}_3)_2$ ), 0.91 (t, 3H,  $^3J_{\text{HH}} = 6.9$  Hz,  $(\text{CH}_2)_5\text{CH}_3$ ), -0.35 (t, 2H,  $^3J_{\text{HH}} = 8.0$  Hz,  $\text{MgCH}_2$ )

$\delta_{\text{C}}$  (100 MHz,  $\text{C}_6\text{D}_6$ , 298K): 167.6 (s, 2C,  $\text{CHC}(\text{CH}_3)_2$ ), 145.8 (s, 2C, *ipso*- $\text{C}^{\text{IV}}$ ), 142.0 (s, 4C, *o*- $\text{C}^{\text{IV}}$ ), 124.8 (s, 2C, *p*- $\text{CH}$ ), 123.5 (s, 4C, *m*- $\text{CH}$ ), 94.3 (s, 1C,  $\text{C}(\text{CH}_3)\text{CH}(\text{CH}_3)\text{C}$ ), 69.6 (s, 2C,  $\text{THF-OCH}_2$ ), 38.7 (s, 1C,  $\text{CH}_2$ ), 32.3 (s, 1C,  $\text{CH}_2$ ), 29.9 (s, 1C,  $\text{CH}_2$ ), 27.9 (s, 4C,  $\text{CH}(\text{CH}_3)_2$ ), 25.0 (s, 2C,  $\text{THF-(CH}_2)_2$ ), 24.9 (s, 4C,  $\text{CH}(\text{CH}_3)_2$ ), 24.2 (s, 4C,  $\text{CH}(\text{CH}_3)_2$ ), 23.8 (s, 2C,  $\text{C}^{\text{IV}}\text{CH}_3$ ), 23.0 (s, 1C,  $\text{CH}_2$ ), 14.4 (s, 1C,  $(\text{CH}_2)_5\text{CH}_3$ ), 5.8 (s, 1C,  $\text{MgCH}_2$ ).

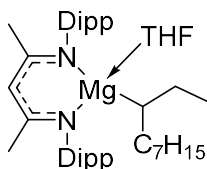


**Independent Synthesis of **1b**.THF:** In a Schlenk flask and under an argon atmosphere, 2-butyl-1-octylbromide (525  $\mu$ L, 2.19 mmol) was added to a suspension of magnesium turnings (153 mg, 6.30 mmol) in THF (15 mL) and the solution heated to reflux for 4 hours. The newly formed Grignard was filtered onto a solution of [Dipp(BDI)K] (1.00 g, 2.19 mmol) in THF (15 mL) and stirred for 20 hours at 22  $^{\circ}$ C. The solvent was removed *in vacuo* then *n*-hexane (30 mL) was added and the suspension stirred for 4 hours. The precipitate was allowed to settle and the yellow solution was transferred to a separate Schlenk flask via cannula filtration. The solution was concentrated to approx. 1/5 volume and the product allowed to crystallise overnight at -35  $^{\circ}$ C. **1b**.THF (165 mg, 11 %) was isolated as a colourless solid by filtration.

$\delta_{\text{H}}$  (400 MHz,  $\text{C}_6\text{D}_6$ , 298K): 7.18 (app s, 6H ArH), 4.80 (s, 1H,  $(\text{CH}_3)\text{C}_2\text{CH}$ ), 3.75 (br t, 4H, THF-OCH<sub>2</sub>), 3.27 (br m, 4H,  $^3J_{\text{HH}} = 6.6$  Hz,  $\text{CH}(\text{CH}_3)_2$ ), 1.64 (s, 6H,  $(\text{C}^{\text{V}}\text{CH}_3)_2$ ), 1.58 (br m, 1H,  $\text{CH}(\text{CH}_2)_3$ ), 1.40 – 1.14 (br m, 16H,  $(\text{CH}_2)_8$ ), 1.35 (d, 12H,  $^3J_{\text{HH}} = 6.8$  Hz,  $\text{CH}(\text{CH}_3)_2$ ), 1.23 (d, 12H,  $^3J_{\text{HH}} = 6.8$  Hz,  $\text{CH}(\text{CH}_3)_2$ ), 0.98 – 0.90 (m, 6H,  $(\text{CH}_3)_2$ ), -0.32 (d, 2H,  $^3J_{\text{HH}} = 6.6$  Hz,  $\text{MgCH}_2$ ).

$\delta_{\text{C}}$  (100 MHz,  $\text{C}_6\text{D}_6$ , 298K): 167.6 (s, 2C,  $\text{CHC}(\text{CH}_3)$ ), 146.0 (s, 2C, *ipso*-C<sup>IV</sup>), 141.9 (s, 4C, *o*-C<sup>IV</sup>), 124.9 (s, 2C, *p*-CH), 123.5 (s, 4C, *m*-CH), 94.6 (s, 1C,  $(\text{C}(\text{CH}_3)\text{CH}(\text{CH}_3)\text{C})$ ), 69.8 (s, 2C, THF-OCH<sub>2</sub>), 41.8 (s, 1C, CH<sub>2</sub>), 41.4 (s, 1C, CH<sub>2</sub>), 38.3 (s, 1C, CH(CH<sub>2</sub>)<sub>2</sub>), 32.4 (s, 1C, CH<sub>2</sub>), 30.2 (s, 1C, CH<sub>2</sub>), 30.1 (s, 1C, CH<sub>2</sub>), 27.9 (s, 4C, CH(CH<sub>3</sub>)<sub>2</sub>), 27.9 (s, 1C, CH<sub>2</sub>), 25.1 (s, 2C, THF-(CH<sub>2</sub>)<sub>2</sub>), 24.8 (s, 4C, CH(CH<sub>3</sub>)<sub>2</sub>), 24.3 (s, 4C, CH(CH<sub>3</sub>)<sub>2</sub>), 23.9 (s, 2C, C<sup>IV</sup>CH<sub>3</sub>), 23.4 (s, 1C, CH<sub>2</sub>), 23.0 (s, 1C, CH<sub>2</sub>), 14.5 (s, 1C, CH<sub>3</sub>), 14.2 (s, 1C, CH<sub>2</sub>), 14.2 (s, 1C, MgCH<sub>2</sub>).

The composition of **1b**, formed from C–F activation, was confirmed by spiking a sample with THF and comparing the data against those of the independently synthesised complex **1b**.THF described above.



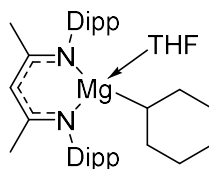
**Independent Synthesis of 1c.THF:** In a Schlenk flask and under an argon atmosphere, 3-bromodecane (484 mg, 2.19 mmol) was added to suspension of magnesium turnings (153 mg, 6.30 mmol) in THF (15 mL) and the solution heated to reflux for 4 hours. The newly formed Grignard was filtered onto a solution of [Dipp(BDI)K] (1.00 g, 2.19 mmol) in THF (15 mL) and stirred for 20 hours at 22 °C. The solvent was removed *in vacuo* then n-hexane (30 mL) was added and the suspension stirred for 4 hours. The precipitate was allowed to settle and the yellow solution was transferred to a separate Schlenk flask via cannula filtration. The solution was concentrated to approx. 1/5 volume and the product allowed to crystallise overnight at -35 °C. **1c.THF** (298 mg, 21 %) was isolated as a colourless solid by filtration.

$\delta_{\text{H}}$  (400 MHz,  $\text{C}_6\text{D}_6$ , 298K): 7.19 (app s, 6H, ArH), 4.80 (s, 1H,  $((\text{CH}_3)\text{C})_2\text{CH}$ ), 3.75 (br t, 4H,  $\text{THF-OCH}_2$ ), 3.30 – 3.21 (br m, 4H,  $\text{CH}(\text{CH}_3)_2$ ), 1.67 (s, 6H,  $(\text{C}^{\text{V}}\text{CH}_3)_2$ ), 1.60 – 1.10 (br m, 18H,  $(\text{CH}_2)_9$ ), 1.34 (d, 12H,  $^3J_{\text{HH}} = 6.2$  Hz,  $\text{CH}(\text{CH}_3)_2$ ), 1.23 (d, 12H,  $^3J_{\text{HH}} = 6.8$  Hz,  $\text{CH}(\text{CH}_3)_2$ ), 0.96 (t, 3H,  $\text{CH}(\text{CH}_2)\text{CH}_3$ ), 0.76 (t, 3H,  $(\text{CH}_2)_6\text{CH}_3$ ), -0.06 (pent, 1H,  $^3J_{\text{HH}} = 7.1$  Hz,  $\text{MgCH}$ ).

$\delta_{\text{C}}$  (100 MHz,  $\text{C}_6\text{D}_6$ , 298K): 167.6 (s, 2C,  $\text{CHC}(\text{CH}_3)$ ), 146.3 (s, 2C, *ipso*- $\text{C}^{\text{IV}}$ ), 141.9 (s, 4C, *o*- $\text{C}^{\text{IV}}$ ), 124.9 (s, 2C, *p*- $\text{CH}$ ), 123.6 (s, 4C, *m*- $\text{CH}$ ), 94.3 (s, 1C,  $(\text{C}(\text{CH}_3)\text{CH}(\text{CH}_3)\text{C})$ ), 69.6 (s, 2C,  $\text{THF-OCH}_2$ ), 36.0 (s, 1C,  $\text{CH}_2$ ), 32.6 (s, 1C,  $\text{CH}_2$ ), 32.4 (s, 1C,  $\text{CH}_2$ ), 30.8 (s, 1C,  $\text{CH}_2$ ), 29.7 (s, 1C,  $\text{CH}_2$ ), 28.3 (s, 1C,  $\text{CH}_2$ ), 28.0 (s, 4C,  $\text{CH}(\text{CH}_3)_2$ ), 26.9 (s, 1C,  $\text{MgCH}_2$ ), 25.1 (s, 2C,  $\text{THF-CH}_2(\text{CH}_2)_2$ ), 24.5 (s, 4C,  $\text{CH}(\text{CH}_3)_2$ ), 24.3 (s, 4C,  $\text{CH}(\text{CH}_3)_2$ ), 24.0 (s, 2C,  $\text{C}^{\text{IV}}\text{CH}_3$ ), 22.3 (s, 1C,  $\text{CH}_2$ ), 17.0 (s, 1C,  $(\text{CHCH}_2)\text{CH}_3$ ), 14.2 (s, 1C,  $(\text{CH}_2)_6\text{CH}_3$ ).

The composition of **1c**, formed from C–F activation, was confirmed by spiking a sample with THF and comparing the data against those of the independently synthesised complex **1c.THF** described above.



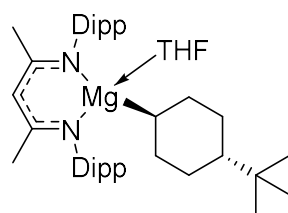


**Independent Synthesis of 1d.THF** Magnesium turnings (160 mg, 6.58 mmol) were dried under reduced pressure in an ampoule. THF (10 mL) was added, followed by bromocyclohexane (270  $\mu$ L, 2.19 mmol) and the solution heated to reflux for 3 hours. The newly formed Grignard was filtered into a solution of [Dipp(BDI)K] (1.00 g, 2.19 mmol) in THF (30 mL) and left to react at 25 °C overnight, a colour change to pale yellow was observed and a white precipitate formed. The solvent was removed *in vacuo* yielding a yellow residue. n-Hexane (20 mL) was added and the mixture stirred for 4 hours. The solution was filtered, concentrated *in vacuo* and the product crystallised over 24 hours at -35 °C yielding colourless crystals of **1d.THF** (540 mg, 41 %).

$\delta_{\text{H}}$  (400 MHz,  $\text{C}_6\text{D}_6$ , 298K): 7.18 (app s, 6H, ArH), 4.78 (s, 1H,  $((\text{CH}_3)\text{C})_2\text{CH}$ ), 3.75 (br t, 4H, THF-OCH<sub>2</sub>), 3.27 (br m, 4H, CH(CH<sub>3</sub>)<sub>2</sub>), 1.64 (s, 6H,  $\text{C}^{\text{IV}}\text{CH}_3$ ), 1.34 (d, 12H,  $^3J_{\text{HH}} = 6.6$  Hz, CH(CH<sub>3</sub>)<sub>2</sub>), 1.23 (d, 12H,  $^3J_{\text{HH}} = 6.8$  Hz, CH(CH<sub>3</sub>)<sub>2</sub>), 0.18 (t, 1H,  $^3J_{\text{HH}} = 11.0$  Hz, MgCH).

$\delta_{\text{C}}$  (100 MHz,  $\text{C}_6\text{D}_6$ , 298K): 167.6 (s, 2C, CHC(CH<sub>3</sub>)), 145.8 (s, 2C, ipso-C<sup>IV</sup>), 141.9 (s, 4C, o-C<sup>IV</sup>), 124.9 (s, 2C, p-CH), 123.4 (s, 4C, m-CH), 94.4 (s, 1C,  $\text{C}(\text{CH}_3)\text{CH}(\text{CH}_3)\text{C}$ ), 69.8 (s, 2C, THF-OCH<sub>2</sub>), 34.8 (s, 2C, CH<sub>2</sub>), 32.1 (s, 2C, CH<sub>2</sub>), 29.3 (s, 1C, 4-CH<sub>2</sub>), 28.0 (s, 4C, CH(CH<sub>3</sub>)<sub>2</sub>), 25.1 (s, 2C, THF-CH<sub>2</sub>(CH<sub>2</sub>)<sub>2</sub>), 24.8 (s, 4C, CH(CH<sub>3</sub>)<sub>2</sub>), 24.3 (s, 1C, MgCH), 24.2 (s, 4C, CH(CH<sub>3</sub>)<sub>2</sub>), 23.7 (s, 2C, C<sup>IV</sup>CH<sub>3</sub>).

The composition of **1d**, formed from C–F activation, was confirmed by spiking a sample with THF and comparing the data against those of the independently synthesised complex **1d.THF** described above.



**Independent Synthesis of *trans-1f*.THF:** Magnesium turnings (200 mg, 8.30 mmol) were dried under reduced pressure in an ampoule. THF (15 mL) was added, followed by *cis*-1-bromo-4-(tert-butyl)cyclohexane (500 mg, 2.28 mmol) and the solution heated to reflux for 5 hours. The newly formed Grignard was filtered into a solution of [Dipp(BDI)K] (1.10 g, 2.30 mmol) in THF (25 mL) and left to react at 25 °C overnight, a colour change to pale yellow was observed and a white precipitate formed. The solvent was removed *in vacuo* yielding a yellow residue. *n*-Hexane (30 mL) was added and the mixture stirred for 4 hours. The solution was filtered, concentrated *in vacuo* and the product crystallised over 24 hours at -35 °C yielding colourless crystals of ***trans-1f*.THF** (310 mg, 21 %).

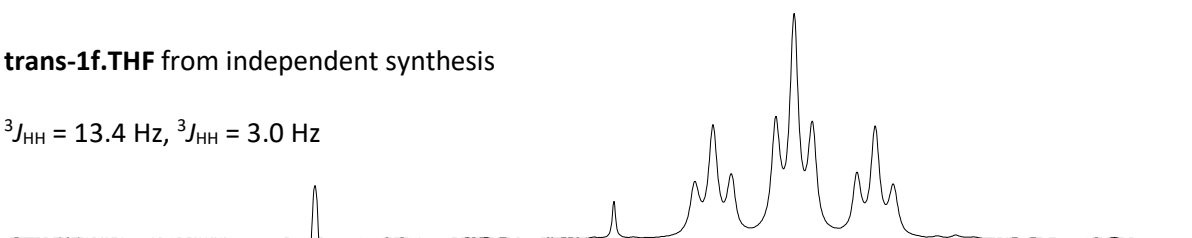
$\delta_{\text{H}}$  (400 MHz, C<sub>6</sub>D<sub>6</sub>, 298K): 7.18 (app s, 6H, ArH), 4.78 (s, 1H, ((CH<sub>3</sub>)C)<sub>2</sub>CH), 3.77 (br t, 4H, THF-OCH<sub>2</sub>), 3.26 (br m, 4H, CH(CH<sub>3</sub>)<sub>2</sub>), 1.82 – 1.73 (m, 2H, <sub>ax</sub>CH), 1.71 – 1.63 (m, 2H, <sub>ax</sub>CH), 1.40 – 1.20 (brm, 4H, <sub>eq</sub>CH), 1.34 (d, 12H, <sup>3</sup>J<sub>HH</sub> = 6.9 Hz, CH(CH<sub>3</sub>)<sub>2</sub>), 1.23 (d, 12H, <sup>3</sup>J<sub>HH</sub> = 6.9 Hz, CH(CH<sub>3</sub>)<sub>2</sub>), 1.07 (tt, 1H, <sup>3</sup>J<sub>HH</sub> = 11.8 Hz, <sup>3</sup>J<sub>HH</sub> = 2.8 Hz, CHC<sup>IV</sup>(CH<sub>3</sub>)<sub>3</sub>), 0.83 (s, 9H, C<sup>IV</sup>(CH<sub>3</sub>)<sub>3</sub>), -0.11 (tt, 1H, <sup>3</sup>J<sub>HH</sub> = 13.4 Hz, <sup>3</sup>J<sub>HH</sub> = 3.0 Hz, MgCH).

$\delta_{\text{C}}$  (100 MHz, C<sub>6</sub>D<sub>6</sub>, 298K): 168.0 (s, 2C, CHC(CH<sub>3</sub>)), 146.1 (s, 2C, *ipso*-C<sup>IV</sup>), 142.4 (s, 4C, *o*-C<sup>IV</sup>), 125.3 (s, 2C, *p*-CH), 123.8 (s, 4C, *m*-CH), 94.7 (s, 1C, (C(CH<sub>3</sub>)CH(CH<sub>3</sub>)C), 70.2 (s, 2C, THF-OCH<sub>2</sub>), 50.7 (s, 1C, CHC<sup>IV</sup>(CH<sub>3</sub>)<sub>3</sub>), 35.8 (s, 2C, CH<sub>2</sub>), 33.2 (s, 2C, CH<sub>2</sub>), 32.8 (s, 1C, C<sup>IV</sup>(CH<sub>3</sub>)<sub>3</sub>), 28.3 (s, 4C, CH(CH<sub>3</sub>)<sub>2</sub>), 27.8 (s, 3C, C<sup>IV</sup>(CH<sub>3</sub>)<sub>3</sub>), 25.5 (s, 2C, THF-CH<sub>2</sub>(CH<sub>2</sub>)<sub>2</sub>), 25.2 (s, 4C, CH(CH<sub>3</sub>)<sub>2</sub>), 24.5 (s, 4C, CH(CH<sub>3</sub>)<sub>2</sub>), 24.1 (s, 2C, C<sup>IV</sup>CH<sub>3</sub>), 23.7 (s, 1C, MgCH).

The composition of ***trans-1f***, formed from C–F activation of *cis* and *trans*-1-fluoro-4-(tert-butyl)cyclohexane, was confirmed by spiking a sample with THF and comparing the data against those of the independently synthesised complex ***trans-1f*.THF** described above.

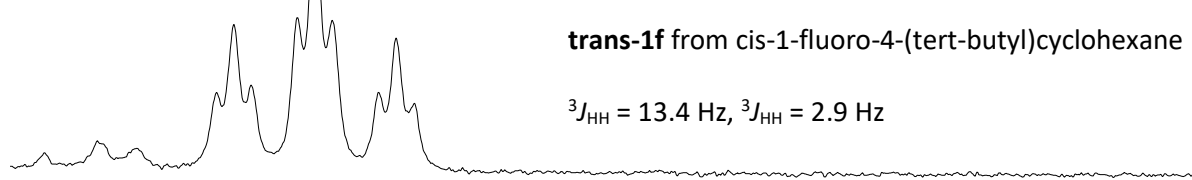
**trans-1f.THF** from independent synthesis

$^3J_{\text{HH}} = 13.4 \text{ Hz}$ ,  $^3J_{\text{HH}} = 3.0 \text{ Hz}$



**trans-1f** from cis-1-fluoro-4-(tert-butyl)cyclohexane

$^3J_{\text{HH}} = 13.4 \text{ Hz}$ ,  $^3J_{\text{HH}} = 2.9 \text{ Hz}$



**trans-1f** from trans-1-fluoro-4-(tert-butyl)cyclohexane

$^3J_{\text{HH}} = 13.4 \text{ Hz}$ ,  $^3J_{\text{HH}} = 2.9 \text{ Hz}$

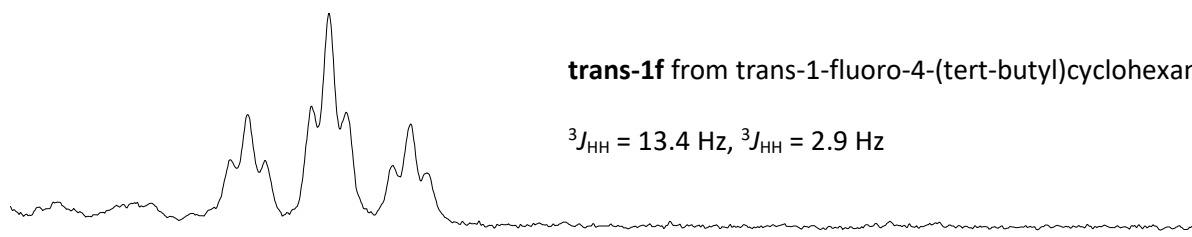
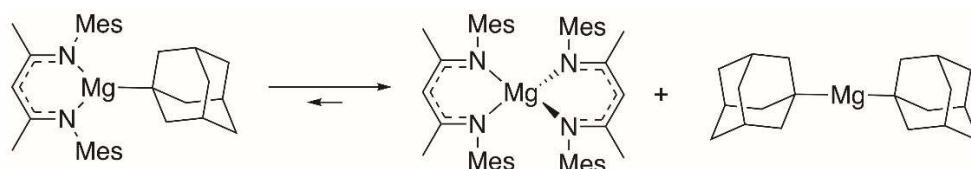


Figure 2.13  $^1\text{H}$  NMR spectra stack plot showing  $\text{MgCH}$  resonance (0.09, tt, 1H) of **trans-1f** upon C-F activation of cis (top) and trans-1-fluoro-4-(tert-butyl)cyclohexane. No intermediate species were observed by  $^1\text{H}$  NMR spectroscopy to indicate the formation of **cis-1f**



**C–F Activation of 1-fluoroadamantane: 2** (8.2 mg, 0.012 mmol) was dissolved in C<sub>6</sub>D<sub>6</sub> (0.6 mL) and added to a J. Young NMR tube equipped with a ferrocene internal standard capillary, then a  $t = 0$  <sup>1</sup>H NMR spectrum recorded. 1-Fluoroadamantane (2.0 mg, 0.013 mmol) was added to the solution and the reaction monitored by <sup>1</sup>H NMR spectroscopy at 22 °C for 16 hours, whereby full conversion of **2** was realised. Upon analysis of the <sup>1</sup>H NMR spectrum, a Schlenk-like ligand redistribution reaction was identified. The homoleptic magnesium species [<sup>Mes</sup>(BDI)<sub>2</sub>Mg] was confirmed by comparison with the literature.<sup>[69]</sup> The other redistributed product [Mg(1-Ad)<sub>2</sub>] (1-Ad = 1-adamantyl) could not be identified spectroscopically, but was confirmed upon reaction with HBpin (see **2.3.4, Preparation of 1-adamantylBpin**).

Data for [<sup>Mes</sup>(BDI)<sub>2</sub>Mg]: δ<sub>H</sub> (400 MHz, C<sub>6</sub>D<sub>6</sub>, 298K): 6.76 (s, 8H, ArH), 4.96 (s, 2H, ((CH<sub>3</sub>)<sub>2</sub>CH)), 2.22 (s, 12H, (C<sup>IV</sup>CH<sub>3</sub>)<sub>2</sub>), 1.94 (s, 24H, *ortho*-C<sup>IV</sup>CH<sub>3</sub>), 1.55 (s, 12H, *para*-C<sup>IV</sup>CH<sub>3</sub>).

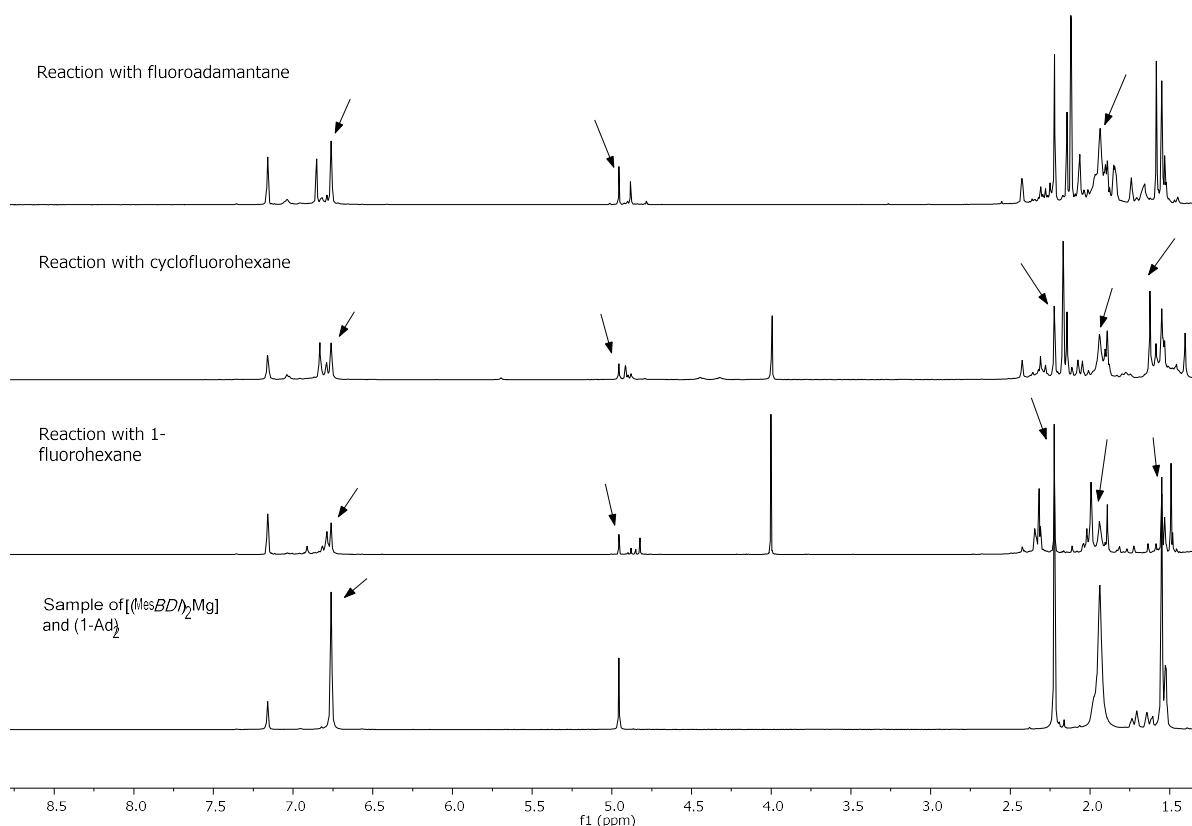


Figure 2.14 <sup>1</sup>H NMR spectra from reactions showing formation of [<sup>Mes</sup>(BDI)<sub>2</sub>Mg] (shown by arrows) upon reaction of **2** with 1°, 2° and 3° fluorocarbons and compared to crystallographically identified species (the latter is contaminated with small amounts of a C–C coupled product [1-Ad]<sub>2</sub>)

### 2.3.3 $sp^3C-F$ activation in the presence of external 'poisons'

**General procedure for the  $sp^3C-F$  activation of 1-fluorohexane in the presence of an external 'poison':** **1** (10.2 mg, 0.012 mmol) was dissolved in  $C_6D_6$  and added to a J. Young NMR tube equipped with a ferrocene capillary insert and a  $t=0$   $^1H$  NMR spectrum was recorded. 1-Fluorohexane (1.7  $\mu L$ , 1.1 equiv.) and competing substrate (x equiv.) was added to the NMR tube and a  $t=1$   $^1H$  NMR spectrum recorded within 15 minutes. The reaction was heated at 80  $^\circ C$  for the stated duration then a  $t=2$   $^1H$  and  $^{19}F$  NMR spectrum recorded. The yield was determined *in situ* upon comparison to the ferrocene internal standard.

### 2.3.4. $sp^3C-F$ to $sp^3C-B$ , $sp^3C-Si$ , and $sp^3C-Sn$ Bond Transformations

**Preparation of 1-Bpin-adamantane: 2** (8.2 mg, 0.012 mmol) was dissolved in  $C_6D_6$  (0.6 mL) and added to a J. Young NMR tube equipped with a ferrocene internal standard capillary, then a  $t=0$   $^1H$  NMR spectrum recorded. 1-Fluoroadamantane (2.0 mg, 0.013 mmol) was added and the reaction was monitored by  $^1H$  NMR spectroscopy at 22 °C. After 16 hours, full conversion of **2** was realised. Pinacolborane (HBpin) (3.4  $\mu$ L, 0.023 mmol) was added, recording  $^1H$  and  $^{11}B$  NMR spectra within 15 minutes. The target product was confirmed by a singlet resonance at  $\delta = 1.05$  ppm and  $\delta = 33.9$  ppm in the  $^1H$  and  $^{11}B$  NMR spectra respectively, which were in accordance with the literature.<sup>[52]</sup> The yield (69 %) was detected by the *in situ* comparison of the new singlet resonance in the  $^1H$  NMR spectrum at 1.05 ppm (12H) to the ferrocene internal capillary.

Mass spec. (EI, +ve) 262 ( $[M]^+$  = 1-Bpin-adamantane, 50 %).

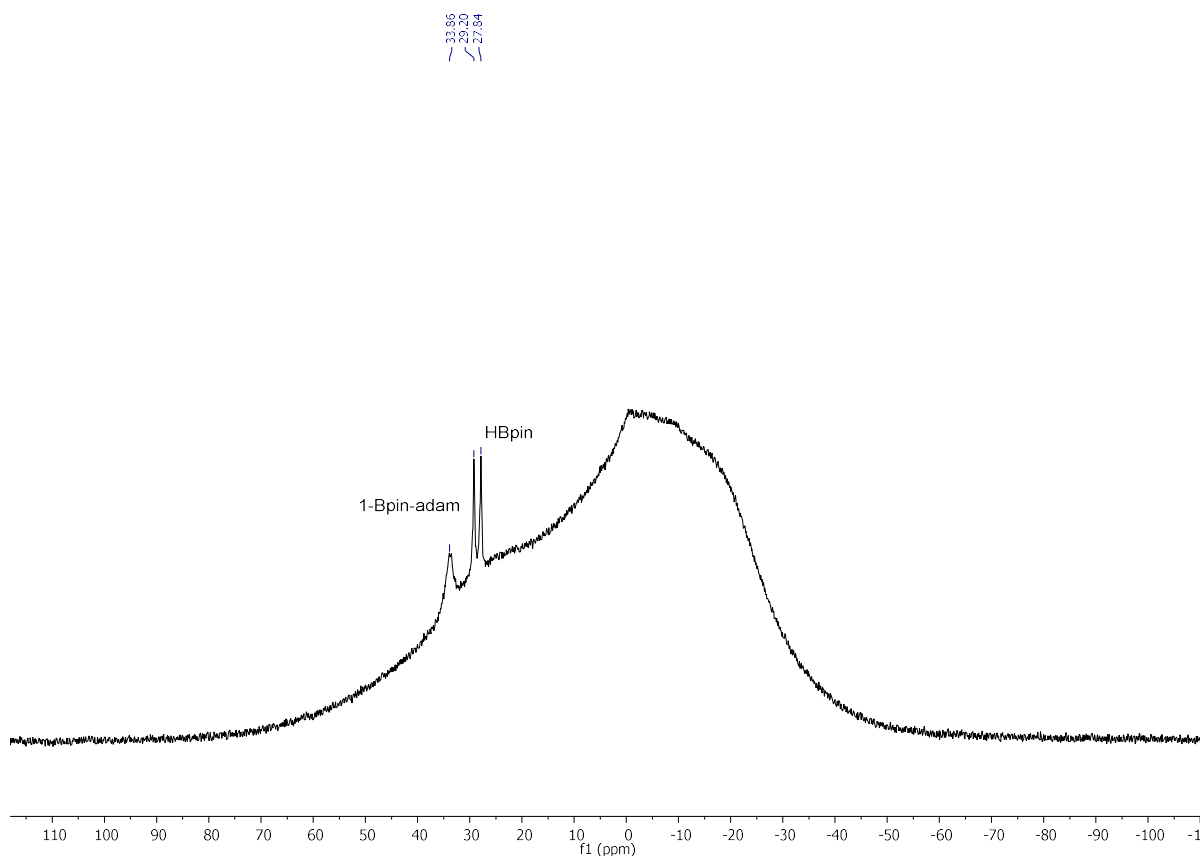
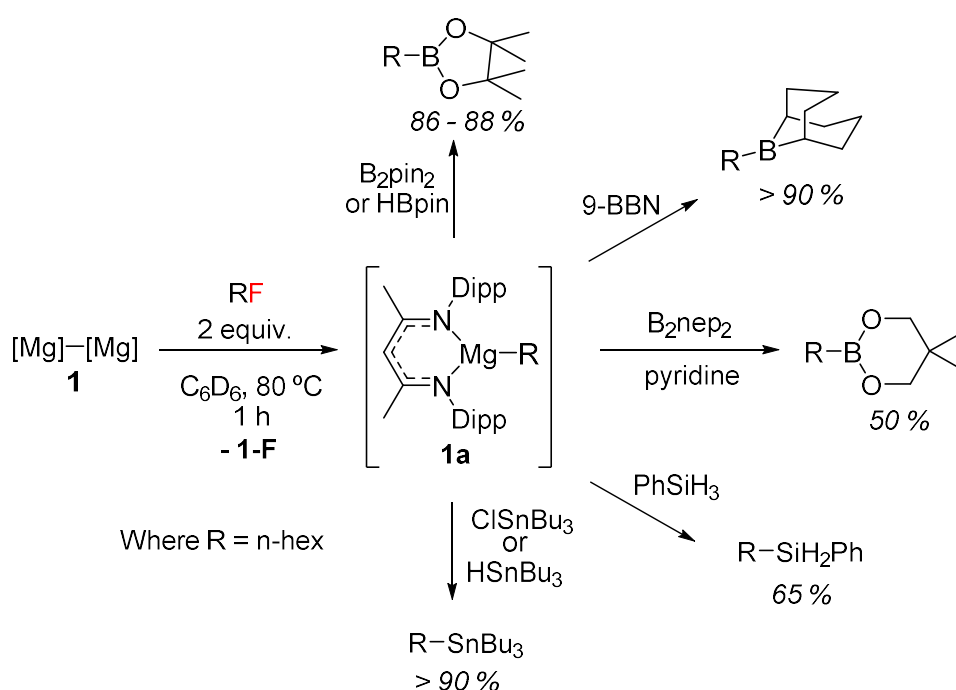


Figure 2.15  $^{11}B$  NMR spectrum showing formation of 1-Bpin-adamantane upon reaction of 1-fluoroadamantane with **2** followed by addition of HBpin

**General procedure for the in situ generation of **1a** for C–F to C–B, C–Si and C–Sn Bond transformation:** **1** (10.2 mg, 0.012 mmol) was dissolved in C<sub>6</sub>D<sub>6</sub> and added to a J. Young NMR tube equipped with a ferrocene capillary insert and a t=0 <sup>1</sup>H NMR spectrum was recorded. 1-Fluorohexane (3.0 μL, 2 equiv.) was added and the reaction heated at 80 °C for 1 hour. A t=1 <sup>1</sup>H NMR was recorded, noting the yield for C–F activation step by integral comparison to the internal standard. The electrophile reagent (x equiv.), where liquid, was added directly to the J. Young NMR tube and <sup>1</sup>H (plus <sup>11</sup>B or <sup>119</sup>Sn) NMR spectra recorded immediately. Where solid, the electrophile reagent (x equiv.) was dissolved in known quantity of C<sub>6</sub>D<sub>6</sub> and added directly to the J. Young NMR, recording the concentration change. The reaction was monitored over time intervals by the relevant NMR spectroscopy and yields measured by comparison to the internal standard.



Scheme 2.45 Derivatisation of **1a** upon reaction with electrophiles

**Preparation of *n*-hexylBPin (Method A):** Pinacolborane (HBpin) (3.6  $\mu$ L, 0.023 mmol, 2 equiv.) was added to an *in situ* generated solution of **1a** from **1** in  $C_6D_6$  (0.6 mL), monitoring the reaction by  $^1H$  and  $^{11}B$  NMR spectroscopy. After 15 minutes at 22  $^\circ C$ , full conversion of **1a** was observed, indicated by the loss of corresponding Mg-CH<sub>2</sub> resonance at  $\delta = -0.22$  ppm in the  $^1H$  NMR spectrum. The product 2-hexyl-4,4,5,5-tetramethyl-1,3,2-dioxaborolane (>90 % NMR yield) was confirmed by the observation of new resonances at  $\delta = 1.07$  ppm and  $\delta = 34.5$  ppm in the  $^1H$  and  $^{11}B$  NMR spectra respectively, which were in accordance with an independently synthesised sample.

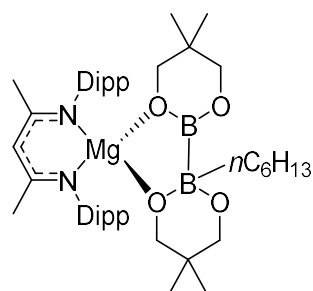
**Preparation of *n*-hexylBPin (Method B):** A stock solution of bis(pinacolato)diboron ( $B_2pin_2$ ) in  $C_6D_6$  (50  $\mu$ L, 0.023 mmol, 2 equiv.) was added to an *in situ* generated solution of **1a** from **1** in  $C_6D_6$  (0.6 mL) and the reaction heated to 80  $^\circ C$  for 1 hour. The reaction mixture was analysed by  $^1H$  and  $^{11}B$  NMR spectroscopy. The product 2-hexyl-4,4,5,5-tetramethyl-1,3,2-dioxaborolane (>85 % NMR yield) was confirmed by the observation of new resonances at  $\delta = 1.07$  ppm and  $\delta = 34.5$  ppm in the  $^1H$  and  $^{11}B$  NMR spectra respectively, which were in accordance with an independently synthesised sample.

**Preparation of *n*-hexyl-9-BBN:** 9-Borabicyclo(3.3.1)nonane (9-BBN) (2.8 mg, 0.023 mmol, 2 equiv.) was added to an *in situ* generated solution of **1a** from **1** in  $C_6D_6$  (0.6 mL), and the reaction monitored by  $^1H$  and  $^{11}B$  NMR spectroscopy. After 24 hours at 22  $^\circ C$ , full conversion of **1a** was observed, indicated by the loss of corresponding Mg-CH<sub>2</sub> triplet resonance at  $\delta = -0.22$  ppm in the  $^1H$  NMR spectrum. The product, 9-hexyl-9-borabicyclo[3.3.1]nonane (>95 % NMR conversion) was confirmed by a new resonance at  $\delta = 88.6$  ppm in the  $^{11}B$  NMR spectrum, which was in accordance with the literature.<sup>[55]</sup>

**Preparation of *n*-hexylBnep:** A stock solution of bis(neopentyl glycolato)diboron ( $B_2nep_2$ ) in  $C_6D_6$  (50  $\mu$ L, 0.023 mmol, 2 equiv.) was added to an *in situ* generated solution of **1a** from **1** in  $C_6D_6$  (0.6 mL) followed by pyridine (4.7  $\mu$ L, 0.575 mmol, 5 equiv.) and the reaction heated to 50  $^\circ C$  for 48 hours. The reaction mixture was analysed by  $^1H$  and  $^{11}B$  NMR spectroscopy. The product 2-hexyl-5,5-dimethyl-1,3,2-dioxaborinane was confirmed by the observation of new resonances  $\delta = 3.30$  ppm and  $\delta = 0.60$  ppm in the  $^1H$  NMR spectrum and 30.7  $^{11}B$  NMR spectra, which were in accordance with an independently synthesised sample.

Compound **6** was observed as an intermediate in this reaction upon addition of  $B_2nep_2$  at 22  $^\circ C$  to an *in situ* solution of **1a**.





**Independent Synthesis of compound 6:** Bis(neopentyl glycolato)diboron ( $B_2nep_2$ ) (51.6 mg, 0.23 mmol, 1.0 equiv.) was added to a solution **1a** (122 mg, 0.23 mmol) in toluene (6 mL) and stirred for 30 minutes at 22 °C. The toluene was removed *in vacuo* and the product recrystallised at -35 °C from *n*-hexane (~5 mL) yielding colourless crystals (104 mg, 0.13 mmol, 60.0 %),

$\delta_H$  (400 MHz,  $C_6D_6$ , 298K): 7.21 – 7.12 (m, 6H, ArH), 4.78 (s, 1H,  $C(CH_3)CH(CH_3)C$ ), 3.77 (d, 2H,  $^3J_{HH} = 10.2$  Hz  $OCH_2$ ), 3.60 (s, 2H,  $OCH_2$ ), 3.33 (s, 2H,  $OCH_2$ ), 3.31 – 3.22 (m, 2H,  $^3J_{HH} = 6.8$  Hz,  $CH(CH_3)_2$ ), 3.14 (d, 2H,  $^3J_{HH} = 10.8$  Hz,  $OCH_2$ ), 3.11 (sept, 2H,  $^3J_{HH} = 6.8$  Hz,  $CH(CH_3)_2$ ), 1.63 (s, 6H,  $(CH)C(CH_3)$ ), 1.52 – 1.41 (br m, 10H,  $(CH_2)_5$ ) 1.46 (d, 6H,  $^3J_{HH} = 6.8$  Hz,  $CH(CH_3)_2$ ), 1.35 (d, 6H,  $^3J_{HH} = 6.8$  Hz,  $CH(CH_3)_2$ ), 1.25 (d, 6H,  $^3J_{HH} = 6.8$  Hz,  $CH(CH_3)_2$ ), 1.16 (d, 6H,  $^3J_{HH} = 6.8$  Hz,  $CH(CH_3)_2$ ), 0.99 (t, 3H,  $(CH_2)_4cH_3$ ), 0.65 (s, 2H,  $C(CH_3)_2$ ), 0.54 (s, 3H,  $CCH_3$ ), 0.39 (s, 3H,  $CCH_3$ ).

$\delta_C$  (100 MHz,  $C_6D_6$ , 298K): 170.6 ( $CHC(CH_3)$ ), 145.2 (*ipso*- $C^{IV}$ ), 142.4 (*o*- $C^{IV}$ ), 142.1 (*o*- $C^{IV}$ ), 126.0 (*p*- $CH$ ), 124.5 (*m*- $CH$ ), 124.2 (*m*- $CH$ ), 94.9 ( $C(CH_3)CH(CH_3)C$ ), 72.5 ( $OCH_2C$ ), 70.8 ( $OCH_2C$ ), 69.1 ( $OCH_2C$ ), 34.2, 33.1 ( $CH_2C^{IV}CH_2$ ), 32.7, 31.3 ( $CH_2C^{IV}CH_2$ ), 29.0 ( $C(CH_3)$ ), 28.3 ( $C(CH_3)$ ), 26.5, 24.9 ( $C(CH_3)$ ), 24.6 ( $C(CH_3)$ ), 23.5, 23.0 ( $C^{IV}CH_3$ ), 22.8 ( $C^{IV}(CH_3)_2$ ), 22.8 ( $(C^{IV}CH_3)$ ), 14.7 ( $(CH_2)_4cH_3$ ).

$\delta_B$  (128 MHz,  $C_6D_6$ , 298K): 30.62, 4.79 ( $B-CH_2$ ).

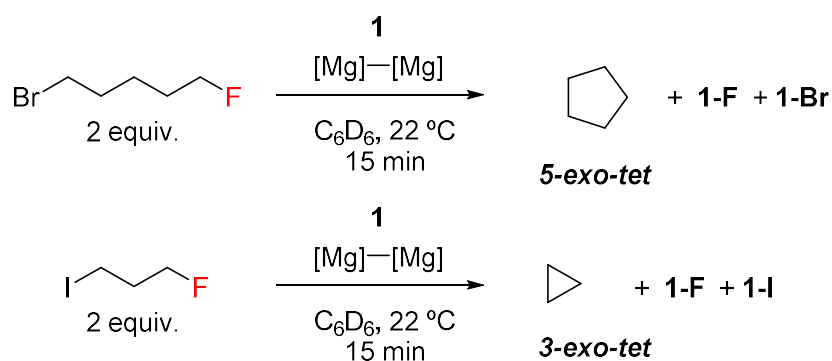
Anal. Calc. ( $MgC_{35}H_{54}N_2$ ): C, 71.78; H, 9.91; N, 3.72. Found: C, 71.63; H, 9.98; N, 3.80.

**Preparation of *n*-hexylSiH<sub>2</sub>Ph:** Phenylsilane (PhSiH<sub>3</sub>) (7.1 μL, 0.0575 mmol, 5 equiv.) was added to an *in situ* generated solution of **1a** from **1** in C<sub>6</sub>D<sub>6</sub> (0.6 mL) and the reaction heated at 80 °C for 20 hours, then analysed by <sup>1</sup>H spectroscopy. Full conversion of **1a** was realised, indicated by the loss of corresponding Mg–CH<sub>2</sub> triplet resonance at δ = -0.22 ppm in the <sup>1</sup>H NMR spectrum. The product, 1-hexyl(phenyl)silane (58% NMR yield), was confirmed by comparison of the <sup>1</sup>H NMR spectrum, to the literature data.<sup>[59]</sup>

**Preparation of *n*-hexylSnBu<sub>3</sub> (Method A):** Tributyltin chloride (Bu<sub>3</sub>SnCl) (6.2 μL, 0.023 mmol, 2 equiv.) was added to an *in situ* generated solution of **1a** from **1** in C<sub>6</sub>D<sub>6</sub> (0.6 mL) and the reaction monitored by <sup>1</sup>H and <sup>119</sup>Sn NMR spectroscopy. Within 15 minutes at 22 °C full conversion of **1a** was realised, indicated by the loss of corresponding Mg–CH<sub>2</sub> triplet resonance at δ = -0.22 ppm in the <sup>1</sup>H NMR spectrum. The product, tributyl(*n*-hexyl)stannane (>95 % NMR conversion) was confirmed by a singlet resonance at δ = -13.96 in the <sup>119</sup>Sn{<sup>1</sup>H} NMR spectrum which was in accordance with analogous tetrabutyltin compound from the literature.<sup>[58]</sup>

**Preparation of *n*-hexylSnBu<sub>3</sub> (Method B):** Tributyltin hydride (Bu<sub>3</sub>SnH) (6.2 μL, 0.023 mmol, 2 equiv.) was added to an *in situ* generated solution of **1a** from **1** in C<sub>6</sub>D<sub>6</sub> (0.6 mL) and the reaction heated at 80 °C whilst monitoring by <sup>1</sup>H and <sup>119</sup>Sn NMR spectroscopy. After 6 days at 80 °C full conversion of **1a** was realised, indicated by the loss of corresponding Mg–CH<sub>2</sub> triplet resonance at δ = -0.22 ppm in the <sup>1</sup>H NMR spectrum. The product, tributyl(*n*-hexyl)stannane (>95 % NMR conversion), was confirmed by a singlet resonance at δ = -13.96 in the <sup>119</sup>Sn{<sup>1</sup>H} NMR spectrum which was in accordance with analogous tetrabutyltin compound from the literature.<sup>[58]</sup>

### 2.3.5. Magnesium-mediated Intramolecular Coupling of $sp^3C-F$ and $sp^3C-X$ Bonds.



Scheme 2.46 Cyclisation of halofluorocarbons upon reaction with **1** via  $sp^3C-F$  and  $sp^3C-X$  C-C coupling

**Formation of cyclopentane:** 1-Bromo-5-fluoropentane (2.9  $\mu$ L, 0.023 mmol, 2 equiv.) was added to a solution of **1** in  $C_6D_6$  (0.6 mL). Within 10 minutes a precipitate had formed. The reaction was analysed by  $^1H$  and  $^{19}F$  NMR spectroscopy. Magnesium-fluoride by-product, **1-F**, was confirmed by a single resonance at  $\delta = -187$  ppm in the  $^{19}F$  NMR spectrum. The volatile reaction products were isolated by trap-to-trap vacuum transfer (22 °C) and analysed by multinuclear NMR spectroscopy. Cyclopentane was confirmed by a singlet resonance at  $\delta = 1.46$  ppm in the  $^1H$  NMR spectrum.

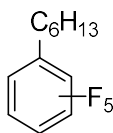
**Formation of cyclopropane:** 1-Iodo-3-fluoropropane (2.3  $\mu$ L, 0.023 mmol, 2 equiv.) was added to a solution of **1** in  $C_6D_6$  (0.6 mL). Within 10 minutes a precipitate had formed. The reaction was analysed by  $^1H$  and  $^{19}F$  NMR spectroscopy. Magnesium-fluoride by-product, **1-F**, was confirmed by a single resonance at  $\delta = -187$  ppm in the  $^{19}F$  NMR spectrum. The volatile reaction products were isolated by trap-to-trap vacuum transfer and analysed by multinuclear NMR spectroscopy. Cyclopropane was confirmed by a singlet resonance at  $\delta = 0.14$  ppm in the  $^1H$  NMR spectrum.

### 2.3.6. Magnesium-mediated Intermolecular Coupling of $sp^3C-F$ and $sp^2C-F$ Bonds.

**General procedure for one-pot C–C coupling:** **1** (10.2 mg, 0.012 mmol) was dissolved in  $C_6D_6$  and added to a J. Young NMR tube equipped with a ferrocene capillary insert and a  $t=0$   $^1H$  NMR spectrum was recorded. 1-Fluorohexane (1.6  $\mu L$ , 1.1 equiv.) was added and the reaction heated at 80 °C for 1 hour. A  $t=1$   $^1H$  NMR spectrum was recorded, noting the yield for the first C–F activation step upon integral comparison to the internal standard. Perfluoroarene (5-20 equiv.) was added to the reaction solution in a J. Young NMR tube and heated at a stated temperature and duration (22 °C, 50 °C or 80 °C). Yields were determined *in situ* by comparison to a ferrocene internal standard capillary, using the new  $Ar^FCH_n$  resonance in the  $^1H$  NMR spectrum. The cross-coupled products, *n*-hexyl alkylated perfluoroarenes, were confirmed by mass spectrometry and by comparison of the  $^1H$  and  $^{19}F$  NMR resonances of independently synthesised samples.

**General procedure for C–C coupling from isolated organomagnesium:**

**1a.THF** (13.8 mg, 0.023 mmol) was dissolved in  $C_6D_6$  (0.6 mL) and transferred to a J. Young NMR tube equipped with a ferrocene internal standard. A  $t=0$   $^1H$  NMR spectrum was recorded, then perfluoroarene (0.115 mmol, 5 equiv.) was added directly to the NMR tube and heated at 80 °C (unless stated otherwise), recording  $^1H$  and  $^{19}F$  NMR spectra at regular time intervals. Yields were determined *in situ* by comparison to a ferrocene internal standard capillary, using the new  $Ar^FCH_2$  resonance in the  $^1H$  NMR spectrum. The cross-coupled products, *n*-hexyl alkylated perfluoroarenes, were confirmed by mass spectrometry and by comparison of the  $^1H$  and  $^{19}F$  NMR resonances of independently synthesised samples.



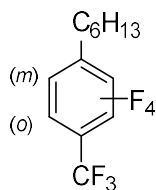
**Synthesis of 7a** (hexylpentafluorobenzene):<sup>[60]</sup> Under an argon atmosphere, n-hexyl magnesium bromide [0.81 M in THF] (10 mL, 8.1 mmol) was filtered onto a THF (5 mL) solution of hexafluorobenzene (0.62 mL, 5.4 mmol) and heated at 60 °C for 36 hours. The reaction was quenched with water (25 mL) and the product extracted into diethyl ether (3 x 50 mL). The organic layers were combined, dried with MgSO<sub>4</sub> then concentrated *in vacuo* yielding a pale yellow liquid. The product was purified by column chromatography on silica gel (eluent : *n*-hexane) yielding a colourless liquid (0.35 mL, 1.175 g/mL, 30 %).

$\delta_{\text{H}}$  (400 MHz, C<sub>6</sub>D<sub>6</sub>, 298K): 2.29 (tt, 2H, <sup>3</sup>J<sub>HH</sub> = 7.7 Hz, C<sup>IV</sup>CH<sub>2</sub>), 1.35 – 1.26 (br m, 2H, CH<sub>2</sub>), 1.25 – 1.16 (br m, 2H, CH<sub>2</sub>), 1.16 – 1.04 (br m, 4H, (CH<sub>2</sub>)<sub>2</sub>), 0.86 (t, 3H, <sup>3</sup>J<sub>HH</sub> = 7.2 Hz, CH<sub>2</sub>CH<sub>3</sub>).

$\delta_{\text{C}}$  (100 MHz, C<sub>6</sub>D<sub>6</sub>, 298K): 145.2 (dm, 2C, <sup>1</sup>J<sub>CF</sub> = 244.4 Hz, *o*-CF), 139.6 (dm, 1C, <sup>1</sup>J<sub>CF</sub> = 250.7 Hz, *p*-CF), 137.6 (dm, 2C, <sup>1</sup>J<sub>CF</sub> = 250.7 Hz, *m*-CF), 115.6 (td, 1C, <sup>2</sup>J<sub>CF</sub> = 19.1 Hz, <sup>3</sup>J<sub>CF</sub> = 3.1 Hz, *ipso*-C<sup>IV</sup>), 31.7 (s, 1C, CH<sub>2</sub>), 29.5 (s, 1C, CH<sub>2</sub>), 29.1 (s, 1C, CH<sub>2</sub>), 22.9 (s, 1C, CH<sub>2</sub>), 22.3 (s, 1C, CH<sub>2</sub>), 14.2 (s, 1C, CH<sub>3</sub>).

$\delta_{\text{F}}$  (376 MHz, C<sub>6</sub>D<sub>6</sub>, 298K): -145.2 (dd, 2F, <sup>3</sup>J<sub>FF</sub> = 22.8 Hz, <sup>4</sup>J<sub>FF</sub> = 7.9 Hz, *o*-CF), -158.7 (t, 1F, <sup>3</sup>J<sub>FF</sub> = 21.3 Hz, *p*-CF), -163.5 (td, 2F, *m*-CF).

Mass spec. (EI, +ve) 252 ([M]<sup>+</sup>, 80 %) 181, 176, 86; High-resolution mass spec. calc. for 252.0937 ([M]<sup>+</sup>), found 252.0937.



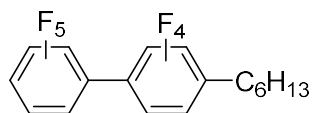
**Synthesis of 7b** (2,3,5,6-Tetrafluoro-4-hexyl trifluoromethylbenzene):<sup>[60]</sup> Under an argon atmosphere, *n*-hexyl magnesium bromide [0.81 M in THF] (10 mL, 8.1 mmol) was filtered onto a THF (5 mL) solution of octafluorotoluene (0.76 mL, 5.4 mmol) and stirred at 22 °C for 24 hours. The reaction was quenched with water and the product extracted into diethyl ether (3 x 50 mL). The organic layers were combined, dried with MgSO<sub>4</sub> then concentrated *in vacuo* yielding a pale yellow liquid. The product was purified through two pads of silica (w x h = 2 cm x 4 cm) (eluent : *n*-hexane) yielding a colourless liquid. (0.95 mL, 73 %, d = 1.248 g mL<sup>-1</sup>).

$\delta_{\text{H}}$  (400 MHz, C<sub>6</sub>D<sub>6</sub>, 298K): 2.27 (t, 2H, <sup>3</sup>J<sub>HH</sub> = 7.7 Hz, C<sup>IV</sup>CH<sub>2</sub>), 1.29 – 1.16 (br m, 4H, (CH<sub>2</sub>)<sub>2</sub>), 1.15 – 1.02 (br m, 4H, (CH<sub>2</sub>)<sub>2</sub>), 0.86 (t, 3H, <sup>3</sup>J<sub>HH</sub> = 7.2 Hz, CH<sub>2</sub>CH<sub>3</sub>).

$\delta_{\text{C}}$  (100 MHz, C<sub>6</sub>D<sub>6</sub>, 298K): 144.8 (dm, 2C, <sup>1</sup>J<sub>CF</sub> = 244.5 Hz, o-C<sup>IV</sup>), 143.7 (dd, 2C, <sup>1</sup>J<sub>CF</sub> = 257.7 Hz, m-C<sup>IV</sup>), 125.4 (t, 1C, <sup>2</sup>J<sub>CF</sub> = 18.5 Hz, p-C<sup>IV</sup>), 123.3 (q, 1C, <sup>1</sup>J<sub>CF</sub> = 273.5 Hz, CF<sub>3</sub>), 106.9 (m, 1C, ipso-C<sup>IV</sup>), 31.3 (s, 1C, CH<sub>2</sub>), 28.9 (s, 1C, CH<sub>2</sub>), 28.6 (s, 1C, CH<sub>2</sub>), 22.7 (s, 1C, CH<sub>2</sub>), 22.4 (s, 1C, CH<sub>2</sub>), 13.8 (s, 1C, CH<sub>3</sub>).

$\delta_{\text{F}}$  (376 MHz, C<sub>6</sub>D<sub>6</sub>, 298K): -56.1 (t, 3F, <sup>4</sup>J<sub>FF</sub> = 21.5 Hz, CF<sub>3</sub>), -142.0 – -142.4 (m, 2F, o-CF), -143.0 – -143.2 (app. q, 2F, <sup>3</sup>J<sub>FF</sub> = 9.6 Hz, m-CF).

Mass spec. (EI, +ve) 302 ([M]<sup>+</sup>, 100 %) 283, 231, 226, 181, 86; High-resolution mass spec. calc. for ([M]<sup>+</sup>) 302.0905, found 302.0897.



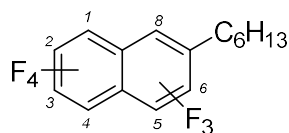
**Synthesis of 7c** (2,2',3,3',4,5,5',6,6'-Nonafluoro-4'-hexyl-1,1'-biphenyl):<sup>[60]</sup> Under an argon atmosphere, *n*-hexyl magnesium bromide [0.6 M in THF] (5 mL, 3.0 mmol) was filtered onto a THF (5 mL) solution of decafluorobiphenyl (668 mg, 2.0 mmol) and stirred at 22 °C for 24 hours. The reaction was quenched with water (25 mL) and the product extracted into diethyl ether (3 x 50 mL). The organic layers were combined, dried with MgSO<sub>4</sub> then concentrated *in vacuo* yielding a pale yellow liquid. The product was purified by column chromatography (eluent : *n*-hexane) yielding a colourless liquid. (0.10 mL, *d* = 1.133 g/mL, 17 %).

$\delta_{\text{H}}$  (400 MHz, C<sub>6</sub>D<sub>6</sub>, 298K): 2.42 (tt, 2H, <sup>3</sup>*J*<sub>HH</sub> = 7.8 Hz, C<sup>V</sup>CH<sub>2</sub>), 1.36 – 1.19 (br m, 8H, (CH<sub>2</sub>)<sub>4</sub>), 0.87 (t, 3H, CH<sub>2</sub>CH<sub>3</sub>).

$\delta_{\text{C}}$  (100 MHz, C<sub>6</sub>D<sub>6</sub>, 298K): 145.0 (dm, 2C, <sup>1</sup>*J*<sub>CF</sub> = 244.8 Hz, *m'*-CF), 144.4 (dm, 2C, <sup>1</sup>*J*<sub>CF</sub> = 250.1 Hz, *o*-CF), 143.9 (dm, 2C, <sup>1</sup>*J*<sub>CF</sub> = 250.6 Hz, *o'*-CF), 141.9 (dm, 1C, <sup>1</sup>*J*<sub>CF</sub> = 256.2 Hz, *p*-CF), 137.6 (dm, 2C, <sup>1</sup>*J*<sub>CF</sub> = 254.0 Hz, *m*-CF), 123.6 (t, 1C, <sup>2</sup>*J*<sub>CF</sub> = 18.6 Hz, C<sup>V</sup>CH<sub>2</sub>), 103.4 (t, 1C, C<sup>IV</sup>), 102.3 (t, 1C, C<sup>IV</sup>), 31.3 (s, 1C, CH<sub>2</sub>), 28.8 (s, 2C, (CH<sub>2</sub>)<sub>2</sub>), 22.9 (s, 1C, CH<sub>2</sub>), 22.4 (s, 1C, CH<sub>2</sub>), 13.7 (s, 1C, CH<sub>3</sub>).

$\delta_{\text{F}}$  (376 MHz, C<sub>6</sub>D<sub>6</sub>, 298K): -138.8 – -139.0 (m, 2F, *o*-Ar-F), -139.8 – -140.0 (m, 2F, *o'*-Ar-F), -143.5 – -143.7 (m, 2F, *m'*-Ar-F), -150.6 (t, 1F, <sup>3</sup>*J*<sub>FF</sub> = 21.8 Hz, *p*-Ar-F), -160.8 – -161.0 (m, 2F, *m*-Ar-F).

Mass spec. (EI, +ve) 400 ([M]<sup>+</sup>, 10 %) 207, 134, 86 ; High-resolution mass spec. calc. for 400.0874 ([M]<sup>+</sup>), found 400.0869.



**Synthesis of 7d** (1,2,3,4,5,6,8-Heptafluoro-7-hexylnaphthalene).<sup>[60]</sup> Under an argon atmosphere, *n*-hexyl magnesium bromide [0.75 M in THF] (5 mL, 3.8 mmol) was filtered onto a THF (5 mL) solution of octafluoronaphthalene (680 mg, 2.5 mmol) and stirred at 22 °C for 24 hours. The reaction was quenched with water (25 mL) and the product extracted into diethyl ether (3 x 50 mL). The organic layers were combined, dried with MgSO<sub>4</sub> then concentrated *in vacuo* yielding a pale yellow liquid. The product was purified by column chromatography (eluent : *n*-hexane) yielding a colourless liquid. (0.14 mL, *d* = 1.39 g/mL, 31 %).

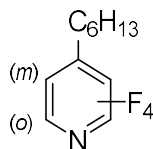
$\delta_{\text{H}}$  (400 MHz, C<sub>6</sub>D<sub>6</sub>, 298K): 2.55 (t, 2H, <sup>3</sup>*J*<sub>HH</sub> = 7.7 Hz, C<sup>IV</sup>CH<sub>2</sub>), 1.53 – 1.43 (m, 2H, CH<sub>2</sub>), 1.31 – 1.15 (br m, 6H, (CH<sub>2</sub>)<sub>3</sub>).

$\delta_{\text{C}}$  (100 MHz, C<sub>6</sub>D<sub>6</sub>, 298K): 149.8 (dm, 1C, <sup>1</sup>*J*<sub>CF</sub> = 257.3 Hz, C<sup>8</sup>F), 146.6 (dt, 1C, <sup>1</sup>*J*<sub>CF</sub> = 250.3 Hz, C<sup>6</sup>F), 140.8 (dm, 2C, <sup>1</sup>*J*<sub>CF</sub> = 258.2 Hz, C<sup>1+4</sup>F), 140.1 (dm, 1C, <sup>1</sup>*J*<sub>CF</sub> = 250.1 Hz, C<sup>5</sup>F), 138.9 (dt, 1C, <sup>1</sup>*J*<sub>CF</sub> = 253.9 Hz, C<sup>3</sup>F), 138.2 (dt, 1C, <sup>1</sup>*J*<sub>CF</sub> = 253.3 Hz, C<sup>2</sup>F), 119.4 (t, 1C, <sup>2</sup>*J*<sub>CF</sub> = 21.2 Hz, C<sup>IV</sup>CH<sub>2</sub>), 109.9 (t, 1C, C<sup>IV</sup>), 107.6 (t, 1C, C<sup>IV</sup>), 31.4 (s, 1C, CH<sub>2</sub>), 29.2 (s, 1C, CH<sub>2</sub>), 28.9 (s, 1C, CH<sub>2</sub>), 22.5 (s, 2C, (CH<sub>2</sub>)<sub>2</sub>), 13.8 (s, 1C, CH<sub>3</sub>).

$\delta_{\text{F}}$  (470 MHz, C<sub>6</sub>D<sub>6</sub>, 298K): -123.6 (dd, 1F, <sup>4</sup>*J*<sub>FF</sub> = 67.6 Hz, <sup>4</sup>*J*<sub>FF</sub> = 18.7 Hz, CF<sup>8</sup>), -139.8 (d, 1F, <sup>3</sup>*J*<sub>FF</sub> = 18.4 Hz, CF<sup>6</sup>), -145.6 (dt, 1F, <sup>4</sup>*J*<sub>FF</sub> = 67.2 Hz, CF<sup>1</sup>), -147.2 (dtd, 1F, <sup>4</sup>*J*<sub>FF</sub> = 56.6 Hz, CF<sup>4</sup>), -150.1 (dtt, 1F, <sup>4</sup>*J*<sub>FF</sub> = 56.6 Hz, CF<sup>5</sup>), -156.0 (t, 1F, CF<sup>3</sup>), -157.4 (m, 1F, CF<sup>2</sup>).

Mass spec. (EI, +ve) 338 ([M]<sup>+</sup>, 100 %) 267, 180, 86; High-resolution mass spec. calc. for ([M]<sup>+</sup>) 338.0905, found 338.0910.





**Synthesis of 7e** (2,3,5,6-Tetrafluoro-4-hexyl pyridine):<sup>[60]</sup> Under an argon atmosphere, *n*-hexyl magnesium bromide [0.81 M in THF] (10 mL, 8.1 mmol) was filtered onto a THF (5 mL) solution of pentafluoropyridine (0.59 mL, 5.4 mmol) and stirred at 22 °C for 24 hours. The reaction was quenched with water (25 mL) and the product extracted into diethyl ether (3 x 50 mL). The organic layers were combined, dried with MgSO<sub>4</sub> then concentrated *in vacuo* yielding a pale yellow liquid. The product was purified through two pads of silica (w x h = 2 cm x 4 cm) (eluent : *n*-hexane) yielding a colourless liquid. (1.05 mL, 77 %, d = 1.180 g mL<sup>-1</sup>).

$\delta_{\text{H}}$  (400 MHz, C<sub>6</sub>D<sub>6</sub>, 298K): 2.18 (tt, 2H, <sup>3</sup>J<sub>HH</sub> = 7.7 Hz, C<sup>V</sup>CH<sub>2</sub>), 1.25 – 1.12 (br m, 4H, (CH<sub>2</sub>)<sub>2</sub>), 1.12 – 0.97 (br m, 4H, (CH<sub>2</sub>)<sub>2</sub>), 0.84 (t, 3H, <sup>3</sup>J<sub>HH</sub> = 7.2 Hz, CH<sub>2</sub>CH<sub>3</sub>).

$\delta_{\text{C}}$  (100 MHz, C<sub>6</sub>D<sub>6</sub>, 298K): 143.1 (dm, 2C, <sup>1</sup>J<sub>CF</sub> = 242.7 Hz, *m*-C<sup>V</sup>), 140.2 (dm, 2C, <sup>1</sup>J<sub>CF</sub> = 255.4 Hz, *o*-C<sup>V</sup>), 134.8 (t, 1C, <sup>2</sup>J<sub>CF</sub> = 17.1 Hz, *p*-C<sup>V</sup>).

$\delta_{\text{F}}$  (376 MHz, C<sub>6</sub>D<sub>6</sub>, 298K): -92.3 – -95.0 (m, 2F, *o*-CF), -146.0 – -146.2 (m, 2F, *m*-CF).

Mass spec. (EI, +ve) 235 ([M]<sup>+</sup>, 100 %) 165, 164, 147, 86; High-resolution mass spec. calc. for 235.0984 ([M]<sup>+</sup>), found 235.0992.

**Synthesis and confirmation of 7e & 7e'** In a dinitrogen filled glovebox, compound **1** (102 mg, 0.115 mmol) was dissolved in toluene (6 mL) followed by the addition of 1-fluorohexane (16  $\mu$ L, 0.127 mmol) and the reaction heated at 80 °C for 90 minutes. An aliquot of the reaction mixture was taken and a <sup>1</sup>H NMR spectrum recorded, noting the full conversion of **1**. To the reaction mixture, pentafluoropyridine (63  $\mu$ L, 0.575 mmol) was added and the reaction heated at 50 °C for 16 hours. The solvent was removed *in vacuo* and the organic products extracted into *n*-hexane (15 mL), washing with water. The organic phases were combined and concentrated under reduced pressure, followed by the recording of <sup>1</sup>H and <sup>19</sup>F NMR spectra in C<sub>6</sub>D<sub>6</sub>. Compound **7e** was confirmed upon <sup>1</sup>H and <sup>19</sup>F NMR comparison to the independently synthesised compound. Compound **7e'** was assigned based upon the observation of 4 new resonances in the <sup>19</sup>F NMR spectrum ( $\delta$  = -85.0, -141.3, -148.4 and -161.6 ppm) and comparison to a related compound in the literature, 2-methyl-tetrafluoropyridine ( $\delta$  = -85.3, -141.5, -146.6 and -161.7 ppm).<sup>[61]</sup>

### 2.3.7 Assessment of Computational Methodology

A series of functional benchmarking calculations were performed to assess their performance in describing the activation energy ( $\Delta\Delta G^\ddagger$ ) and enthalpy ( $\Delta\Delta H^\ddagger$ ) associated with key C–F bond cleavage steps.

The functional selection was based on earlier computational benchmarking studies conducted on related C–F activation of  $sp^2$ C–F bonds in fluoroarenes using compound **1**.<sup>[63]</sup> The functionals include the hybrid GGA functional, B3PW91<sup>[73–77]</sup>; Minnesota meta functional, M06-L<sup>[90]</sup> and long range-corrected functional,  $\omega$ B97X<sup>[91]</sup> whilst maintaining the same basis set and pseudopotential combination. All values were single point corrected for solvent. Dispersion single point correction using D3<sup>[84]</sup> for B3PW91 and D2<sup>[92]</sup> single point correction for  $\omega$ B97X. C–F bond cleavage steps were also computed using B3PW91 incorporating solvent and dispersion into the optimisation process (B3PW91-D3(PCM)).

|             | B3PW91             | B3PW91-D3 (PCM)    | $\omega$ B97X      | M06L               |
|-------------|--------------------|--------------------|--------------------|--------------------|
| <b>TS-1</b> | <b>23.6</b> (16.7) | <b>22.5</b> (17.9) | <b>31.7</b> (25.9) | <b>20.8</b> (12.5) |
| <b>TS-4</b> | <b>26.2</b> (22.2) | <b>29.5</b> (24.6) | <b>31.1</b> (27.4) | <b>31.9</b> (27.9) |

Table 2.5 Relative energy barriers associated with C–F bond cleavage steps involving **TS-1** and **TS-4** calculated using specified density functionals. All values single point corrected for solvent. Dispersion single point correction using D3 for B3PW91, D2 single point correction for  $\omega$ B97X.  $\Delta\Delta G$  in bold and  $\Delta\Delta H$  in parenthesis.

The final functional choice, B3PW91, is well established in describing bond activation mechanisms with dimeric main group reagents.<sup>[68,93–96]</sup> Calculations performed using B3PW91 indicate the second  $sp^2$ C–F bond cleavage and C–C coupling step has a higher associated energy barrier than  $sp^3$ C–F bond activation. This is represented experimentally by the elevated temperatures (80 °C) and longer reaction times (days) required to couple **1a** with C<sub>6</sub>F<sub>6</sub>. This reactivity trend was not reflected in the activation barriers calculated using  $\omega$ B97X functional. Results from previous studies revealed that although  $\omega$ B97X accurately described various bond distances in **1** the enthalpy and free energy barriers did not correlate as well as B3PW91 based upon data from the Eyring analysis.<sup>[63]</sup>

Comparison of barriers associated with B3PW91 and B3PW91-D3(PCM) highlights a negligible difference between the methods. The calculations suggest that there is no advantage from including a dispersion and solvent correction during the optimization step of the calculations, the disadvantage is that the calculations are more costly.

## 2.4 References

- [1] N. Kambe, T. Iwasaki, J. Terao, *Chem. Soc. Rev.*, **2011**, *40*, 4937–4947.
- [2] B. Saito, G. C. Fu, *J. Am. Chem. Soc.* **2007**, *129*, 9602–9603.
- [3] J. Choi, G. C. Fu, *Science*, **2017**, *356*, 7230.
- [4] T. Ahrens, J. Kohlmann, M. Ahrens, T. Braun, *Chem. Rev.*, **2015**, *115*, 931–972.
- [5] W. Chen, C. Bakewell, M. R. Crimmin, *Synthesis* **2017**, *49*, 810–821.
- [6] J. L. Kiplinger, T. G. Richmond, C. E. Osterberg, *Chem. Rev.*, **1994**, *94*, 373–431.
- [7] S. J. Blanksby, G. B. Ellison, *Acc. Chem. Res.* **2003**, *36*, 255–263.
- [8] P. J. Davidson, M. F. Lappert, R. Pearce, *Chem. Rev.*, **1976**, *76*, 219–242.
- [9] W. Scherer, G. S. McGrady, *Angew. Chem. Int. Ed.*, **2004**, *43*, 1782–1806.
- [10] J. L. Kiplinger, T. G. Richmond, *J. Am. Chem. Soc.*, **1996**, *118*, 1805–1806.
- [11] W. D. Jones, *Dalton Trans.*, **2003**, *3*, 3991–3995.
- [12] B. M. Kraft, R. J. Lachicotte, W. D. Jones, *J. Am. Chem. Soc.*, **2000**, *122*, 8559–8560.
- [13] B. M. Kraft, R. J. Lachicotte, W. D. Jones, *J. Am. Chem. Soc.*, **2001**, *123*, 10973–10979.
- [14] E. Clot, C. Mégret, B. M. Kraft, O. Eisenstein, W. D. Jones, *J. Am. Chem. Soc.*, **2004**, *126*, 5647–5653.
- [15] K. E. Liu, S. J. Lippard, C. C. Johnson, M. Newcomb, *J. Am. Chem. Soc.*, **1993**, *115*, 939–947.
- [16] E. L. Werkema, E. Messines, L. Perrin, L. Maron, O. Eisenstein, R. A. Andersen, *J. Am. Chem. Soc.*, **2005**, *127*, 7781–7795.
- [17] C. Douvris, O. V. Ozerov, *Science*, **2008**, *321*, 1188–1190.
- [18] C. B. Caputo, D. W. Stephan, *Organometallics*, **2012**, *31*, 27–30.
- [19] M. Ahrens, G. Scholz, T. Braun, E. Kemnitz, *Angew. Chem. Int. Ed.*, **2013**, *52*, 5328–5332.
- [20] R. Panisch, M. Bolte, T. Müller, *J. Am. Chem. Soc.*, **2006**, *128*, 9676–9682.
- [21] V. J. Scott, R. Çelenligil-Çetin, O. V. Ozerov, *J. Am. Chem. Soc.*, **2005**, *127*, 2852–2853.
- [22] W. Gu, M. R. Haneline, C. Douvris, O. V. Ozerov, *J. Am. Chem. Soc.*, **2009**, *131*, 11203–11212.
- [23] C. B. Caputo, L. J. Hounjet, R. Dobrovetsky, D. W. Stephan, *Science*, **2013**, *341*, 1374–1377.
- [24] B. Pan, F. P. Gabbaï, *J. Am. Chem. Soc.*, **2014**, *136*, 9564–9567.
- [25] J. Choi, D. Y. Wang, S. Kundu, Y. Choliy, T. J. Emge, K. Krogh-Jespersen, A. S. Goldman, *Science*, **2011**, *332*, 1545–1548.
- [26] H. W. Roesky, C. Cui, H.-G. Schmidt, M. Noltemeyer, H. Hao, F. Cimpoesu, *Angew. Chem. Int. Ed.*, **2000**, *39*, 4274–4276.
- [27] S. P. Green, C. Jones, A. Stasch, *Science*, **2007**, *318*, 1754–1757.
- [28] S. S. Sen, J. Hey, R. Herbst-Irmer, H. W. Roesky, D. Stalke, *J. Am. Chem. Soc.*, **2011**, *133*, 12311–12316.

- [29] Y. Segawa, M. Yamashita, K. Nozaki, *Science*, **2006**, *314*, 113–115.
- [30] T. J. Hadlington, M. Driess, C. Jones, *Chem. Soc. Rev.*, **2018**, *47*, 4176–4197.
- [31] C. Jones, *Nat. Rev. Chem.* **2017**, *1*, 59.
- [32] M. N. S. Rao, H. W. Roesky, G. Anantharaman, *J. Organomet. Chem.* **2002**, *646*, 4–14.
- [33] M. R. Crimmin, M. J. Butler, A. J. P. White, *Chem. Commun.*, **2015**, *51*, 15994–15996.
- [34] T. Chu, Y. Boyko, I. Korobkov, G. I. Nikonov, *Organometallics*, **2015**, *34*, 5363–5365.
- [35] Y. Kim, H. Cho, S. Hwang, *Bull. Korean Chem. Soc.* **2017**, *38*, 282–284.
- [36] C. E. Pitsch, X. Wang, *Chem. Commun.*, **2017**, *53*, 8196–8198.
- [37] X. W. Liu, C. Zarate, R. Martin, *Angew. Chem. Int. Ed.*, **2019**, *58*, 2064–2068.
- [38] S. Mallick, P. Xu, E. U. Würthwein, A. Studer, *Angew. Chem. Int. Ed.*, **2019**, *58*, 283–287.
- [39] B. Cui, S. Jia, E. Tokunaga, N. Shibata, *Nat. Commun.* **2018**, *9*, 4393–4400.
- [40] C. Bakewell, A. J. P. White, M. R. Crimmin, *J. Am. Chem. Soc.*, **2016**, *138*, 12763–12766.
- [41] F. L. M. Pattison, W. C. Howell, *J. Org. Chem.* **1956**, *21*, 879–882.
- [42] E. C. Ashby, S. H. Yu, *J. Org. Chem.* **1970**, *36*, 2123–2128.
- [43] R. D. Rieke, S. E. Bales, P. M. Hudnall, T. P. Burns, G. S. Poindexter, *Org. Synth.* **2003**, 85–85.
- [44] A. Stasch, C. Jones, *Dalton Trans.*, **2011**, *40*, 5659–5672.
- [45] N. W. Goldberg, X. Shen, J. Li, T. Ritter, *Org. Lett.*, **2016**, *18*, 6102–6104.
- [46] R. E. Banks, P. Y. François, P. N. Preston, *Polymer* **1992**, *33*, 3974–3975.
- [47] J. Guo, K. L. Bamford, D. W. Stephan, *Org. Biomol. Chem.* **2019**, *17*, 5258–5261.
- [48] P. A. Champagne, Y. Benhassine, J. Desroches, J. F. Paquin, *Angew. Chem. Int. Ed.*, **2014**, *53*, 13835–13839.
- [49] H. Chen, Z. Liu, Y. Lv, X. Tan, H. Shen, H. Z. Yu, C. Li, *Angew. Chem. Int. Ed.*, **2017**, *56*, 15411–15415.
- [50] I. Bucsi, B. Török, A. I. Marco, G. Rasul, G. K. S. Prakash, G. A. Olah, *J. Am. Chem. Soc.*, **2002**, *124*, 7728–7736.
- [51] S. J. Bonyhady, C. Jones, S. Nembenna, A. Stasch, A. J. Edwards, G. J. McIntyre, *Chem. Eur. J.*, **2010**, *16*, 938–955.
- [52] S. K. Bose, K. Fucke, L. Liu, P. G. Steel, T. B. Marder, *Angew. Chem. Int. Ed.*, **2014**, *53*, 1799–1803.
- [53] M. Arrowsmith, T. J. Hadlington, M. Hill, G. Kociok-Köhn, *Chem. Commun.*, **2012**, *48*, 4567–4569.
- [54] M. À. M. Bonds, S. P. Green, C. Jones, A. Stasch, *Angew. Chem. Int. Ed.*, **2008**, *49*, 9079–9083.
- [55] G. Y. Fang, O. A. Wallner, N. Di Blasio, X. Ginesta, J. N. Harvey, V. K. Aggarwal, *J. Am. Chem. Soc.*, **2007**, *129*, 14632–14639.

- [56] D. J. Liptrot, M. S. Hill, M. F. Mahon, A. S. S. Wilson, *Angew. Chem. Int. Ed.*, **2015**, *54*, 13362–13365.
- [57] A. L. Colebatch, M. S. Hill, C. L. McMullin, M. F. Mahon, C. Weetman, *Nature Comm.*, **2017**, *8*, 15022.
- [58] A. J. Saunders, I. R. Crossley, *Dalton Trans.*, **2016**, *45*, 2148–2155.
- [59] E. Shirakawa, D. Ikeda, S. Masui, M. Yoshida, T. Hayashi, *J. Am. Chem. Soc.*, **2012**, *134*, 272–279.
- [60] Y. Sun, H. Sun, J. Jia, A. Du, X. Li, *Organometallics*, **2014**, *33*, 1079–1081.
- [61] T. Braun, S. Parsons, R. N. Perutz, M. Voith, *Organometallics*, **1999**, *18*, 1710–1716.
- [62] H. R. Rogers, J. Houk, *J. Am. Chem. Soc.*, **1982**, *104*, 522–525.
- [63] C. Bakewell, B. J. Ward, A. J. P. White, M. R. Crimmin, *Chem. Sci.*, **2018**, *9*, 2348–2356.
- [64] D. M. Cyr, M. G. Scarton, K. B. Wiberg, M. A. Johnson, S. Nonose, J. Hirokawa, H. Tanaka, T. Kondow, R. A. Morris, A. A. Viggiano, *J. Am. Chem. Soc.*, **1995**, *117*, 1828–1832.
- [65] G. Li, W. L. Hase, *J. Am. Chem. Soc.*, **1999**, *121*, 7124–7129.
- [66] I. Szabó, B. Olsz, G. Czako, *J. Phys. Chem. Lett.* **2017**, *8*, 2917–2923.
- [67] X. Zhang, J. Ren, S. M. Tan, D. Tan, R. Lee, C. H. Tan, *Science*, **2019**, *363*, 400–404.
- [68] C. E. Kefalidis, A. Stasch, C. Jones, L. Maron, *Chem. Commun.*, **2014**, *50*, 12318–12321.
- [69] S. J. Bonyhady, C. Jones, S. Nembenna, A. Stasch, A. J. Edwards, G. J. McIntyre, *Chem. Eur. J.*, **2010**, *16*, 938–955.
- [70] M. J. Monreal, R. J. Wright, D. E. Morris, B. L. Scott, J. T. Golden, P. P. Power, J. L. Kiplinger, *Organometallics*, **2013**, *32*, 1423–1434.
- [71] M. Spiniello, J. M. White, *Org. Biomol. Chem.* **2003**, *1*, 3094–3101.
- [72] M. J. Frisch, G. W. Trucks, H. B. Schlegel, G. E. Scuseria, M. A. Robb, J. R. Cheeseman, G. Scalmani, V. Barone, B. Mennucci, G. A. Petersson, et al., *Gaussian Inc.* **2009**.
- [73] A. D. Becke, *J. Chem. Phys.* **1993**, *98*, 5648.
- [74] J. P. Perdew, K. Burke, M. Ernzerhof, *Phys. Rev. Lett.* **1996**, *77*, 3865–3868.
- [75] J. P. Perdew, J. A. Chevary, S. H. Vosko, K. A. Jackson, M. R. Pederson, D. J. Singh, C. Fiolhais, *Phys. Rev. B* **1993**, *48*, 4978.
- [76] J. P. Perdew, J. A. Chevary, S. H. Vosko, K. A. Jackson, M. R. Pederson, D. J. Singh, C. Fiolhais, *Phys. Rev. B* **1992**, *46*, 6671–6687.
- [77] J. P. Perdew, K. Burke, Y. Wang, *Phys. Rev. B* **1996**, *54*, 16533–16539.
- [78] W. J. Hehre, R. Ditchfield, J. A. Pople, *J. Chem. Phys.* **1972**, *56*, 2257–2261.
- [79] P. C. Hariharan, J. A. Pople, *Theor. Chim. Acta* **1973**, *28*, 213–222.
- [80] T. Clark, J. Chandrasekhar, G. W. Spitznagel, P. V. R. Schleyer, *J. Comput. Chem.* **1983**, *4*, 294–

- 301.
- [81] K. Fukui, *Acc. Chem. Res.* **1981**, *14*, 363–368.
- [82] H. P. Hratchian, H. B. Schlegel, in *Theory Appl. Comput. Chem.*, **2005**, pp. 195–249.
- [83] J. Tomasi, B. Mennucci, R. Cammi, *Chem. Rev.*, **2005**, *105*, 2999–3094.
- [84] S. Grimme, J. Antony, S. Ehrlich, H. Krieg, *J. Chem. Phys.* **2010**, *132*, 154104.
- [85] R. Dennington, T. Keith, J. Millam, *Semichem Inc., Shawnee Mission. KS* **2009**, Semichem Inc.
- [86] NBO Version 5.9, E.D. Glendening, J. K. Badenhoop, A. E. Reed, J. E. Carpenter, J. A. Bohmann, C. M. Morales, F. Weinhold. Theoretical Chemistry Institute, University of Wisconsin: Madison January 1, **2001**.
- [87] R. F. W. Bader, *Chem. Rev.*, **1991**, *91*, 893–928.
- [88] R. F. W. Bader, *Atoms In Molecules - A Quantum Theory*, Oxford University Press, New York, **1994**.
- [89] AIMAll (Version 17.01.25), T. A. Keith, TK Gristmill Software: Overland Park KS, USA January 1, **2017**.
- [90] Y. Zhao, D. G. Truhlar, *J. Chem. Phys.* **2006**, *125*, 194101.
- [91] J.-D. Chai, M. Head-Gordon, *J. Chem. Phys.* **2008**, *128*, 84106.
- [92] J.-D. Chai, M. Head-Gordon, *Phys. Chem. Chem. Phys.* **2008**, *10*, 6615.
- [93] C. E. Kefalidis, C. Jones, L. Maron, *Dalton Trans.*, **2016**, *45*, 14789–14800.
- [94] A. J. Boutland, C. A. Lamsfus, B. Maitland, L. Maron, A. Stasch, C. Jones, *Chem. Eur. J.*, **2017**, *23*, 14049–14055.
- [95] A. J. Boutland, A. Carroll, C. Alvarez Lamsfus, A. Stasch, L. Maron, C. Jones, *J. Am. Chem. Soc.*, **2017**, *139*, 18190–18193.
- [96] S. Schnitzler, T. P. Spaniol, L. Maron, J. Okuda, *Chem. Eur. J.*, **2015**, *21*, 11330–11334.

## Chapter 3 –Defluorosilylation of Fluoroalkenes and Industrially Relevant HFOs

Results from this chapter have been published by Wiley in *Angewandte Chemie*.

G. Coates, H. Y. Tan, C. Kalff, A. J. P. White, M. R. Crimmin, *Angew. Chem. Int. Ed.* **2019**, 58, 12514 – 12518.

### 3.1 Introduction

$sp^2$  Hybridised C–F bonds of fluoroalkenes are typically stronger than their  $sp^3$  hybrid counterparts (BDEs  $C_2H_3F = 123.3 \pm 0.8$ ,  $CH_3F = 115 \pm 4.0$  kcal mol<sup>-1</sup>), yet more methods and procedures have been found to activate the former – transforming them into C–H, C–C or C–element bonds. Many of these processes require metals or metal complexes. Early examples of  $sp^2$ C–F activation were mainly limited to hydrodefluorination (HDF) processes, whereby a C–F bond is converted to a C–H bond.<sup>[1]</sup> This interconversion arguably brings limited value, as one unreactive bond is converted into a similarly unreactive bond which can lead to a synthetic ‘dead-end’. However, selective processes for the hydrodefluorination of C–F bonds in per- or polyfluorinated olefins can be of utility. Partially fluorinated olefins, HFOs are proposed as the next generation of refrigerants and their production is set to increase greatly as the phase-out of HFCs accelerate.

Typical techniques to generate hydrofluoroolefins involve the installation then removal of chlorine atoms. This not only reduces the overall atom economy but can lead to toxic by-products and pollutants. Perfluorinated olefins such as hexafluoropropene are cheap bulk chemicals, simple to produce through perfluorination processes. The selective HDF of these compounds can add value and possibly lead to new, more efficient routes to HFO refrigerant gases.

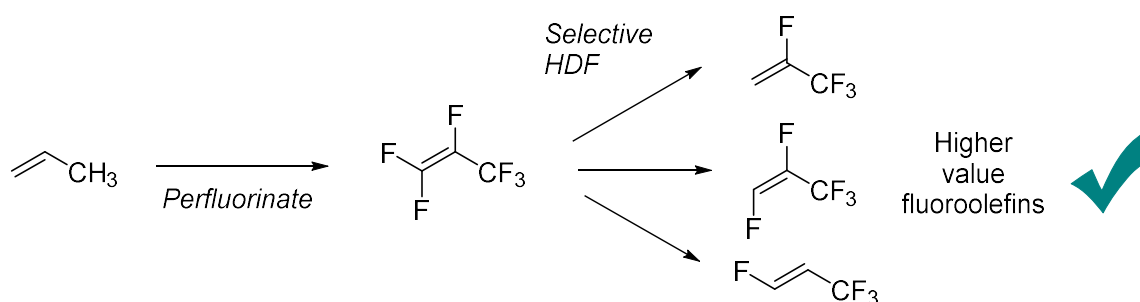
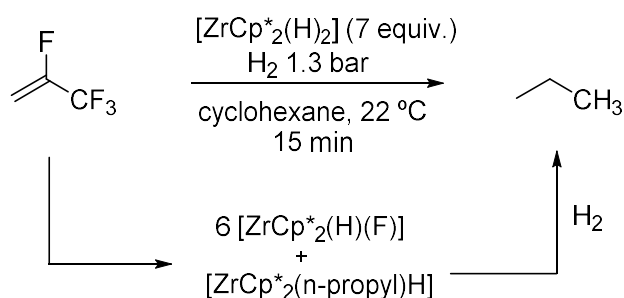


Figure 3.1 Overview of a value-adding HDF process

#### 3.1.1 Unselective hydrodefluorination

The earliest examples of fluoroalkene HDF were not selective and often led to the complete removal of fluorine from the substrate. For example, in 2000 Jones and co-workers demonstrated the

hydrodefluorination of fluoroaromatics, fluoroalkanes and fluoroolefins including refrigerant gas R-1234yf.<sup>[2]</sup> They found decamethyl zirconocene dihydride  $[\text{ZrCp}^*_2(\text{H})_2]$  under an atmosphere of  $\text{H}_2$  to be an effective reagent to achieve the complete hydrodefluorination and subsequent hydrogenation of 3,3,3-trifluoropropene and 2,3,3,3-tetrafluoropropene to yield n-propane.  $[\text{ZrCp}^*_2(\text{n-propyl})\text{H}]$  was detected in small amounts indicating the final step of the process to be a stepwise hydrogenation of the C=C  $\pi$ -bond via a hydrozirconated intermediate upon the addition of  $\text{H}_2$  to this complex.



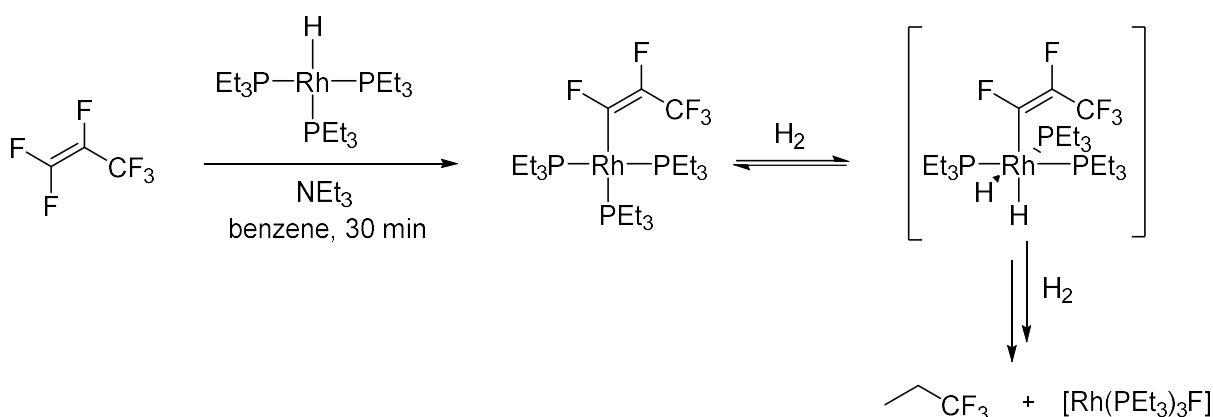
Scheme 3.1 The complete hydrodefluorination and hydrogenation of refrigerant gas R-1234yf using a zirconocene reagent

In the context of refrigeration, Jones also showed in this publication that CFCs such as dichlorodifluoromethane could be converted to methane (GWP = ~ 21), albeit requiring a longer reaction time. Downsides to this technique are evident, the formation of a simple alkane from a fluorinated alkene is undoubtedly a chemical devaluation, however it was a significant discovery that paved the way for methodology with higher utility.

In 2002, Thomas Braun *et al.* developed a rhodium based system to selectively convert hexafluoropropene (HFP) into 1,1,1-trifluoropropane.<sup>[3]</sup> This was an advance over a publication by Whittlesey whereby a ruthenium dihydride complex *trans*- $[\text{Ru}(\text{dmpe})_2\text{H}_2]$  (dmpe =  $\text{Me}_2\text{PCH}_2\text{CH}_2\text{PMe}_2$ ) converted hexafluoropropene into a mixture of hydrodefluorinated products.<sup>[4]</sup> It also improved upon Jones' method described above whereby dihydrogen became the hydride source, compared to using stoichiometric  $[\text{ZrCp}^*_2(\text{H})_2]$ .

Addition of HFP in the presence of triethylamine ( $\text{Et}_3\text{N}$ ) to a solution of  $[\text{Rh}(\text{PEt}_3)_3\text{H}]$  resulted in rapid rhodiation of the C–F bond *trans* to the  $\text{CF}_3$  group, as determined by  $^{19}\text{F}$  NMR spectroscopy and single crystal X-ray diffraction analysis. Upon addition of  $\text{H}_2$  to the resultant rhodium–fluoroolefin species 1,1,1-trifluoropropane was generated in an 80 % yield, based upon  $^{19}\text{F}$  NMR spectrum analysis. The exact nature of C–F activation process that led to the triply defluorinated and hydrogenated product was unknown upon publication.



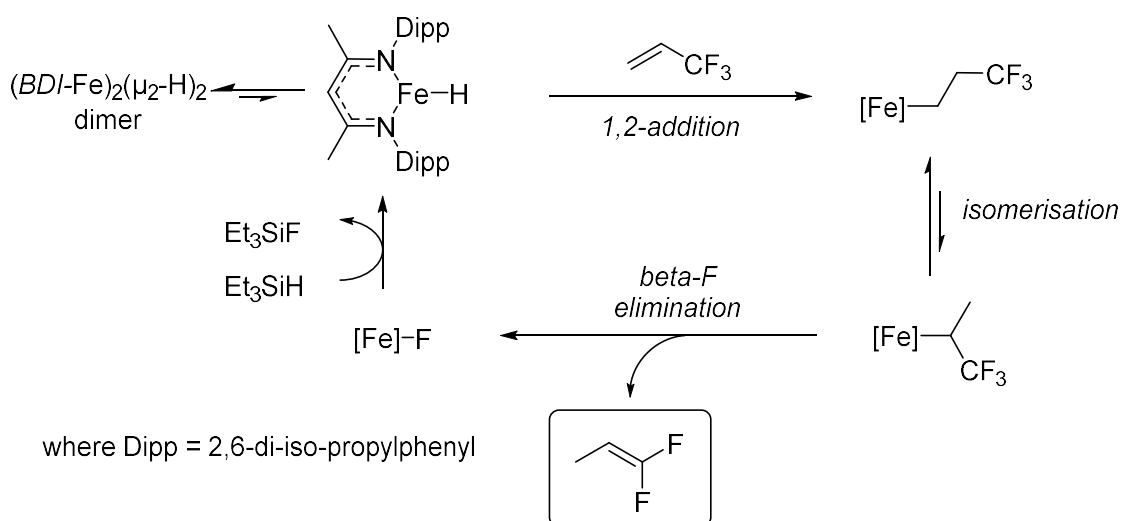


Scheme 3.2 Selective  $sp^2$  hydrodefluorination of HFP by  $[Rh(PEt_3)_3H]$

A more in depth study of this system was performed later.<sup>[5]</sup> It was found that reaction of (*E*)-1,2,3,3,3-pentafluoropropene with the rhodium complex led to the selective defluorination of the internal C–F bond to generate (*Z*)-1,3,3,3-tetrafluoropropene and that the rhodium fluoride by-products could be converted back to the active species upon reaction with a silane (such as  $Et_3SiH$ ).

### 3.1.2 Transition Metal Catalysed Partial Hydrodefluorination

Catalytic systems are limited in the field of C–F activation, due largely to the strong M–F bonds that are subsequently formed. In 2005, Holland and co-workers developed one such method however. A  $\beta$ -diketiminato (BDI) supported iron hydride system was shown to catalyse the HDF of 3,3,3-trifluoropropene to 1,1-difluoropropene, albeit still requiring stoichiometric triethylsilane as a fluorine acceptor.<sup>[6]</sup>



Scheme 3.3 Catalytic HDF of 3,3,3-trifluoropropene to 1,1-difluoropropene mediated by an iron hydride complex

The iron hydride exists as a bridging hydride dimer in its resting state, which can separate into its monomer active species. This active monomer undergoes a concerted 1,2-addition of the C=C  $\pi$ -bond

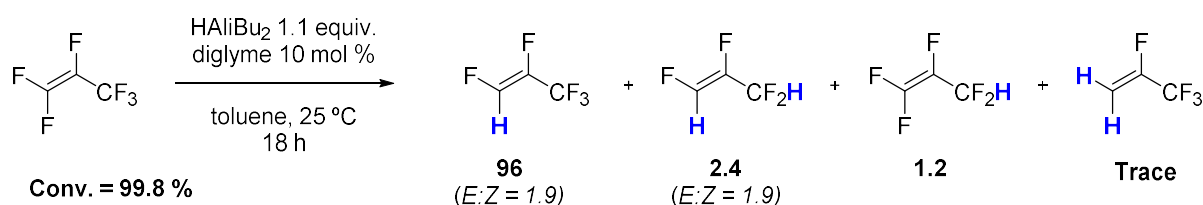
with anti-Markovnikov selectivity, followed by isomerisation to its branched form. This isomerisation is key to accessing the  $\beta$ -fluoride elimination step to finally generate the unsaturated fluoroolefin plus the iron fluoride by-product. Turnover is achieved upon addition of triethylsilane. A sigma-bond metathesis reaction occurs, with the formation of the very strong Si–F bond supplying a driving force for this reaction and perpetuating the cycle. Unfortunately, turn-over numbers were low (TONs = 1 - 10) and fairly forcing conditions of 100 °C for multiple days were required.

Other systems for the hydrodefluorination of alkenes have been developed over the past two decades, mediated by various transition metals such as osmium,<sup>[7]</sup> titanium,<sup>[8]</sup> copper<sup>[9,10]</sup> among others.<sup>[11]</sup>

### 3.1.3 Main Group Mediated Partial Hydrodefluorination

More recently, less expensive and more naturally abundant main group metals have offered promising results in the area of selective hydrodefluorination. Main group metals are typically cheaper and less toxic, therefore development of this methodology to generate valuable, partially fluorinated olefins is particularly attractive.

For example, Lentz and co-workers designed a process to partially defluorinate HFP to form a mixture of products including industrially relevant HFOs.<sup>[12]</sup> Stoichiometric alane reagent HAl*i*Bu<sub>2</sub> (DIBAL) was used in conjunction with an ethereal solvent such as diglyme, used in substoichiometric quantities. Within 18 hours under ambient conditions, hexafluoropropene was converted into a mixture of HFOs, with a single defluorination at the vinylic position being highly favoured (~90%). They found the incorporation of a coordinating solvent, diglyme, to be required for the reaction to occur. The HDF process was shown not to occur in pure toluene. This highlights the importance of solvent effects and diglyme could be considered a ligand in this scenario with three coordinating oxygen atoms available. The choice of ligand could potentially be used to control the reactivity, as its coordination to the aluminium centre is likely to be involved in the rate-determining step (since no reaction occurs without it).



*Scheme 3.4 Mild HDF process of HFP with DIBAL*

Upon broadening the substrate scope to trifluoroethylene only trace quantities of HDF products were identified by <sup>19</sup>F NMR spectroscopy, revealing the limitations to this reaction. Competition reactions

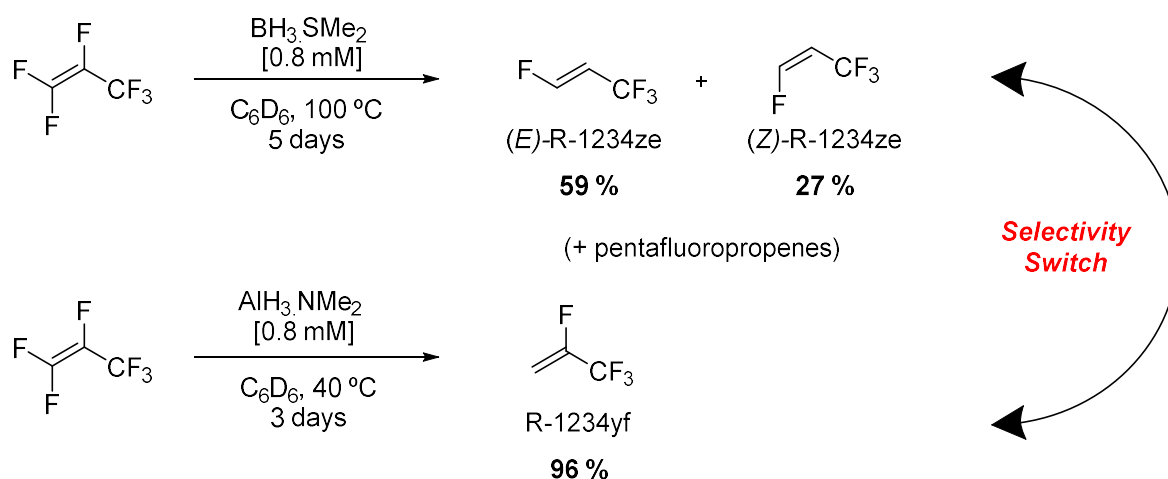
were undertaken on a range of halogenated trifluoroethylenes,  $C_2F_3X$  (where  $X = Cl, Br$  or  $I$ ). In the case of  $X = Cl$  or  $Br$ , the  $C-F$  bond was found to react preferentially, however the chemoselectivity switched when  $X = I$ , yielding trifluoroethylene.

DFT studies were performed to elucidate the reaction mechanism. In hydrocarbon solvents, DIBAL exists as a dimer. Upon coordination of a single THF molecule, this dimer becomes asymmetric and one  $Al-H-Al$  bridge is weakened. This weakened bridge results in a lower activation barrier for HDF, which is reported to proceed via  $S_NV$  mechanism.

In related studies, the Crimmin group recently reported the selective HDF of HFP using commercial borane and alanes as stoichiometric reagents to synthesise fourth generation refrigerants, namely R-1234yf and R-1234ze.<sup>[13]</sup> This work offered an improvement over existing methods by Lentz whereby more complex and expensive *N*-heterocyclic carbene alane adducts ( $AlH_3 \bullet NHC$  where  $NHC = N$ -heterocyclic carbene, 5 examples) were used to generate fluoroolefin R-1234yf from hexafluoropropene.<sup>[14]</sup>

Reaction of a 0.8 mM solution of  $BH_3 \bullet SMe_2$  in  $C_6D_6$  with hexafluoropropene at 1 bar pressure at 100 °C initially led to the formation of 1,2,3,3,3-pentafluoropropene (as *cis/trans* isomers) after just one day. An additional 4 days of reaction led to the formation of R-1234ze isomers in a combined yield of 86 % ( $E:Z = 2:1$ ).

It was found that substitution of boron with the heavier group 13 analogue aluminium allowed for a switch in selectivity to now generate 2,3,3,3-tetrafluoropropene (R-1234yf), with HDF occurring primarily at the vinylic positions with high selectivity and conversion. This selectivity switch was the result of a change in reaction mechanism, as determined upon extensive DFT studies. The borane reagent reacts *via* an initial ligand dissociation step followed by 1,2-addition-elimination sequences. The alane however reacts in an  $S_NV$  manner which favours HDF at the more electrophilic terminal carbon position.

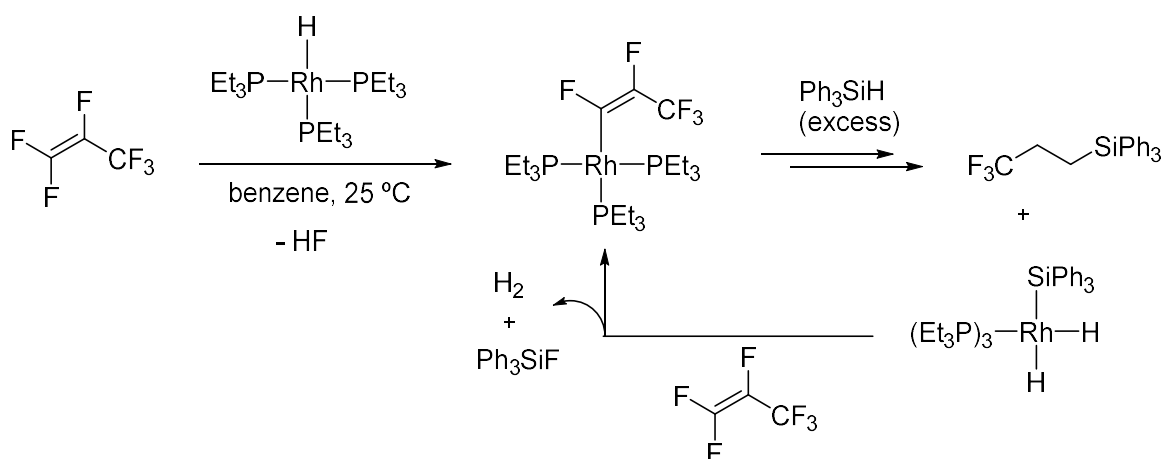


Scheme 3.5 HDF of HFP with simple boranes and alanes to yield industrially relevant HFOs

This represents an attractive method for the synthesis of refrigerant HFOs, particularly in the case of the aluminium reagent as only one isomer is produced. However the use of stoichiometric reagents is not ideal for industrial application, as large quantities of metal–fluoride would be produced as a by-product. For this specific example however, the problem can be partially mitigated due to the inherent value of  $\text{AlF}_3$  and  $\text{BF}_3$  as catalysts or reagents which can be re-used or re-sold.

### 3.1.4 Hydrodefluorination with C–Element Bond Formation

Braun *et al.* developed their rhodium-based hydrodefluorination process, now demonstrating the formation of C–Si bonds as the final step in the process.<sup>[15]</sup> Previously, only hydrodefluorination products were reported. Addition of hexafluoropropene to a solution of  $[\text{Rh}(\text{PEt}_3)_3\text{H}]$  catalyst in the presence of excess triphenylsilane ( $\text{Ph}_3\text{SiH}$ ) as the hydrogen source led to the selective formation of (3,3,3-trifluoropropyl)triphenylsilane. A TON of 90 was achieved under ambient conditions, representing the number of fluorine atoms abstracted per Rh centre. Other silanes such as  $\text{Et}_3\text{SiH}$ ,  $\text{PhMe}_2\text{SiH}$  and  $(\text{MeO})_3\text{SiH}$  were effective albeit with lower TONs.

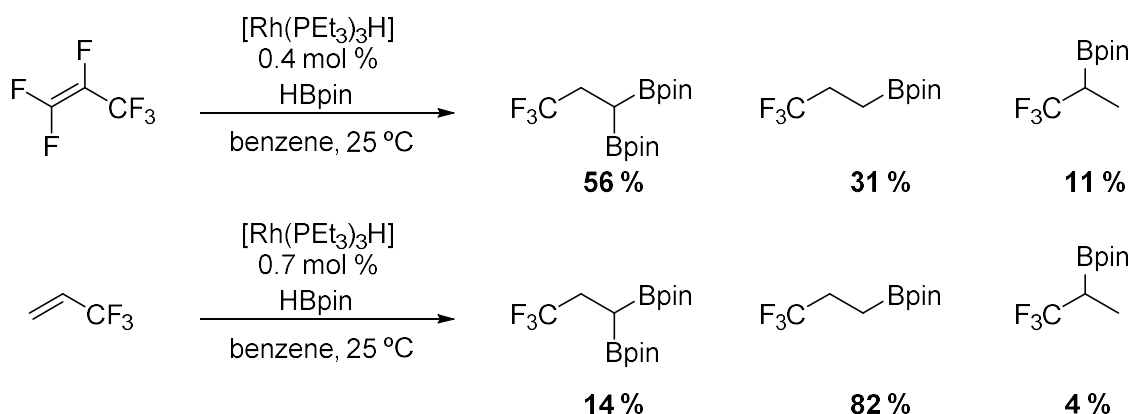


Scheme 3.6 Rhodium catalyzed hydrodefluorination and subsequent C–Si bond forming reactions of HFP

This represented an advance as it was one of the first examples of catalytic C–F bond cleavage that was not a simple HDF process. A new C–Si bond was formed, giving the new compound a site for further derivatisation *via* well understood silicon chemistry. However, the saturation of the C=C  $\pi$ -bond may be undesirable in many cases as it narrows the scope for further reactivity.

Braun later showed a similar transformation to form new carbon–boron bonds.<sup>[16]</sup> Employing the same rhodium catalyst under similar conditions, whilst replacing the silane with a commercial dioxaborolane reagent, HBpin (4,4,5,5-tetramethyl-1,3,2-dioxaborolane) the formation of a mixture of fluoroalkyl boronate esters could be achieved. This represented the first example of a catalytic C–F borylation process on fluoroalkenes.

Bubbling HFP through a benzene solution of  $[\text{Rh}(\text{PEt}_3)_3\text{H}]$  (0.4 mol %) in the presence of HBpin full conversion of HBpin was achieved to generate three products, with a bis-borylated species predominating (Scheme 3.7).



Scheme 3.7 Rhodium catalyzed C–F borylation of fluoroalkenes yielding fluoroalkyl boronate esters

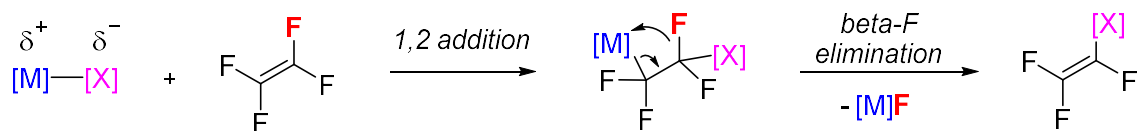
There was evidence for the formation of a Rh(I) boryl species in the reaction. When performing the reaction with 3,3,3-trifluoropropene, the favoured product was a mono-borylated product showing anti-Markovnikov selectivity (no C–F activation occurred). This is conceivable through a simple catalysed hydroboration, however a doubly borylated product was also observed in a 14 % yield. This observation would suggest that dehydrogenative borylation reactions are plausible as the formation of a C–H borylated alkene is a necessary precursor of the doubly substituted product that was observed experimentally. Although this was a significant advancement in the field, the formation of product mixtures is not ideal and the process will continue until all C=C  $\pi$ -bonds are saturated.

### 3.1.5 Mono Defluoroborylation and Defluorosilylation

Hydrodefluorination has its limitations with regards to adding value, with only lower fluorine-containing alkenes or alkanes accessible. As discussed in Chapter 1, the discovery of new fluorine containing chemicals for pharmaceutical or agrochemical purposes have relied on the use of easy-to-handle fluorinating agents or fluorinated building blocks. In this context, the upgrading of fluoroolefins *via* C–F activation to form new carbon–element bonds represents an attractive entry point to this field.

Fluoroolefins can react through multiple plausible mechanisms. The unsaturated bond offers the possibility of 1,2-addition, vinylic substitution ( $S_NV$ ) or conjugate nucleophilic addition ( $S_N2'$ ) reactivity.

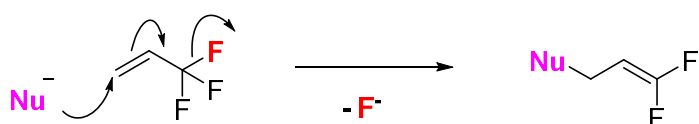
## 1,2 Addition Elimination



## $S_NV$ - Nucleophilic vinylic substitution



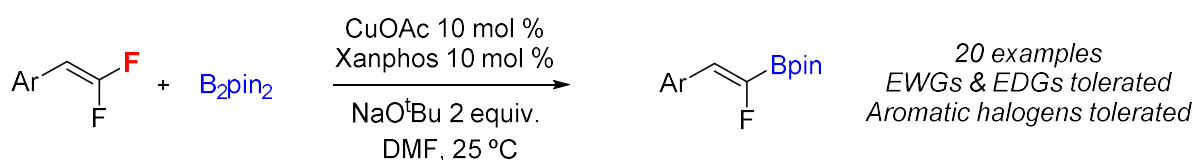
## $S_N2'$ - Nucleophilic conjugate substitution



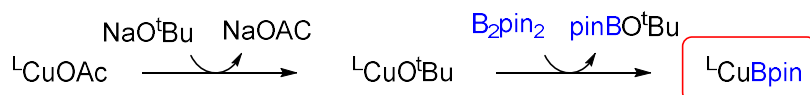
Scheme 3.8 Three plausible reactivity pathways of fluoroolefins

Whilst much progress has been made in catalytic aromatic C–F functionalisation such as the borylation reactions by the groups of Zhang,<sup>[17]</sup> Martin,<sup>[18]</sup> Hosoya,<sup>[19]</sup> Marder and Radius,<sup>[20]</sup> examples of olefinic C–F bond functionalisation remained relatively sparse for much of the 2010's. This dry spell ended in 2017 when Cao and co-workers successfully demonstrated C–F borylation reactions of vinyl fluorides.<sup>[21]</sup> Their system employed a simple copper(I) catalyst (CuOAc) in conjunction with a commercial diboron reagent ( $B_2pin_2$ ), a phosphine based ligand and a base. Gem-difluoroalkenes are susceptible to nucleophilic attack due to the electron deficiency of the double bond.

The reaction was found to be heavily solvent dependant, only proceeding in DMF or DMA (DMF = *N,N*-dimethylformamide, DMA = *N,N*-dimethylacetamide). Copper(II) catalysts were shown not to be active. A large substrate scope was presented, with examples including electron-rich and electron-poor aromatic gem-difluoroalkenes. Aromatic halogen ( $X = Cl, Br$ ) and ether functional groups were tolerated. The active species is generated *in situ* upon ligand exchange of the acetate with the base to form the alkoxide,  $B_2pin_2$  then reacts with the alkoxide to form the copper(I) boryl. This key intermediate can undergo addition to the fluoroalkene by a 1,2-addition elimination pathway to generate the desired products.



generation of active species:



Scheme 3.9 Copper catalysed defluoroborylation of gem-difluoroalkenes

Borylation was always achieved in a *trans*-orientation, which can be rationalised through the Newman projection. Rotation around the C–C bond is required to minimise steric repulsion between the arene and boron groups.

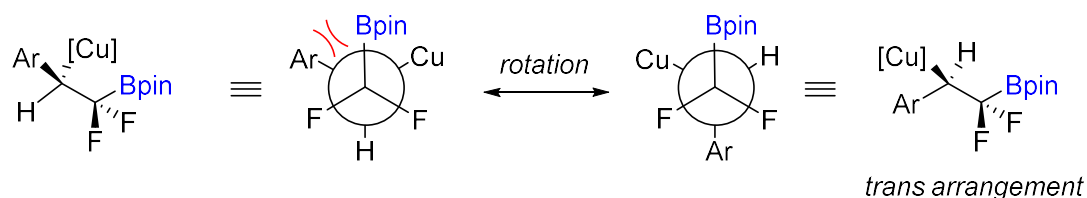
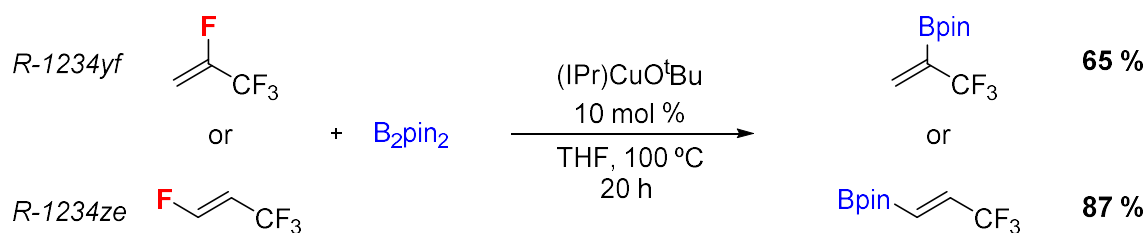


Figure 3.2 Newman projection to show origin of *trans*-selectivity in defluoroborylation reaction

It was also demonstrated that mono-fluorinated vinyl substrates could be effectively defluoroborylated in a similar fashion. To illustrate the versatility of these new boron based fluorinated building blocks, a range of functional group interconversion (FGI) reactions were performed on one product, derivatising the product into eight new chemicals.

Copper catalysts have been found to be important reagents for the breaking of olefinic C–F bonds over recent years. This method was further developed by Ogoshi and Hosoya to allow access to HFO substrates upon modification of the copper catalyst and conditions.<sup>[22]</sup> A strongly donating N-heterocyclic carbene ligand was required as well as forcing conditions (100 °C) to achieve good yields of defluoroborylated HFOs, but nevertheless this represented a step forward as the functionalisation of industrially relevant fluoroolefins (R-1234yf and R-1234ze) was now accessible.



Scheme 3.10 Copper catalysed defluoroborylation of R-1234ze and R-1234yf



The limited stability of the defluoroborylated products was one downside to this transformation. The C–B bonds were found to be susceptible to moisture and the products were also relatively volatile. To overcome these issues, Ogoshi *et al.* modified their process developing a method for the silyl–cupration of fluoroolefins.<sup>[23]</sup> By employing a silyl–boronate ester (PhMe<sub>2</sub>SiBpin) a reactive copper silyl species could now be generated. This intermediate can undergo a 1,2-addition to the C=C π-bond and a subsequent β-fluoride elimination step yields the desired defluorosilylated products.

A variety of fluoroolefins were accessible, including those used for refrigeration purposes such as R-1234yf and R-1234ze. Yields were typically high after 20 hours at 100 °C in THF solvent. A set of stoichiometric reactions provided compelling evidence for the mechanism in play. Isolation of a silyl–copper intermediate was achieved upon addition of *in situ* generated (IPr)CuSiMe<sub>2</sub>Ph (where IPr = 1,3-bis(2,6-di-iso-propylphenyl)imidazol-2-ylidene) to a tetrafluoroethylene solution at 25 °C, which was characterised by single crystal X-ray diffraction. FBpin was found to have a crucial role in the β-fluoride elimination step. Thermolysis of the isolated silyl–copper intermediate gave an analogous defluorocuprated product [Cu(IPr)C<sub>2</sub>F<sub>3</sub>] in 48 % yield. Only upon repetition of this reaction in the presence of excess FBpin was the desired product observed. This result suggested a bi-molecular, Lewis acid assisted β-fluorine elimination process was occurring.

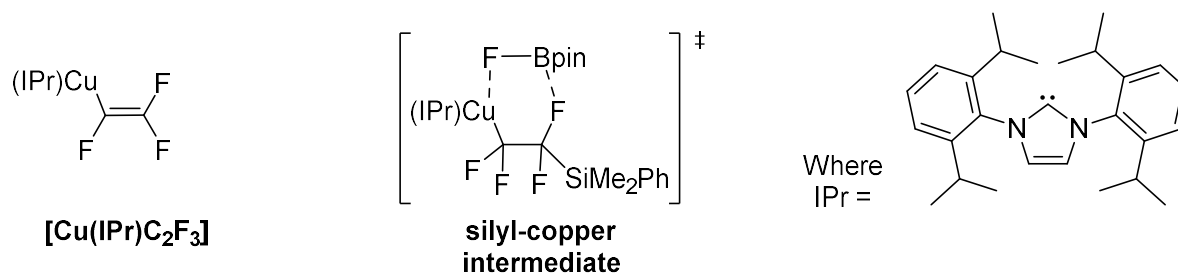
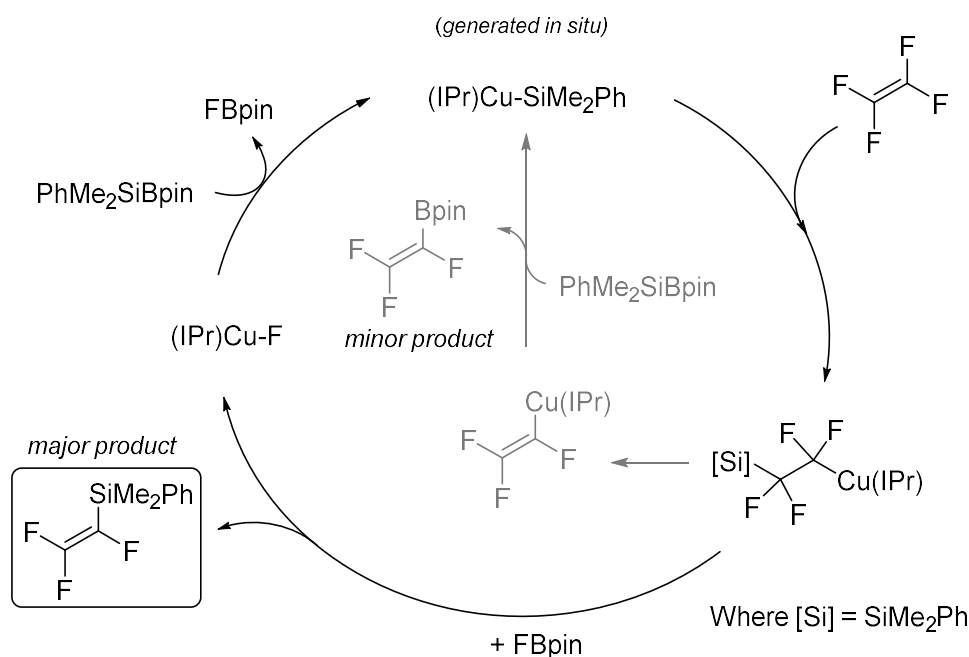


Figure 3.3 Structure of [Cu(IPr)C<sub>2</sub>F<sub>3</sub>] and proposed bi-molecular transition state for β-fluoride elimination of silyl-cuprate species

Upon reaction of the copper fluoroalkene species [Cu(IPr)C<sub>2</sub>F<sub>3</sub>] with PhMe<sub>2</sub>SiBpin (under reaction conditions), the borylated product was observed rather than the silylated one. This rules out the possibility of a transmetalation process occurring to generate the desired product. From these stoichiometric reactions, a plausible catalytic cycle was proposed, whilst accounting for the small quantity of borylated product.



Scheme 3.11 Plausible catalytic cycle for defluorosilylation of tetrafluoroethylene

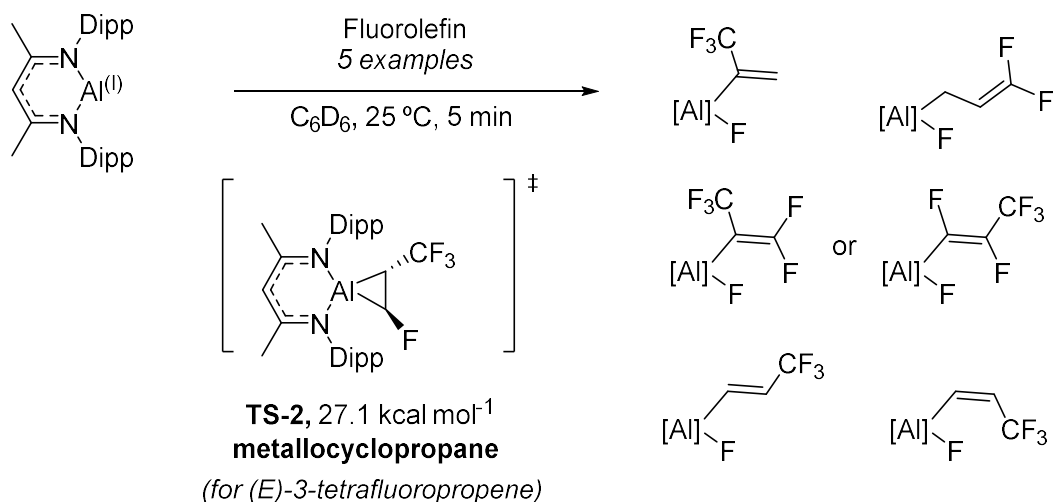
This reaction showed some limitations with respect to substrate scope.  $\alpha,\beta,\beta$ -Trifluorostyrene and octafluorocyclopentene did not react under reaction conditions whilst chlorotrifluoroethylene and perfluoropropoxyethylene underwent cleavage of C–X bonds (where X = Cl, O respectively) in low yields. Nevertheless, this was an improvement on their previous work. Organosilicon reagents are highly versatile, bench stable reagents that are employed ubiquitously in organic chemistry, used for functional group interconversions (FGIs) or C–C bond forming reactions such as Hiyama couplings and Fleming-Tamao oxidations.<sup>[24,25]</sup>

### 3.1.6 C–F Almination of Fluoroolefins

Recently, our group demonstrated a method to oxidatively cleave C–F bonds in six fluoroolefins, including refrigerant HFOs, using a low valent aluminium(I) species.<sup>[26]</sup> The aluminium reagent was first synthesised in 2000 by Roesky and has since displayed many interesting applications in the context of breaking strong bonds.<sup>[27]</sup> This reagent has been shown in previous studies to effectively oxidatively cleave C–F bonds in fluoroarenes and fluoroalkanes.<sup>[28,29]</sup>

Addition of (*E*)-R-1234ze to a benzene-*d*<sub>6</sub> solution of Al(I) led to the formal cleavage of the vinylic sp<sup>2</sup>C–F bond and the formation of *E*:*Z* isomers of an aluminated product in a 4:1 ratio. Contrastingly, repetition of this reaction with (*Z*)-R-1234ze led to the formation of a 9:10 (*E*:*Z*) mixture of products. These results revealed that there was a process occurring along the reaction pathway that could cause inversion of the stereochemistry at the C=C  $\pi$ -bond, leading to an erosion of the stereochemistry in the final product. Computational calculations ( $\omega$ B97X/D2/PCM) on the reaction with (*E*)-R-1234ze with

Al(I) led to the discovery of two plausible processes. 1) The direct oxidative addition of a C–F bond, which would lead to stereoretention (**TS-1**,  $\Delta G^{\ddagger}_{298\text{K}} = 23.5 \text{ kcal mol}^{-1}$ ). 2) The formation of a metallocyclopropane intermediate upon initial oxidative addition to the alkene (**TS-2**,  $\Delta G^{\ddagger}_{298\text{K}} = 27.1 \text{ kcal mol}^{-1}$ ). This intermediate can then undergo a  $\beta$ -fluoride elimination process. This trend was supported upon functional testing the computational methods. **TS-2** was consistently higher in energy to **TS-1** ( $\Delta\Delta G^{\ddagger}_{298\text{K}} = +0.6 - +3.6 \text{ kcal mol}^{-1}$ ). The energies of these two pathways would suggest that stereoretention should dominate, supporting the experimental observations.

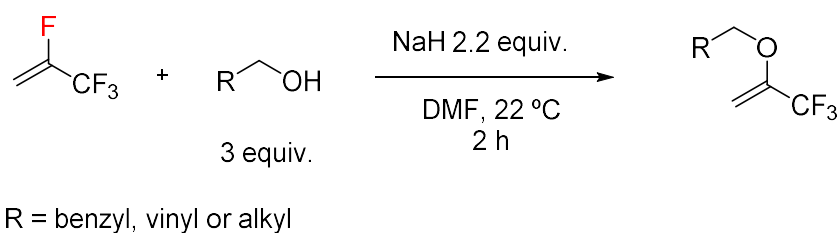


Scheme 3.12 C–F almination of fluoroolefins using a low valent Al(I) reagent

The use of aluminium as the metal is desirable as it is relatively cheap, abundant and non-toxic. However, the large scale synthesis of  $\beta$ -diketiminate supported aluminium(I) is non-trivial and the products of this reaction are themselves sensitive to air and moisture meaning their applications in further synthesis are limited. If the final product contain  $\beta$ -fluorides in relation to Al, elimination processes can occur which lead to an aluminium difluoride species and a HFO by-product, as was observed with R-1336mzz yielding 1,1,4,4-tetrafluorobutadiene (25 °C, 30 min). The discovery of cyclopropane intermediates during this study was itself important and led to the revelation of reversible alkene binding to aluminium.<sup>[30]</sup>

### 3.1.7 Reaction with Oxygen Nucleophiles

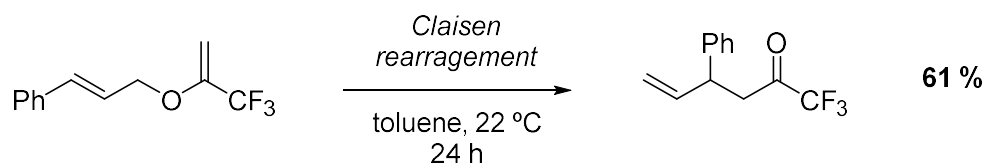
The group of Yamazaki reported the simple synthesis of fluorinated vinyl ethers from R-1234yf and alkoxide nucleophiles.<sup>[31]</sup> The reaction was found to be most effective when employing 3 equivalents of alcohol and 2.2 equivalents of sodium hydride base (NaH) in DMF solvent. The reactions in most cases were complete within 2 hours at 22 °C.



*Scheme 3.13 Synthesis of fluorinated vinyl ethers from R-1234yf and alcohol substrates*

The reactions occurred regioselectively at the C2 position of the fluoroolefin, with the authors proposing an addition-elimination reaction mechanism. Calculation of the natural charges on R-1234yf using computational methods (B3LYP/6-311++G\*\*) revealed that the C2 position of the olefin is more electron deficient than the C1 position (0.318 vs. -0.408), indicating nucleophilic attack would occur at the central carbon. This results in direct C–F oxygenation, leaving the trifluoromethyl and C=C  $\pi$ -bond intact. Benzyl, vinyl and aliphatic alcohols were shown to take part in the reaction with good efficiency – examples include cinammyl alcohol and cyclohexanol. Electron rich benzyl alcohols performed better, such as *p*-methoxy substituted whilst electron poor benzyl alcohol species were not as efficient. This can be rationalised by the nucleophilicity of the resulting alkoxide. In the case of *p*-nitro benzyl alcohol, reactivity was completely inhibited. Phenols could not be used as nucleophiles in this reaction.

Further derivatisation of the product from parent cinammyl alcohol could be achieved *via* a [3,3] sigmatropic oxy-Claisen rearrangement, yielding a trifluoroketone product.



*Scheme 3.14 [3,3] Sigmatropic rearrangement of cinammyl alcohol derived product*

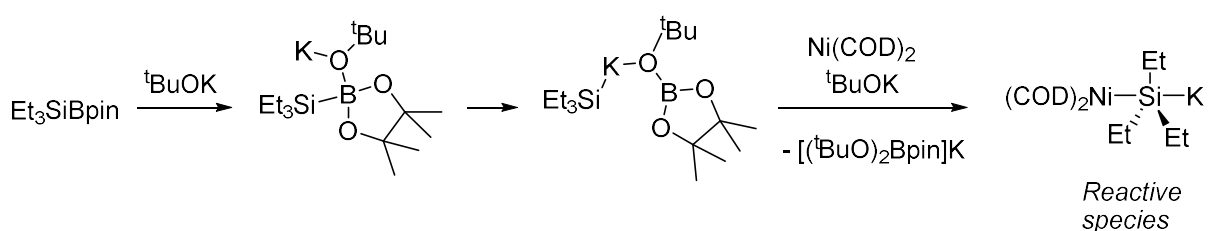
Overall, this methodology represents a very simple approach to upgrade an industrially relevant fluoroolefin (R-1234yf) to higher value targets.

### 3.1.8 Defluorosilylation With *s*-Block Anions

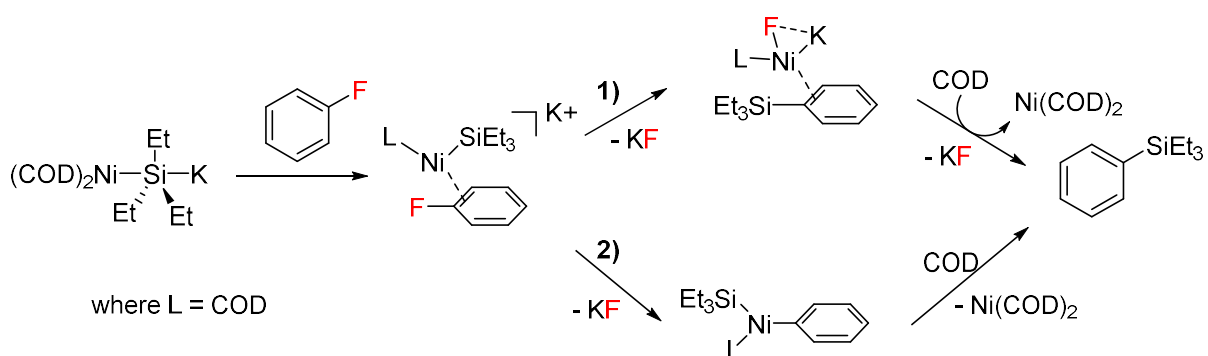
Recently, there has been growing interest into the use of nucleophilic main group reagents, in particular silicon, to break strong carbon–fluorine bonds. In 2018, Shibata described an elegant method for the defluorosilylation of fluoroarenes and displayed a large scope including some pharmaceutically relevant structures.<sup>[32]</sup>

This method relied upon a simple nickel catalyst  $\text{Ni}(\text{COD})_2$  (where COD = 1,5-cyclooctadiene) and alkali metal base ( $^t\text{BuOK}$ ), required no external ligand and could be conducted under mild conditions. The system tolerated methoxy, phenoxy and silyl ether substrates, though significantly electron deficient fluoroarenes did not participate in the reaction. The authors suggest these results ruled out a conventional oxidative-addition process and the presence of  $\text{Ni}^{(0)}$  species, as electron deficient fluoroarenes should be favoured. Instead, a highly nucleophilic potassium–silyl complex was proposed as the reactive species.

A more complex reaction mechanism was proposed whereby silylboronate reagent ( $\text{Et}_3\text{SiBpin}$ ) reacts with  $^t\text{BuOK}$  to generate a 4-coordinate boronate salt. This can then react with  $\text{Ni}(\text{COD})_2$  and another molecule of  $^t\text{BuOK}$  to form a five-coordinate potassium–silyl compound bound to nickel (*Scheme 3.15*). This species is proposed to form a  $\pi$ -complex with the fluoroarene substrate and then two pathways are possible; 1) the nucleophilic silyl can attack the *ipso*-carbon *via* an  $\text{S}_{\text{N}}\text{Ar}$  reaction with the potassium counterion aiding the removal of the fluoride or 2) defluoronickelation occurs (with loss of  $\text{KF}$ ) followed by the reductive elimination of  $\text{Si}-\text{C}$  upon recombination of  $\text{Ni}(\text{COD})_2$  (*Scheme 3.16*).



*Scheme 3.15 Generation of reactive potassium silyl species*

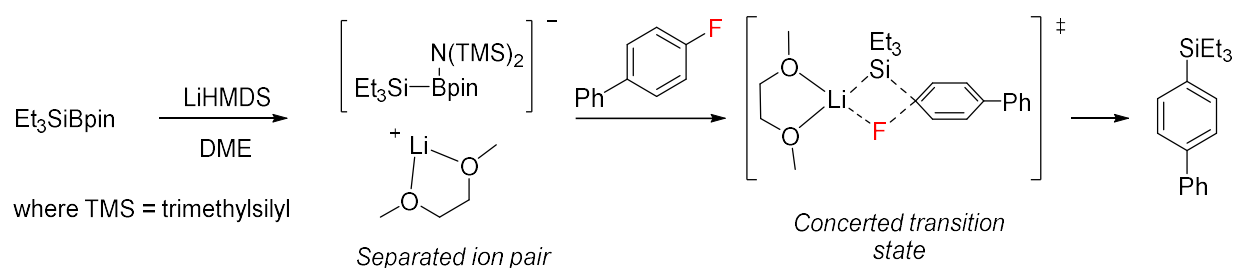


*Scheme 3.16 Formation of reactive potassium silyl species and two plausible pathways (1 & 2) to defluorosilylation*

When they studied their system using fluorocarbon substrates, they found that the nickel catalyst was not necessary for the reaction to proceed, requiring only the silyl boronate and potassium base.

A similar system was also recently described by Martin.<sup>[33]</sup> In this example, successful C–F silylation of fluoroarenes and fluoroalkanes could be achieved without a transition metal catalyst upon opting for a lithium amide base,  $\text{LiHMDS}$  (where HMDS = hexamethyldisilazane) in conjunction with a silyl boronate ester.

A screen of the reaction conditions found that only the combination of LiHMDS in dimethoxyethane (DME) solvent was effective at producing the desired defluorosilylated product in high yields. When altering the alkali metal from Li to Na the yield fell by almost half and moving down the group further to K, the yield became negligible. The authors suggest that the degree of covalency in the Li–F bond is important for the bond cleavage reaction. These Li---F interactions can elongate the C–F bond and facilitate C–Si formation. Furthermore, the higher lattice enthalpy for LiF compared to NaF and KF ( $\Delta H_{\text{lattice}} = 251, 222$  and  $198 \text{ kcal mol}^{-1}$  respectively)<sup>[34]</sup> could also be a contributing factor, supplying a driving force for the reaction. Switching to other polar or ethereal solvents resulted in no C–F bond silylation occurring. The solvation or denticity of the lithium ion could be crucial and suggests the involvement of a separated ion pair, which the authors propose as the reactive species in the reaction. This species can then undergo a concerted  $S_{\text{N}}\text{Ar}$  reaction with fluoroarenes, or  $S_{\text{N}}2$  with fluoroalkane substrates (Scheme 3.17).



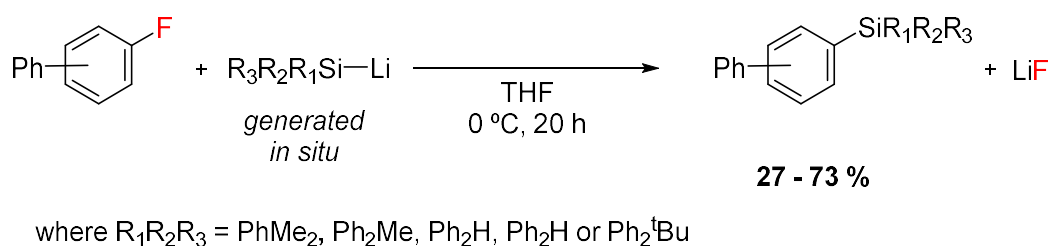
Scheme 3.17 Defluorosilylation of fluorobenzene via formation of reactive ion pair

Deuterium labelling experiments supported the proposed  $S_{\text{N}}2$  reaction pathway. The stereocentre of a fluoroalkane substrate was inverted during the C–F bond cleaving reaction. The process was shown to favour  $\text{sp}^3\text{C–F}$  bonds in the presence of  $\text{sp}^2\text{C–F}$  bonds located on the same substrate. A range of fluoroarenes could be successfully silylated, with tolerance to methoxy, amine, acetal groups as well as nitrogen containing heterocycles. The scope was further extended to a range of pharmaceutically relevant structures, such as fluorinated estrone.

Although a simple modification from Shibata's earlier work, the avoidance of transition metal catalyst offered a significant advantage. The removal of trace transition metals from end products, particularly pharmaceuticals, is a vital yet timely and expensive process. Although the authors suggest this method could be valuable for the upgrading of fluorinated refrigerant gases, no examples were given.

The previous two examples of defluorosilylation methods have both relied on the *in situ* generation of nucleophilic silicon ( $\text{K–Si}$ , or  $\text{Li–Si}$  respectively). It was shown by Studer *et al.* that silyl lithium solutions can be used directly without any other additives for the successful transformation of  $\text{sp}^2\text{C–F}$  bonds in fluoroarenes.<sup>[35]</sup> This technique is conceptually simple. A silyl lithium THF solution ( $\text{R}_3\text{SiLi}$  where  $\text{R}_3 = \text{PhMe}_2, \text{Ph}_2\text{Me}, \text{Ph}_2\text{H}, \text{Ph}_2\text{H}$  or  $\text{Ph}_2\text{tBu}$ ) is filtered onto a THF solution of fluoroarene at  $0^\circ\text{C}$

and stirred for 20 hours. A range of fluoroarenes are included in the scope, exhibiting similar functional group tolerances to methods by Martin and Shibata. Furthermore, the silyl moiety can be varied with five examples shown. It should be noted that as the groups on silicon get larger and contain more conjugated systems the yields of defluorosilylated product decreases.



Scheme 3.18 Direct defluorosilylation of fluoroarenes by silyl lithium solutions

Nucleophilic aromatic substitution ( $\text{S}_{\text{N}}\text{Ar}$ ) was hypothesised to be the dominant mechanism. However, in scenarios where the  $\text{S}_{\text{N}}\text{Ar}$  transition state is not accessible, *ortho*-deprotonation of the substrate can occur. This can lead to an aryne intermediate followed by unselective (*ipso* and *ortho*) silylation, as observed on a bulky fluoro-biphenyl substrate. These two processes were corroborated by computational calculations (TPSS/def2-TZVP+PCM(THF)+GD3BJ) upon reaction of  $\text{PhMe}_2\text{SiLi}\cdot 2\text{THF}$  with fluorobenzene. Transition state energies were located for the  $\text{S}_{\text{N}}\text{Ar}$  vs. aryne pathways ( $\Delta\text{G}^\ddagger_{298\text{K}} = 18.8$  and  $\Delta\text{G}^\ddagger_{298\text{K}} = 21.7$  kcal mol<sup>-1</sup> respectively).

Very recently, Shi *et al.* reported the defluorosilylation of a variety of fluoroalkene substrates, under similar conditions to Shibata and Martin.<sup>[36]</sup> Employing a silylboronate ester ( $\text{PhMe}_2\text{SiBpin}$ ) in conjunction with sodium methoxide ( $\text{NaOMe}$ ), C–F activation could be achieved under relatively mild conditions with good yields on a wide substrate scope.

Two different mechanisms were shown to be in operation, depending on the fluorinated substrate. *gem*-Difluoroalkenes would undergo a nucleophilic vinylic substitution ( $\text{S}_{\text{N}}\text{V}$ ) whereas trifluorovinyl species undergo nucleophilic conjugate substitution ( $\text{S}_{\text{N}}2'$ ). This work described by Shi was published after our results on the defluorosilylation of industrially relevant fluoroolefins.

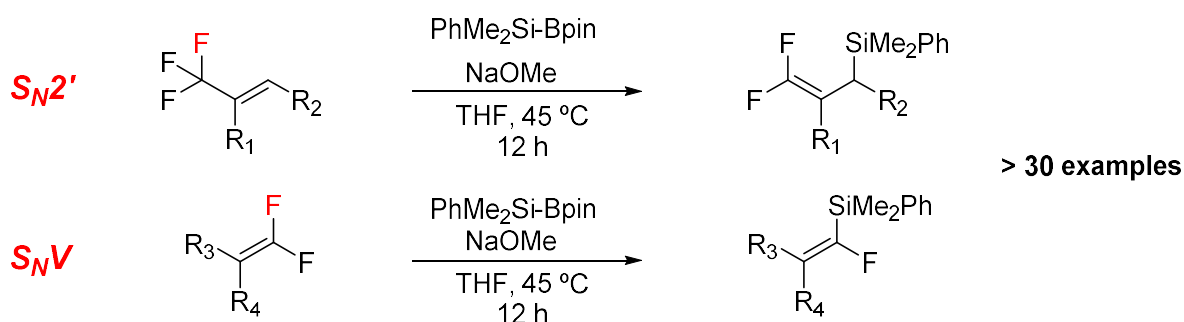


Figure 3.4 Defluorosilylation of fluoroalkenes using silylboronate ester in conjunction with NaOMe





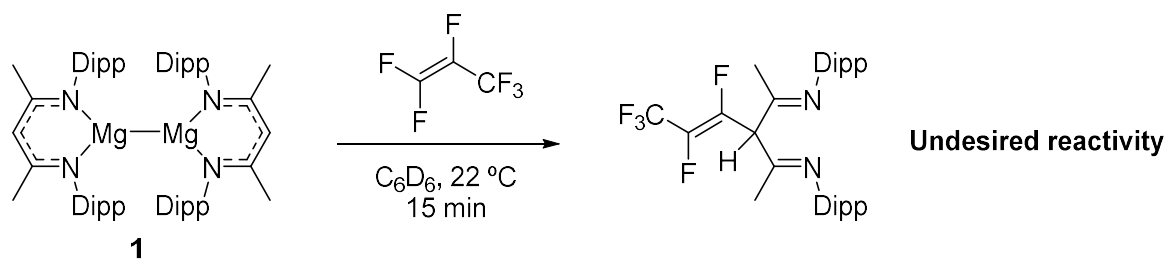
## 3.2 Defluorosilylation of Industrially Relevant Fluoroolefins

### 3.2.1 Synthesis of Magnesium and Lithium Silyl Compounds

The production and use of hydrofluoroolefins for industrial refrigeration purposes is set to accelerate over the coming decades as their predecessors, hydrofluorocarbons, are phased out under climate change initiatives. As discussed in the introduction, the long-term environmental impact of the release of HFOs into the environment remains understudied. Due to the decreased atmospheric lifetimes however, they are likely to contribute to local pollution closer to the source of emission and could break down into more toxic compounds, such as trifluoroacetic acid. It is therefore a timely challenge to develop methods to recycle and reuse these fluorinated gases.

We aimed to build on the recent successes in the group on the use of main group reagents with fluoroalkenes.<sup>[13,26]</sup> Our interest lay with five fluoroolefins, three that are industrially relevant as the new generation of refrigerants. These were, hexafluoropropene (HFP), 3,3,3-trifluoropropene, (*Z*)-1,3,3,3-tetrafluoropropene (R-1234ze), 2,3,3,3-tetrafluoropropene (R-1234yf) and 1,1,1,4,4,4-hexafluorobut-2-ene (R-1336-mzz)

The C–F activation reaction of hexafluoropropene with  $[\text{Dipp}(\text{BDI})\text{Mg}]_2$  (**1**) had been attempted in the group, hoping to generate one equivalent of  $\text{Mg-R}^{\text{F}}$  and one  $\text{Mg-F}$  species, similar to the reactivity observed with the Al(I) reagent and our previous studies on fluorocarbons.<sup>[26,37]</sup> Unfortunately, addition of 1 bar HFP to a degassed sample of **1** resulted in the formation of a complex mixture of products as determined by multinuclear NMR spectroscopy. One of these products was shown to be the result of undesired reaction at the ligand backbone upon  $^{19}\text{F}$  NMR spectrum analysis ( $\delta = -67.7, -138.2$  and  $-170.9$  ppm) which indicated substitution at one terminal vinylic C–F bond. Furthermore, the  $^1\text{H}$  NMR spectrum revealed the methine proton resonates as a doublet of doublets, indicating coupling to two fluorine environments ( $\delta = 4.52$  ppm,  $^3J_{\text{HF}} = 28.9$  Hz and  $^4J_{\text{HF}} = 4.7$  Hz).

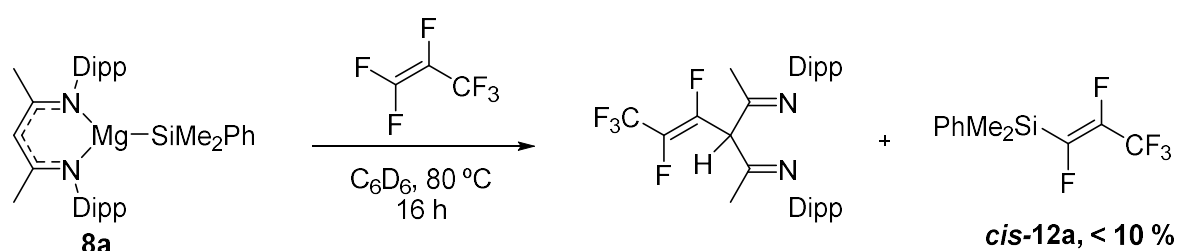


Scheme 3.19 Reaction of HFP with **1a** yielding complex mixture of undesired products

We proposed that  $\beta$ -fluorine elimination would also be a likely decomposition route from the desired organomagnesium products due to strong Mg–F interactions.

Based upon emerging literature it appeared that silicon-based nucleophiles bound to a fluoride-acceptor are ideal reagents for breaking C–F bonds.<sup>[32,33,35]</sup> We therefore investigated the reactivity of industrially relevant fluoroolefins with a range of s-block silicon reagents. The fluorinated products of these reactions would also be particularly attractive for further reactivity. Organosilicon reagents are well studied and versatile in synthetic chemistry, are typically bench stable and can be used directly in cross coupling reactions.

Hill and co-workers have previously reported the synthesis and reactivity of a related magnesium silyl [<sup>Dipp</sup>(BDI)MgSiMe<sub>2</sub>Ph] (**8a**).<sup>[38]</sup> Upon addition of HFP to an *in situ* generated sample of **8a** in C<sub>6</sub>D<sub>6</sub>, the product of the ligand decomposition pathway resulting from nucleophilic attack of the central carbon of the β-diketiminate ligand on HFP was again observed. Despite ligand based reactivity being the major pathway, investigation of the <sup>19</sup>F NMR spectrum confirmed the generation of the desired product, *cis*-**12a**, in approximately 10 % yield upon comparison to literature data (δ = -67.8 dd, -155.9 dq and -166.2 dq).<sup>[23]</sup>



Scheme 3.20 Undesired reactivity of HFP with magnesium silyl **8a**

Confident that appropriate ligand modification would remove or dampen the nucleophilic carbon site and suppress the undesired pathway, related compounds **9a/b** – **10a/b** were prepared. These reagents feature an imino-anilide ligand, blocking the nucleophilic position when compared to the β-diketiminate ligand. When considering the mesomeric structures of both ligands, **2** and **3** for the imino-anilide (Figure 3.5) are highly unfavoured and hence reduce the nucleophilicity at the backbone carbon. Harder *et al.* exploited this effect when developing magnesium based FLP catalysts for CO<sub>2</sub> activation.<sup>[39]</sup>

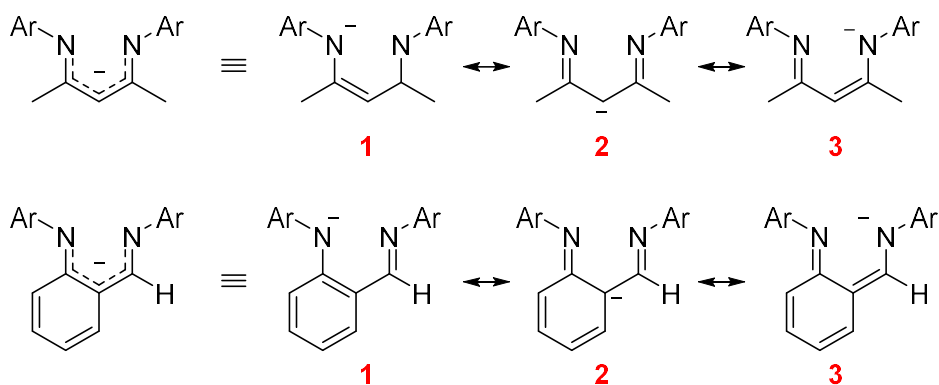
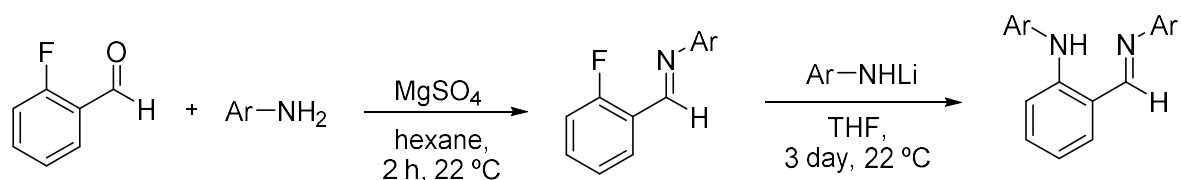


Figure 3.5 Mesomeric structures of  $\beta$ -diketiminato ligand vs imino-anilide ligand

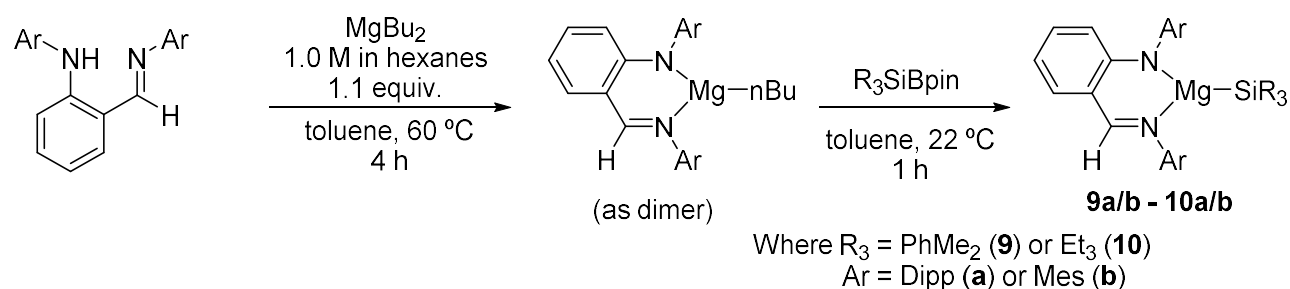
Imino-anilide ligands containing mesityl (1,3,5-trimethylbenzene) and 2,6-di-iso-propylphenyl groups could be synthesised on large scales in three steps from the parent 2-fluoroacetophenone and respective anilines.<sup>[40]</sup>



Where Ar = 1,3,5-trimethylbenzene or 2,6-di-iso-propylphenyl

Scheme 3.21 Two-step synthesis of imino-anilide ligands

The magnesium silyl reagents could in turn be synthesised in two steps from the imino-anilide ligands – reaction with  $\text{Mg}^n\text{Bu}_2$  to yield the magnesium alkyl species followed by metathesis with a silylboronate ester ( $\text{R}_3\text{SiBpin}$ , where R =  $\text{PhMe}_2$  or  $\text{Et}_3$ ).



Scheme 3.22 Two-step synthesis of magnesium silyl reagents from parent imino-anilide ligands

Due to difficulties in their isolation, some of these compounds were isolated as THF adducts. Their stability in solution without ethereal solvation (generation *in situ* from  $^L\text{Mg}^n\text{Bu}$ , where L = imino-anilide ligand) was good however and they did not display significant degradation even upon heating at 80 °C. Full characterisation of four compounds was achieved using multinuclear NMR spectroscopy and single crystal X-ray diffraction in the case of **9a.THF** and **9b**.

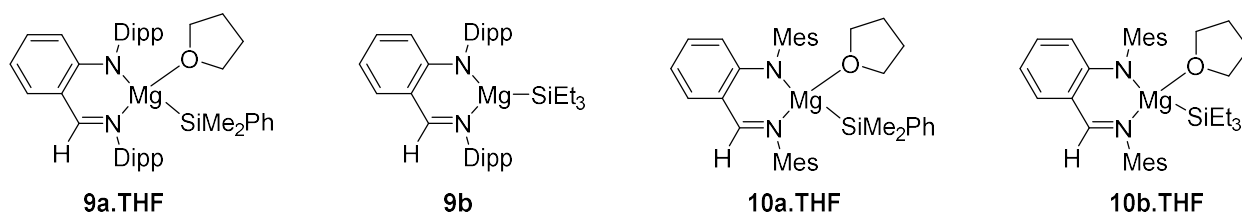


Figure 3.6 Novel magnesium silyl compounds

To the best of our knowledge, compound **9b** represents the second example of a three-coordinate magnesium bound to silicon. The Mg–Si bond is 2.6022(9) Å, slightly longer to that reported by Hill for related compound **8a** (Mg–Si = 2.5900(7) Å).<sup>[38]</sup> Compound **9a.THF** displays a Mg–Si interaction of 2.614(1) Å, which falls well within the range reported in the literature for similar silicon analogues of Grignard reagents (c.f. [Mg( $\kappa^2$ -TMEDA)(Br)(SiMe<sub>3</sub>)], Mg–Si = 2.651(6) Å).<sup>[41,42]</sup>

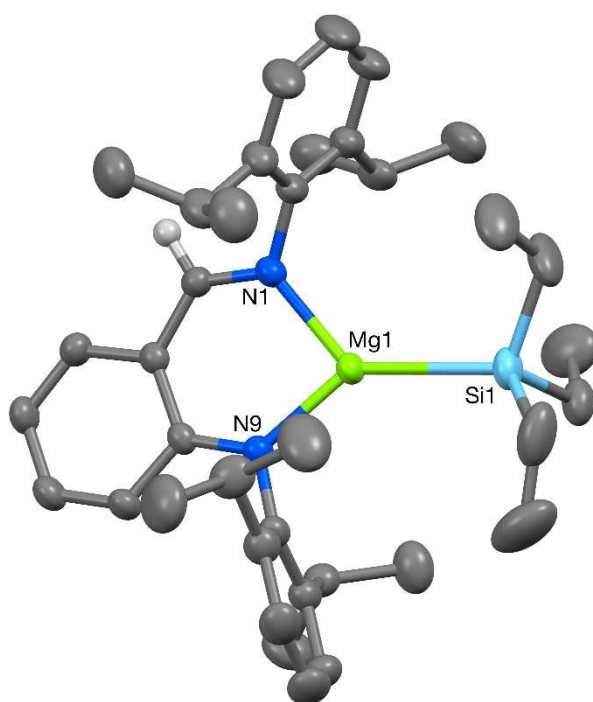


Figure 3.7 The crystal structure of **9b** Mg–Si 2.6022(9) Å (50% probability ellipsoids).

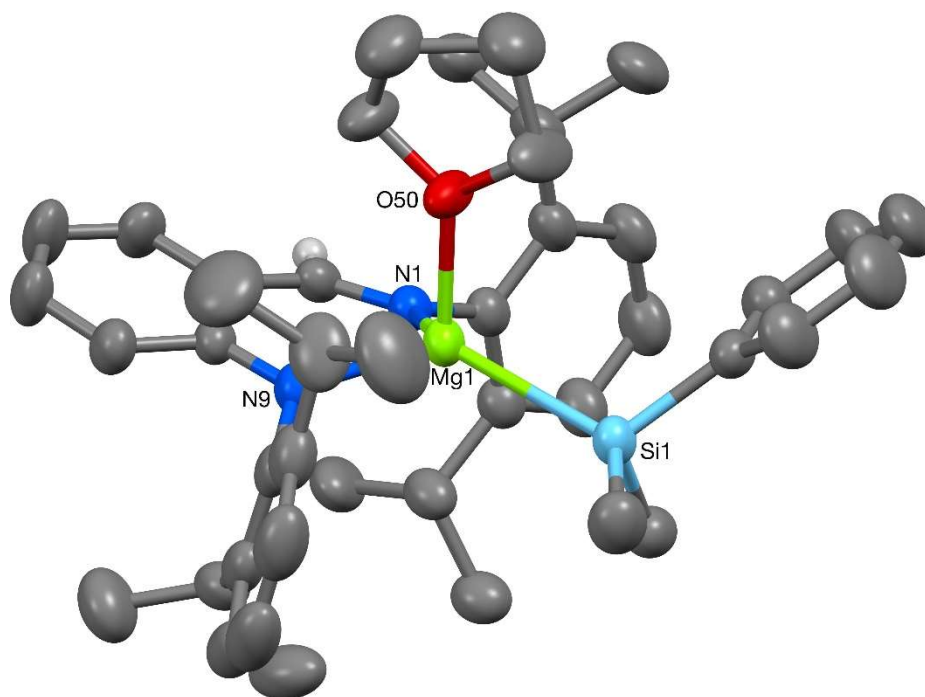


Figure 3.8 The crystal structure of **9a**·THF Mg–Si 2.614(1) Å (50% probability ellipsoids).

In an alternative approach taking inspiration from recent literature, [Li(SiMe<sub>2</sub>Ph)(THF)<sub>1.5</sub>] (**11.THF**), [Li(SiMe<sub>2</sub>Ph)(TMEDA)<sub>1.5</sub>] (**11.TMEDA**) and [Li(SiMe<sub>2</sub>Ph)(PMDETA)] (**11.PMDETA**) were prepared (TMEDA = tetramethylethylenediamine, PMDETA = pentamethyldiethylenetriamine). Electrostatic Li---F interactions are particularly strong (LiF<sub>(s)</sub>, lattice enthalpy = 251 kcal mol<sup>-1</sup>)<sup>[34]</sup> therefore we hoped this would provide a strong driving force for the C–F bond cleaving transformations. The decreased steric bulk of THF and amine ligands should also allow for greater access to the reactive Li–Si bond.

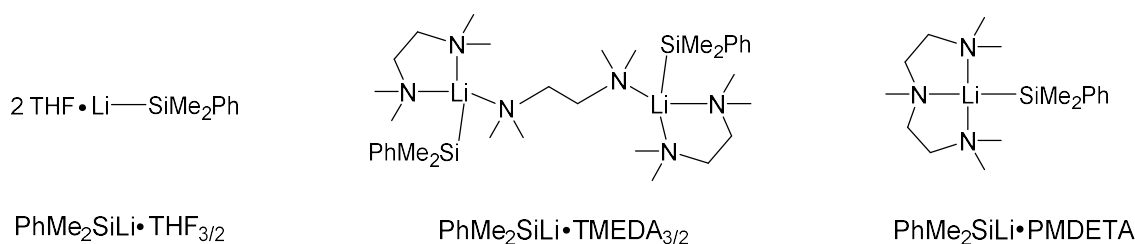


Figure 3.9 Isolated lithium silyl species

**11.THF** was isolated as a dark red oil and based on <sup>1</sup>H NMR spectroscopic analysis contained between 1.5 – 2 THF molecules per silicon atom. The remaining members of the series were isolated as crystalline solids and have been characterised by multinuclear NMR spectroscopy and single crystal X-ray diffraction (Figure 3.9).

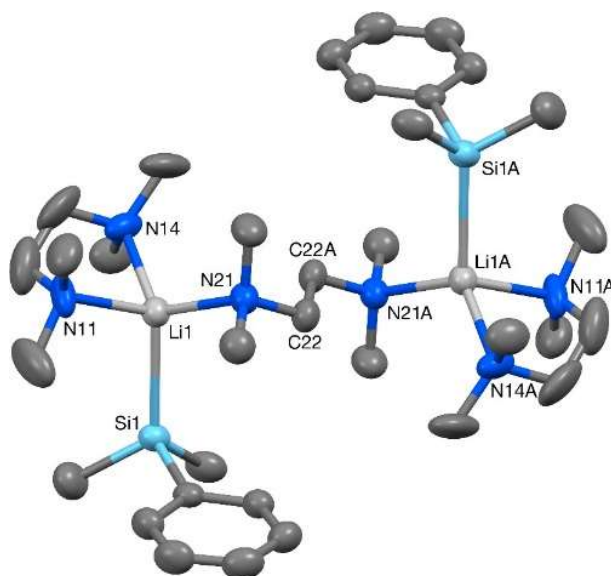


Figure 3.10 Crystal structure of **11.TMEDA**: Li–Si 2.736(3) Å. (50% probability ellipsoids).

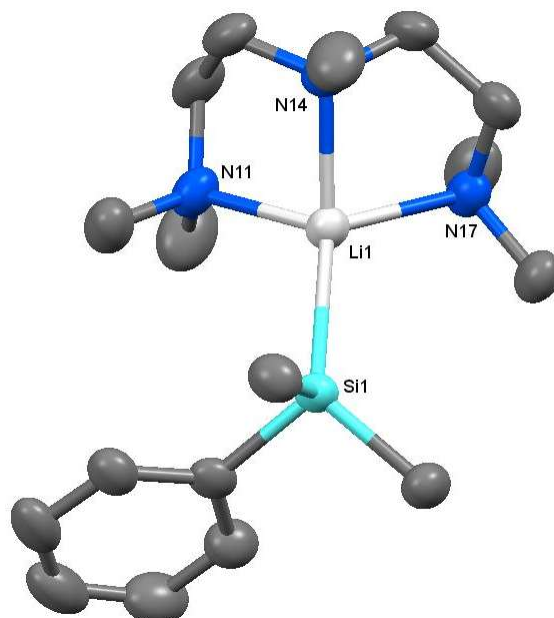


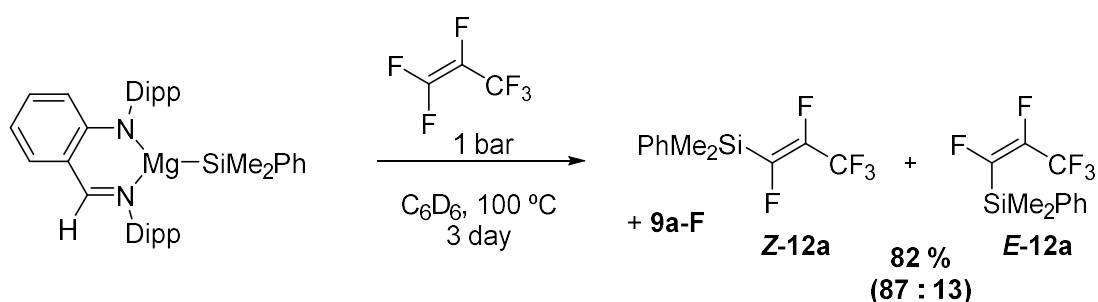
Figure 3.11 Crystal structure of **11.PMDETA**: Li–Si 2.644(2) Å. (50% probability ellipsoids).

The structure of **11.PMDETA** has been reported previously by Strohmann *et al.*<sup>[43]</sup> **11.TMEDA** crystallised as a bridging dimer with three N atoms bound to each lithium centre. The Si–Li bond distance was towards the upper end of similar structures reported in the literature (Li–Si = 2.736(3) Å) with typical distances ranging from 2.52 – 2.76 Å.<sup>[41,43,44]</sup>

### 3.2.2 Defluorosilylation with Magnesium Silyl Compounds

A 0.05 M benzene- $d_6$  solution of **9a**, generated *in situ* from the parent magnesium alkyl complex, was heated to 100 °C under an atmosphere of hexafluoropropene and the reaction was monitored by  $^1\text{H}$

and  $^{19}\text{F}$  NMR spectroscopy. After three days, the desired product **12a** was generated in 82 % yield upon *in situ* comparison to a ferrocene internal standard ( $\delta = 4.0$  ppm) along with the magnesium fluoride by-products (**9a-F**).  $^{19}\text{F}$  NMR spectrum analysis confirmed the formation of *cis/trans* isomers with a ratio of 87:13 (**Z-12a** : **E-12a**).



*Scheme 3.23 Reaction of 9a with hexafluoropropene*

3,3,3-Trifluoropropene reacted under the same conditions albeit with a diminished yield of 44 % to generate the  $\text{S}_{\text{N}}2'$  product (**12c**) whereby the  $\text{C}=\text{C}$   $\pi$ -bond migrates and overall cleavage of a  $\text{sp}^3\text{C}-\text{F}$  bond. Disappointingly, further experiments with other HFOs failed to result in the formation of any defluorosilylated products. We speculated that triethyl silyl analogue **9b** may show better reactivity towards fluoroolefins. This hypothesis was disproven however, observing no desired reactivity with hexafluoropropene after three days at 100 °C.

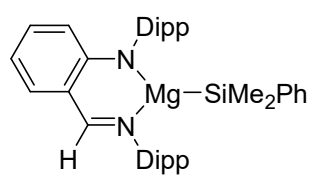
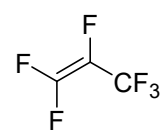
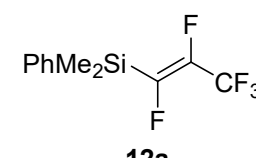
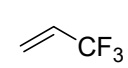
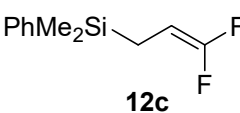
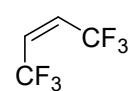
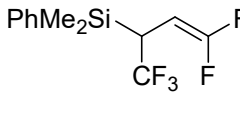
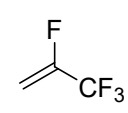
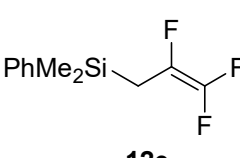
| <b>9a</b><br>(generated <i>in situ</i> )  | Temp / Time  | Product  | Yield %                            |
|---|--|--|------------------------------------|
|                | fluoroolefin<br>~1 bar<br>C <sub>6</sub> D <sub>6</sub> , temp °C,<br>time | PhMe <sub>2</sub> Si-R <sup>F</sup> + <b>9a-F</b><br>(magnesium fluoride by-products)              |                                    |
|                | 100 °C, 3 day  | <br><b>12a</b>   | <b>82</b><br>( <i>E:Z</i> = 87:13) |
|                | 100 °C, 3 day  | <br><b>12c</b>   | <b>42</b>                          |
| <br>R-1336mzz | 100 °C, 3 day  | <br><b>12d</b>  | <b>0</b>                           |
| <br>R-1234yf | 100 °C, 3 day  | <br><b>12e</b> | <b>0</b>                           |

Table 3.1 Results of defluorosilylation reaction of **9a** with fluoroolefins

It had been previously shown in the group that accessibility to the reactive metal–metal bond of Mg–Mg and Mg–Zn nucleophiles is the most important factor in determining reactivity. Consistent with this finding, the enlarged pocket around the Mg–Si bond in **10a** leads to an increased reaction scope that now includes R-1234ze and R-1336-mzz.

Two-step reactions were performed in J. Young NMR tubes from the magnesium alkyl precursors, as isolation of **10a** proved elusive. **10a** was consistently generated *in situ* with 80 – 85 % yield from the magnesium alkyl precursor, upon addition of Suginome reagent (PhMe<sub>2</sub>SiBpin). Fluoroolefins, at 1 bar pressure were added to the de-gassed solution of **10a** and the reactions monitored by <sup>1</sup>H and <sup>19</sup>F NMR spectroscopy. Reactions of **10a** with fluoroolefins proceeded under ambient temperatures (apart from R-1234yf) and the speed of the reactions could be increased slightly upon heating at 60 °C. This contrasted to the reaction with **9a** which required forcing conditions (100 °C) and long reaction times.



Yields for the single C–F activation process were between 60 – 68 % and still maintained good selectivity for the case of hexafluoropropene.

| <b>10a</b><br>(generated in situ) | <b>Temp / Time</b> | <b>Product</b> | <b>Yield %</b>                     |
|-----------------------------------|--------------------|----------------|------------------------------------|
|                                   | 60 °C, 72 h        |                | <b>60</b><br>( <i>E:Z</i> = 90:10) |
|                                   | 22 °C, 24 h        |                | <b>68</b>                          |
| <i>R-1234ze</i>                   |                    | <b>12b</b>     |                                    |
|                                   | 60 °C, 24 h        |                | <b>63</b>                          |
|                                   |                    | <b>12c</b>     |                                    |
|                                   | 22 °C, 72 h        |                | <b>62</b>                          |
| <i>R-1336mzz</i>                  |                    | <b>12d</b>     |                                    |
|                                   | 60 °C, 24 h        |                | <b>0</b>                           |
| <i>R-1234yf</i>                   |                    | <b>12e</b>     |                                    |

Table 3.2 Results of defluorosilylation reaction between **10a** and fluoroolefins

Unfortunately, the C–F activation of R-1234yf still remained elusive even under forcing conditions.

### 3.2.3 Defluorosilylation with Lithium Silyl Compounds

Although the reaction of fluoroolefins with magnesium silyl reagents were mostly successful, the yields were modest and extended reaction times were required at elevated temperatures. We hoped that modification of the fluoride acceptor would enhance the efficiency.

Upon addition of hexafluoropropene to a 0.2 M benzene-*d*<sub>6</sub> solution of **11.THF** at 22 °C, an immediate colour change was observed from dark red to pale orange. Pleasingly, after analysis of the <sup>1</sup>H and <sup>19</sup>F

NMR spectra the formation of the desired product was confirmed in an 81 % yield (selectivity **Z-12a** : **E-12a** = 92:8).

Repeating this reaction employing 3,3,3-trifluoropropene and R-1336mzz gave good yields at 22 °C (88 and 75 % respectively) based upon *in situ* comparison to a ferrocene internal standard. The reaction with R-1234ze showed a diminished yield of 64 % however upon further examination of the <sup>19</sup>F NMR spectrum, a doubly silylated product was revealed in 18 % yield (*vide infra*). This reaction could be further optimised by adding the fluoroolefin at -78 °C in toluene-d<sub>8</sub> solvent then allowing the solution to warm to 22 °C, now achieving 77 % yield based upon *in situ* NMR spectrum analysis.

Addition of R-1234yf to a 0.2 M benzene-d<sub>6</sub> solution of **11.THF** at 22 °C resulted in a similarly rapid reaction, yet analysis by multinuclear NMR spectroscopy showed just 24 % of the S<sub>N</sub>2' product plus other unidentified species. In our case, no defluorosilylation was observed to have taken place at the internal C2 position upon comparison of the <sup>19</sup>F NMR spectroscopic data to the literature.<sup>[23]</sup> We speculated that further silylation reactions could be taking place after generation of the initial mono-silylated product.

Delightfully, optimisation of the conditions (THF, -78 to 22 °C, 3 h) allowed for a much cleaner reaction between **11.THF** and R-1234yf generating the desired product **12e** as the sole species in good yield. It was found generally that performing the reactions at -78 °C in either THF or toluene and slowly allowing the solutions to warm to room temperature (over approximately 4 hours) gave the best selectivity towards the desired products whilst also enhancing the yields.



|                  | Product    | Conditions   | Yield % (isolated)   |
|------------------|------------|--|--|
|                  |            | C <sub>6</sub> D <sub>6</sub> , 22 °C, 15 min<br>toluene, -78 °C, 14 h | <b>81</b> ( <i>E:Z</i> = 92:8)<br><b>(57)</b> ( <i>E:Z</i> = 97:3) |
|                  |            | C <sub>6</sub> D <sub>6</sub> , 22 °C, 15 min<br>toluene, -78 °C, 14 h | <b>64</b><br><b>77</b>   |
| <i>R-1234ze</i>  | <b>12b</b> |  |  |
|                  |            | C <sub>6</sub> D <sub>6</sub> , 22 °C, 15 min<br>toluene, -78 °C, 14 h | <b>88</b><br><b>(47)</b>   |
|                  |            | C <sub>6</sub> D <sub>6</sub> , 22 °C, 15 min<br>toluene, -35 °C, 3 h  | <b>75</b><br><b>(47)</b>   |
| <i>R-1336mzz</i> | <b>12d</b> |  |  |
|                  |            | C <sub>6</sub> D <sub>6</sub> , 22 °C, 15 min<br>THF, -78 °C, 3 h      | <b>24</b><br><b>(69)</b>   |
| <i>R-1234yf</i>  | <b>12e</b> |  |  |

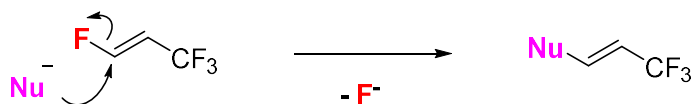
Table 3.3 Results of defluorosilylation reactions of fluoroolefins with **11.THF**. Internal yields given determined upon *in situ* comparison of dimethyl resonance ( $\text{SiMe}_2\text{Ph}$ ) to a ferrocene internal standard capillary ( $\delta = 4.00$  ppm)

The reactions were then repeated on modest scales of approximately 1 mmol at their optimised (low temperature) conditions. The reaction of R-1336mzz was conducted at -35 °C rather than -78 °C as it was performed in the glovebox using a Polar Bear Cub cooling apparatus. After a short work up of the reaction mixture, the fluorinated organosilanes could be isolated as colourless oils by short path distillation in reasonable yields (47 – 69 %). It should be possible to enhance these yields upon further reaction scale up, minimising losses during the distillation process. The *Z:E* selectivity was improved upon isolation of compound **12a** (97:3) highlighting the benefit of performing the reactions at low temperatures.

From these reactions, two different reactivity pathways are being displayed. This depends on the substitution pattern of the fluorine atoms. The fluoroolefins act as Michael acceptors, what differs is the location of the leaving group. When the substrate possesses a terminal vinylic fluorine, a

nucleophilic vinylic substitution or  $S_NV$  process is favoured. When these are absent on the substrate, a nucleophilic conjugate substitution,  $S_N2'$ , reaction will occur.

### $S_NV$ - Nucleophilic vinylic substitution



### $S_N2'$ - Nucleophilic conjugate substitution

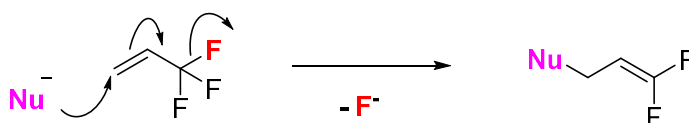


Figure 3.12 Two reactivity modes for fluoroolefins depending on fluorine substitution pathway

The reaction of metal-silyls with R-1234yf and R-1336mzz produce, to the best of our knowledge, novel products. The reactivity of R-1234yf contrasts to the work by Ogoshi, whereby defluorosilylation at the internal vinylic position takes place keeping the trifluoromethyl group in intact.<sup>[23]</sup> This is a result of the opposing mechanisms, whereby the copper-silyl first undergoes 1,2-addition to the fluoroalkene followed by  $\beta$ -fluoride elimination. Due to this opposing mechanism, our system also displays much higher selectivity for *Z:E* isomers of **12.HFP** compared to those of Ogoshi.

#### 3.2.3.1 Reactions with *PhMe<sub>2</sub>SiLi.TMEDA* & *PhMe<sub>2</sub>SiLi.PMDETA*

Ligand exchange reactions with **11.THF** upon addition of bidentate or tridentate amine ligands (TMEDA or PMDETA) yielded crystals of related compounds **11.TMEDA** and **11.PMDETA** in high purity. We envisaged that these would react in a similar manner to their THF adduct parent and a higher purity reagent would hopefully allow for enhanced product yields.

Surprisingly, addition of hexafluoropropene to a 0.13 M benzene-*d*<sub>6</sub> solution of **11.PMDETA** led to a reduced yield of **12a** (46 %, *Z:E* = 91:9) for the desired product. We saw previously that performing these reactions at lower temperatures would allow for greater selectivity and enhanced yields. Repeating this reaction at -78 °C in toluene-*d*<sub>8</sub> led to a further diminished yield of **12a** (31 %) and displayed lower *Z:E* selectivity (86:14).

Unpredictably, repeating these reactions with **11.TMEDA** failed to generate any of the desired product at -78 °C. A reaction was immediate however, as observed by the rapid colour change upon addition of HFP. Inspection of the <sup>19</sup>F NMR spectrum revealed the formation of a complex mixture of products,

including  $\text{PhMe}_2\text{SiF}$  ( $\delta = -161.8$  ppm, sept  $^3J_{\text{HF}} = 7.2$  Hz).<sup>[45]</sup> This was a surprising observation and the process to form a Si–F bond is not immediately obvious. Repeating this reaction at 22 °C led to approximately 30 % of the desired product being generated and an overall cleaner reaction.

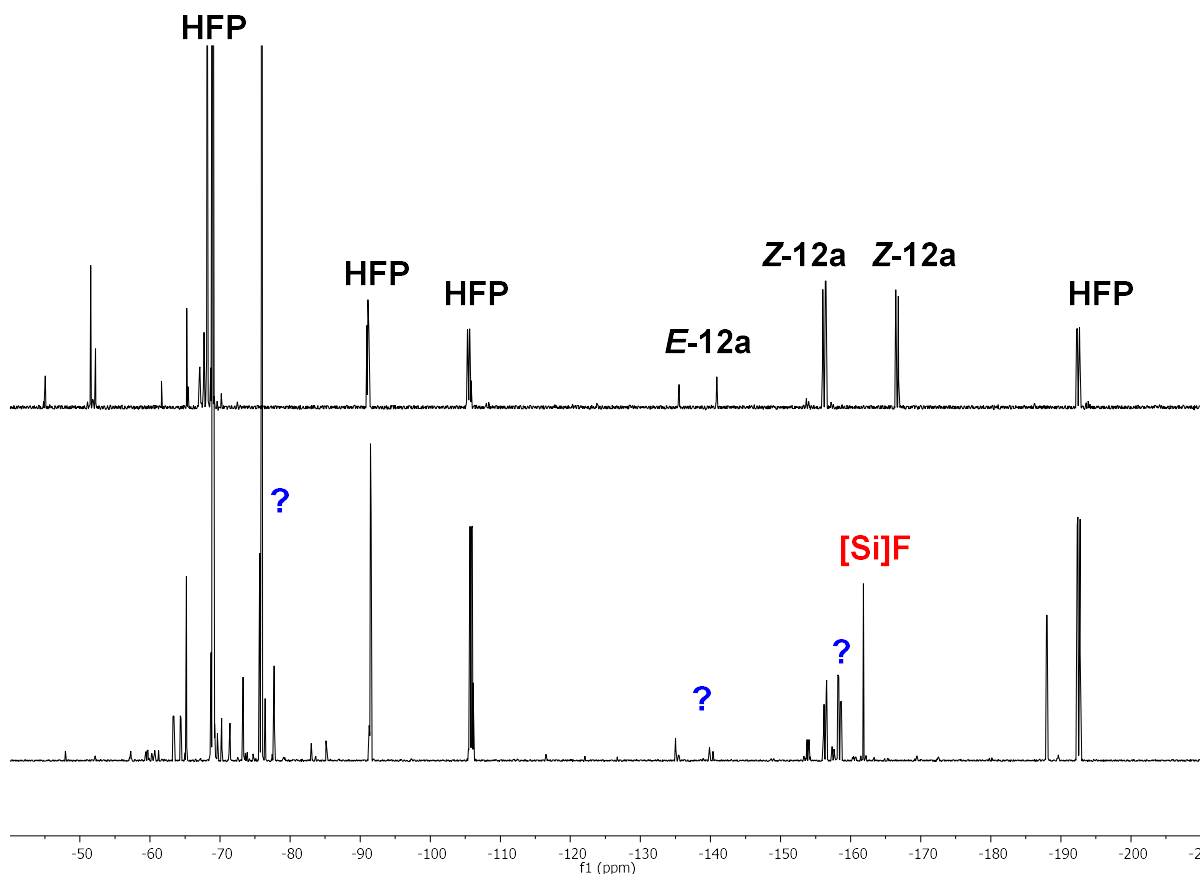


Figure 3.13  $^{19}\text{F}$  NMR stack plot of reaction of **11.TMEDA** with HFP in  $\text{tol-d}_8$  at  $-78$  °C (bottom) and in  $\text{C}_6\text{D}_6$  at 22 °C (top).

These reactions showed that the ligand environment around lithium has a large influence on the reactivity. It could be expected that **11.TMEDA** and **11.PMDETA** are more potent silicon nucleophiles due to increased charge separation between Si–Li. This could correlate to the decreased selectivity and hence yields we observe. It does not provide much insight into the marked difference between the reactions at  $-78$  °C and 22 °C, particularly in the case of **11.TMEDA** whereby none of the desired product was observed.

Several other attempts were made at altering the nature of silicon nucleophile. Addition of  $\text{KO}^t\text{Bu}$  to a sample of **11.THF** in *n*-hexane led to the formation of a black precipitate. Subsequent centrifugation of the solution and isolation yielded a black powder that was insoluble in hydrocarbon solvent and was assumed to be  $\text{PhMe}_2\text{SiK}$ . Addition of 3,3,3-trifluoropropene to a benzene- $\text{d}_6$  suspension of this compound led to the slow formation of compound **12a**, but this showed no benefit or improvement over the established method with **11.THF**.

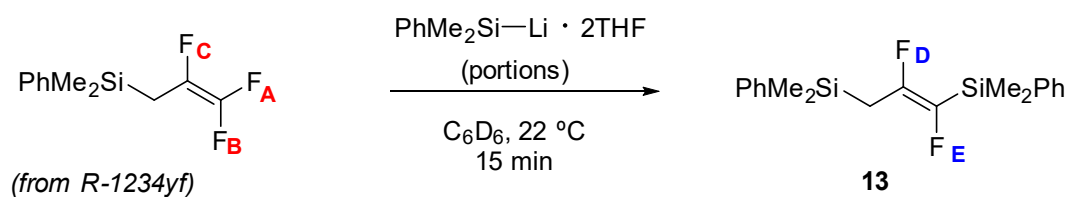
Trialkoxysilyl groups are ubiquitous partners in palladium catalysed Hiyama cross coupling reactions. It would be of synthetic interest therefore to install  $(RO)_3Si$  groups onto HFOs. Addition of methyl lithium (MeLi) to a sample of  $(EtO)_3SiH$  in THF at  $-78\text{ }^\circ\text{C}$  and subsequent warming to  $22\text{ }^\circ\text{C}$  led to the formation of a thick white precipitate as  $(EtO)_3SiLi$  (this preparation was adapted from one described within a patent [KR 1687374] for the synthesis of the trimethoxy analogue). The product was washed with n-hexane and isolated as a white powder. Addition of HFP to a 0.15 M solution of  $(EtO)_3SiLi$  led to the very slow consumption of fluoroolefin. A defluorosilylated product was suspected upon consultation with the  $^{19}\text{F}$  NMR spectrum, however upon removal of volatile species from the reaction, no fluorinated compounds remained. This reagent was deemed to offer no benefit to the so far optimised methods as clean formation of trialkoxysilyl species appeared unlikely.

The synthesis of triphenyl silyl lithium was attempted *via* the analogous technique for **11.THF** (reduction of parent silyl chloride with lithium metal).<sup>[46,47]</sup> A pink-white powder was isolated upon work up that was largely insoluble in hydrocarbon and THF solvent making analysis of the compound difficult. Multiple resonances were observed in the  $^7\text{Li}$  NMR spectrum, however upon addition of HFP to a benzene- $d_6$  suspension of  $\text{Ph}_3\text{SiLi}$  no reactivity was noted as determined by  $^{19}\text{F}$  NMR spectroscopy. Again investigation of this reagent was halted, as it was deemed to offer no benefit to established methods.

### 3.2.4 Multiple Silylation Reactions

It kept coming to our attention that the reactions of fluoroolefins with **11.THF** at  $22\text{ }^\circ\text{C}$  were not as selective as those at  $-78\text{ }^\circ\text{C}$ . Further investigation of the  $^{19}\text{F}$  NMR spectra led us to believe multiple silylations could be occurring on the same molecule (notably with R-1234ze and R-1234yf). This is understandable, as the products of the defluorosilylation reactions remain chemically similar to their HFO precursors. Furthermore, the organosilicon products will exist exclusively in solution whereas the HFO gases can also exist in the reaction vessel head space. This could bias the reaction towards multiple additions.

To test this theory, a pure sample of **12e** was subject to a titration with **11.THF** and the reaction was monitored by  $^1\text{H}$  and  $^{19}\text{F}$  NMR spectroscopy. To our delight, the formation of one new product was observed upon portion-wise addition of a benzene- $d_6$  solution of **11.THF**.



Scheme 3.24 Second defluorosilylation reaction of R-1234yf with **11.THF**

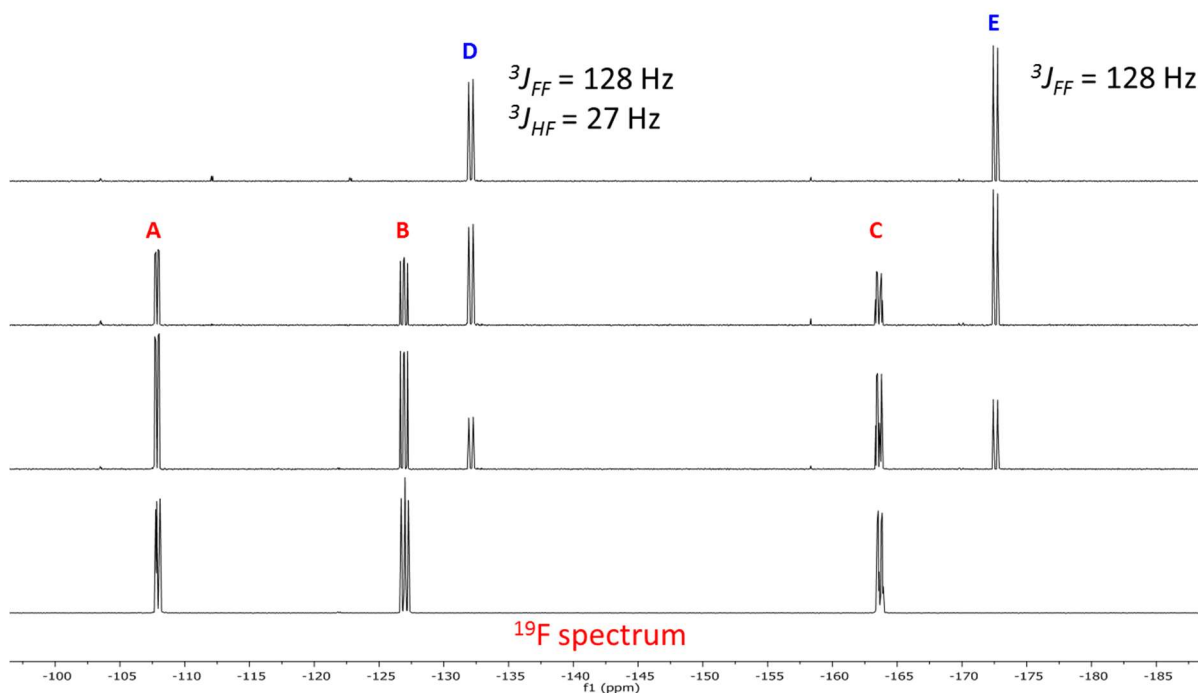


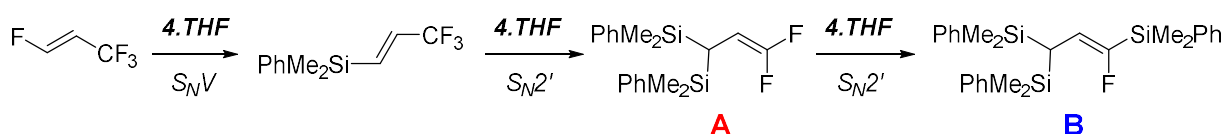
Figure 3.14  $^{19}\text{F}$  NMR stack plot spectrum of the sequential addition of **11.THF** to a sample of **12e** to form one new product (0.5 equivalents of **11.THF** at each interval). Fluorine environments from Scheme 3.24 indicated

Interestingly, although there are still two plausible reactive sites for silylation, exposing the doubly silylated fluoroolefin to further portions of **11.THF** failed to produce any triply functionalised species.

This reaction displays both variants of the possible mechanisms for C–F activation. The first defluorosilylation occurs through the  $\text{S}_{\text{N}}2'$  mechanism whilst the second functionalisation proceeds through the direct  $\text{S}_{\text{N}}\text{V}$  mechanism.

A similar study was repeated using R-1234ze directly, rather than from an isolated sample of **12b**. In this instance there was evidence for greater than two defluorosilylation steps, as determined by  $^{19}\text{F}$  NMR spectroscopy. Full consumption of HFO was achieved after addition of two portions of **11.THF** (0.07 mmol), yielding **12b** as the major component. Two small resonances in the  $^{19}\text{F}$  NMR spectrum were emerging in the region that would indicate a gem-difluoroalkene (Compound **A**, Scheme 3.25). Further portion-wise addition of **11.THF** benzene- $\text{d}_6$  solution led to the full consumption of **12b** whereby compound **A** became the dominant compound. Continued addition led to the slow formation

of a new resonance in the  $^{19}\text{F}$  NMR spectrum, indicating a single new fluorine environment and believed to be compound **B** (Scheme 3.25).



Scheme 3.25 Plausible multiply silylated product from *R*-1234ze upon reaction with **11.THF**

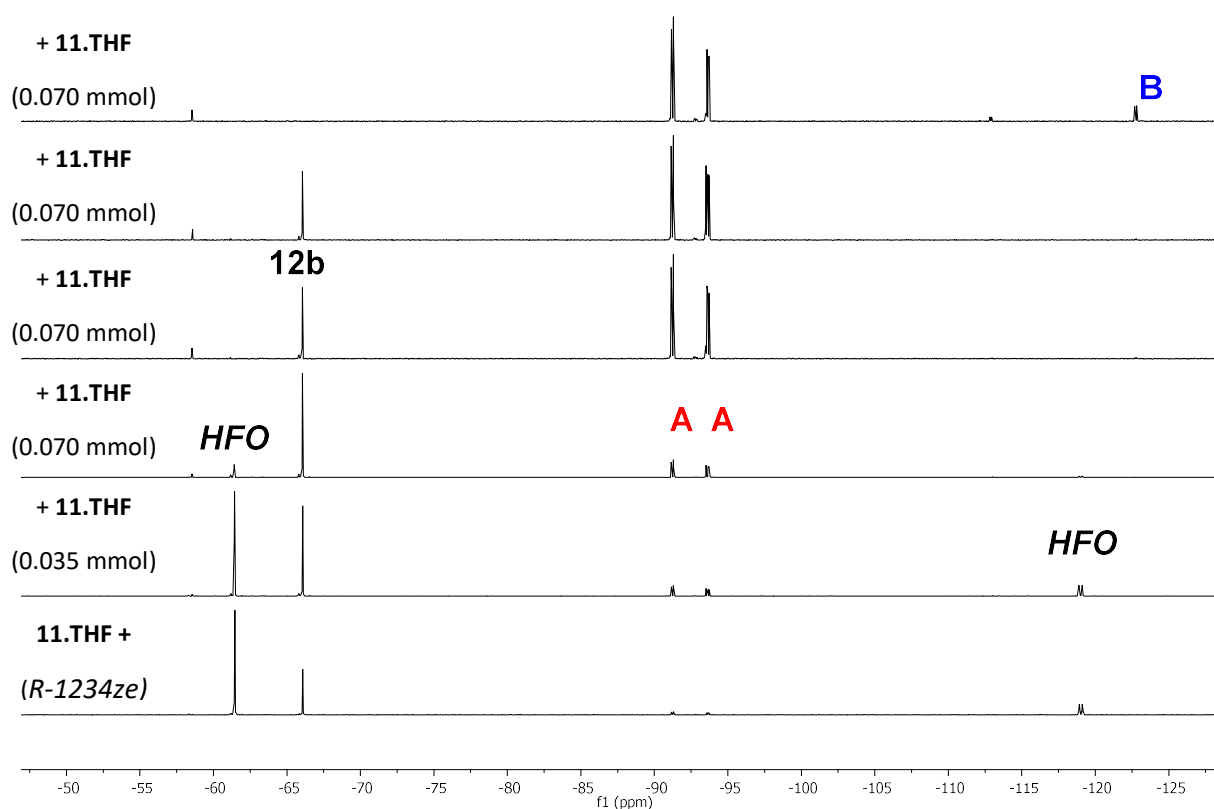


Figure 3.15  $^{19}\text{F}$  NMR stack plot spectrum of sequential addition of **11.THF** to *R*-1234ze. Likely fluorinated products from Scheme 3.25 indicated

These reactions represent an exciting opportunity for further chemistry. Partially fluorinated alkenes have been produced with multiple points of attachment through traditional organosilicon chemistry. Further development of this methodology could hopefully allow for the addition of orthogonal silicon groups to differentiate their onward reactivity.

### 3.2.5 Reactivity of Fluorosilicon Products towards Electrophiles

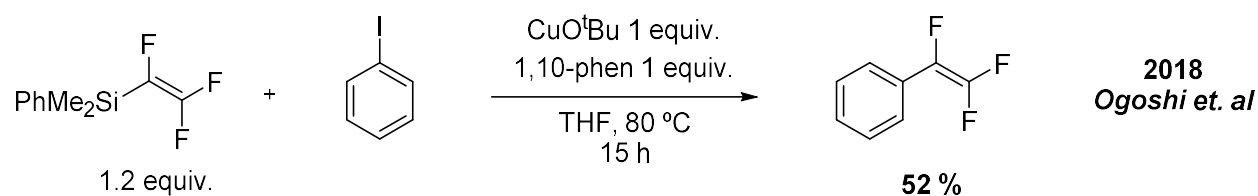
With an efficient method for upgrading HFOs to bench-stable silicon reagents in hand, we were intrigued to investigate what further reactivity these compounds would display. Do they satisfy our aim of developing versatile fluorinated building blocks?

The field of organosilicon chemistry is well established, with many procedures to perform cross-coupling and functional group reactions documented. A notable reaction is Hiyama coupling, a



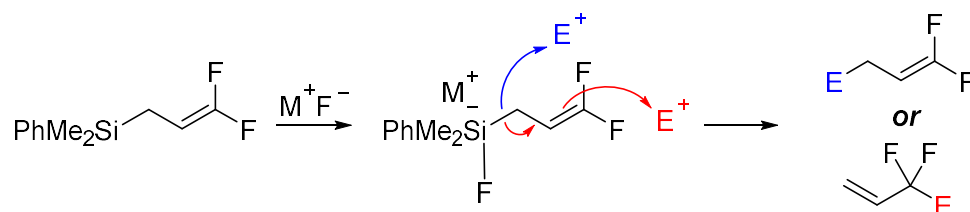
palladium catalysed C–C cross coupling reaction that employs aryl, alkyl and alkenyl silicon reagents with organic halides.<sup>[48]</sup>

Ogoshi *et al.* recently showed that an analogous fluoroalkene silicon reagent can be successfully cross-coupled with iodobenzene, aided by copper *tert*-butoxide (CuO<sup>t</sup>Bu) and 1,10-phenanthroline (1,10-phen).<sup>[23]</sup>



*Scheme 3.26 Cross coupling of fluoroalkene silicon reagent with iodobenzene*

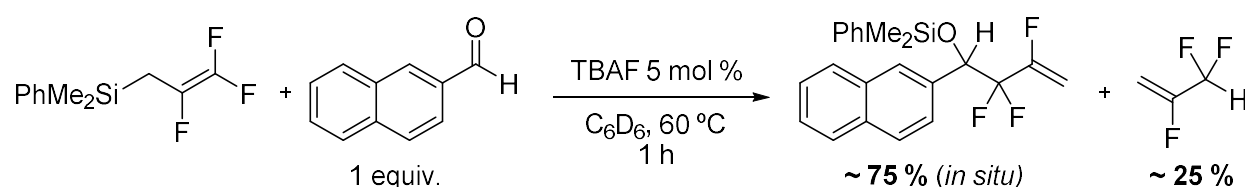
Another well-established protocol in organosilicon chemistry is the installation of trifluoromethyl groups using the Rupert-Prakash reagent (TMSCF<sub>3</sub>).<sup>[49]</sup> In conjunction with an anion activator (typically fluoride), the CF<sub>3</sub><sup>-</sup> synthon can be efficiently delivered to a range of electrophiles. We were particularly interested in this type of reactivity. Our compounds **12a** – **12e** are somewhat different in character however, therefore analogous reactivity was far from certain. Would the Si–C<sup>F</sup> bond be significantly activated and distinguishable from the PhMe<sub>2</sub> groups to allow for nucleophilic transfer? Furthermore, the nature of those products derived through S<sub>N</sub>2' reactions with fluoroolefins suggests two plausible reactivity pathways, through the C1 carbon (blue pathway, *Scheme 3.27*) or *via* transposition of the C=C π-bond and nucleophilic attack through the terminal carbon (red pathway, *Scheme 3.27*).



*Scheme 3.27 Two plausible modes of reactivity with electrophiles (organosilicon reagent derived from 3,3,3-trifluoropropene)*

One equivalent of 2-naphthaldehyde and 5 mol % tetrabutylammonium fluoride (TBAF) catalyst were added to a 0.14 M solution of **12e** in C<sub>6</sub>D<sub>6</sub> and the reaction heated at 60 °C for one hour. The reaction was analysed by <sup>1</sup>H and <sup>19</sup>F NMR spectroscopy. Full consumption of the organosilicon reagent was realised and the formation of two new fluorinated products was elucidated upon <sup>19</sup>F NMR spectrum analysis. Upon consultation with the literature, a hydrodesilylation product 2,3,3-trifluoroprop-1-ene was elucidated in approximately 25 % yield (<sup>19</sup>F δ = -122.2 and -123.7 <sup>2</sup>J<sub>HF</sub> = 55 Hz ppm).<sup>[50]</sup> The formation of two sets of roofed doublet of doublet of doublets in the <sup>19</sup>F NMR spectrum (δ = -110.5 and -117.6 ppm) gave strong evidence for the formation of an α,α-difluoro alcohol-type species,

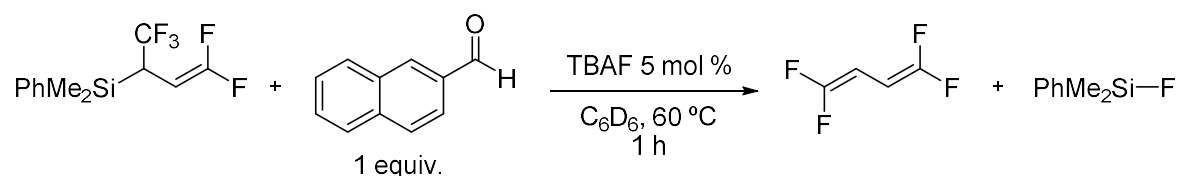
suggesting that the reaction had occurred *via* transposition of the double bond (red pathway, Scheme 3.27). This was supported by evidence in the proton spectrum as three sets of resonances with equal integration were observed in the alkenic/benzylic region ( $\delta = 5.24, 4.69$  and  $4.55$  ppm). Based upon *in situ* comparison to an internal standard, 75 % yield of the fluorinated silyl ether was achieved.



Scheme 3.28 Fluoroalkene addition to 2-naphthaldehyde from **12e** catalysed by TBAF

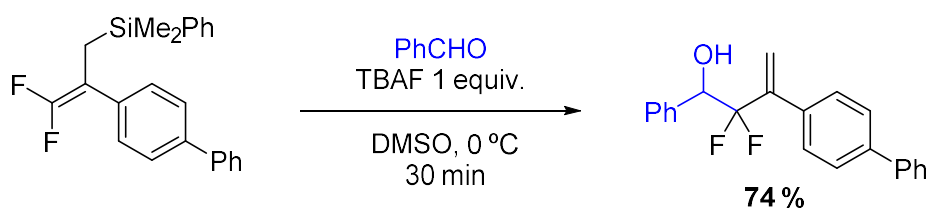
This was a very encouraging result. The conditions were reasonably mild and the reaction occurred with a high yield in a short reaction time of just one hour. Further optimisation should allow for higher yields and wider scope of carbonyl electrophiles.

Unfortunately, repeating this reaction with an isolated sample of **12e** under the same conditions led to an undesired outcome. Full conversion of the starting material was realised within 1 hour at  $60\text{ }^{\circ}\text{C}$ , however transfer of the fluoroalkene moiety to the carbonyl had not been achieved. Instead, upon consultation to the literature a  $\beta$ -fluoride elimination process was suspected, yielding 1,1,4,4-tetrafluorobutadiene ( $^1\text{H } \delta = 4.28$  ppm and  $^{19}\text{F } \delta = -86.6$  and  $-87.8$  ppm) and  $\text{PhMe}_2\text{SiF}$ .<sup>[26]</sup>



Scheme 3.29 Unsuccessful fluoroalkene transfer of **12e** to 2-naphthaldehyde, instead leading to  $\beta$ -fluoride elimination

It was recently shown by Shi *et al.*, that silicon containing fluoroalkenes can add to carbonyl substrates in a similar fashion to generate related  $\alpha,\alpha$ -difluoroalcohol species. They could also react with an electrophilic bromine source, *N*-bromosuccinimide (NBS) to generate 1,bromo-1,1-difluoroalkenes.



Scheme 3.30 Addition of fluorinated alkene to benzaldehyde under mild conditions

Further investigation into the versatility of our fluorinated organosilicon reagents is being undertaken in our group. The fluorinated species formed upon reaction with carbonyl compounds could be particularly interesting to medicinal chemists, potentially acting as amide, ester or alcohol mimics.

### 3.2.6 Computational Studies

To gain a deeper mechanistic understanding of the C–F bond activation processes, an extensive series of computational calculations were undertaken to investigate the reaction of fluoroolefins with compounds **9a** and **10a**. The imino-anilide ligands surrounding the magnesium centre are well defined in solution and the resulting Mg–F compounds are known to remain in solution, therefore the energies associated with the formation of metal fluoride lattices can be circumvented.<sup>[51]</sup> We were cautious of calculating the energy profiles for related silyl lithium reagents due to their ambiguous nuclearity and number of coordinated solvent molecules.

The B3PW91 functional and a hybrid basis set was utilised (6-31G\*\*/SDDALL), incorporating single point energy calculations to account for dispersion (GD3) and solvation (pcm, benzene). These computational methods have been previously benchmarked in the group against experimentally determined activation parameters.<sup>[52]</sup>

These calculations capture both modes of reactivity that occur,  $S_NV$  and  $S_N2'$  plus the effects of the steric environment around the magnesium centre. Transition states were located through scan calculations, incrementally decreasing the distance between the Si atom and the C atom on the fluoroolefin where the new bond is known to form.

#### 3.2.6.1 Nucleophilic Vinylic Substitution Calculations

Hexafluoropropene and R-1234ze were shown experimentally to undergo  $S_NV$  type reactivity. This mechanism was supported by the calculations. After an initial thermodynamically favourable coordination of HFP to **10a** ( $\Delta G_{298K} = -1.6 \text{ kcal mol}^{-1}$ ), **Z-12a** is generated *via* a low energy  $S_NV$  transition state ( $\Delta G^\ddagger_{298K} = 15.2 \text{ kcal mol}^{-1}$ ). In this concerted transition state (**TS-1-Z**) the Mg---Si and C---F distances lengthen from 2.62 to 2.78 Å and 1.32 to 1.44 Å respectively, whilst the Mg–Si–C<sup>IV</sup>(phenyl) angle becomes more acute by 26.0° reaching a value of 81.7°. The products are thermodynamically favourable ( $\Delta G^\circ_{298K} = -58.9 \text{ kcal mol}^{-1}$ ) and form a weak encounter complex whereby the magnesium fluoride species is coordinated to the  $\pi$ -system of the phenyl ring on the organosilicon moiety.

By altering the orientation of the hexafluoropropene molecule in the bond scanning calculations, an alternative  $S_NV$  transition state (**TS-1-E**) can be located that accounts for the experimentally observed minor product of this reaction ( $\Delta G^\ddagger_{298K} = 17.1 \text{ kcal mol}^{-1}$ ). The energy difference between these pathways ( $\Delta\Delta G^\ddagger_{298K} = 1.9 \text{ kcal mol}^{-1}$ ) is in line with the experimentally observed selectivity (approximately 9:1, **Z-12a** : **E-12a**).

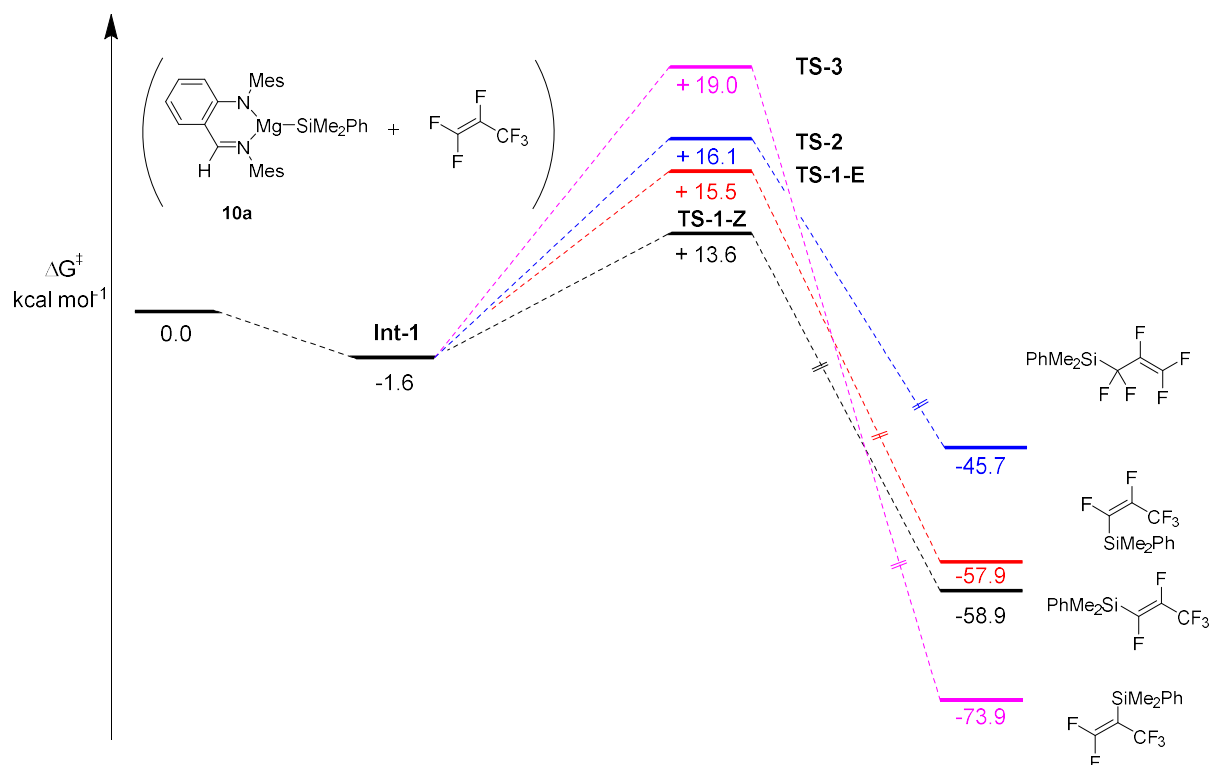


Figure 3.16 Calculated potential energy surfaces for reaction of HFP with **10a** to generate four products (only the two lowest energy products were observed experimentally). B3PW91 functional and a hybrid basis set was utilised (6-31G\*\*/SDDALL), incorporating single point energy calculations to account for dispersion (GD3) and solvation (PCM, benzene). Product energies are those of a weak encounter complex between **12a** and the magnesium fluoride side product (**10a-F**).

Two other plausible products can be envisaged. One that results through the alternative  $S_N2'$  pathway and one where direct vinylic substitution occurs at the internal position of the fluoroolefin. Transition states could be located for these pathways (**TS-2**,  $\Delta G^\ddagger_{298K} = 17.7$  and **TS-3**,  $20.6 \text{ kcal mol}^{-1}$ ). Both exhibit larger energy requirements than for the experimentally observed products confirming calculation and experiment are in concordance. Overall, the computed energy barriers to generate the experimentally observed product **12a** could be deemed somewhat low, based on the length of time the reactions require at temperatures between  $22 - 60 \text{ }^\circ\text{C}$ . The single point corrections could overestimate the stabilisation of the transition states. Functional testing of this method would be worthwhile, comparing to experimentally determined parameters through analysis of the reaction kinetics.

The reaction profile for the defluorosilylation of R-1234ze with **10a** is comparable to that for the major product upon reaction with HFP. A low energy  $S_NV$  transition state was located ( $\Delta G^\ddagger_{298K} = 13.9 \text{ kcal mol}^{-1}$ ) leading to the experimentally observed product **12b** ( $\Delta G^\circ_{298K} = -58.0 \text{ kcal mol}^{-1}$ ).

### 3.2.6.2 Nucleophilic Conjugate Substitution Calculations

Whilst the  $S_NV$  pathway was shown to be favoured in the cases of HFP and R-1234ze, an  $S_N2'$  pathway was shown to dominate when no terminal vinylic C-F bonds are present.

For example, 6-membered concerted transition states could be located for the reaction of **10a** with R-1234yf and R-1336mzz ( $\Delta G^\ddagger_{298\text{K}} = 22.5$  and  $19.6$  kcal mol<sup>-1</sup> respectively). These energies are significantly larger than the barriers determined for the S<sub>N</sub>V reactions with HFP and R-1234ze. This is in accordance with experimental findings that R-1336mzz and R-1234yf are more difficult to activate.

Surprisingly, a two-step process was elucidated when calculating reaction of 3,3,3-trifluoropropene with **10a**.

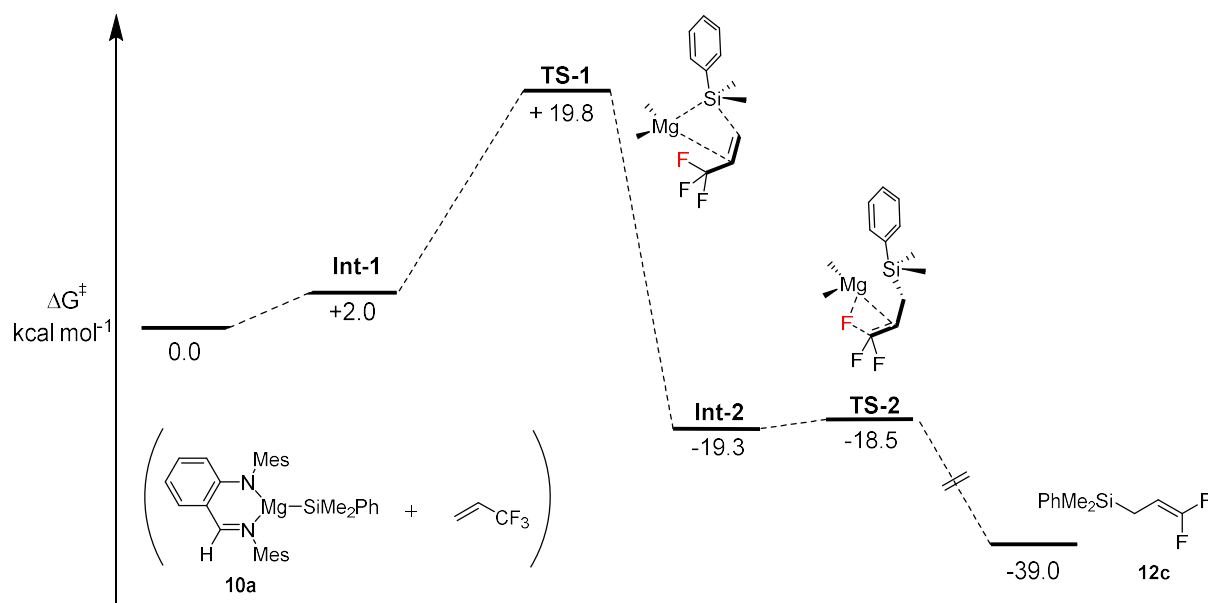


Figure 3.17 Calculated potential energy surface for the reaction of 3,3,3-trifluoropropene with **10a**. B3PW91 functional and a hybrid basis set was utilised (6-31G\*\*/SDDALL), incorporating single point energy calculations to account for dispersion (GD3) and solvation (PCM, benzene). Product energies are those of a weak encounter complex between **12c** and the magnesium fluoride side product.

An initial 1,2-addition of the Mg–Si bond occurs across the alkene (**TS-1**,  $\Delta G^\ddagger_{298\text{K}} = 19.8$  kcal mol<sup>-1</sup>), to form **Int-2**. This represents a silyl-magnesiation of the C=C  $\pi$ -bond generating a saturated intermediate. This is an unstable species that can undergo facile  $\beta$ -fluoride elimination (**TS-2**,  $\Delta G^\ddagger_{298\text{K}} = 0.8$  kcal mol<sup>-1</sup>), resulting in the formation of the experimentally observed product whereby the C=C  $\pi$ -bond migrates and a formal sp<sup>3</sup>C–F bond is cleaved. This resembles the step-wise addition elimination processes determined by Ogoshi using copper(I) silyl or boryl species.<sup>[22,23]</sup> In our case, the transition state for  $\beta$ -fluoride elimination is virtually barrierless and these two pathways (S<sub>N</sub>2' and addition–elimination) are believed to be related aspects of a continuum. This is further underpinned when investigating the reaction of 3,3,3-trifluoropropene with **9a**, whereby a single concerted transition state is now located ( $\Delta G^\ddagger_{298\text{K}} = 23.2$  kcal mol<sup>-1</sup>) representing the S<sub>N</sub>2' pathway.

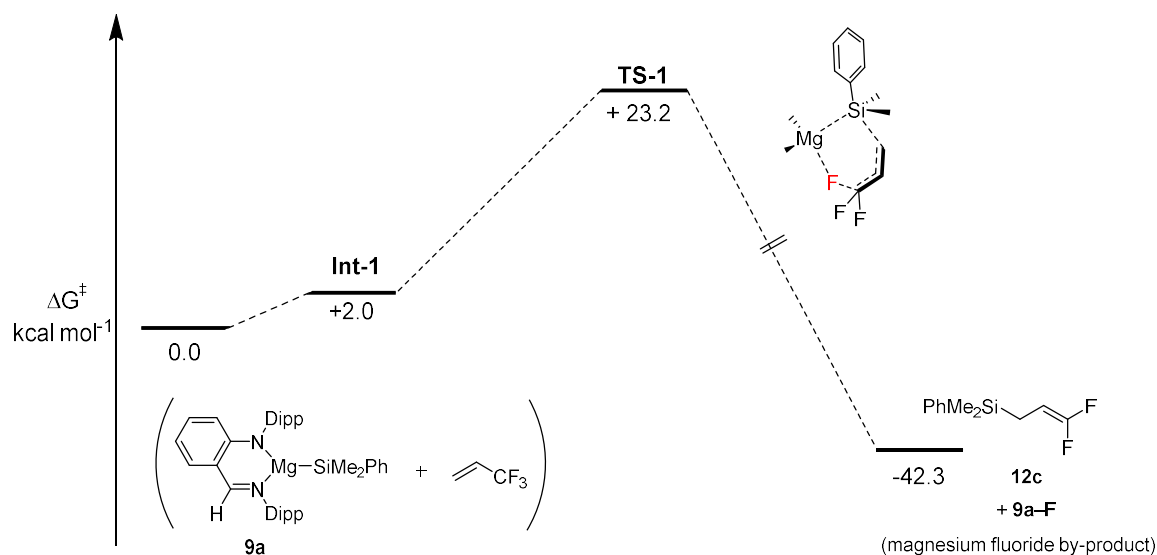


Figure 3.18 Calculated potential energy surface for the reaction of 3,3,3-trifluoropropene with **9a**. B3PW91 functional and a hybrid basis set was utilised (6-31G\*\*/SDDALL), incorporating single point energy calculations to account for dispersion (GD3) and solvation (PCM, benzene). Product energies are those of a weak encounter complex between **12c** and the magnesium fluoride side product **9a-F**.

In all other cases, substitution of **10a** with more sterically encumbering **9a** results in similar transition states ( $S_NV$  or  $S_{N2}'$ ) albeit with higher transition state energy barriers throughout. This supported what was observed experimentally, namely that the reactions with **9a** required more forcing conditions.

The favoured reactivity pathways occur through nucleophilic attack of the terminal vinylic carbon. The mechanism then depends on the location of the fluoride leaving group.  $S_NV$  reactivity will occur if there is a terminal vinylic fluorine, whereas  $S_{N2}'$  reactivity will take over when this position does not have a C-F bond. Nucleophilic attack at the internal position of the fluoroolefin is disfavoured in all cases due to substrate polarisation. The reactivity pathways can be rationalised by a charge analysis of the substrates. For HFP and R-1234ze that contain terminal  $sp^2C-F$  bonds, the terminal vinylic carbon is the most electropositive ( $sp^2$  carbon) due to the electron withdrawing nature of fluorine. The electronegative build-up on the terminal carbon can be stabilised by the fluoride leaving group.

When considering the reactivity of R-1234yf and trifluoropropene, the situation is slightly more complex. As was shown by Yamazaki, the C2 position of R-1234yf is the most electropositive and one might expect direct C-F silylation to occur at that position.<sup>[31]</sup>

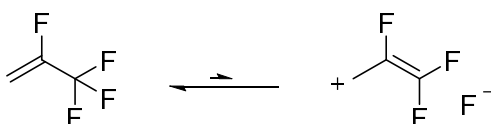


Figure 3.19 Mesomeric structures of R-1234yf

The mesomeric effects become important in this substrate. The magnesium promotes the loss of fluoride and can stabilise the mesomeric structure of R-1234yf in the transition state. Magnesium can

be considered to be acting as a Lewis acid and the process has a degree of 'push and pull' by both the nucleophile (Si) and electrophile (Mg). These stabilisation effects over-ride the electron withdrawing effect of the fluorine at the C2 position and hence the reaction favours the S<sub>N</sub>2' pathway.

## 3.3 Experimental

### 3.3.1 General Experimental

Standard Schlenk line and glovebox techniques were used for all manipulations under an inert atmosphere of dinitrogen or argon unless otherwise stated. NMR scale reactions were performed in J. Young's tap NMR tubes equipped with internal standard capillaries of ferrocene ( $^1\text{H}$  NMR spectroscopy) or 1-trifluoromethylnaphthalene ( $^{19}\text{F}$  NMR spectroscopy) and prepared in a glovebox. An MBraun Labmaster glovebox was utilised, operating at  $<0.1$  ppm and  $\text{H}_2\text{O} <0.1$  ppm  $\text{O}_2$ .  $^1\text{H}$ ,  $^{13}\text{C}$ ,  $^{11}\text{B}$ ,  $^{29}\text{Si}$ ,  $^7\text{Li}$  and  $^{19}\text{F}$  NMR spectra were recorded on BRUKER 400 MHz or 500 MHz machines. Data were processed using the MestReNova software package.

Solvents were dried over activated alumina from a solvent purification system (SPS) based upon the Grubbs design and de-gassed before use. Glassware was dried for  $>6$  h prior to use at  $120$  °C. Benzene- $d^6$  was stored over  $3\text{Å}$  molecular sieves, distilled and de-gassed before use. All heating mentioned was done using silicone oil baths.

All reagents were acquired from Sigma Aldrich (Merck), Honeywell or Fluorochem and used without further purification unless specified. Fluorinated gases were acquired from Apollo Scientific and used without further purification. Where liquids at  $25$  °C, reagents were dried over activated  $3\text{Å}$  molecular sieves and freeze-pump-thaw degassed prior to use. (Dimethylphenylsilyl)boronic acid pinacol ester ( $\text{PhMe}_2\text{SiBpin}$ ) and (triethylsilyl)boronic acid pinacol ester ( $\text{Et}_3\text{SiBpin}$ ) were synthesised according to the literature, distilled and stored over  $3\text{Å}$  molecular sieves.<sup>[53,54]</sup> [ $^{\text{Dipp}}(\text{BDI})\text{MgSiMe}_2\text{Ph}$ ], compound **8a**, was synthesised according to the literature.<sup>[38]</sup> ((2,6-diisopropylphenyl)imino)methyl)phenyl)-2,6-diisopropylaniline ( $^{\text{Dipp}}\text{L}^{\text{H}}$ ) and N-(2-((mesitylimino)methyl)phenyl)-2,4,6-trimethylaniline ( $^{\text{Mes}}\text{L}^{\text{H}}$ ) were synthesised according to adapted literature procedures.<sup>[39,40,55]</sup>

Single crystal X-ray data were obtained on Agilent Diffraction Xcalibur PX Ultra A and Xcalibur 3 diffractometers, and the structures were refined using the SHELXTL, SHELX-97, and SHELX-2013 program systems. The carrier gas was helium (at a flow rate of  $25$  mL/min). CHN analysis was run by Stephen Boyer of London Metropolitan University.

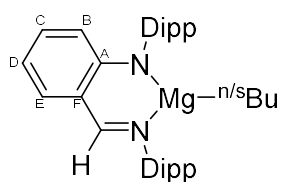


DFT calculations were run using Gaussian 09 (Revision D.01)<sup>[56]</sup> using the B3PW91 density functional.<sup>[57–61]</sup> Mg and Si centres were described with Stuttgart SDDAll RECPs and associated basis sets whereas 6-31G\*\* basis sets was used for all other atoms.<sup>[62–64]</sup>

Geometry optimisation calculations were performed without symmetry constraints. The Gaussian 09 default optimisation criteria were tightened to  $10^{-9}$  on the density matrix and  $10^{-7}$  on the energy matrix. The default numerical integration grid was also improved using a pruned grid with 99 radial shells and 590 angular points per shell. Frequency analyses for all stationary points were performed using the enhanced criteria to confirm the nature of the structures as either minima (no imaginary frequency) or transition states (only one imaginary frequency). Intrinsic reaction coordinate (IRC) calculations followed by full geometry optimisations on final points were used to connect transition states and minima located on the potential energy surface allowing a full energy profile (calculated at 298.15 K, 1 atm) of the reaction to be constructed.<sup>[65,66]</sup> Free energies reported within the main text are corrected for the effects of benzene solvent ( $\epsilon=2.2706$ ) using the polarizable continuum model (PCM).<sup>[67]</sup> In addition, single point dispersion corrections were applied to the B3PW91 optimised geometries employing Grimme's D3 correction.<sup>[68]</sup>

The graphical user interface used to visualise the various properties of the intermediates and transition states was GaussView 5.0.9.<sup>[69]</sup>

### 3.3.2 Preparation of Magnesium Reagents

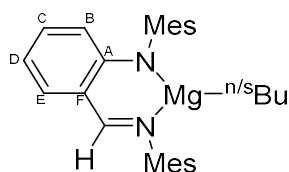


(as dimer)

**Synthesis of  $[^{Dipp}P(L)MgC_4H_9]$ :** In a Schlenk flask under an argon atmosphere, ((2,6-diisopropylphenyl)imino)methylphenyl-2,6-diisopropylaniline ( $^{Dipp}L^H$ ) (3.00 g, 6.81 mmol) was dissolved in toluene (50 mL) and the solution cooled to 0 °C.  $MgBu_2$  (mixture of nBu and sBu, ~88:12), 1.0 M solution in heptanes, (7.49 mL, 7.49 mmol) was added dropwise, observing a colour change to bright yellow. The solution was allowed to warm to room temperature. The solvent was removed *in vacuo* then n-hexane (60 mL) added. The precipitate was heated into solution, then the product crystallised upon cooling to -35 °C, yielding the product  $[^{Dipp}P(L)MgC_4H_9]$  as bright yellow fine crystals (2.99 g, 93 %, 5.74 mmol)

$\delta_H$  (400 MHz,  $C_6D_6$ , 298K): 7.91 (s, 1H,  $NCH$ ), 7.23 (apparent s, 3H,  $DippCH$ ), 7.15 – 7.05 (m, 3H,  $DippCH$ ), 6.90 (d, 1H,  $^3J_{HH} = 8.0$  Hz  $CH_E$ ), 6.88 – 6.82 (m, 1H,  $CH_C$ ), 6.40 (d, 1H,  $^3J_{HH} = 8.8$  Hz,  $CH_A$ ), 6.33 – 6.26 (m, 1H,  $CH_D$ ), 3.32 (sept, 2H,  $^3J_{HH} = 6.9$  Hz,  $CH(CH_3)_2$ ), 3.06 (sept, 2H,  $^3J_{HH} = 6.8$  Hz,  $CH(CH_3)_2$ ), 1.53 – 1.43 (m, 2H,  $CH_2$ ), 1.24 (d, 6H,  $^3J_{HH} = 6.9$  Hz,  $CH(CH_3)_2$ ), 1.18 (d, 6H,  $^3J_{HH} = 6.8$  Hz,  $CH(CH_3)_2$ ), 1.15 – 1.02 (m, 2H,  $CH_2$ ) 1.13 (d, 6H,  $^3J_{HH} = 6.8$  Hz,  $CH(CH_3)_2$ ), 1.06 (d, 6H,  $^3J_{HH} = 6.8$  Hz,  $CH(CH_3)_2$ ), 0.81 (t, 3H,  $^3J_{HH} = 7.3$  Hz,  $(CH_2)_3CH_3$ ), -0.09 (t, 2H,  $^3J_{HH} = 7.9$  Hz,  $MgCH_2$ ).

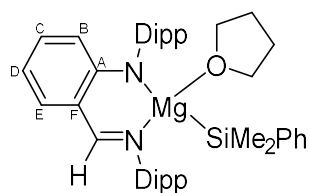
$\delta_C$  (100 MHz,  $C_6D_6$ , 298K): 172.8 (s, 1C,  $HCNC^{IV}$ ), 160.2 (s, 1C,  $NC^{IV}_A$ ), 146.3 (s, 1C,  $NC^{IV}$ ), 144.2 (s, 2C,  $o-C^{IV}$ ), 143.7 (s, 1C,  $NC^{IV}$ ), 141.0 (s, 2C,  $o-C^{IV}$ ), 138.7 (s, 1C,  $C_E$ ), 135.2 (s, 1C,  $C_C$ ), 127.1 (s, 1C,  $p-(Dipp)CH$ ), 125.9 (s, 1C,  $p-(Dipp)CH$ ), 124.7 (s, 2C,  $m-(Dipp)CH$ ), 124.2 (s, 2C,  $m-(Dipp)CH$ ), 117.4 (s, 1C,  $C_B$ ), 115.6 (s, 1C,  $C^IV_F$ ), 113.4 (s, 1C,  $C_D$ ), 31.1 (s, 1C,  $CH_2$ ), 31.0 (s, 1C,  $CH_2$ ), 29.4 (s, 2C,  $CH(CH_3)_2$ ), 28.7 (s, 2C,  $CH(CH_3)_2$ ), 24.9 (s, 2C,  $CH(CH_3)_2$ ), 24.4 (s, 2C,  $CH(CH_3)_2$ ), 24.2 (s, 2C,  $CH(CH_3)_2$ ), 23.9 (s, 2C,  $CH(CH_3)_2$ ), 14.4 (s, 1C,  $(CH_2)_3CH_3$ ), 5.5 (s, 1C,  $MgCH_2$ ).



**Synthesis of  $[^{Mes}(L)MgC_4H_9]$ :** In a Schlenk flask under an argon atmosphere, N-(2-((mesitylimino)methyl)phenyl)-2,4,6-trimethylaniline ( $^{Mes}L^H$ ) (2.00 g, 5.61 mmol) was dissolved in n-hexane (60 mL) and the solution cooled to 0 °C.  $MgBu_2$  (mixture of nBu and sBu, ~88:12), 1.0 M solution in heptanes, (6.17 mL, 6.17 mmol) was added dropwise, observing a colour change to dark orange. The solution was allowed to warm to room temperature, forming a thick yellow precipitate. Toluene (20 mL) was added and the suspension stirred for 2 hours at 22 °C. The precipitate was heated into solution, then the product crystallised upon cooling to -35 °C, yielding the product  $[^{Dipp}(L)MgC_4H_9]$  as bright yellow fine crystals (1.89 g, 77 %, 4.33 mmol)

$\delta_H$  (400 MHz,  $C_6D_6$ , 298K): 7.71 (s, 1H,  $NCH$ ), 7.08 – 6.62 (m, 6H,  $Mes-m-CH + CH_E + CH_C$ ), 6.37 (d, 1H,  $^3J_{HH} = 8.8$  Hz,  $CH_A$ ), 6.29 – 6.23 (m, 1H,  $CH_D$ ), 2.39 (s, 3H,  $p-CH_3$ ), 2.31 (s, 3H,  $p-CH_3$ ), 2.18 - 1.79 (br m, 12H,  $o-CH_3$ ), 1.44 – 1.13 (br m, 4H,  $(CH_2)_2CH_3$ ), 0.76 (t, 3H,  $^3J_{HH} = 7.1$  Hz,  $(CH_2)_2CH_3$ ), -0.16 – -0.60 (br m, 2H,  $MgCH_2$ )

$\delta_C$  (100 MHz,  $C_6D_6$ , 298K): 173.5 (s, 1C,  $HCNC^{IV}$ ), 159.8 (s, 1C,  $NC^{IV}_A CH$ ), 147.9 (s, 1C,  $NC^{IV}$ ), 145.9 (s, 1C,  $NC^{IV}$ ), 138.8 (s, 1C,  $C_E$ ), 134.9 (s, 1C,  $C_C$ ), 133.8 (s, 2C,  $o-C^{IV}$ ), 130.5 (s, 2C,  $o-C^{IV}$ ), 130.2 (s, 2C,  $MesCH$ ), 130.1 (s, 2C,  $MesCH$ ), 129.3 (s, 1C,  $Mes-p-C^{IV}$ ), 128.6 (s, 1C,  $Mes-p-C^{IV}$ ), 117.0 (s, 1C,  $C_B$ ), 116.0 (s, 1C,  $NCHC^{IV}_F$ ), 112.4 (s, 1C,  $C_D$ ), 31.5 (s, 1C,  $CH_2$ ), 28.5 (s, 1C,  $CH_2$ ), 21.2 (s, 1C,  $p-CCH_3$ ), 21.0 (s, 1C,  $p-CCH_3$ ), 18.6 (br s, 4C,  $o-CCH_3$ ), 13.6 (s, 1C,  $(CH_2)_3CH_3$ ), 10.5/9.9 (2s, 1C,  $MgCH_2$ ).



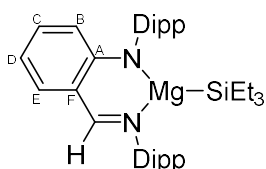
**Synthesis of compound 2a.THF:** In a dinitrogen filled glovebox, [<sup>Dipp</sup>(L)MgC<sub>4</sub>H<sub>9</sub>] (74 mg, 0.15 mmol) was dissolved in toluene (6 mL) followed by the addition of THF (20 μL, 0.25 mmol). Me<sub>2</sub>PhSiBpin (54 μL, 0.20 mmol) was added and the reaction was stirred in a scintillation vial for 2 hours at 22 °C then the solvent removed *in vacuo*. The product was crystallised from n-hexane (~4 mL) at -35 °C yielding yellow precipitate (77 mg, 76 %, 0.12 mmol).

$\delta_{\text{H}}$  (400 MHz, C<sub>6</sub>D<sub>6</sub>, 298K): 7.96 (s, 1H, NCH), 7.34 (apparent s, 3H, *Dipp*CH), 7.25 – 7.03 (m, 8H, *Dipp*CH + SiCH), 6.97 – 6.91 (m, 1H, CH<sub>E</sub>), 6.86 – 6.79 (m, 1H, CH<sub>C</sub>), 6.43 (d, 1H, <sup>3</sup>J<sub>HH</sub> = 8.9 Hz, CH<sub>A</sub>), 6.27 – 6.21 (m, 1H, CH<sub>D</sub>), 3.34 – 3.38 (m, 4H, (OCH<sub>2</sub>)<sub>2</sub>), 3.42 – 3.18 (br m, 2H, CH(CH<sub>3</sub>)<sub>2</sub>), 3.21 – 2.91 (br m, 2H, CH(CH<sub>3</sub>)<sub>2</sub>), 1.35 – 1.11 (m, 18H, CH(CH<sub>3</sub>)<sub>2</sub>), 1.08 (d, 6H, <sup>3</sup>J<sub>HH</sub> = 6.9 Hz, CH(CH<sub>3</sub>)<sub>2</sub>), 1.06 – 1.00 (m, 4H, OCH<sub>2</sub>(CH<sub>2</sub>)<sub>2</sub>), 0.26 (s, 6H, Si(CH<sub>3</sub>)<sub>2</sub>).

$\delta_{\text{C}}$  (100 MHz, C<sub>6</sub>D<sub>6</sub>, 298K): 171.4 (s, 1C, HCNC<sup>IV</sup>), 160.5 (s, 1C, NC<sup>IV</sup><sub>A</sub>), 151.9 (s, 1C, SiC<sup>IV</sup>), 148.1 (s, 1C, NC<sup>IV</sup>), 146.2 (s, 1C, NC<sup>IV</sup>) 144.3 (s, 2C, o-C<sup>IV</sup>), 138.1 (s, 1C, C<sub>E</sub>), 134.2 (s, 2C, Si-o-CH), 133.9 (s, 1C, C<sub>C</sub>), 127.5 (s, 2C, Si-m-CH), 126.7 (s, 1C, p-(*Dipp*)CH), 125.9 (s, 1C, Si-p-CH), 125.2 (s, 1C, p-(*Dipp*)CH), 124.1 (s, 2C, m-(*Dipp*)CH), 119.1 (s, 1C, C<sub>B</sub>), 116.1 (s, 1C, C<sup>IV</sup><sub>F</sub>), 112.4 (s, 1C, C<sub>D</sub>), 70.2 (s, 2C, THF-OCH<sub>2</sub>), 28.5 (br s, 4C, CH(CH<sub>3</sub>)<sub>2</sub>), 25.8 (s, 2C, CH(CH<sub>3</sub>)<sub>2</sub>), 25.5 (s, 2C, CH(CH<sub>3</sub>)<sub>2</sub>), 25.3 (s, 2C, THF-OCH<sub>2</sub>(CH<sub>2</sub>)<sub>2</sub>), 24.8 (s, 2C, CH(CH<sub>3</sub>)<sub>2</sub>), 23.3 (s, 2C, CH(CH<sub>3</sub>)<sub>2</sub>), 3.7 (s, 1C, Si(CH<sub>3</sub>)<sub>2</sub>).

2 \* *Dipp*-o-C<sup>IV</sup> and 2 \* *Dipp*-m-CH resonances could not be located.

$\delta_{\text{Si}}$  (79.5 MHz, C<sub>6</sub>D<sub>6</sub>, 298K): -26.9 (s).



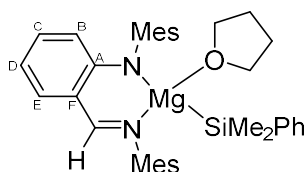
**Synthesis of compound 9b:** In a dinitrogen filled glovebox, [<sup>Dipp</sup>(L)MgC<sub>4</sub>H<sub>9</sub>] (156 mg, 0.30 mmol) was dissolved in toluene (6 mL) followed by the addition of Et<sub>3</sub>SiBpin (97  $\mu$ L, 0.36 mmol). The reaction was stirred in a scintillation vial for 18 hours at 22 °C then the solvent removed *in vacuo*. The product was crystallised from n-hexane (~5 mL) at -35 °C yielding yellow crystals (121 mg, 70 %, 0.21 mmol).

$\delta_{\text{H}}$  (400 MHz, C<sub>6</sub>D<sub>6</sub>, 298K): 7.95 (s, 1H, NCH), 7.26 – 7.23 (m, 3H, *Dipp*CH), 7.13 – 7.06 (m, 3H, *Dipp*CH), 6.95 – 6.91 (m, 1H, CH<sub>E</sub>), 6.90 – 6.84 (m, 1H, CH<sub>C</sub>), 6.44 (d, 1H, <sup>3</sup>J<sub>HH</sub> = 8.8 Hz, CH<sub>A</sub>), 6.35 – 6.29 (m, 1H, CH<sub>D</sub>), 3.29 (sept, 2H, <sup>3</sup>J<sub>HH</sub> = 6.9 Hz, CH(CH<sub>3</sub>)<sub>2</sub>), 3.02 (sept, 2H, <sup>3</sup>J<sub>HH</sub> = 6.8 Hz, CH(CH<sub>3</sub>)<sub>2</sub>), 1.32 (d, 6H, <sup>3</sup>J<sub>HH</sub> = 6.9 Hz, CH(CH<sub>3</sub>)<sub>2</sub>), 1.27 (d, 6H, <sup>3</sup>J<sub>HH</sub> = 6.9 Hz, CH(CH<sub>3</sub>)<sub>2</sub>), 1.12 (d, 6H, <sup>3</sup>J<sub>HH</sub> = 6.8 Hz, CH(CH<sub>3</sub>)<sub>2</sub>), 1.03 (d, 6H, <sup>3</sup>J<sub>HH</sub> = 6.8 Hz, CH(CH<sub>3</sub>)<sub>2</sub>), 0.79 (t, 9H, <sup>3</sup>J<sub>HH</sub> = 7.9 Hz, Si(CH<sub>2</sub>CH<sub>3</sub>)<sub>3</sub>), 0.62 – 0.52 (m, 6H, Si(CH<sub>2</sub>CH<sub>3</sub>)<sub>3</sub>).

$\delta_{\text{C}}$  (100 MHz, C<sub>6</sub>D<sub>6</sub>, 298K): 172.6 (s, 1C, HCNC<sup>IV</sup>), 159.8 (s, 1C, NC<sup>IV</sup><sub>A</sub>), 146.5 (s, 1C, NC<sup>IV</sup>), 144.2 (s, 1C, NC<sup>IV</sup>), 143.8 (s, 2C, *o*-C<sup>IV</sup>), 140.9 (s, 2C, *o*-C<sup>IV</sup>), 138.6 (s, 1C, C<sub>E</sub>), 135.2 (s, 1C, C<sub>C</sub>), 127.2 (s, 1C, *p*-*Dipp*CH), 126.0 (s, 1C, *p*-*Dipp*CH), 124.7 (s, 2C, *m*-*Dipp*CH), 124.2 (s, 2C, *m*-*Dipp*CH), 117.6 (s, 1C, C<sub>B</sub>), 115.6 (s, 1C, C<sup>IV</sup><sub>F</sub>CHN), 113.4 (s, 1C, C<sub>D</sub>), 29.6 (s, 2C, CH(CH<sub>3</sub>)<sub>2</sub>), 28.8 (s, 2C, CH(CH<sub>3</sub>)<sub>2</sub>), 25.1 (s, 2C, CH(CH<sub>3</sub>)<sub>2</sub>), 24.6 (s, 2C, CH(CH<sub>3</sub>)<sub>2</sub>), 24.5 (s, 2C, CH(CH<sub>3</sub>)<sub>2</sub>), 23.4 (s, 2C, CH(CH<sub>3</sub>)<sub>2</sub>), 9.9 (s, 3C, Si(CH<sub>2</sub>CH<sub>3</sub>)<sub>3</sub>), 8.2 (s, 3C, Si(CH<sub>2</sub>CH<sub>3</sub>)<sub>3</sub>).

$\delta_{\text{Si}}$  (79.5 MHz, C<sub>6</sub>D<sub>6</sub>, 298K): 0.28 (s).

Anal. Calc. (C<sub>37</sub>H<sub>54</sub>MgN<sub>2</sub>Si): C, 76.72; H, 9.40; N, 4.84. Found: C, 76.68; H, 9.64; N, 4.86.

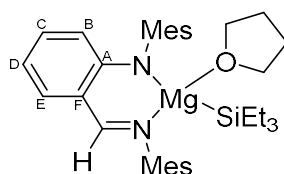


**Synthesis of compound 10a.THF:** In a dinitrogen filled glovebox, [<sup>Mes</sup>(L)MgC<sub>4</sub>H<sub>9</sub>] (100 mg, 0.23 mmol) was suspended in toluene (6 mL) followed by the addition of THF (20 μL, 0.25 mmol). Me<sub>2</sub>PhSiBpin (67 μL, 0.51 mmol) was added and a colour change from yellow to orange was observed. The reaction was stirred in a scintillation vial for 2 hours at 22 °C then the solvent removed *in vacuo*. The product was crystallised from n-hexane (~4 mL) at -35 °C yielding yellow precipitate (41 mg, 30 %, 0.7 mmol). Attempts to crystallise pure samples of **3a.THF** repeatedly led to the incorporation of a side product, *pinB-C<sub>4</sub>H<sub>9</sub>* (approx. 30 %).

$\delta_{\text{H}}$  (400 MHz, C<sub>6</sub>D<sub>6</sub>, 298K): 7.77 (s, 1H, NCH), 7.25 – 7.19 (m, 2H, *o*-CH), 7.19 – 7.10 (m, 3H, Si-*m/p*-CH), 7.06 (s, 2H, *Mes-m*-CH), 7.01 – 6.92 (m, 2H, CH<sub>E</sub> + CH<sub>C</sub>), 6.84 (s, 2H, *Mes-m*-CH), 6.54 (d, 1H, <sup>3</sup>J<sub>HH</sub> = 8.8 Hz, CH<sub>A</sub>), 6.29 – 6.23 (m, 1H, CH<sub>B</sub>), 6.38 – 6.33 (m, 1H, CH<sub>D</sub>), 3.26 – 3.19 (m, 4H, THF-OCH<sub>2</sub>), 2.32 (s, 3H, *p*-CH<sub>3</sub>), 2.32 – 2.01 (br m, 12H, *o*-CH<sub>3</sub>), 2.19 (s, 3H, *p*-CH<sub>3</sub>), 0.89 (m, 4H, THF-OCH<sub>2</sub>(CH<sub>2</sub>)<sub>2</sub>), 0.34 (s, 6H, Si(CH<sub>3</sub>)<sub>2</sub>). Residual *pinB-C<sub>4</sub>H<sub>9</sub>* (~0.3 equiv.): 1.64 – 1.54 (m, 2H, CH<sub>2</sub>), 1.43 – 1.37 (m, 2H, CH<sub>2</sub>), 1.06 (s, 12H, (CH<sub>3</sub>)<sub>4</sub>), 1.02 – 0.86 (m, 5H).

$\delta_{\text{C}}$  (100 MHz, C<sub>6</sub>D<sub>6</sub>, 298K): 171.1 (s, 1C, HCNC<sup>IV</sup>), 159.0 (s, 1C, NC<sup>IV</sup><sub>A</sub>CH), 152.4 (s, 1C, SiC<sup>IV</sup>), 147.7 (s, 1C, NC<sup>IV</sup>), 146.1 (s, 1C, NC<sup>IV</sup>), 138.5 (s, 1C, C<sub>E</sub>), 135.0 (s, 2C, *Mes-o*-C<sup>IV</sup>), 134.6 (s, 1C, C<sub>C</sub>), 134.3 (s, 2C, Si-*o*-CH), 133.0 (s, 2C, *Mes-o*-C<sup>IV</sup>), 129.7 (br s, 4C, *Mes*CH), 127.3 (s, 2C, Si-*m*-CH), 125.9 (s, 1C, Si-*p*-CH), 116.9 (s, 1C, C<sub>B</sub>), 116.3 (s, 1C, NCHC<sup>IV</sup><sub>F</sub>), 112.0 (s, 1C, C<sub>D</sub>), 69.5 (s, 2C, THF-OCH<sub>2</sub>), 24.9 (s, 2C, THF-OCH<sub>2</sub>(CH<sub>2</sub>)<sub>2</sub>), 21.1 (s, 1C, *p*-CH<sub>3</sub>), 20.9 (s, 1C, *p*-CH<sub>3</sub>), 19.0 (br s, 4C, *o*-CH<sub>3</sub>), 3.1 (s, 2C, Si(CH<sub>3</sub>)<sub>2</sub>). The *Mes-p*-C<sup>IV</sup> resonance could not be identified.

$\delta_{\text{Si}}$  (79.5 MHz, C<sub>6</sub>D<sub>6</sub>, 298K): -26.4 (s).



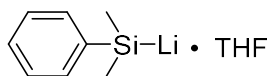
**Synthesis of compound 10b.THF:** In a dinitrogen filled glovebox, [<sup>Mes</sup>(L)MgC<sub>4</sub>H<sub>9</sub>] (100 mg, 0.23 mmol) was dissolved in toluene (6 mL) followed by the addition of THF (20 μL, 0.25 mmol). Et<sub>3</sub>SiBpin (67 μL, 0.25 mmol) was added and the reaction was stirred in a scintillation vial for 2 hours at 22 °C then the solvent removed *in vacuo*. The product was crystallised from n-hexane (~3 mL) at -35 °C yielding yellow crystals (90 mg, 78 %, 0.18 mmol).

$\delta_{\text{H}}$  (400 MHz, C<sub>6</sub>D<sub>6</sub>, 298K): 7.79 (s, 1H, NCH), 7.03 (s, 2H, MesCH), 7.02 – 6.99 (m, 1H, CH<sub>E</sub>), 6.97 – 6.91 (m, 1H, CH<sub>C</sub>), 6.84 (s, 2H, MesCH), 6.55 (d, 1H, <sup>3</sup>J<sub>HH</sub> = 8.2 Hz, CH<sub>A</sub>), 6.38 – 6.33 (m, 1H, CH<sub>D</sub>), 3.51 – 3.44 (m, 4H, O(CH<sub>2</sub>)<sub>2</sub>), 2.29 (s, 3H, *p*-CH<sub>3</sub>), 2.27 (s, 6H, *o*-CH<sub>3</sub>), 2.17 (s, 3H, *p*-CH<sub>3</sub>), 2.15 (br s, 6H, *o*-CH<sub>3</sub>), 1.09 – 1.04 (m, 4H, OCH<sub>2</sub>(CH<sub>2</sub>)<sub>2</sub>), 0.94 (t, 9H, <sup>3</sup>J<sub>HH</sub> = 7.9 Hz, Si(CH<sub>2</sub>CH<sub>3</sub>)<sub>3</sub>), 0.61 (q, 6h <sup>3</sup>J<sub>HH</sub> = 7.9 Hz, Si(CH<sub>2</sub>CH<sub>3</sub>)<sub>3</sub>).

$\delta_{\text{C}}$  (100 MHz, C<sub>6</sub>D<sub>6</sub>, 298K): 170.8 (s, 1C, HCNC<sup>IV</sup>), 159.0 (s, 1C, NC<sup>IV</sup><sub>A</sub>CH), 147.8 (s, 1C, NC<sup>IV</sup>), 146.4 (s, 1C, NC<sup>IV</sup>), 138.3 (s, 1C, C<sub>E</sub>), 134.9 (s, 2C, *p*-C<sup>IV</sup>), 134.4 (s, 1C, C<sub>C</sub>), 133.4 (s, 2C, Mes-*o*-C<sup>IV</sup>), 132.8 (s, 1C, Mes-*p*-C<sup>IV</sup>), 130.0 (s, 2C, MesCH), 130.0 (s, 2C, Mes-*o*-C<sup>IV</sup>), 129.6 (s, 2C, MesCH), 117.1 (s, 1C, C<sub>B</sub>), 116.5 (s, 1C, NHC<sup>IV</sup><sub>F</sub>), 111.9 (s, 1C, C<sub>D</sub>), 69.5 (s, 2C, OCH<sub>2</sub>), 25.1 (s, 2C, OCH<sub>2</sub>(CH<sub>2</sub>)<sub>2</sub>), 21.1 (s, 1C, *p*-CH<sub>3</sub>), 20.9 (s, 1C, *p*-CH<sub>3</sub>), 19.2 (s, 2C, *o*-CH<sub>3</sub>), 19.0 (s, 2C, *o*-CH<sub>3</sub>), 10.3 (s, 3C, Si(CH<sub>2</sub>CH<sub>3</sub>)<sub>3</sub>), 8.8 (s, 3C, Si(CH<sub>2</sub>CH<sub>3</sub>)<sub>3</sub>).

$\delta_{\text{Si}}$  (79.5 MHz, C<sub>6</sub>D<sub>6</sub>, 298K): -6.4 (s).

### 3.3.4 Preparation of Lithium Reagents



**Synthesis of compound 11.THF (PhMe<sub>2</sub>SiLi.THF<sub>3/2</sub>):** Lithium wire, from paraffin oil (328 mg, 47.2 mmol) was washed with n-hexane and added to an oven dried Schlenk flask. The lithium was stirred under vacuum for 10 minutes then backfilled with argon and this process repeated three times. Dry THF (40 mL) was added and the solution cooled to 0 °C, followed by the addition of chloro(dimethyl)phenylsilane (3.00 mL, 17.8 mmol). The solution was stirred for 16 hours at 22 °C observing a colour change to deep red. The solvent was removed *in vacuo* then toluene (40 mL) was added and the solution stirred for 3 hours at 22 °C. The solution was transferred to another Schlenk flask via cannula filtration and the solvent removed *in vacuo* yielding a dark red oil as the target compound containing 2 THF molecules (2.59 g, 51 %, 9.0 mmol). *The number of THF molecules varied slightly batch to batch between of 1.5 – 2 THF.*

$\delta_{\text{H}}$  (400 MHz, C<sub>6</sub>D<sub>6</sub>, 298K): 7.74 (d, 2H, <sup>3</sup>J<sub>HH</sub> = 7.0 Hz, *o*-CH), 7.33 – 7.28 (m, 2H, *m*-CH), 7.11 (tt, 1H, <sup>3</sup>J<sub>HH</sub> = 7.4 Hz, *p*-CH), 3.38 – 3.33 (m, 6H, (CH<sub>2</sub>)<sub>2</sub>O), 1.24 – 1.17 (m, 6H, (CH<sub>2</sub>)<sub>2</sub>CH<sub>2</sub>O), 0.67 (s, 6H, CH<sub>3</sub>Si).

$\delta_{\text{C}}$  (100 MHz, C<sub>6</sub>D<sub>6</sub>, 298K): 160.2 (s, 1C, C<sup>IV</sup>Si), 133.8 (s, 2C, *o*-CH), 127.6 (s, 2C, *m*-CH), 124.7 (s, 1C, *p*-CH), 68.6 (s, 4C, OCH<sub>2</sub>), 25.3 (s, 4C, OCH<sub>2</sub>(CH<sub>2</sub>)<sub>2</sub>), 6.26 (s, 1C, Si(CH<sub>3</sub>)<sub>2</sub>).

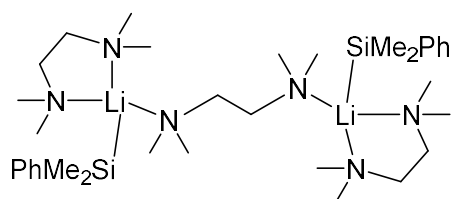
$\delta_{\text{Li}}$  (38.8 MHz, C<sub>6</sub>D<sub>6</sub>, 298K): 1.2 (s).

$\delta_{\text{Si}}$  (79.5 MHz, C<sub>6</sub>D<sub>6</sub>, 298K): -29.8 (s).

#### Procedure for purity determination of 5.THF:

A batch of silyl–lithium was synthesised according to our procedure above. Purity by mass was determined by <sup>1</sup>H NMR comparison to a known quantity of internal standard. Assuming 100 % purity, PhMe<sub>2</sub>SiLi.<sup>3/2</sup>THF (25 mg, 0.10 mmol) was dissolved in C<sub>6</sub>D<sub>6</sub> (0.6 mL) then mesitylene (13.9 μL, 0.10 mmol) was added. A <sup>1</sup>H NMR spectrum was recorded and the silyl lithium measured to be 84 % pure upon integral comparison of mesitylene (s, 9H) to PhMe<sub>2</sub>SiLi.<sup>3/2</sup>THF (s, 6H). Inspection of the <sup>1</sup>H NMR spectrum reveals the presence of between 1.5 – 2 THF molecules per lithium, which varies from batch to batch.





**Synthesis of compound 11.TMEDA (PhMe<sub>2</sub>SiLi.TMEDA<sub>3/2</sub>):** **11.THF** (33 mg, 0.134 mmol) was dissolved in C<sub>6</sub>D<sub>6</sub> (0.6 mL) and added to a J. Young NMR tube then TMEDA (18.7 μL, 0.12 mmol) was added and a <sup>1</sup>H NMR spectrum recorded. The solvent was removed *in vacuo* and the product crystallised from a saturated pentane/toluene solution (0.5 mL, 10:1), yielding X-ray quality brown crystals (10 mg, 26 %, 0.032 mmol).

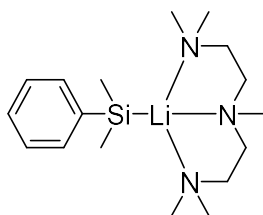
CHN analysis was attempted on **11.TMEDA** and **11.PMEDTA** but failed, likely due to their high sensitivity to atmospheric conditions.

$\delta_{\text{H}}$  (400 MHz, C<sub>6</sub>D<sub>6</sub>, 298K): 7.98 – 7.96 (m, 2H, *o*-CH), 7.45 (apparent t, 2H, <sup>3</sup>J<sub>HH</sub> = 7.4 Hz, *m*-CH), 7.21 (tt, 1H, <sup>3</sup>J<sub>HH</sub> = 7.3 Hz, *p*-CH), 2.02 – 1.41 (br m, 23H, PMEDTA), 0.90 (s, 6H, CH<sub>3</sub>Si).

$\delta_{\text{C}}$  (100 MHz, C<sub>6</sub>D<sub>6</sub>, 298K): 163.5 (s, 1C, C<sup>V</sup>), 134.0 (s, 2C, *o*-CH), 127.2 (s, 2C, *m*-CH), 123.8 (s, 1C, *p*-CH), 56.7 (s, 3C, (N(CH<sub>2</sub>))<sub>3</sub>), 45.4 (s, 6C, N(CH<sub>3</sub>)<sub>6</sub>), 7.4 (s, 2C, Si(CH<sub>3</sub>)<sub>2</sub>).

$\delta_{\text{Li}}$  (38.8 MHz, C<sub>6</sub>D<sub>6</sub>, 298K): 1.4 (s).

$\delta_{\text{Si}}$  (79.5 MHz, C<sub>6</sub>D<sub>6</sub>, 298K): -27.6 (s).



**Synthesis of compound 11.PMDETA (PhMe<sub>2</sub>SiLi.PMDETA):** PhMe<sub>2</sub>SiLi.<sup>3/2</sup>THF (700 mg, 2.90 mmol) was dissolved in toluene (4 mL) and then PMDETA (930  $\mu$ L, 4.50 mmol) was added. The solution was left for 30 minutes then filtered into a scintillation vial followed by the addition of n-hexane (4 mL). The product was allowed to crystallise at -35 °C yielding brown crystals (588 mg, 64 %, 1.86 mmol).

$\delta_{\text{H}}$  (400 MHz, C<sub>6</sub>D<sub>6</sub>, 298K): 7.99 – 7.91 (m, 2H, *o*-CH), 7.44 (apparent t, 2H, <sup>3</sup>J<sub>HH</sub> = 7.5 Hz, *m*-CH), 7.20 (tt, 1H, <sup>3</sup>J<sub>HH</sub> = 7.3 Hz, <sup>4</sup>J<sub>HH</sub> = 1.3 Hz, *p*-CH), 1.79 (s, 18H, N(CH<sub>3</sub>)<sub>6</sub>), 1.73 (s, 6H, N(CH<sub>3</sub>)<sub>2</sub>), 0.87 (s, 6H, CH<sub>3</sub>Si).

$\delta_{\text{C}}$  (100 MHz, C<sub>6</sub>D<sub>6</sub>, 298K): 165.3 (s, 1C, C<sup>V</sup>), 133.9 (s, 2C, *o*-CH), 127.0 (s, 2C, *m*-CH), 123.3 (s, 1C, *p*-CH), 57.0 (s, 2C, NCH<sub>2</sub>), 53.4 (s, 2C, NCH<sub>2</sub>), 45.8 (br s, 4C, N(CH<sub>3</sub>)<sub>2</sub>), 44.8 (s, 1C, N(CH<sub>3</sub>)), 7.7 (s, 2C, Si(CH<sub>3</sub>)<sub>2</sub>)

$\delta_{\text{Li}}$  (38.8 MHz, C<sub>6</sub>D<sub>6</sub>, 298K): 1.4 (s).

$\delta_{\text{Si}}$  (79.5 MHz, C<sub>6</sub>D<sub>6</sub>, 298K): -27.5 (s).

### 3.3.5 Preparation of Silicon Products Through sp<sup>2</sup> and sp<sup>3</sup>C–F Activation

#### General procedure for NMR scale C–F activation with Mg–Si reagents:

In a J. Young NMR tube compound **10a** (11 mg, 0.025 mmol) was dissolved in C<sub>6</sub>D<sub>6</sub> (0.6 mL) and a t=0 <sup>1</sup>H NMR spectrum recorded. The solution was degassed three times *via* freeze-pump-thaw technique then fluoroolefin gas, at 1 bar pressure, was added. The reaction was heated (22 – 100 °C) for up to 144 hours, monitoring reaction progression with <sup>1</sup>H and <sup>19</sup>F NMR spectroscopy. Yields were determined *in situ* upon integral comparison between Si(CH<sub>3</sub>)<sub>2</sub> singlet and a ferrocene or mesitylene internal capillary.

Characteristic Mg–F resonances were observed in the <sup>19</sup>F NMR spectrum between -180 and -210 ppm during *in situ* studies.<sup>[37,51]</sup> Related ( $\beta$ -diketiminato)Mg–F species are known to exist as dimers and trimers, with the formation of insoluble MgF<sub>2</sub> also being possible.

### General procedure for NMR scale C–F activation with Li–Si reagents:

**A) Room Temperature Reactions:** In a J. Young NMR tube silyl lithium compounds **11** (0.08 – 0.11 mmol) were dissolved in C<sub>6</sub>D<sub>6</sub> (0.6 mL) to generate an 0.13-0.17 M solution of the silyl lithium reagent, based upon 84 % purity (see above) of **11.THF**, from the silyl chloride and 100 % purity of **11.TMEDA** and **11.PMDETA**. A t=0 <sup>1</sup>H NMR spectrum was recorded. The solution was degassed three times *via* freeze-pump-thaw technique then fluoroolefin gas at 1 bar pressure was added. <sup>1</sup>H and <sup>19</sup>F NMR spectra were recorded within 20 minutes indicating full conversion from **11** had occurred in all cases. Yields were determined *in situ* by NMR spectroscopy on comparison of the integrals between Si(CH<sub>3</sub>)<sub>2</sub> singlet and a ferrocene internal capillary.

**B) Low Temperature Reactions:** In a J. Young NMR tube silyl lithium compounds **11** (0.08 – 0.11 mmol) were dissolved in C<sub>6</sub>D<sub>6</sub> (0.6 mL) to generate a 0.13-0.17 M solution of the silyl lithium reagent, based upon 84 % purity (see above) of **11.THF**, from the silyl chloride and 100 % purity of **11.TMEDA** and **11.PMDETA**. A t=0 <sup>1</sup>H NMR spectrum recorded. The solution was degassed three times *via* freeze-pump-thaw technique then cooled to -78 °C. Fluoroolefin gas, at 1 bar pressure, was added and the reaction maintained at -78 °C for 1 hour then warmed to 22 °C. <sup>1</sup>H and <sup>19</sup>F NMR spectra were recorded, indicating full conversion from **11** had occurred in all cases. The selectivity of the reactions was determined *in situ* by <sup>19</sup>F NMR spectroscopy.

### General procedures for large scale reaction:

**A) For Gases:** In a dinitrogen filled glovebox, **11.THF** (300-310 mg, 1.22-1.26 mmol) was dissolved in solvent (toluene or THF, 6.0 mL) and transferred to a 20 mL ampoule, to generate a 0.17 M solution of the silyl lithium reagent, based upon 84 % purity (see above) of **11.THF**. The ampoule was transferred to a Schlenk line and the contents de-gassed *via* freeze-pump-thaw technique and maintained under a static vacuum. The reaction was cooled to -78 °C. Fluoroolefin (~1 bar pressure) was purged three times through the regulator and ampoule sidearm, then allowed to fill the headspace of the reaction vessel (*see Figure 3.20*). The reaction was maintained at -78 °C for 1h before slowly warming to 22 °C over 16 hours.

**B) For Liquids:** In a dinitrogen filled glovebox, PhMe<sub>2</sub>Si–Li.<sup>3/2</sup>THF (310 mg, 1.26 mmol) was dissolved in toluene (6.0 mL) in a 20 mL scintillation vial to generate a 0.17 M solution of the silyl lithium reagent, based upon 84 % purity (see above) of **11.THF**. The contents were cooled to -35 °C over 1 hour in a freezer. Hexafluorobut-2-ene (300 μL, 3.85 mmol) was added and an immediate colour change was observed from deep red to pale orange. The reaction was left at -35 °C for one hour before allowing to warm to 22 °C. Crude <sup>1</sup>H and <sup>19</sup>F NMR spectra recorded.

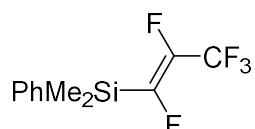
Particular care should be taken when performing these reactions on a large scale due to the possibility of exotherms upon the formation of LiF.



Figure 3.20 Standard set-up for large scale reactions of fluoroolefins at -78 °C

### Purification of organosilicon compounds:

The contents of the ampoule were transferred to a pre-weighed round bottom flask and the solvent removed by rotary evaporation. The crude mass was recorded. The contents were dissolved as much as possible in n-hexane (15 mL) then filtered through a plug of silica into another pre-weighed round bottomed flask. The mass was recorded. The product was purified by vacuum distillation (40 – 60 °C, 0.1 mbar) yielding colourless liquids (47 – 69 % isolated yields).



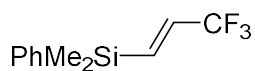
**Compound Z-12a, (Z)-dimethyl(perfluoroprop-1-en-1-yl)(phenyl)silane:** Reaction performed in toluene *via* general procedure A (155 mg, 57 %, 0.59 mmol).<sup>[23]</sup>

$\delta_{\text{H}}$  (400 MHz,  $\text{C}_6\text{D}_6$ , 298K): 7.37 – 7.30 (m, 2H, *o*-CH), 7.17 – 7.07 (m, 3H, *m/p*-CH), 0.23 – 0.20 (m, 6H, Si(CH<sub>3</sub>)<sub>2</sub>).

$\delta_{\text{C}}$  (100 MHz,  $\text{C}_6\text{D}_6$ , 298K): 162.3 (dd, 1C,  $^1J_{\text{CF}} = 288$  Hz,  $^2J_{\text{CF}} = 66$  Hz, SiCF), 150.0 (dm, 1C,  $^1J_{\text{CF}} = 239$  Hz, CFCF<sub>3</sub>), 134.1 (s, 2C, *o*-CH), 132.8 (s, 1C, SiC<sup>IV</sup>), 130.7 (s, 1C, *p*-CH), 128.5 (s, 2C, *m*-CH), 119.2 (qd, 1C,  $^1J_{\text{CF}} = 274$  Hz,  $^2J_{\text{CF}} = 39$  Hz, CF<sub>3</sub>), -4.7 (t, 2C,  $^3J_{\text{CF}} = 3$  Hz).

$\delta_{\text{F}}$  (376 MHz,  $\text{C}_6\text{D}_6$ , 298K): -67.8 (dd, 3F,  $^3J_{\text{FF}} = 21.6$  Hz,  $^4J_{\text{FF}} = 10.5$  Hz, CF<sub>3</sub>), -155.9 (dq,  $^3J_{\text{FF}} = 138.2$  Hz,  $^3J_{\text{FF}} = 21.6$  Hz, CFCF<sub>3</sub>), -166.2 (dq, 1F,  $^3J_{\text{FF}} = 138.2$  Hz,  $^3J_{\text{FF}} = 10.7$  Hz, SiCF).

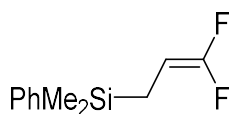
$\delta_{\text{Si}}$  (79.5 MHz,  $\text{C}_6\text{D}_6$ , 298K): -9.6 (d,  $^2J_{\text{SiF}} = 27.5$  Hz).



**Compound 12b, (E)-dimethyl(phenyl)(3,3,3-trifluoroprop-1-en-1-yl)silane:** Was synthesised according to literature procedures for NMR scale reactions and characterised *in situ* as a single isomer, with both  $^1\text{H}$  and  $^{19}\text{F}$  NMR resonances matching the literature.<sup>[23]</sup>

$\delta_{\text{H}}$  (400 MHz,  $\text{C}_6\text{D}_6$ , 298K): 6.64 (dm, 1H,  $^3J_{\text{HH}} = 18.9$  Hz, SiCH), 5.92 (dq, 1H,  $^3J_{\text{HH}} = 18.9$  Hz,  $^3J_{\text{HF}} = 5.8$  Hz, CHCF<sub>3</sub>), 0.08 (s, 6H, Si(CH<sub>3</sub>)<sub>2</sub>).

$\delta_{\text{F}}$  (376 MHz,  $\text{C}_6\text{D}_6$ , 298K): -66.3 (s, 3F, CF<sub>3</sub>).



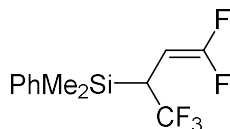
**Compound 12c, (3,3-difluoroallyl)dimethyl(phenyl)silane:** Reaction performed in toluene *via* general procedure A (101 mg, 47 %, 0.48 mmol).<sup>[70]</sup>

$\delta_{\text{H}}$  (400 MHz,  $\text{C}_6\text{D}_6$ , 298K): 7.37 – 7.30 (m, 2H, *o*-CH), 7.21 – 7.15 (m, 3H, *m/p*-CH), 3.87 (dtd,  $^3J_{\text{HF}} = 25.4$  Hz,  $^3J_{\text{HH}} = 8.7$  Hz,  $^3J_{\text{HF}} = 2.5$  Hz, CHCF<sub>2</sub>), 1.25 (dm, 2H,  $^3J_{\text{HH}} = 8.7$  Hz, CH<sub>2</sub>Si), 0.11 (s, 6H, Si(CH<sub>2</sub>)<sub>3</sub>).

$\delta_{\text{C}}$  (100 MHz,  $\text{C}_6\text{D}_6$ , 298K): 155.9 (t, 1C,  $^1J_{\text{CF}} = 283$  Hz, CF<sub>2</sub>), 137.9 (s, 1C, SiC<sup>IV</sup>), 133.9 (s, 2C, *o*-CH), 129.7 (s, 1C, *p*-CH), 128.3 (s, 2C, *m*-CH), 74.7 (t, 1C,  $^2J_{\text{CF}} = 23$  Hz, CHCF<sub>2</sub>), 10.3 (s, 1C, SiCH<sub>2</sub>CH), -3.6 (s, 2C, Si(CH<sub>3</sub>)<sub>2</sub>).

$\delta_{\text{F}}$  (376 MHz,  $\text{C}_6\text{D}_6$ , 298K): -90.7 (d, 1F,  $^2J_{\text{FF}} = 52.6$ , (*E*)-CF), -93.9 (dd, 1F,  $^2J_{\text{FF}} = 52.6$  Hz,  $^3J_{\text{HF}} = 25.3$  Hz, (*Z*)-CF).

$\delta_{\text{Si}}$  (79.5 MHz,  $\text{C}_6\text{D}_6$ , 298K): -3.7 (s).



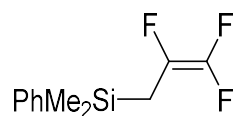
**Compound 12d, dimethyl(1,1,1,4,4-pentafluorobut-3-en-2-yl)(phenyl)silane:** Reaction performed in toluene *via* general procedure B (139 mg, 47 %, 0.50 mmol).

$\delta_{\text{H}}$  (400 MHz,  $\text{C}_6\text{D}_6$ , 298K): 7.27 – 7.23 (m, 2H, *o*-CH), 7.18 – 7.09 (m, 3H, *m/p*-CH), 3.93 (qd, 1H,  $^3J_{\text{HF}} = 11.8$  Hz,  $^3J_{\text{HH}} = 1.8$  Hz, CHCF<sub>2</sub>), 2.47 (dp, 1H,  $^3J_{\text{HF}} = 11.7$  Hz,  $^3J_{\text{HH}} = 2.7$  Hz, CHCF<sub>3</sub>), 0.16 (s, 6H, Si(CH<sub>3</sub>)<sub>2</sub>).

$\delta_{\text{C}}$  (100 MHz,  $\text{C}_6\text{D}_6$ , 298K): 157.2 (t, 1C,  $^1J_{\text{CF}} = 288$  Hz, CF<sub>2</sub>), 134.4 (s, 1C, SiC<sup>IV</sup>), 134.2 (s, 2C, *o*-CH), 130.2 (s, 1C, *p*-CH), 128.2 (s, 1C, *m*-CH), 128.1 (q, 1C,  $^1J_{\text{CF}} = 276$  Hz, CF<sub>3</sub>), 72.3 (tm, 1C,  $^2J_{\text{CF}} = 25$  Hz, CHCF<sub>2</sub>), 30.8 (qd, 1C,  $^2J_{\text{CF}} = 30$  Hz,  $^3J_{\text{CF}} = 2.1$  Hz, -4.1 (s, 1C, SiCH<sub>3</sub>), -4.7 (s, 1C, SiCH<sub>3</sub>).

$\delta_{\text{F}}$  (376 MHz,  $\text{C}_6\text{D}_6$ , 298K): -59.9 (d, 2F,  $^3J_{\text{HF}} = 11.5$  Hz, CF<sub>3</sub>), -86.1 (d, 1F,  $^2J_{\text{FF}} = 37.8$  Hz, (*E*)-CF), -88.2 (dd, 1F,  $^2J_{\text{FF}} = 37.8$  Hz,  $^3J_{\text{HF}} = 23.5$  Hz, (*Z*)-CF).

$\delta_{\text{Si}}$  (79.5 MHz,  $\text{C}_6\text{D}_6$ , 298K): -2.5 (s).



**Compound 12e, dimethyl(phenyl)(2,3,3-trifluoroallyl)silane:** Reaction performed in THF via general procedure A (168 mg, 69 %, 0.73 mmol).

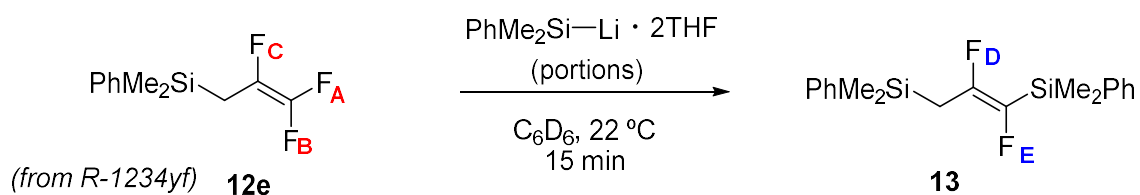
$\delta_{\text{H}}$  (400 MHz,  $\text{C}_6\text{D}_6$ , 298K): 7.34 – 7.27 (m, 2H, *o*-CH), 7.20 – 7.12 (m, 3H, *m/p*-CH), 1.51 (dm, 2H,  $^3J_{\text{HF}} = 25.1$  Hz,  $\text{CH}_2\text{Si}$ ), 0.17 (s, 6H,  $\text{Si}(\text{CH}_3)_2$ ).

$\delta_{\text{C}}$  (100 MHz,  $\text{C}_6\text{D}_6$ , 298K): 153.6 (qd, 1C,  $^1J_{\text{CF}} = 269$  Hz,  $^2J_{\text{CF}} = 49$  Hz,  $\text{CF}_2$ ), 137.0 (s, 1C,  $\text{SiC}^{\text{IV}}$ ), 133.7 (s, 2C, *o*-CH), 129.8 (s, 1C, *p*-CH), 128.6 (dm, 1C,  $\text{CFCH}_2$ ), 128.3 (s, 2C, *m*-CH), 14.7 (d, 1C,  $^2J_{\text{CF}} = 26$  Hz,  $\text{CH}_2\text{CF}$ ), -3.1 (s, 2C,  $\text{Si}(\text{CH}_3)_2$ ).

$\delta_{\text{F}}$  (376 MHz,  $\text{C}_6\text{D}_6$ , 298K): -107.9 (dd, 1F,  $^2J_{\text{FF}} = 95.8$  Hz,  $^3J_{\text{FF}} = 30.9$  Hz, (*Z*)-CF), -127.0 (dd, 1F,  $^3J_{\text{FF}} = 111.9$  Hz,  $^3J_{\text{FF}} = 96.5$  Hz, (*E*)-CF), -163.6 (dm, 1F,  $^3J_{\text{FF}} = 113.4$  Hz,  $\text{CFCH}_2$ ).

$\delta_{\text{Si}}$  (79.5 MHz,  $\text{C}_6\text{D}_6$ , 298K): -3.9 (s).

### 3.3.6 Multiple Silylation Reactions



Scheme 3.31 Plausible multiply silylated products from HF0-1234yz upon reaction with **11.THF**

**Sequential silylation of compound 12e:** PhMe<sub>2</sub>SiLi·2THF (10 mg, 0.035 mmol) was dissolved in C<sub>6</sub>D<sub>6</sub> (0.6 mL) and transferred to a J. Young NMR tube. **12e** (16 mg, 0.070 mmol) was added and the reaction allowed to react at 22 °C for 15 minutes. <sup>1</sup>H and <sup>19</sup>F NMR spectra were recorded. Two new major resonances were observed at -132.1 (dt, 1F, <sup>3</sup>J<sub>FF</sub> = 128 Hz, <sup>3</sup>J<sub>HF</sub> = 27 Hz) and -172.6 (dt, 1F, <sup>3</sup>J<sub>FF</sub> = 128 Hz, <sup>4</sup>J<sub>HF</sub> = 6 Hz) corresponding to **13**. Further addition of **11.THF** (10 mg, 0.035 mmol) in C<sub>6</sub>D<sub>6</sub> (0.05 mL) resulted in no further reaction as monitored by <sup>19</sup>F and <sup>1</sup>H NMR spectroscopy.



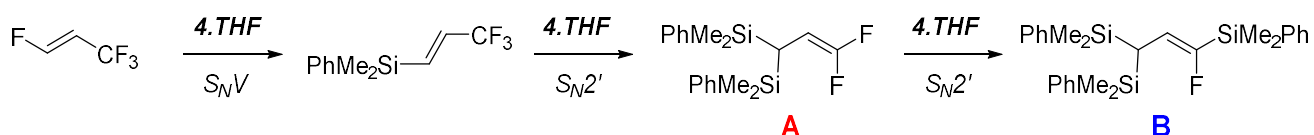
**Sequential silylation of *R*-1234ze:** **11.THF** (10 mg, 0.035 mmol) was dissolved in C<sub>6</sub>D<sub>6</sub> (0.6 mL) and transferred to a J. Young NMR tube. The contents were degassed three times *via* freeze-pump-thaw technique and *R*-1234ze added at 1 bar pressure. <sup>1</sup>H and <sup>19</sup>F NMR spectra were recorded, indicating the presence of desired product, **11d** as the major component, plus a small quantity of unknown compound (*sp*<sup>2</sup> CF bonds were suspected due to resonances). PhMe<sub>2</sub>SiLi.2THF (10 mg, 0.035 mmol) was dissolved in C<sub>6</sub>D<sub>6</sub> (0.1 mL) and added to the reaction. <sup>1</sup>H and <sup>19</sup>F NMR spectra were recorded, then this process repeated until no change to the NMR spectra were observed.

**Compound A** (*cf.* compound 12c)

δ<sub>F</sub> (376 MHz, C<sub>6</sub>D<sub>6</sub>, 298K): -91.2 (d, 1F, <sup>2</sup>J<sub>FF</sub> = 53 Hz), -93.6 (dd, 1F, <sup>2</sup>J<sub>FF</sub> = 53 Hz, <sup>3</sup>J<sub>HF</sub> = 24 Hz)

**Compound B**

δ<sub>F</sub> (376 MHz, C<sub>6</sub>D<sub>6</sub>, 298K): -122.8 (d, 1F, <sup>3</sup>J<sub>HF</sub> = 46 Hz)



Scheme 3.32 Plausible multiply silylated product from R1234ze upon reaction with **11.THF**

### 3.3.7 Low Temperature reactions with PhMe<sub>2</sub>SiLi.TMEDA and PhMe<sub>2</sub>SiLi.PMDETA

In toluene-d<sub>8</sub> at -78 °C, **11.PMDETA** and **11.TMEDA** displayed diminished reactivity towards fluoroolefins. Most notably, **11.TMEDA** failed to produce any of the desired product upon reaction with hexafluoropropene. Analysis of the <sup>19</sup>F NMR spectrum shows many, mostly unidentifiable, fluorinated species have been formed including PhMe<sub>2</sub>SiF and small quantities of 1,H-pentafluoropropene. The major, unidentified, component displays a multiplet resonance at -75.9 ppm in the <sup>19</sup>F NMR spectrum.

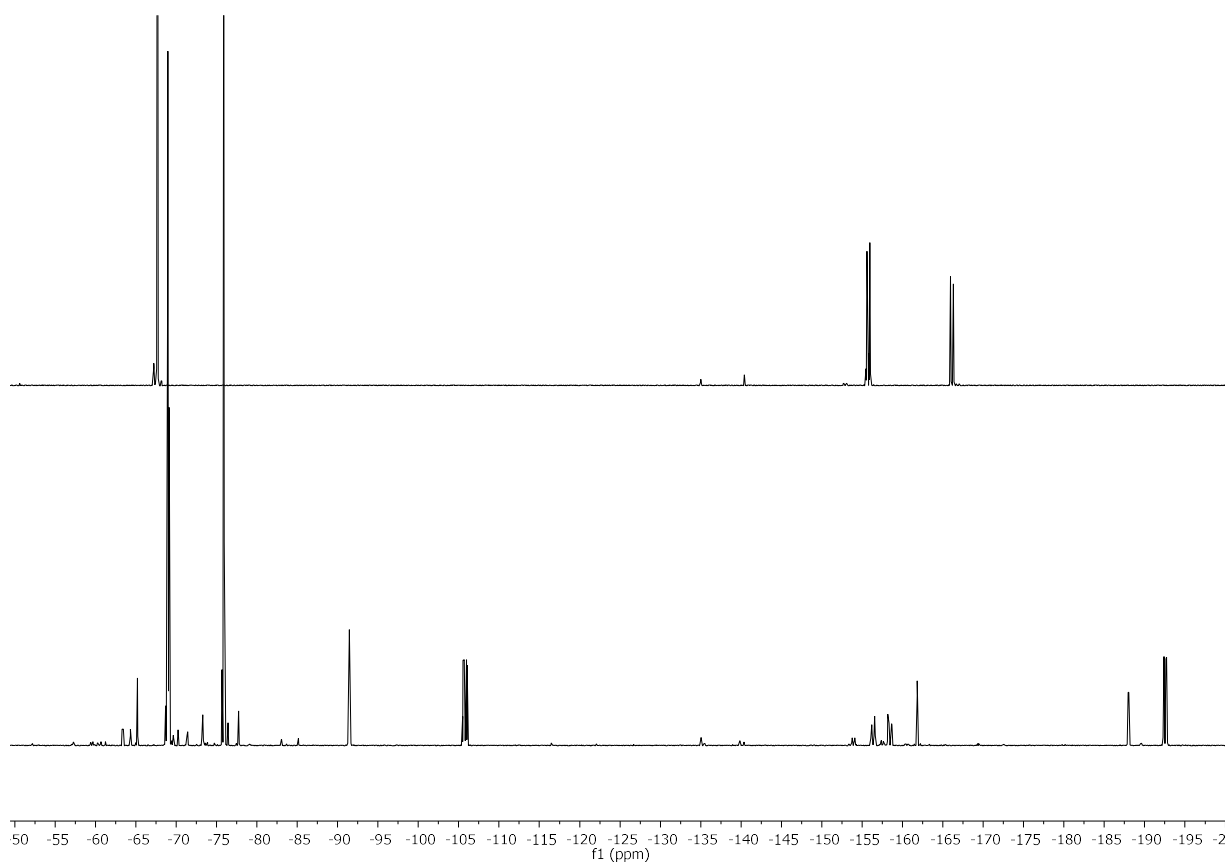
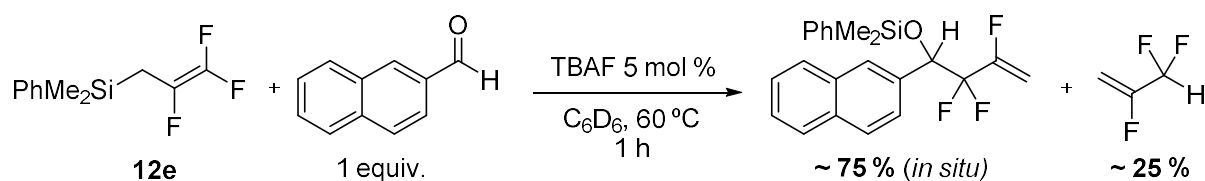


Figure 3.21 <sup>19</sup>F NMR stack plot of isolated **6a** (top) and reaction of **11.TMEDA** with HFP in toluene-d<sub>8</sub> at -78 °C (bottom). For reference, residual HFP = -70.0 (m, 3F), -91.5 (tm, 1F), -105.8 (dm, 1F) and -192.5 (dm, 1F); 1,H-pentafluoropropene = -180.0 (1F), -165.3 (1F), -69.7 (3F); PhMe<sub>2</sub>SiF = -161.5 (sept, 1F)

### 3.3.8 Fluoroalkene Addition to 2-Naphthaldehyde



Compound **12e** (20  $\mu$ L, 0.08 mmol) and 2-naphthaldehyde (12 mg, 0.08 mmol) were dissolved in C<sub>6</sub>D<sub>6</sub> (0.6 mL) and added to J. Young NMR tube. <sup>1</sup>H and <sup>19</sup>F NMR spectra were recorded to check the substrates do not react with each other. TBAF (1.0 M in THF, 3  $\mu$ L, 0.003 mmol) was added to the J. Young NMR tube and the reaction heated at 60 °C for 1 hour. <sup>1</sup>H and <sup>19</sup>F NMR spectra were recorded and the fluoroalkene addition product was determined in a 75 % yield based upon <sup>1</sup>H NMR spectrum comparison to an internal standard.

Characteristic NMR resonances:

$\delta_{\text{H}}$  (400 MHz, C<sub>6</sub>D<sub>6</sub>, 298K): 5.28 – 5.20 (m, 1H, benzylic C–H), 4.70 (dm, 1H, <sup>3</sup>J<sub>HF</sub> = 46.8 Hz), 4.55 (dm, 1H, <sup>3</sup>J<sub>HF</sub> = 17 Hz)

$\delta_{\text{F}}$  (376 MHz, C<sub>6</sub>D<sub>6</sub>, 298K): -110.5 (dm, 1F, <sup>2</sup>J<sub>FF</sub> = 262 Hz), -116.9 (dm, 1F, H<sub>2</sub>CCE), -117.7 (dm, 1F, <sup>2</sup>J<sub>FF</sub> = 262 Hz)

**2,3,3-trifluoroprop-1-ene:**<sup>[50]</sup>

$\delta_{\text{F}}$  (376 MHz, C<sub>6</sub>D<sub>6</sub>, 298K): -122.2 (m, 1F), -123.7 (dm, 2F, <sup>2</sup>J<sub>HF</sub> = 55 Hz, CF<sub>2</sub>H)

### 3.4 References

- [1] J. L. Kiplinger, T. G. Richmond, C. E. Osterberg, *Chem. Rev.*, **1994**, *94*, 373–431.
- [2] B. M. Kraft, R. J. Lachicotte, W. D. Jones, *J. Am. Chem. Soc.*, **2000**, *122*, 8559–8560.
- [3] T. Braun, D. Noveski, B. Neumann, H. G. Stammler, *Angew. Chem. Int. Ed.*, **2002**, *41*, 2745–2748.
- [4] M. S. Kirkham, M. F. Mahon, M. K. Whittlesey, *Chem. Commun.*, **2001**, 813–814.
- [5] D. Noveski, T. Braun, M. Schulte, B. Neumann, H. G. Stammler, *J. Chem. Soc. Dalton Trans.* **2003**, *3*, 4075–4083.
- [6] J. Vela, J. M. Smith, Y. Yu, N. A. Ketterer, C. J. Flaschenriem, R. J. Lachicotte, P. L. Holland, *J. Am. Chem. Soc.*, **2005**, *127*, 7857–7870.
- [7] G. Ferrando-Miguel, H. Gérard, O. Eisenstein, K. G. Caulton, *Inorg. Chem.* **2002**, *41*, 6440–6449.
- [8] M. F. Kühnel, D. Lentz, *Angew. Chem. Int. Ed.*, **2010**, *49*, 2933–2936.
- [9] N. O. Andrella, N. Xu, B. M. Gabidullin, C. Ehm, R. T. Baker, *J. Am. Chem. Soc.*, **2019**, *141*, 11506–11521.
- [10] J. Hu, X. Han, Y. Yuan, Z. Shi, *Angew. Chem. Int. Ed.*, **2017**, *56*, 13342–13346.
- [11] J. Y. Hu, J. L. Zhang, in *Organomet. Fluor. Chem.*, **2015**, pp. 143–196.
- [12] A. D. Jaeger, C. Ehm, D. Lentz, *Chem. Eur. J.*, **2018**, *24*, 6769–6777.
- [13] N. Phillips, A. White, M. Crimmin, *Adv. Synth. Catal.* **2019**, *361*, 3351–3358.
- [14] H. Schneider, A. Hock, A. D. Jaeger, D. Lentz, U. Radius, *Eur. J. Inorg. Chem.* **2018**, 4031–4043.
- [15] T. Braun, F. Wehmeier, K. Altenhöner, *Angew. Chem. Int. Ed.*, **2007**, *46*, 5321–5324.
- [16] T. Braun, M. A. Salomon, K. Altenhöner, M. Teltewskoi, S. Hinze, *Angew. Chem. Int. Ed.*, **2009**, *48*, 1818–1822.
- [17] W. H. Guo, Q. Q. Min, J. W. Gu, X. Zhang, *Angew. Chem. Int. Ed.*, **2015**, *54*, 9075–9078.
- [18] X. W. Liu, J. Echavarren, C. Zarate, R. Martin, *J. Am. Chem. Soc.*, **2015**, *137*, 12470–12473.
- [19] T. Niwa, H. Ochiai, Y. Watanabe, T. Hosoya, *J. Am. Chem. Soc.*, **2015**, *137*, 14313–14318.
- [20] J. Zhou, M. W. Kuntze-Fechner, R. Bertermann, U. S. D. Paul, J. H. J. Berthel, A. Friedrich, Z.

- Du, T. B. Marder, U. Radius, *J. Am. Chem. Soc.*, **2016**, *138*, 5250–5253.
- [21] J. Zhang, W. Dai, Q. Liu, S. Cao, *Org. Lett.*, **2017**, *19*, 3283–3286.
- [22] H. Sakaguchi, Y. Uetake, M. Ohashi, T. Niwa, S. Ogoshi, T. Hosoya, *J. Am. Chem. Soc.*, **2017**, *139*, 12855–12862.
- [23] H. Sakaguchi, M. Ohashi, S. Ogoshi, *Angew. Chem. Int. Ed.*, **2018**, *57*, 328–332.
- [24] Y. Nakao, T. Hiyama, *Chem. Soc. Rev.*, **2011**, *40*, 4893–4901.
- [25] G. R. Jones, Y. Landais, *Tetrahedron* **1996**, *52*, 7599–7662.
- [26] C. Bakewell, A. J. P. White, M. R. Crimmin, *Angew. Chem. Int. Ed.*, **2018**, *57*, 6638–6642.
- [27] H. W. Roesky, C. Cui, H. W. Roesky, H.-G. Schmidt, M. Noltemeyer, H. Hao, F. Cimpoesu, *Angew. Chem. Int. Ed.*, **2000**, *39*, 4274–4276.
- [28] M. R. Crimmin, M. J. Butler, A. J. P. White, *Chem. Commun.*, **2015**, *51*, 15994–15996.
- [29] T. Chu, Y. Boyko, I. Korobkov, G. I. Nikonov, *Organometallics*, **2015**, *34*, 5363–5365.
- [30] C. Bakewell, A. J. P. White, M. R. Crimmin, *Chem. Sci.*, **2019**, *10*, 2452–2458.
- [31] Y. Hiraoka, T. Kawasaki-Takasuka, Y. Morizawa, T. Yamazaki, *J. Fluor. Chem.* **2015**, *179*, 71–76.
- [32] B. Cui, S. Jia, E. Tokunaga, N. Shibata, *Nat. Commun.* **2018**, *9*, 4393–4400.
- [33] X. W. Liu, C. Zarate, R. Martin, *Angew. Chem. Int. Ed.*, **2019**, *58*, 2064–2068.
- [34] B. E. Smart, *The Chemistry of Functional Groups, Supplement D*, Wiley, New York, **1983**.
- [35] S. Mallick, P. Xu, E. U. Würthwein, A. Studer, *Angew. Chem. Int. Ed.*, **2019**, *58*, 283–287.
- [36] P. Gao, G. Wang, L. Xi, M. Wang, S. Li, Z. Shi, *Chinese J. Chem.* **2019**, *37*, 1009–1014.
- [37] G. Coates, B. J. Ward, C. Bakewell, A. J. P. White, M. R. Crimmin, *Chem. Eur. J.*, **2018**, *24*, 16282–16286.
- [38] D. J. Liptrot, M. Arrowsmith, A. L. Colebatch, T. J. Hadlington, M. S. Hill, G. Kociok-Köhn, M. F. Mahon, *Angew. Chem. Int. Ed.*, **2015**, *54*, 15280–15283.
- [39] S. Brand, J. Pahl, H. Elsen, S. Harder, *Eur. J. Inorg. Chem.* **2017**, *2017*, 4187–4195.
- [40] P. G. Hayes, G. C. Welch, D. J. H. Emslie, C. L. Noack, W. E. Piers, M. Parvez, *Organometallics*, **2003**, *22*, 1577–1579.

- [41] H. W. Lerner, *Coord. Chem. Rev.* **2005**, *249*, 781–798.
- [42] R. Goddard, C. Krüger, N. A. Ramadan, A. Ritter, *Angew. Chem. Int. Ed.*, **1995**, *34*, 1030–1032.
- [43] C. Strohmann, C. Däschlein, *Chem. Commun.*, **2008**, 2791–2793.
- [44] C. Strohmann, D. Schildbach, D. Auer, *J. Am. Chem. Soc.*, **2005**, *127*, 7968–7969.
- [45] W. Liu, K. Welch, C. O. Trindle, M. Sabat, W. H. Myers, W. D. Harman, *Organometallics*, **2007**, *26*, 2589–2597.
- [46] H. Gilman, G. D. Lichtenwalter, *J. Am. Chem. Soc.*, **1958**, *80*, 608–611.
- [47] H. V. R. Dias, M. M. Olmstead, K. Ruhlandt-Senge, P. P. Power, *J. Organomet. Chem.* **1993**, *462*, 1–6.
- [48] Y. Hatanaka, T. Hiyama, *J. Org. Chem.* **1988**, *53*, 918–920.
- [49] G. K. S. Prakash, A. K. Yudin, *Chem. Rev.*, **1997**, *97*, 757–786.
- [50] Y. L. Yagupolskii, N. V. Pavlenko, S. V. Shelyazhenko, A. A. Filatov, M. M. Kremlev, A. I. Mushta, I. I. Gerus, S. Peng, V. A. Petrov, M. Nappa, *J. Fluor. Chem.* **2015**, *179*, 134–141.
- [51] C. Bakewell, A. J. P. White, M. R. Crimmin, *J. Am. Chem. Soc.*, **2016**, *138*, 12763–12766.
- [52] C. Bakewell, B. J. Ward, A. J. P. White, M. R. Crimmin, *Chem. Sci.*, **2018**, *9*, 2348–2356.
- [53] M. Suginome, *Organometallics*, **2000**, *19*, 4647–4649.
- [54] T. A. Boebel, J. F. Hartwig, *Organometallics*, **2008**, *27*, 6013–6019.
- [55] J. Zhang, X. Qin, J. Fu, X. Wang, X. Su, F. Hu, J. Jiao, M. Shi, *Organometallics*, **2012**, *31*, 8275–8282.
- [56] M. J. Frisch, G. W. Trucks, H. B. Schlegel, G. E. Scuseria, M. A. Robb, J. R. Cheeseman, G. Scalmani, V. Barone, B. Mennucci, G. A. Petersson, et al., *Gaussian Inc.* **2009**.
- [57] A. D. Becke, *J. Chem. Phys.* **1993**, *98*, 5648.
- [58] J. P. Perdew, K. Burke, M. Ernzerhof, *Phys. Rev. Lett.* **1996**, *77*, 3865–3868.
- [59] J. P. Perdew, J. A. Chevary, S. H. Vosko, K. A. Jackson, M. R. Pederson, D. J. Singh, C. Fiolhais, *Phys. Rev. B* **1993**, *48*, 4978.
- [60] J. P. Perdew, J. A. Chevary, S. H. Vosko, K. A. Jackson, M. R. Pederson, D. J. Singh, C. Fiolhais, *Phys. Rev. B* **1992**, *46*, 6671–6687.

- [61] J. P. Perdew, K. Burke, Y. Wang, *Phys. Rev. B* **1996**, *54*, 16533–16539.
- [62] W. J. Hehre, R. Ditchfield, J. A. Pople, *J. Chem. Phys.* **1972**, *56*, 2257–2261.
- [63] P. C. Hariharan, J. A. Pople, *Theor. Chim. Acta* **1973**, *28*, 213–222.
- [64] T. Clark, J. Chandrasekhar, G. W. Spitznagel, P. v. R. Schleyer, *J. Comput. Chem.* **1983**, *4*, 294–301.
- [65] K. Fukui, *Acc. Chem. Res.* **1981**, *14*, 363–368.
- [66] H. P. Hratchian, H. B. Schlegel, in *Theory Appl. Comput. Chem.*, **2005**, pp. 195–249.
- [67] J. Tomasi, B. Mennucci, R. Cammi, *Chem. Rev.*, **2005**, *105*, 2999–3094.
- [68] S. Grimme, J. Antony, S. Ehrlich, H. Krieg, *J. Chem. Phys.* **2010**, *132*, 154104.
- [69] R. Dennington, T. Keith, J. Millam, *Semichem Inc. , Shawnee Mission. KS* **2009**, Semichem Inc.
- [70] M. Fujita, M. Obayashi, T. Hiyama, *Tetrahedron* **1988**, *44*, 4135–4145.

## Chapter 4 – Defluorosilylation of Trifluoromethane and HFCs

### 4.1 Introduction

Trifluoromethane (trifluoromethane,  $\text{CF}_3\text{H}$  or R-23) is produced in vast quantities (*c.a.* 20 kt year<sup>-1</sup>) as a by-product from a range of industrial processes such as the production of PTFE (Teflon), refrigerant gases and fire suppressing agents.<sup>[1,2]</sup> Trifluoromethane is a non-ozone depleting but highly potent greenhouse gas, with a 100 year global warming potential 14800 times that of  $\text{CO}_2$  and an approximate atmospheric lifetime of 250 years.<sup>[3]</sup>

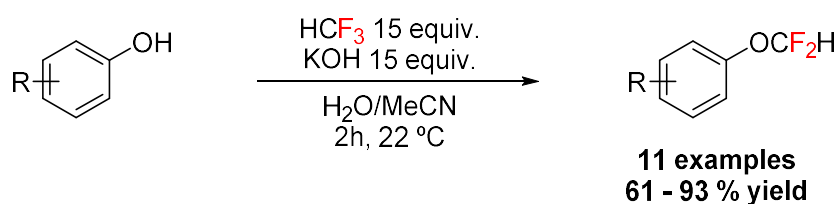
Despite its widespread production and abundant availability, limited application has been found for trifluoromethane itself. Considered primarily as a waste product, trifluoromethane needs to be stored or destroyed to limit its emission into the atmosphere (of which is predicted to already surpass 20 kt) both which are negative cost processes. For example, current methods for the destruction of trifluoromethane are catalytic hydrolysis, thermal oxidation and plasmolysis processes.<sup>[3]</sup> These two realities, its abundance and cost of mitigation, present a unique opportunity to synthetic chemists to develop value adding processes that can upgrade trifluoromethane.

Trifluoromethane has a relatively acidic C–H bond ( $\text{pK}_a \sim 25$  in  $\text{H}_2\text{O}$ ) and therefore most of its chemistry is based upon deprotonation reactions. Over recent years, many examples have exploited this reactivity to construct trifluoromethyl moieties in organic compounds.<sup>[1,4–9]</sup> The facile decomposition of the trifluoromethyl anion to difluoromethyl carbene *via*  $\alpha$ -fluorine elimination is well studied and represents a significant challenge for chemists when developing new processes. Carbenes are highly reactive species and are difficult to control.<sup>[10]</sup> Regardless of their high reactivity, the difluoromethyl carbene intermediate has found useful application in synthetic chemistry as a difluoromethyl synthon.<sup>[11]</sup> However, the majority of current sources to produce the difluoromethyl carbene are complex precursors, such as difluorochloro or difluorosulfonyl based compounds.<sup>[12]</sup> The difluoromethyl group is gaining traction as a useful bioisostere in pharmaceutical chemistry to affect the pharmacokinetic behaviour of drugs. The incorporation of difluoromethyl groups can significantly increase lipophilicity, membrane permeability, metabolic stability and compound solubilities in aqueous media – examples of such pharmaceuticals are Gemcitabine or Desflurane.<sup>[13,14]</sup> Providing suitable methodology, the increasing interest into difluoromethyl substituted products could represent a new application for trifluoromethane gas.<sup>[15]</sup>

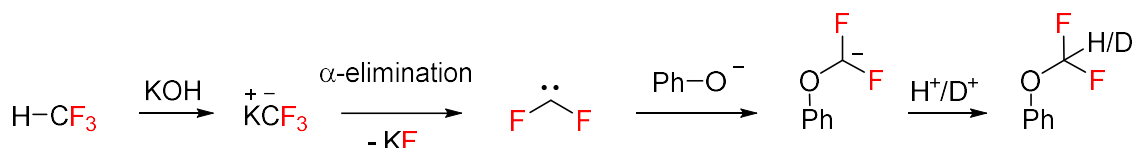


#### 4.1.1 Difluoromethylation of Alcohols and Thiols using Trifluoromethane

In 2013 Dolbier Jr. *et al.* described a method to difluoromethylate a range of phenols and aromatic thiols to generate difluoromethyl ethers and thioethers using trifluoromethane.<sup>[16]</sup> A biphasic system is employed.<sup>[17]</sup> KOH was found to be the optimum base and H<sub>2</sub>O/dioxane or H<sub>2</sub>O/MeCN the best solvent mixture (depending on substrate). The reaction was hypothesised to proceed through carbene formation and recombination with the alcohol functionality. No direct nucleophilic fluoride displacement methods are known in the literature. H/D isotope experiments highlighted the incorporation of deuterium in the final difluoromethyl product, which would not be possible if a direct C–F activation process was operating. Subjecting the final Ar–OCF<sub>2</sub>H products to the reaction conditions (KOH in D<sub>2</sub>O/MeCN) did not show any evidence of H/D exchange, further cementing the proposed pathway. The authors do not rule out the possibility of H/D scrambling upon deprotonation of trifluoromethane by KOH then subsequent deuteration to form DCF<sub>3</sub>. This pathway could also result in the observation of H/D incorporation to the reaction products.



Proposed mechanism:



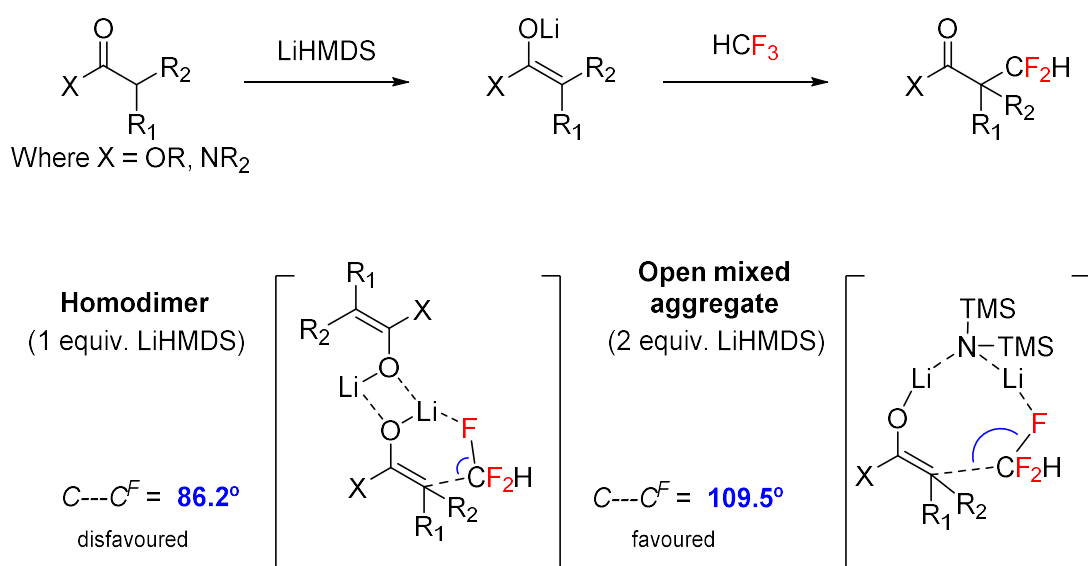
Scheme 4.1 Difluoromethylation of phenols with trifluoromethane proceeding via difluorocarbene intermediates

This method alleviates the need to use ozone depleting HCF<sub>2</sub>Cl, the long-standing preferred method to synthesise the reaction products. However, large excesses of trifluoromethane are required due to its facile consumption by KOH, although this excess trifluoromethane was shown to be recoverable. The reaction was shown to display low functional group tolerances due to the strong base (KOH) that was employed. Despite these drawbacks, this method shows promise for the commercial synthesis of selected simple aryltrifluoromethylethers.

#### 4.1.2 Reactions of Lithium Enolates with Trifluoromethane

The Mikami group demonstrated a novel technique to install difluoromethyl groups in the *alpha* position of carbonyl substrates using trifluoromethane as the CF<sub>2</sub>H synthon and LiHMDS (where HMDS

= hexamethyldisilazane) as a base.<sup>[18]</sup> They found that lithium enolates would react with trifluoromethane in an umpolung manner to generate the desired quaternary centres. Lithium was shown to be the only alkaline metal that could promote the C–F activation, presumably due to the higher strength of Li---F interactions compared to those of Na---F and K---F ( $\Delta H_{lattice} = 251, 222$  and  $198$  kcal mol<sup>-1</sup> respectively).<sup>[19]</sup> Using two equivalents of LiHMDS was the preferred stoichiometry over one or three equivalents and the authors attributed this result to a stable aggregate that can be formed with the extra equivalent of base with the lithium enolate, rather than the homodimer whereby two lithium enolates are complexed through Li---O---Li interactions (*Scheme 4.2*).



*Scheme 4.2*  $\alpha$ -difluoromethylation of lithium enolates using trifluoromethane, highlighting suggested origin of enhanced reaction with 2 equiv. LiHMDS as calculated computationally

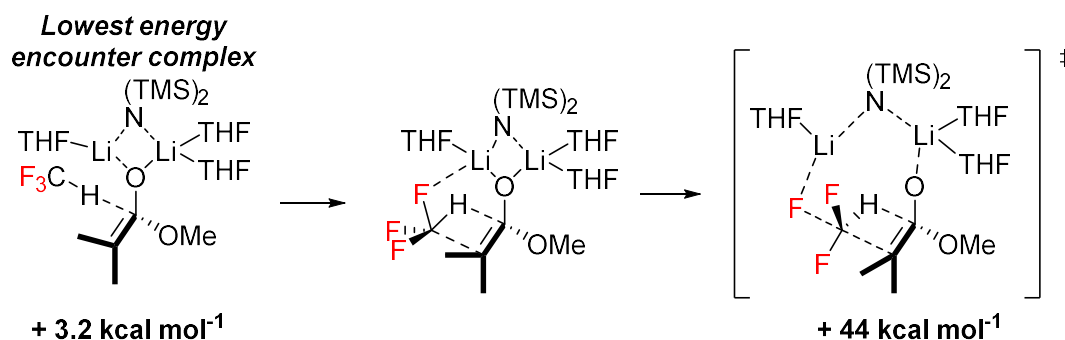
This method was not thought to proceed through a difluorocarbene intermediate. Quenching reactions with D<sub>2</sub>O showed no incorporation of deuterium in the product, whilst carbene trapping reactions showed no evidence for the formation of cyclopropanes when performing the reaction in the presence of electron-rich alkenes. Instead, a cyclic S<sub>N</sub>2-type pathway was advocated and supported by computational calculations. At the  $\omega$ B97XD/6-31G(d) level of theory, the coordination of trifluoromethane to the lithium enolate was probed at both the homodimer and mixed aggregate structures. Whilst S<sub>N</sub>2 reactivity was plausible at the homodimer, the non-ideal angle of 86.2° for C---C<sup>F</sup> attack (C<sup>F</sup> = trifluoromethane carbon) would suggest a relatively slow process. Comparing this now to the mixed aggregate enolate, the C---C<sup>F</sup> angle opens to a much more favourable 109.5° – suggesting a more facile S<sub>N</sub>2 reaction. In both cases the C–F and C=C bonds lengthen as well as exhibiting substantial Li---F interactions (2.280 Å).

A range of cyclic and acyclic amides and esters were shown to undergo reaction with moderate yields (33 – 82 %) under relatively mild conditions (0 °C, 2 – 24 h). They also demonstrated the  $\alpha$ -

difluoromethylation of ibuprofen, to form an analogue which still retains pain relieving activity. This result was important, representing one of the first examples of direct C–F activation on trifluoromethane that, at the time, was suggested not to proceed *via* carbene formation or an initial deprotonation reaction. It also highlights the significance of lithium counterions with respect to C–F activation processes, as we have seen in previous chapters.

This mechanism did not hold up to much scrutiny when the group undertook a more extensive, purely computational study a few years later.<sup>[20]</sup> A much more complex process unravelled, concluding that C–H activation was now likely to occur as the first bond breaking step in the reaction of trifluoromethane with these lithium enolates.

They opted for the B3LYP-D3BJ level of theory including polarised continuum model (PCM) for THF solvation effects. They do not discuss why they change their functional from the first publication. Initial studies investigate the multiple structures for lithium enolates with varying number of THF molecules to find the lowest energy coordination complex. A mixed aggregate (Li enolate + LiHMDS) complex with three THF molecules coordinated in total was found to be the lowest in energy. Taking this structure they then simulated multiple modes of trifluoromethane coordination (seven in total), with  $\Delta\Delta G_{298K}$  values ranging from + 3.2 to + 13.8 kcal mol<sup>-1</sup> compared to the free lithium enolate. The lowest energy of these structures corresponded to a weak encounter complex with the trifluoromethane proton coordinating weakly to the C1 position of the enolate.

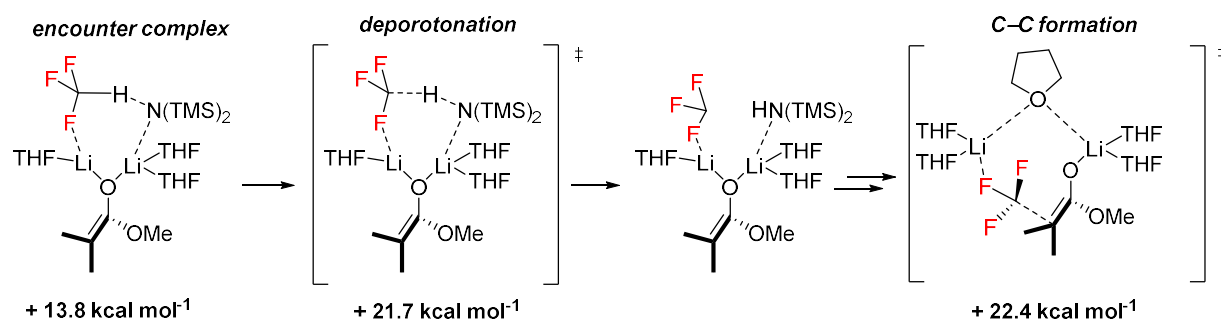


Scheme 4.3 Structure of lowest energy encounter complex of lithium enolate with trifluoromethane plus the high energy transition state for direct C–F bond cleavage

From this lowest energy encounter complex, a transition state for the direct C–C bond forming reaction was obtained. Unfortunately, the S<sub>N</sub>2-type transition state was high in energy ( $\Delta G_{298K}^{\ddagger} = 44.0$  kcal mol<sup>-1</sup>), suggesting the C–F bond is not activated enough in this structure for the experimentally observed outcome to be achieved.

A new model was proposed, which involved fluoride abstraction from a lithium carbenoid species. This process is initiated from the highest energy trifluoromethane–enolate encounter complex ( $\Delta G_{298K}$

= + 13.8 kcal mol<sup>-1</sup>). Deprotonation of trifluoromethane by HMDS could then take place to form the lithium carbenoid ( $\Delta G^{\ddagger}_{298\text{K}} = 21.7$  kcal mol<sup>-1</sup>) which then rearranges to set up for C–C bond formation ( $\Delta G^{\ddagger}_{298\text{K}} = 22.4$  kcal mol<sup>-1</sup>). This yields a lithiated difluoromethyl product which can undergo subsequent protonation under reaction conditions.



*Scheme 4.4 C–C bond formation structures beginning with deprotonation from highest energy encounter complex to generate lithium carbenoid*

The authors describe this mechanism as bimetallic, one lithium activates the leaving group whilst a second interacts with the carbenoid carbon.

After C–F activation, a –CF<sub>2</sub>Li substituted product is formed which requires protonation as the final step to generate the desired product (with H<sub>2</sub>O or excess trifluoromethane as the source). Their experimental results during a D<sub>2</sub>O quench seems to counter their proposal however, as deuterium incorporation should occur under this new mechanism, to form a CF<sub>2</sub>D group, but was not observed.

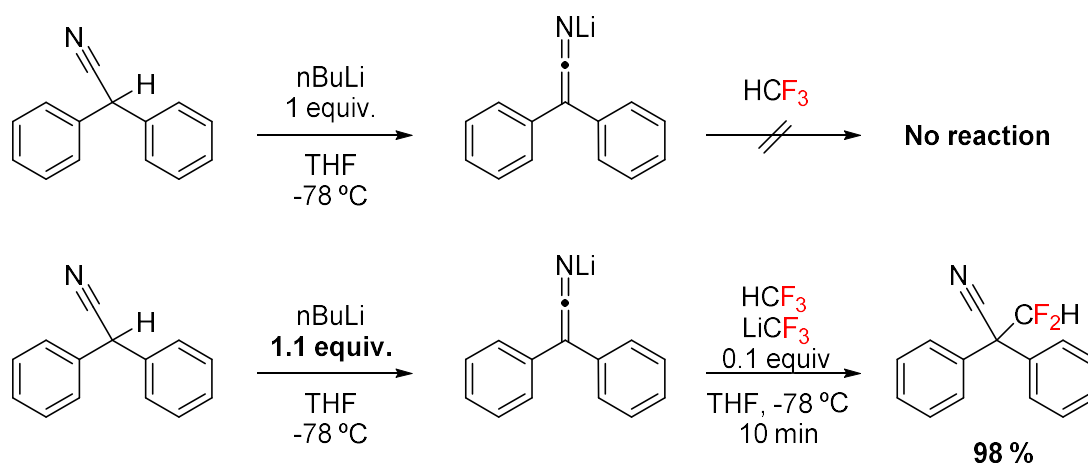
Overall, this proposed process is far from conclusive. Many lower energy structures are shown to be plausible and not all pathways have been investigated in as much detail, but again the study highlights the importance lithium plays when activating C–F bonds.

#### 4.1.3 $\alpha$ -Difluoromethylation of Nitriles and $sp$ , $sp^2$ and $sp^3$ Carbon Centres using Trifluoromethane

The group of Mikami have been prevalent in the area of difluoromethylation reactions using trifluoromethane. In these studies, they have demonstrated the  $\alpha$ -difluoromethylation of nitriles as well as at  $sp$ ,  $sp^2$  and  $sp^3$  carbon centres.<sup>[21,22]</sup> In the first of these publications, interesting insight into the reaction process was obtained through a range of mechanistic probe experiments, garnering support for the pathway suggested by their computational calculations.

Trifluoromethane gas is bubbled through a solution of 2,2-diphenylacetonitrile in the presence of lithium base at -78 °C. The first important observation was that no reaction would occur when a sub-

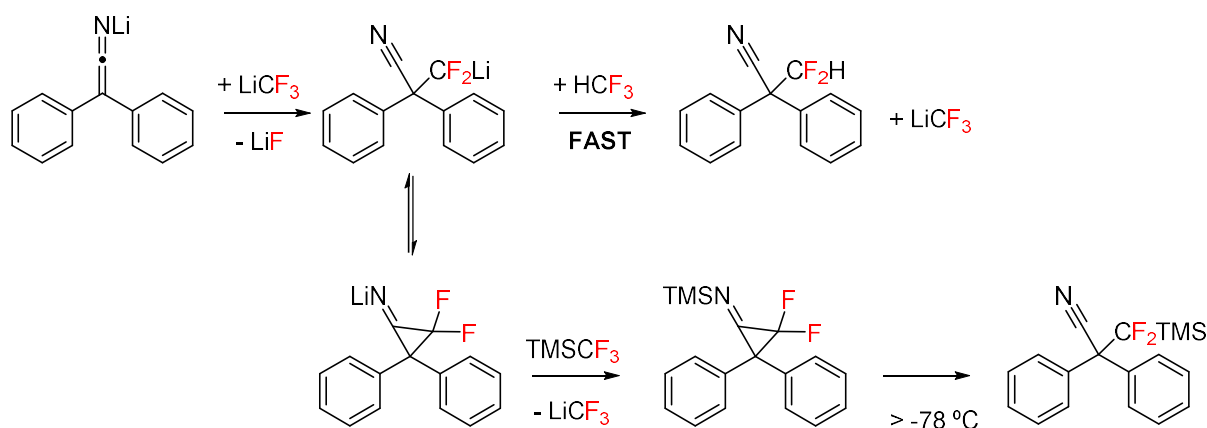
stoichiometric quantity of lithium base (*n*-BuLi) was employed. However, adding just a slight excess (1.1 equivalents) resulted in near quantitative formation of the desired  $\alpha$ -difluoromethylated nitrile product within 10 minutes. The initial hypothesis was that the lithium ketene imine intermediate would react directly with trifluoromethane, but the necessity of excess *n*-BuLi suggests that deprotonation of trifluoromethane is also required. The reaction can be considered autocatalytic in LiCF<sub>3</sub>.



Scheme 4.5 Necessity of excess *n*-BuLi in the difluoromethylation of 2,2-diphenylacetone nitrile

The difluoromethyl source was then changed to the Ruppert–Prakash reagent (TMSCF<sub>3</sub>, where TMS = SiMe<sub>3</sub>). Similarly to the previous example, no reaction was observed when 1 equivalent or less of *n*-BuLi was employed. However, increasing this to 1.1 equivalents and allowing the solution to react at -78 °C for 10 minutes resulted in the formation of the -CF<sub>2</sub>H substituted nitrile (after reaction quench with H<sub>2</sub>O). Intriguingly, leaving the reaction for 1 hour at -78 °C resulted in a mix of both -CF<sub>2</sub>H and -CF<sub>2</sub>TMS substituted products in 54 and 27 % yield respectively. When performing the reaction at warmer temperatures, -40 and -20 °C the desired -CF<sub>2</sub>TMS  $\alpha$ -substituted nitrile product was now favoured. Finally, the authors found that at 22 °C this product could be generated exclusively in high yields within just 10 minutes.

A divergent mechanism was proposed, based on observations from D<sub>2</sub>O quenching reactions (**Scheme 4.6**). One equivalent of *n*-BuLi quantitatively forms the lithium ketene imine intermediate. The excess *n*-BuLi deprotonates or desilylates the fluorinated substrate to generate LiCF<sub>3</sub>. LiCF<sub>3</sub> is proposed to react with the lithium ketene imine to generate the R-CF<sub>2</sub>Li (R =  $\alpha,\alpha$ -diaryl acetonitrile) reactive intermediate in both cases. From here the mechanism diverges. This intermediate can deprotonate another equivalent of trifluoromethane directly to generate the experimentally observed product, regenerating LiCF<sub>3</sub> which then perpetuates the cycle, but it will not react with TMSCF<sub>3</sub>.

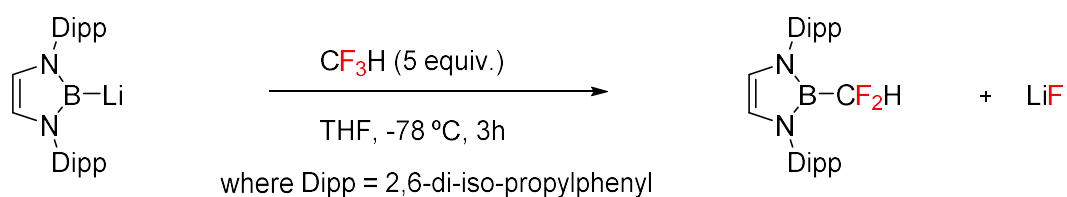


Scheme 4.6 Divergent reaction mechanisms for difluoromethylation of  $\alpha,\alpha$ -diaryl acetonitrile substrates

A difluorocyclopropane intermediate is in equilibrium with  $R-CF_2Li$ . This cyclic species will react with  $TMSCF_3$  which will subsequently ring open to form the observed product at temperatures higher than  $-78\text{ }^\circ\text{C}$ . Quenching the reaction with  $D_2O$  at  $-78\text{ }^\circ\text{C}$  will therefore lead to the  $-CF_2D$   $\alpha$ -substituted product, which was not observed during the reaction with trifluoromethane. Evidence for this reactivity was also determined computationally, whilst low temperature  $^{19}\text{F}$  NMR spectroscopy revealed trace quantities of a difluorocyclopropane intermediate ( $\delta = -125\text{ ppm}$ ).

#### 4.1.4 C–F Borylation of Trifluoromethane using a Nucleophilic Boron Reagent

Another example of a C–F functionalisation process of trifluoromethane was demonstrated using a highly nucleophilic boryl lithium reagent.<sup>[23]</sup> A new  $-CF_2H$  substituted boron species is generated upon addition of trifluoromethane at  $-78\text{ }^\circ\text{C}$  to a THF solution of boryl lithium.



Scheme 4.7 Defluoroborylation of trifluoromethane upon reaction with a nucleophilic boryl lithium reagent

The authors suggest the mechanism follows what they previously reported for the difluoromethylation of lithium enolates.<sup>[20]</sup> The speculative mechanism proposed involves an initial deprotonation of trifluoromethane to form a  $LiCF_3$  intermediate. This deprotonation could be initiated by the boryl lithium or lithium naphthalide, the latter which is present due to the *in situ* generation of the boryl lithium. The next key postulated step is dubious, but has been supported computationally by their previous work.<sup>[20,21]</sup> They suggest an  $S_N2$  attack on  $LiCF_3$  by the boryl lithium (an effective nucleophilic attack on a carbanion species), with the C–F cleavage step aided by a lithium atom. This

process forms a [B]–CF<sub>2</sub>Li species. Subsequent protonation by another trifluoromethane molecule will then yield the desired product.

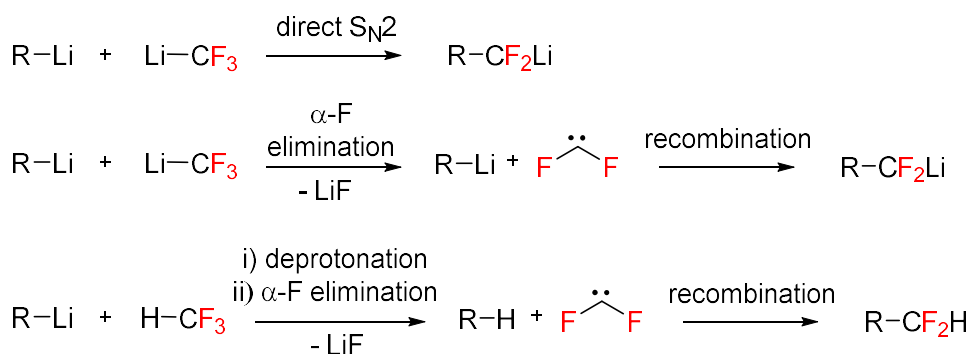
Trifluoromethane is known to undergo deprotonation provided a suitable base (pK<sub>a</sub> ~25 in H<sub>2</sub>O), the anion of which is then susceptible to α-fluorine elimination to generate difluoromethyl carbene (:CF<sub>2</sub>), however this was not countenanced by the authors

They also report the C–F activation of TMSCF<sub>3</sub> which cannot follow the exact same pathway. The steps in the mechanism could be similar if X–CF<sub>3</sub> (where X = H, SiMe<sub>3</sub>) act in the same way, *i.e.* SiMe<sub>3</sub> is significantly similar in reactivity to the proton on trifluoromethane. The last step of the reaction is supposedly deprotonation of trifluoromethane by [B]–CF<sub>2</sub>Li to form [B]–CF<sub>2</sub>H. In the case of TMSCF<sub>3</sub>, [B]–CF<sub>2</sub>Li would need to abstract SiMe<sub>3</sub> to generate the observed [B]–CF<sub>2</sub>TMS. The Mikami group had previously suggested that R–CF<sub>2</sub>Li ( where R = α,α-diaryl acetonitrile) would not desilylate TMSCF<sub>3</sub>.<sup>[21]</sup>

The boryl lithium was synthesised *in situ* and the bromo diazaborane precursor was only 82 % pure. This makes it difficult to establish the whole reaction sequence with certainty as lithium powder, naphthalene, LiBr plus other compounds are present in the reaction vessel and their participation cannot be ruled out.

Despite the lack of conclusive mechanistic insight, this reaction represents an attractive upgrade of an industrial waste product, generating a bench-stable reagent that could be used as a synthetic source of the difluoromethyl unit. The boryl lithium synthesis is non-trivial requiring very precise temperature controls and is highly susceptible to degradation which may hamper its synthetic utility on larger scales. However, this result again reiterates the effectiveness of atypical nucleophilic main group reagents towards activating C–F bonds.

The key step in all of Mikami's publications is an S<sub>N</sub>2 attack on LiCF<sub>3</sub> by the lithiated anion of the substrate. Provided a suitable base, trifluoromethane is known to undergo facile deprotonation followed by rapid α-fluorine elimination steps to generate difluoromethyl carbene. They do not consider this possible process in their publications however, but it would still fit with their plausible mechanism. Difluoromethyl carbene could recombine with the lithium boryl reagent to generate the same [B]–CF<sub>2</sub>Li species and the rest of the mechanism would be the same (*Scheme 4.8*). Furthermore, the recombination of :CF<sub>2</sub> could take place with the [B]–H species, that would be generated upon initial deprotonation of trifluoromethane.



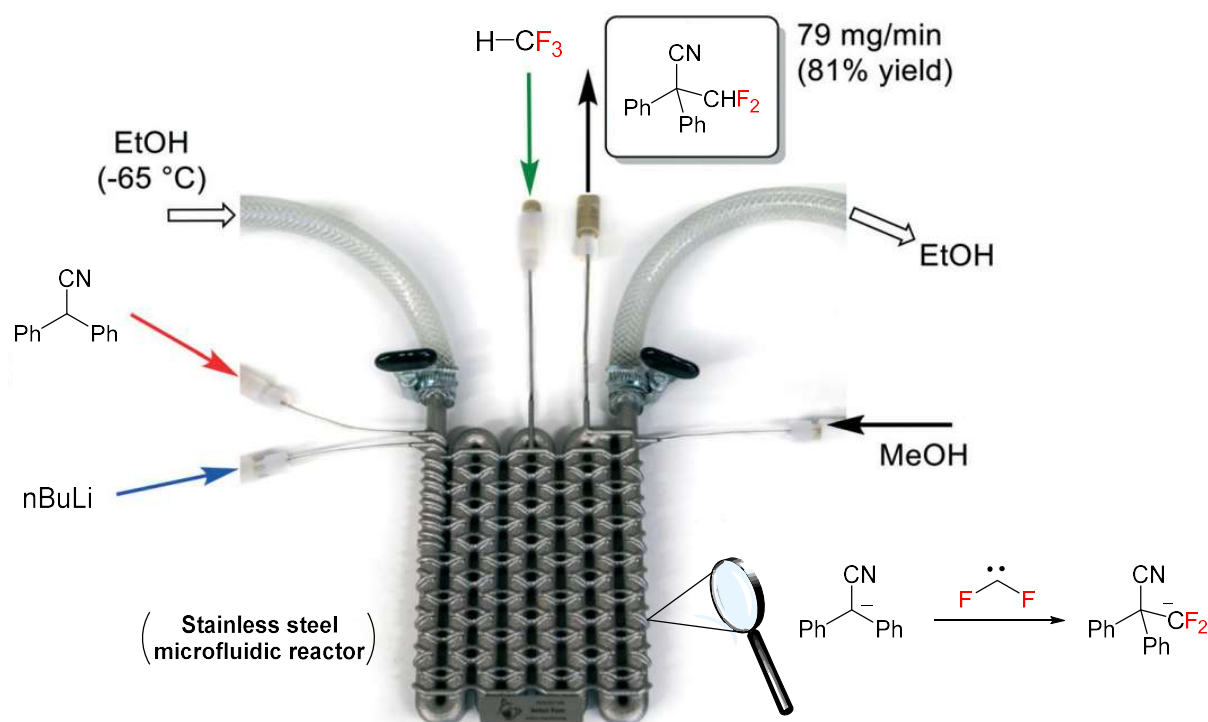
Scheme 4.8 Three plausible routes to the same difluorolithium or (difluoromethyl species). Direct  $S_N2$  on  $\text{LiCF}_3$  proposed by Mikami and supported computationally or known  $\alpha$ -fluorine elimination and recombination processes

#### 4.1.5 Difluoromethylation Reactions using Trifluoromethane under Continuous Flow Conditions

One of the key advantages of using trifluoromethane as a source of the trifluoromethyl or difluoromethyl moiety is its relative abundance and hence, low cost. However, this only becomes a significant factor when considering large scale processes as the benefits are amplified. Therefore, it is important to demonstrate scalability when using trifluoromethane as a feedstock.

The group of Oliver Kappe in Austria has developed novel micro-fluidic reactors, made from 3D printed stainless steel, that can withstand the often harsh conditions required to activate and utilise trifluoromethane.<sup>[24]</sup> By using a specifically designed stainless steel reactor they can overcome many of the problems inherent with more traditional microfluidic and continuous flow reactors, such as low mechanical strengths, low temperature ranges and solvent compatibility issues. With stainless steel, high pressures and efficient heat transfer can be achieved which suits exothermic reactions at cryogenic conditions. In this seminal publication, they took one reaction as a model – the difluoromethylation of diphenylacetonitrile. Adopting Mikami's conditions<sup>[21]</sup> the desired difluoromethyl product was realised with high purity and short reaction times of less than two minutes at  $-65^\circ\text{C}$ .



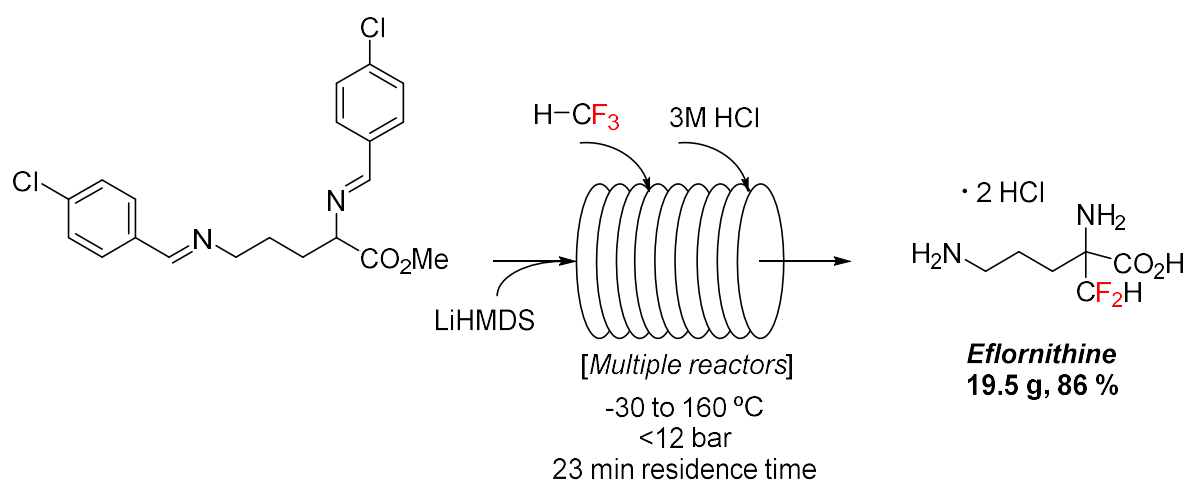


Scheme 4.9 Illustration of continuous flow process for difluoromethylation of diphenylacetonitrile<sup>[24]</sup>

Kappe *et al.* suggested that the reaction generates difluorocarbene and does not proceed directly via the  $\text{LiCF}_3$  intermediate as is reported in all of Mikami's examples. It is difficult to conclude with certainty which process is taking place, as no positive results for the formation of difluoromethyl carbene have been observed in any cases.

In a follow up publication, they demonstrated that Mikami's conditions could be adapted to suit the continuous flow process for the synthesis of  $\alpha$ -difluoromethyl amino acids with a wide substrate scope.<sup>[22,25]</sup>

The Kappe group conclude this series by applying their process towards a commercial target. The synthesis of Eflornithine was achieved, an active pharmaceutical agent (API) listed on the World Health Organisation's essential medicines used to treat African trypanosomiasis – sleeping sickness.<sup>[26]</sup> They showed that almost stoichiometric trifluoromethane could be used (1.05 equivalents), greatly improving on the batch results of Mikami.



Scheme 4.10 Simplified representation for the continuous flow synthesis of Eflornithine

Overall, 19.5 g of the active agent Eflornithine hydrochloride monohydrate was isolated in 86 % yield. This outperforms traditional methods that takes chlorodifluoromethane as the difluoromethyl source (~ 40 % yield) and the reaction time was drastically decreased from 23 hours to less than 25 minutes under continuous flow conditions. This work highlights the potential advantages of developing continuous flow methods in parallel to batch reactions, particularly if considering future industrial application.

## 4.2 C–F Silylation of Trifluoromethane

The industrial production and use of hydrofluorocarbons are currently more pervasive than that of hydrofluoroolefins. HFC gases are orders of magnitude more potent greenhouse gases than HFOs and are significant contributors to global warming and climate change.

We have seen in *Chapter 3* that the reaction of industrially relevant fluoroolefins with highly nucleophilic silicon reagents can generate bottleable and easy-to-use fluorinated building blocks with high efficiency. We now questioned whether this methodology was transferable to HFC substrates. Particular interest was focused on the defluorosilylation of trifluoromethane (R-23) and 1,1,1,2-tetrafluoroethane (R-134a), both of which are produced in vast quantities industrially as a by-product and commercial refrigerant respectively.

We began by adopting the conditions from our previous report for the defluorosilylation of fluoroolefins using silyl lithium reagents and focused on trifluoromethane as the substrate. Trifluoromethane has a relatively acidic C–H bond ( $pK_a \sim 25$  in  $H_2O$ ) therefore a lot of its chemistry favours deprotonation as an initial step, followed by possible  $\alpha$ -fluorine elimination to yield a highly reactive difluoromethyl carbene. The C–H bonds of R-134a are still reasonably accessible ( $pK_a \sim 35$  in  $H_2O$ ).<sup>[27]</sup> During the development of this reactivity, we aim to conclusively deduce the operating mechanisms.

### 4.2.1 Silyl Lithium Reagent Comparisons – Ligand Effects

Initial reactions investigated the effect of the lithium ligand (THF, PMDETA and TMEDA) and were performed in J. Young NMR tubes using 0.13 M solutions of silyl lithium reagent in  $C_6D_6$  solvent. The reactions were monitored by  $^1H$  and  $^{19}F$  NMR spectroscopy with yields and conversions determined upon comparison of integrals to a ferrocene internal standard ( $\delta = 4.00$  ppm).

The addition of trifluoromethane to a 0.13 M solution of  $PhMe_2SiLi.THF$  (**11.THF**) resulted in a slow discolouration of the sample from deep red to pale orange. Upon analysis of the  $^1H$  NMR spectrum full conversion of the silyl lithium reagent was observed. There was no obvious suggestion the desired product had been generated, expecting a broad triplet at approximately  $\delta = 5.8$  ppm in the  $^1H$  NMR spectrum. Inspection of the  $^{19}F$  NMR spectrum however showed a small doublet resonance at  $\delta = -137.7$  ppm, which collapsed to a singlet resonance upon  $^1H$  decoupling. The desired product,  $PhMe_2SiCF_2H$ , is reported to exhibit a doublet resonance in the  $^{19}F$  NMR spectrum in this region (when accounting for the difference in  $^{19}F$  NMR reference standard,  $CCl_3F$   $\delta = 0.00$  ppm and  $CF_3COOH$   $\delta = -76.55$  ppm).<sup>[28]</sup> This result, although representing less than 5 % yield, was promising and provided a

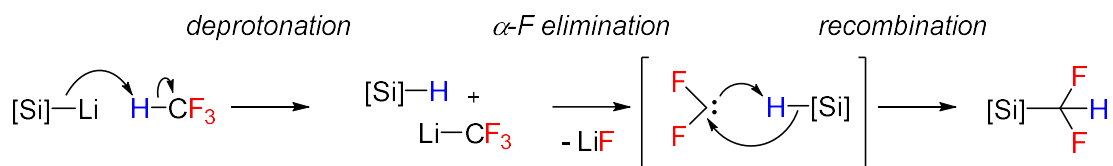


#### 4.2.2 Solvent Screen

We next investigated the effect of the solvent in this reaction. The reaction was performed in  $C_6H_6$  to investigate whether the quantity of product or silane could be underrepresented, due to the incorporation of deuterium atoms. Upon integral comparison to the  $t=0$   $^1H$  NMR spectrum, a yield of 27 % was determined plus 14 % corresponding to the silane. This result would suggest there is no significant deuterium incorporation.

Performing the reaction in a polar aprotic solvent, THF, resulted in a decreased yield being realised. Using the PMDETA resonances as internal standard, a yield of approximately 10 % was established. Upon investigation of the  $^{19}F$  NMR spectrum multiple new resonances were seen, indicating a more complex process could be taking part. Similarly, employing the tridentate amine ligand (PMDETA) as the solvent also resulted in a decreased yield, of just 13 %.

Finally we investigated the effect of viscosity on the reaction. Plausibly, the mechanism for this reaction could involve the deprotonation of trifluoromethane to initially generate lithium trifluoromethyl. This could then undergo an  $\alpha$ -fluorine elimination to form a difluoromethyl carbene. In turn, this reactive species could recombine with the Si-H bond (formed *via* first deprotonation) to generate the desired and experimentally observed product (*Scheme 4.11*)



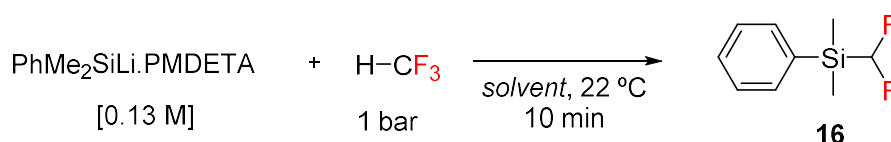
*Scheme 4.11 Plausible reaction mechanism based on carbene formation and recombination*

The phenomenon known as the cage effect states that a molecule is affected by its surroundings and that molecules in solvents can be treated as encapsulated particles. This effect is particularly relevant to radicals and can be quantified by the cage recombination efficiency ( $F_c$ ).<sup>[29]</sup>  $F_c$  has been shown to be dependent on several parameters such as; radical shape, radical size and solvent viscosity. With a more viscous solvent, the solvent cage is more pronounced and the recombination within the cage should be more favourable ( $F_c$  increases).

In the context of this work, the deprotonation of trifluoromethane by **11.PMDETA** and  $\alpha$ -elimination could occur within a solvent cage. Using a more viscous solvent, diffusion of these species outside the solvent cage could be minimised. Therefore, the proposed recombination of the difluoromethyl carbene with the Si-H bond could be enhanced, minimising undesired side reactions occurring with

other reagents outside of the solvent cage. Hence, a positive result would see an increase in product yield and decrease in silane yield.

Unfortunately, employing mesitylene (1,3,5-trimethylbenzene) as the solvent showed no improvement yielding 24 % of the product (as determined by  $^{19}\text{F}$  NMR spectroscopy using 1,2,4,5-tetrafluorobenzene as the internal standard added after the reaction was complete). This result does not rule out a carbene insertion mechanism, nor does it support one.



| Solvent                | Compound 16 Yield (%) | Viscosity (cP) |
|------------------------|-----------------------|----------------|
| $\text{C}_6\text{D}_6$ | 30                    | –              |
| $\text{C}_6\text{H}_6$ | 27                    | 0.65           |
| THF                    | ~10 <sup>b</sup>      | 0.55           |
| Mesitylene             | 24 <sup>c</sup>       | 0.834          |
| PMDETA                 | 13 <sup>c</sup>       | 1.52           |

Table 4.2 Results of solvent screen. <sup>b</sup> = PMDETA was used as internal standard <sup>c</sup> = 1,2,4,5-tetrafluorobenzene was used as internal standard added after the reaction was complete.

The solvent investigation showed our initial conditions using **11.PMDETA** to be optimum, however the reaction was still limited to approximately 30 % product yield.

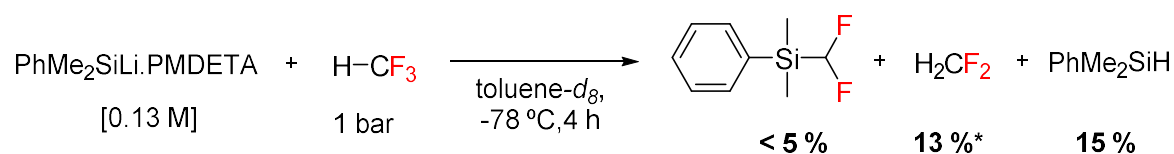
#### 4.2.3 Temperature Screen

In our previous study on the defluorosilylation of fluoroolefins, the reaction temperature was shown to be important for certain substrates. We showed that performing the reaction at  $-78^\circ\text{C}$  ensured the highest selectivity and yields with all five fluoroolefins investigated.

A 0.13 M solution of **11.PMDETA** was dissolved in toluene- $\text{d}_8$ , degassed, then cooled to  $-78^\circ\text{C}$  using a cardice/acetone bath. Trifluoromethane (1 bar pressure) was added and the reaction temperature maintained at  $-78^\circ\text{C}$  for 4 hours. The reaction was warmed to room temperature then  $^1\text{H}$  and  $^{19}\text{F}$  NMR spectra were recorded.

Integration of the  $^1\text{H}$  NMR spectrum indicated less than 5 % of the desired product (**16**) had been formed alongside 15 %  $\text{PhMe}_2\text{SiH}$ . A major product of this reaction was determined to be

difluoromethane – a triplet resonance was observed at  $\delta = 4.80$  ppm ( $^2J_{\text{H}} = 50.3$  Hz) in the  $^1\text{H}$  NMR spectrum which coincided with the intense triplet resonance at  $\delta = -141.7$  ppm ( $^2J_{\text{HF}} = 50.3$  Hz) in the  $^{19}\text{F}$  spectrum.



Scheme 4.12 Result of low temperature reaction of **11.PMDETA** and trifluoromethane in toluene- $d_8$ . Yield of difluoromethane 13 % as calculated in solution by  $^1\text{H}$  NMR spectroscopy, quantity in headspace was unknown therefore 13 % is the lower limit

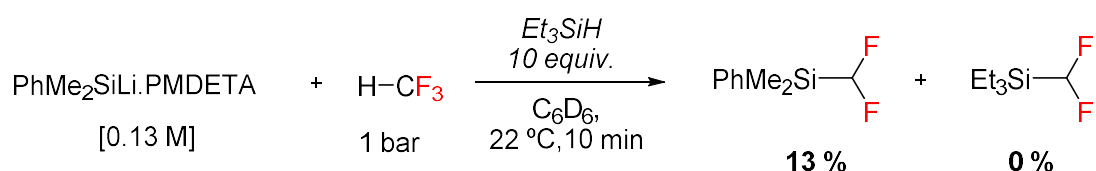
#### 4.2.4 Carbene Trap Experiments

At this stage we attempted to gain insight into the reaction mechanism. A carbene formation and re-insertion mechanism was proposed as initial deprotonation appeared the obvious first step and was supported in the literature.<sup>[16,20]</sup>

To probe this theory, we expanded the series of radical trap experiments. Carbenes are known to undergo cyclopropanation reactions with electron rich alkenes.<sup>[10]</sup> Performing the reaction in the presence of 10 equivalents of tetramethylethylene (TME) showed no significant inhibition of the reaction, achieving 25 % of the desired product upon *in situ* NMR spectrum analysis. Furthermore, the  $^{19}\text{F}$  NMR spectrum displayed no signs for the formation of difluorocyclopropane products or any other resonances that were not present in the reaction without TME. This did not rule out the formation of difluoromethylcarbene.

Repetition of this reaction in neat TME led to an unexpected result. Upon addition of TME to **11.PMDETA** (to form a 0.03 M solution) a colourless solution was generated. This contrasts to the colour in all other solvents whereby orange-brown solutions are observed. This colour change could indicate a reaction has occurred between the two compounds. The  $^1\text{H}$  NMR spectrum displayed unexpected singlet resonances at  $\delta = 5.24$  ppm and  $\delta = 5.54$  ppm. The addition of trifluoromethane gas to this solution showed no effect on the  $^1\text{H}$  and  $^{19}\text{F}$  NMR spectra, indicating the reagent had been consumed by TME to generate an unreactive species.

It has previously been shown that fluorinated carbenes, including  $:\text{CF}_2$ , can insert into the Si–H bonds of silanes such as  $\text{H}_3\text{SiX}$  (where X = F, Cl, Br or I).<sup>[10,30,31]</sup> However, to the best of our knowledge, the insertion of  $:\text{CF}_2$  into  $\text{PhMe}_2\text{SiH}$  has not been explicitly reported. We hypothesised that the addition of excess  $\text{PhMe}_2\text{SiH}$  could act as carbene trap, whilst producing the desired product.



A silane that would generate a different product was also explored. **11.PMDETA** should not deprotonate  $\text{Et}_3\text{SiH}$  to form  $\text{Et}_3\text{SiLi.PMDETA}$ , therefore any triethyl product is highly likely to occur through Si–H bond insertion. If  $\text{Et}_3\text{SiCF}_2\text{H}$  is formed, this would be good evidence for the carbene process.

A tenfold excess of triethyl silane ( $\text{Et}_3\text{SiH}$ ) was added to a 0.13 M solution of **11.PMDETA** and a  $t=1$   $^1\text{H}$  NMR spectrum recorded as a background. Trifluoromethane was then added at  $22^\circ\text{C}$  and the reaction allowed to react for 10 minutes before recording  $^1\text{H}$  and  $^{19}\text{F}$  NMR spectra. Upon analysis by  $^1\text{H}$  NMR spectroscopy, 13 % of a difluoromethyl product was observed based upon the observation of the characteristic triplet resonance at approximately  $\delta = 5.77$  ppm and a doublet at  $\delta = -137.7$  ppm in the  $^1\text{H}$  and  $^{19}\text{F}$  NMR spectra respectively. It was not immediately clear if the product was  $\text{Et}_3\text{SiCF}_2\text{H}$  or  $\text{PhMe}_2\text{SiH}$  as they have very similar resonances in these regions.<sup>[32]</sup> The NMR spectra did suggest the formation of only one product, as only one triplet and one doublet were observed in those expected regions.

The product was confirmed to be  $\text{PhMe}_2\text{SiCF}_2\text{H}$  upon vacuum transfer and analysis of the non-volatile fraction. A characteristic singlet resonance was observed at  $\delta = 0.18$  ppm in the  $^1\text{H}$  NMR spectrum corresponding to the dimethyl moiety which integrated approximately 6:1 with the triplet resonance at  $\delta = 5.77$  ppm. Furthermore, the complete loss of triplet and quartet resonances between  $\delta = 0.50$  ppm and  $\delta = 1.20$  ppm was determined, characteristic for the  $\text{Et}_3\text{Si}$ – moiety. The singlet resonance at  $\delta = -132.8$  ppm in the  $^{19}\text{F}$  NMR spectrum, corresponding to the yet unidentified by-product of this reaction was also observed. Again, this reaction did not rule out the formation of difluoromethyl carbene but it also did not support it.

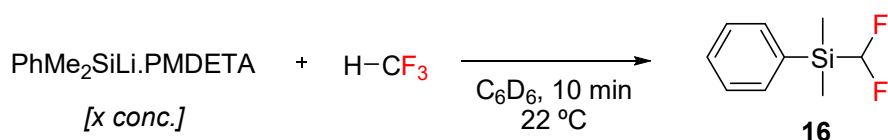
#### 4.2.5 Silyl Lithium Concentration Studies

We next investigated the effect of **11.PMDETA** concentration on the reaction yields and distributions. We kept observing the formation of a fluorinated by-product in the reaction ( $\delta = -132.8$  ppm in the  $^{19}\text{F}$  NMR spectrum) and perhaps this was the result of further reactivity occurring between **11.PMDETA** and the desired product, eroding our yield.

Doubling the concentration in solution from 0.13 M to 0.26 M, whilst keeping all other parameters constant, led to a decrease in reaction yield from 30 to 15 %. Halving the concentration to 0.067 M



gratifyingly led to a 48 % yield – the highest observed for this reaction so far. Further decreases in concentration led again to the enhancement of yields. At 0.011 M a maximum yield of 93 % was achieved as determined by *in situ* NMR spectrum analysis. The yield varied only slightly between 0.011 M and 0.022 M therefore a solution concentration of 0.02 M was determined to be optimum, due to the quantity of solvent that would be spared.



| 11.PMDETA mass (mg) | Conc. [M] | Product yield % |
|---------------------|-----------|-----------------|
| 50                  | 0.26      | 15              |
| 25 <sup>a</sup>     | 0.13      | 30              |
| 12.5                | 0.067     | 48              |
| 6                   | 0.033     | 67              |
| 3                   | 0.022     | 87              |
| 2                   | 0.011     | 93              |

Table 4.3 Effect of concentration on product yield. <sup>a</sup> = Standard reaction conditions from previous optimisations

In addition to enhancing the yield by decreasing the concentration, the reaction also became cleaner with respect to side products. Analysis of the <sup>19</sup>F NMR spectra in each reaction showed that the concentration of by-product, as determined by the resonance at  $\delta = -132.8$  ppm, decreased with decreasing **11.PMDETA** concentration. At concentrations of 0.022 M and 0.011 M, the resonance representing this by-product was only present in trace quantities. This observation could suggest that the by-product is being generated upon facile reaction of **11.PMDETA** with PhMe<sub>2</sub>SiCF<sub>2</sub>H. A singlet resonance in this region of the <sup>19</sup>F NMR spectrum is characteristic of a difluoromethyl species (–CF<sub>2</sub>–).

Repeating the reaction with **11.TMEDA** at the new optimum concentration led to no product being formed. This result highlights the importance of the tridentate PMDETA ligand in assisting this reaction.

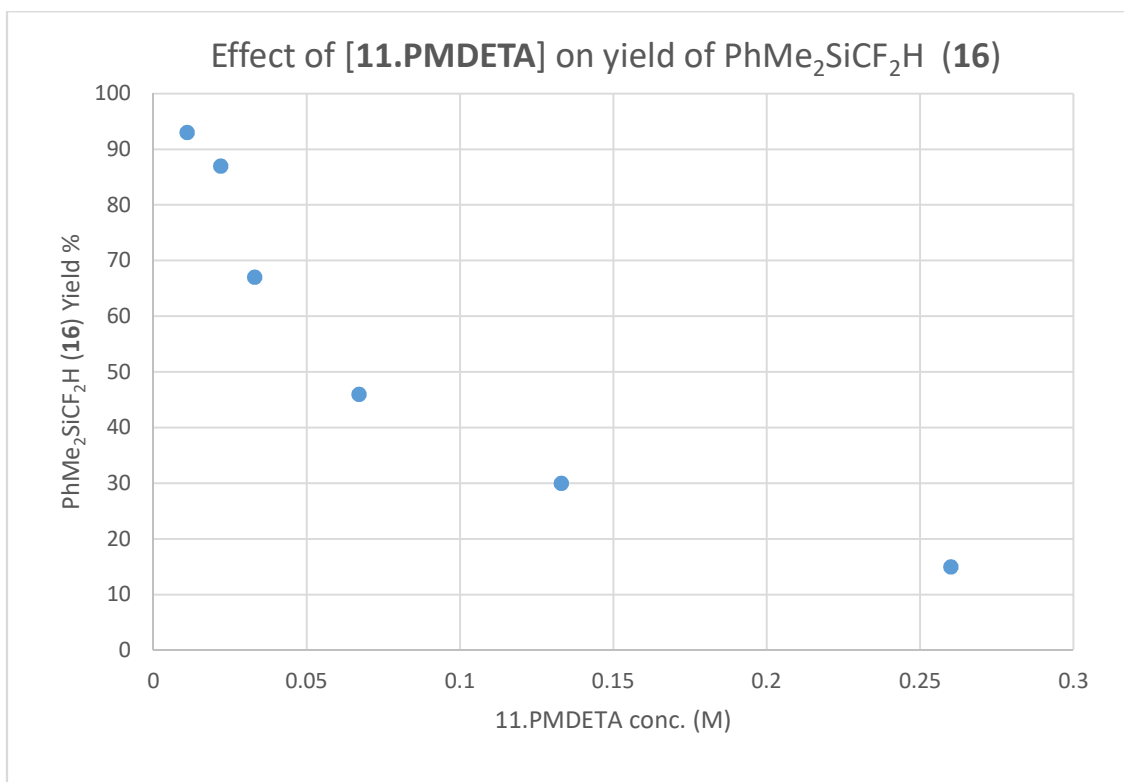


Figure 4.1 Graph displaying results of **11.PMDETA** concentration variation on yield of desired product PhMe<sub>2</sub>SiCF<sub>2</sub>H. A clear trend is shown decreasing the concentration increases the yield. Optimum compromise approximately 0.02 M.

#### 4.2.6 Large Scale Defluorosilylation of Trifluoromethane

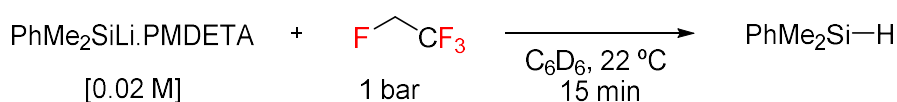
With optimum reaction conditions in hand, we now targeted the scale-up and isolation of the pure compound, PhMe<sub>2</sub>SiCF<sub>2</sub>H. We aimed to demonstrate the defluorosilylation of trifluoromethane on gram scale. For this to be achieved, certain considerations had to be made; the vessel size, stirring method and temperature control. With a 0.02 M concentration being favoured, a considerable quantity of solvent is required (160 mL toluene for 1.00 g **11.PMDETA**). The volume of headspace is also important and loosely represents the equivalents of trifluoromethane available for reaction. For example, assuming the volume of a J. Young NMR tube is 2.8 mL, then approximately 0.1 mmol of gas is added. This translates to approximately eight equivalents in relation to 0.6 mL of a 0.02 M **11.PMDETA** benzene solution. To keep this as representative as possible to the NMR scale reaction, a 500 mL Strauss flask was opted for. It is also able to hold the vacuum efficiently during the freeze-pump-thaw step. We have seen previously that PTFE stirrer bars will slowly carbonise (turn black) in the presence of silyl lithium reagents. Therefore, stirring of the sample would be performed manually. Finally, the formation of LiF is a highly exothermic process. For a safe and constant reaction, suitable measures to maintain the reaction temperature are required. This was satisfied by a simple water bath at 22 °C.

The reaction was performed as reported in the *experimental* section. The toluene solvent was removed under reduced pressure and the product extracted into n-hexane, washing with aqueous HCl (0.1 M), brine then water. This process removed inorganic by-products and PMDETA. The organic fractions were concentrated and the product isolated by short path distillation as a colourless oil (404 mg, 68 %, 2.17 mmol).

#### 4.2.7 C–F Silylation of Other CF<sub>3</sub> Containing Species

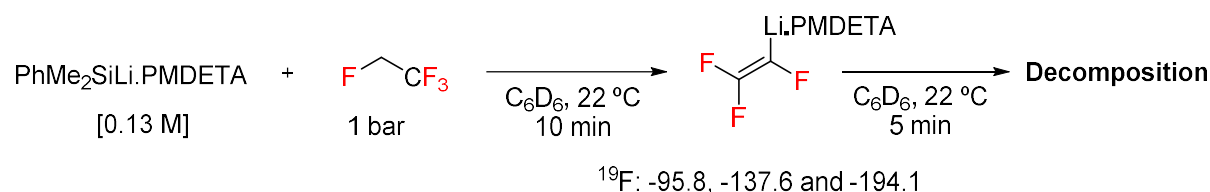
We explored the scope in fluorocarbons probing other industrially relevant HFCs and trifluoromethyl-containing compounds.

The reactivity of 1,1,1,2-tetrafluoroethane (R-134a) was investigated. Full conversion of silyl–lithium was achieved within 15 minutes upon addition of R-134a to a 0.02 M benzene-d<sub>6</sub> solution of **11.PMDETA**. The major product of the reaction was PhMe<sub>2</sub>SiH as evidenced by <sup>1</sup>H NMR spectroscopy. Unfortunately, analysis of the <sup>19</sup>F NMR spectrum revealed no new fluorinated species.



*Scheme 4.13 Reaction of 1,1,1,2-tetrafluoroethane (R-134a) with 11.PMDETA*

R-134a was added to a higher concentration solution of **11.PMDETA** (0.13 M) and <sup>1</sup>H and <sup>19</sup>F NMR spectra were recorded within 10 minutes. Three significant resonances were observed as doublet of doublet of doublets ( $\delta = -95.8, -137.6$  and  $-194.1$  ppm) in the <sup>19</sup>F NMR spectrum. Upon removal of the J. Young NMR tube from the spectrometer, the solution immediately turned black and the solution noticeably increased in temperature. Recording further <sup>1</sup>H and <sup>19</sup>F NMR spectra revealed the previously observed resonances had been lost. The PMDETA resonances in the <sup>1</sup>H NMR spectrum were now sharp, suggesting it was de-coordinated.

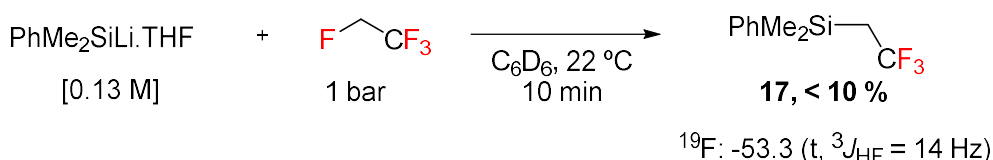


*Scheme 4.14 Reaction of 1,1,1,2-tetrafluoroethane (R-134a) with 11.PMDETA in higher concentration of silyl–lithium*

This led us to hypothesise the initial formation of lithium trifluoroethylene (LiC<sub>2</sub>F<sub>3</sub>), which then decomposes. This was supported upon consultation of the literature, as the <sup>19</sup>F NMR resonances matched well with a related compound [IZnC<sub>2</sub>F<sub>3</sub>].<sup>[33]</sup>

Repeating this study at -78 °C in toluene-d<sub>8</sub> solvent led to the formation of trace quantities of trifluoroethylene as determined by <sup>19</sup>F NMR spectrum analysis and comparison to the literature.<sup>[33]</sup>

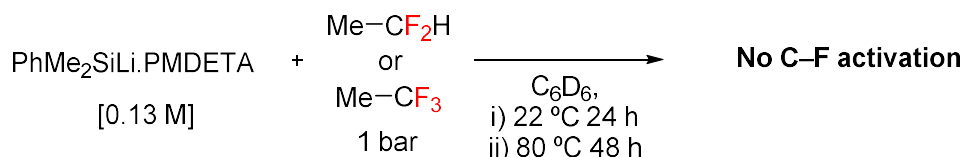
The defluorosilylation reaction of R-134a was attempted with **11.THF**. Consumption of **11.THF** occurred slowly over 16 hours. Gratifyingly, the formation of the desired defluorosilylated product, PhMe<sub>2</sub>SiCH<sub>2</sub>CF<sub>3</sub> (**17**) was achieved upon analysis of the <sup>19</sup>F NMR spectrum, revealing a characteristic triplet resonance at δ = -53.2 ppm (<sup>3</sup>J<sub>HF</sub> = 14 Hz) which matched the reported data.<sup>[34]</sup>



*Scheme 4.15 Defluorosilylation of R-134a with 11.THF*

Unfortunately, the <sup>1</sup>H NMR spectrum was quite messy, with many undesired and unidentifiable products present. Overall, compound **17** was determined to be consistently generated in 5 – 10 % yields. Further optimisation of this reaction is on-going but so far no improvement has been made to product yields.

Two other industrially relevant gases 1,1,1-trifluoroethane and 1,1-difluoroethane (R-143a and R-152a) were subject to the reaction conditions. No colour change was observed upon addition of fluorinated gas to a solution of **11.PMDETA** in both cases. Upon <sup>1</sup>H and <sup>19</sup>F NMR spectrum analysis, there was no suggestion that any reaction had occurred. Allowing the solutions to react for a further 24 hours at room temperature led to the formation of approximately 25 % PhMe<sub>2</sub>SiH in both cases. No new resonances were observed in the <sup>19</sup>F NMR spectrum. Heating these solutions to 80 °C led to the complete consumption of **11.PMDETA**. Further silane was produced however no new resonances in the <sup>19</sup>F NMR spectrum were identified, suggesting these two HFCs are not taking part in the C–F silylation process observed with trifluoromethane. The acidity of the C–H bond in trifluoromethane could therefore be an important feature (pK<sub>a</sub> ~25 in H<sub>2</sub>O).



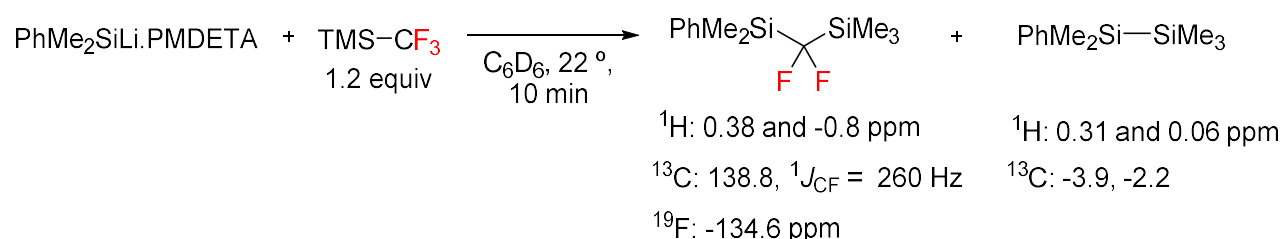
*Scheme 4.16 Failed C–F silylation reactions with 1,1,1-trifluoroethane and 1,1-difluoroethane (R-143a and R-152a)*

Defluorosilylation of α,α,α-trifluorotoluene was attempted using the optimised conditions. Upon addition, no colour change was observed and NMR spectrum analysis suggested no obvious reaction had taken place. After a further two hours, the solution had turned a darker orange-red colour. Over

the course of three days, the solution turned red-pink.  $^{19}\text{F}$  NMR analysis revealed no new fluorinated species however, indicating a lack of C–F cleavage. The  $^1\text{H}$  NMR spectrum exhibited new singlet resonances at  $\delta = 0.30, 0.65$  and  $0.94$  ppm that were not assigned. New, unassigned, resonances were also seen in the aromatic region,  $\delta = 6.00 - 8.40$  ppm.

Ito and co-workers reported the C–F activation of  $\text{TMSCF}_3$  with a boryl lithium reagent.<sup>[23]</sup> Upon addition of  $\text{TMSCF}_3$  to a 0.02 M solution of **11.PMDETA** an immediate loss of colour was observed. Analysis of the  $^1\text{H}$  and  $^{19}\text{F}$  NMR spectra revealed the complete consumption of **11.PMDETA** and the formation of one new fluorinated product (singlet at  $\delta = -134.6$  ppm). Removal of volatile species revealed 4 new singlet resonances in the  $^1\text{H}$  NMR spectrum. The two sets of resonances roughly integrated as 6:9 and 6:9 ratios ( $\delta = 0.38$  and  $-0.8$  ppm,  $\delta = 0.31$  and  $0.06$  ppm).

This reaction was repeated on a 300 mg scale then worked up, removing inorganic material and PMDETA. Analysis of the multinuclear NMR spectra elucidated the presence of two species, one that was fluorinated. Two sets of singlet resonances were observed in the  $^1\text{H}$  NMR spectrum, corresponding to Si–CH<sub>3</sub> moieties and both sets with approximately 6:9 ratios ( $\delta = 0.38$  and  $-0.8$  ppm,  $\delta = 0.31$  and  $0.06$  ppm). Characteristic resonances in the  $^{19}\text{F}$  and  $^{13}\text{C}$  NMR spectra ( $\delta = -134.6$  (s) and  $138.8$  (t)  $^1J_{\text{CF}} = 260$  Hz respectively) are consistent with the formation of  $\text{PhMe}_2\text{Si}(\text{CF}_2)\text{SiMe}_3$ .<sup>[35]</sup>



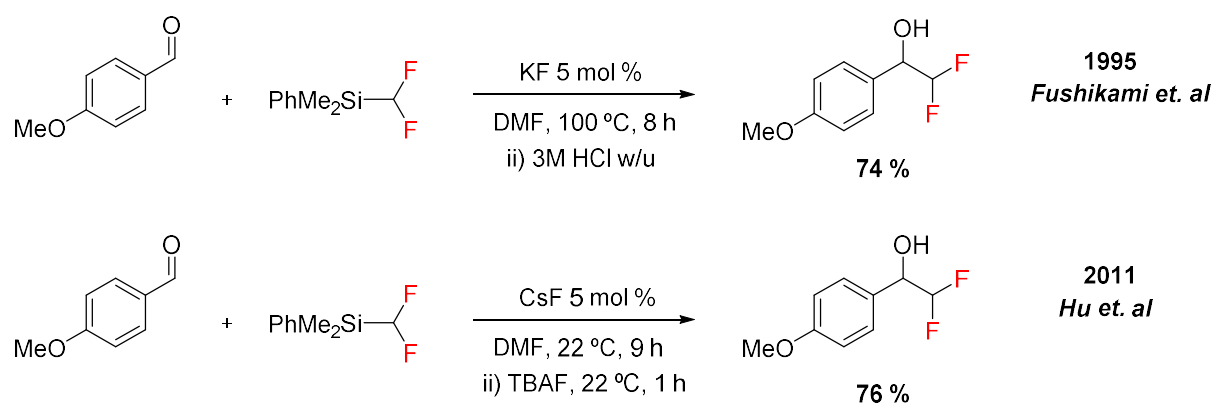
*Scheme 4.17 Likely products of reaction based upon  $^1\text{H}$  and  $^{13}\text{C}$  NMR spectroscopy, plus identifying  $^1\text{H}$ ,  $^{13}\text{C}$  and  $^{19}\text{F}$  NMR spectrum data<sup>[35]</sup>*

Consultation of the literature strongly suggested the formation of  $\text{PhMe}_2\text{SiSiMe}_3$  as the minor product ( $^1\text{H}$ ,  $\delta = 0.31$  and  $0.06$  ppm,  $^{13}\text{C}$ ,  $\delta = -3.9$  and  $-2.2$  ppm).<sup>[36,37]</sup>

#### 4.2.8 Use of C–F Activated Product as Fluorinated Building Block

The use of  $\text{PhMe}_2\text{SiCF}_2\text{H}$  as a difluoromethylating agent has been reported in the literature.<sup>[38,39]</sup> Initial studies focused on the difluoromethylation of carbonyl substrates. Moderate to good yields could be achieved under forcing conditions ( $100^\circ\text{C}$ , 6–48 h) using catalytic KF as an activator. DMF was shown to be the best solvent. Aromatic and aliphatic aldehydes could be selectively difluoromethylated. Ketones were also shown to undergo reaction to form 2,2-difluoroethanol derivatives, though longer reaction times and higher KF loadings were required (up to 50 %).

Molecular orbital calculations (MOPAC, PM3 method) showed that  $\text{PhMe}_2\text{SiCF}_2\text{H}$  has a  $\text{Si}-\text{C}^{\text{F}}$  bond order of 0.44. This is markedly higher than the Ruppert-Prakash reagent ( $\text{TMSCF}_3$ ) of 0.22, suggesting that cleavage of  $\text{Si}-\text{C}$  bond in  $\text{PhMe}_2\text{SiCF}_2\text{H}$  is more difficult, therefore requiring more forcing conditions to deliver ' $\text{HF}_2\text{C}^{\cdot}$ '.



*Scheme 4.18 Difluoromethylation of 4-methoxybenzaldehyde*

This result was improved by Hu *et. al*. Employing catalytic caesium fluoride ( $\text{CsF}$ ) as the activator, the difluoromethylation of aldehydes was now possible at room temperature.<sup>[39]</sup>

We probed the difluoromethylation of 2-naphthaldehyde with a pure sample of **16** on an NMR scale. Conditions reminiscent to those used for the Ruppert-Prakash reagent were used – tetrabutyl ammonium fluoride (TBAF) catalyst in  $\text{C}_6\text{D}_6$  solvent. Pleasingly, after addition of 20 % TBAF to a 0.06 M solution of naphthaldehyde and  $\text{PhMe}_2\text{SiCF}_2\text{H}$  the formation of characteristic resonances (for  $\alpha$ -difluoromethyl alcohols) were observed in the  $^1\text{H}$  and  $^{19}\text{F}$  NMR spectra. The formation of difluoromethane was also determined, possibly as a result of a proto-desilylation process in the presence of water from the TBAF solution (1.0 M in THF).

$\text{PhMe}_2\text{SiCF}_2\text{H}$  shows promise as a difluoromethylating agent but there is a distinct lack of its use in the literature. This could be due to the difficulty or cost in synthesis, or better access to alternatives. Our method allows for the large scale synthesis of  $\text{PhMe}_2\text{SiCF}_2\text{H}$  in a simple, quick procedure using desirable starting materials.

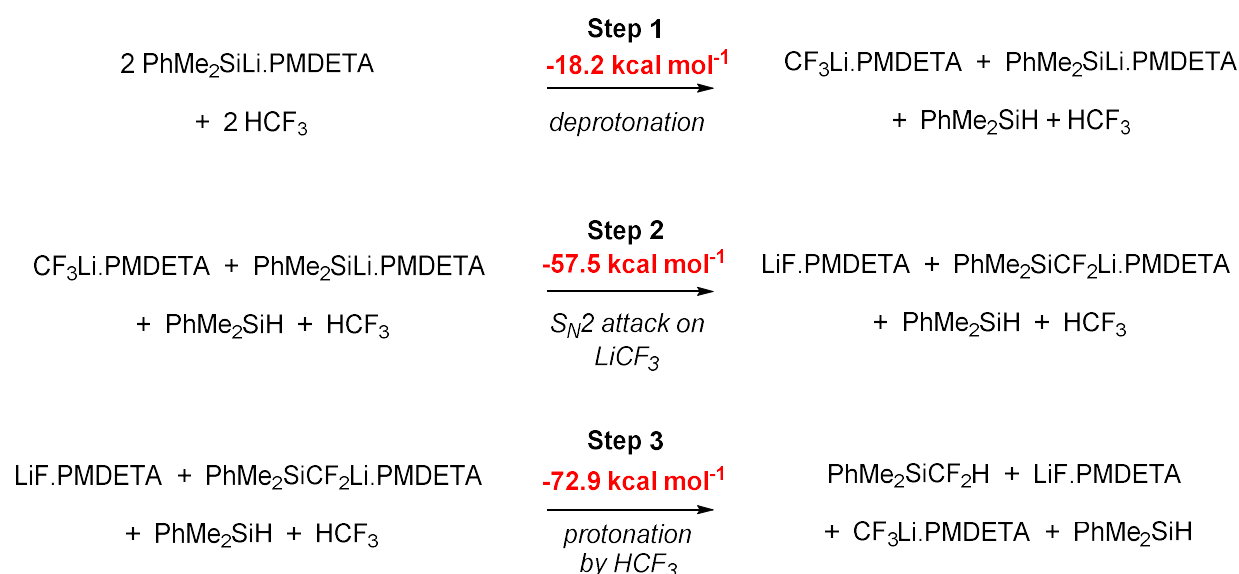
Further work will be undertaken to explore the capabilities of these reagents to deliver the difluoromethyl synthon.

#### 4.2.9 Preliminary Computational Calculations

The mechanism so far remained elusive. Carbene trap and solvent cage experiments had not given a positive result, yet this did not rule out their formation.

The group of Mikami reported that the formation of  $\text{LiCF}_3$  was the important initial step in numerous difluoromethylation reactions.<sup>[18,20,22]</sup> The key bond forming step was a dubious, yet computationally supported  $\text{S}_{\text{N}}2$  attack on  $\text{LiCF}_3$  by their lithiated substrate. We were keen to test this hypothesis on our defluorosilylation reaction.

Preliminary DFT calculations were undertaken at the B3PW91/6-31G level of theory (*c.f.* Mikami, B3LYP-D3/6-31G\*<sup>[20]</sup>). Initial investigation explored the thermodynamics of the multistep process, without analysing the transition state energies. The reactions under investigation are as so:



*Scheme 4.19 Balanced equations for the three step pathway based on Mikami's findings.<sup>[20]</sup> Thermodynamic energies given without considered energy barriers*

Gratifyingly, each step of the process was thermodynamically downhill, but the barriers to get there were unknown. We expanded the DFT studies to investigate the transitions states for the plausible first step of the process. The majority of literature examples reveal deprotonation to be the first step in trifluoromethane reactivity pathways.

A low energy transition state was located for the deprotonation of  $\text{CF}_3\text{H}$  by silyl–lithium compound **11.PMDETA** (**TS-1**,  $\Delta G^\ddagger_{298\text{K}} = 12.3 \text{ kcal mol}^{-1}$ ), to generate  $\text{PhMe}_2\text{SiH}$  and  $\text{CF}_3\text{Li.PMDETA}$ . A high energy barrier was located for the direct  $\text{S}_{\text{N}}2$  attack of  $\text{CF}_3\text{H}$  to form **16** in a single step (**TS-2**,  $\Delta G^\ddagger_{298\text{K}} = 44.0 \text{ kcal mol}^{-1}$ ). We also investigated the unusual front-side attack pathway on one C–F bond ( $\text{S}_{\text{N}}2\text{X}$ -type reactivity) as we had garnered previous computational evidence for this pathway upon reaction of fluorocarbons with Mg–Mg compounds (**1** and **2**). A transition state was located (**TS-3**,  $\Delta G^\ddagger_{298\text{K}} = 33.3 \text{ kcal mol}^{-1}$ ) that was reminiscent of what was observed in Chapter 2 for the reaction at Mg–Mg bonds.

In this reaction, the fluorine atom is transferred to silicon to generate PhMe<sub>2</sub>SiF plus a carbanionic species (CF<sub>2</sub>HLi.PMDETA).

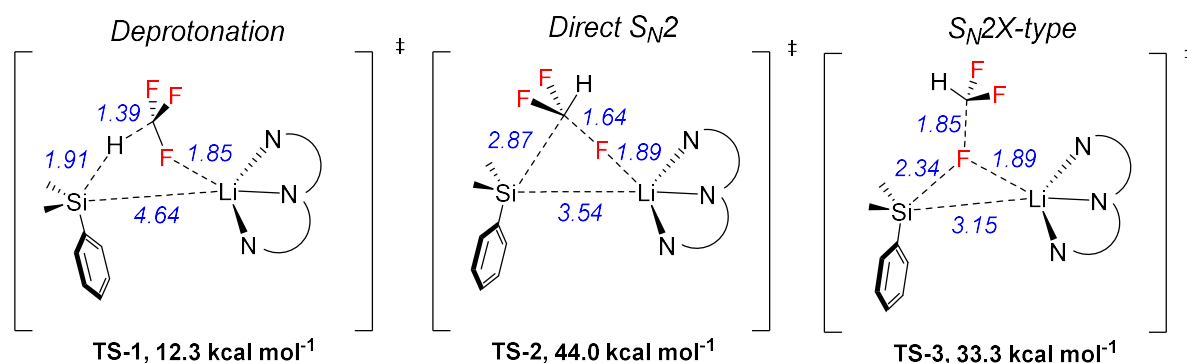


Figure 4.2 Transition state geometries and energies for the reactions of **11**.PMDETA with trifluoromethane. Bond lengths given in Å. PMDETA simplified in the representations by three N atoms

From this analysis, the relative energy barriers highly suggest that deprotonation of trifluoromethane would occur as the first step in the reaction.

Assuming deprotonation to be the first step, we investigated step two of the Mikami-like pathway, the S<sub>N</sub>2 attack of lithium carbenoid species (CF<sub>3</sub>Li.PMDETA) by another equivalent of **11**. Pleasingly, an accessible (assuming energies would be lower when incorporating solvent and dispersion corrections) transition state was identified (**TS-4**, ΔG<sup>‡</sup><sub>298K</sub> = 30.6 kcal mol<sup>-1</sup>), for the formation of PhMe<sub>2</sub>SiCF<sub>2</sub>Li.PMDETA (**Step 2**, figure 4.19).

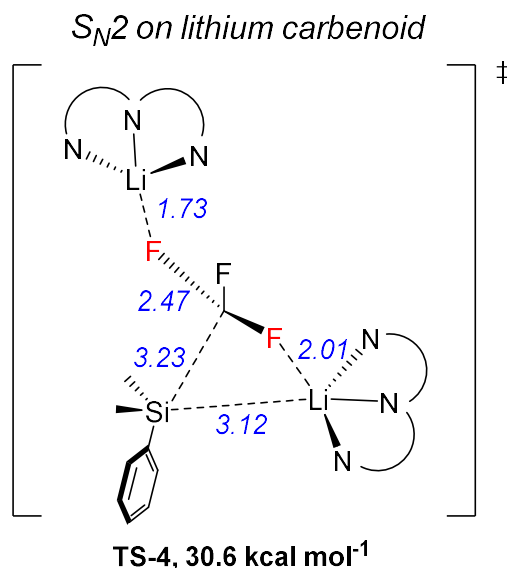


Figure 4.3 Transition state geometry for **TS-4**, an S<sub>N</sub>2 attack of **11** on a lithium carbenoid species (F<sub>3</sub>CLi.PMDETA)

So far, we have not investigated the formation of difluorocarbene or its insertion into either the Si-Li bond of **11** or the Si-H bond of the silane. Further calculations need to be undertaken to generate an



overall pathway, including the final step (**Step 3**, figure 4.19) where a second deprotonation of trifluoromethane to generate the experimentally observed product **16**.

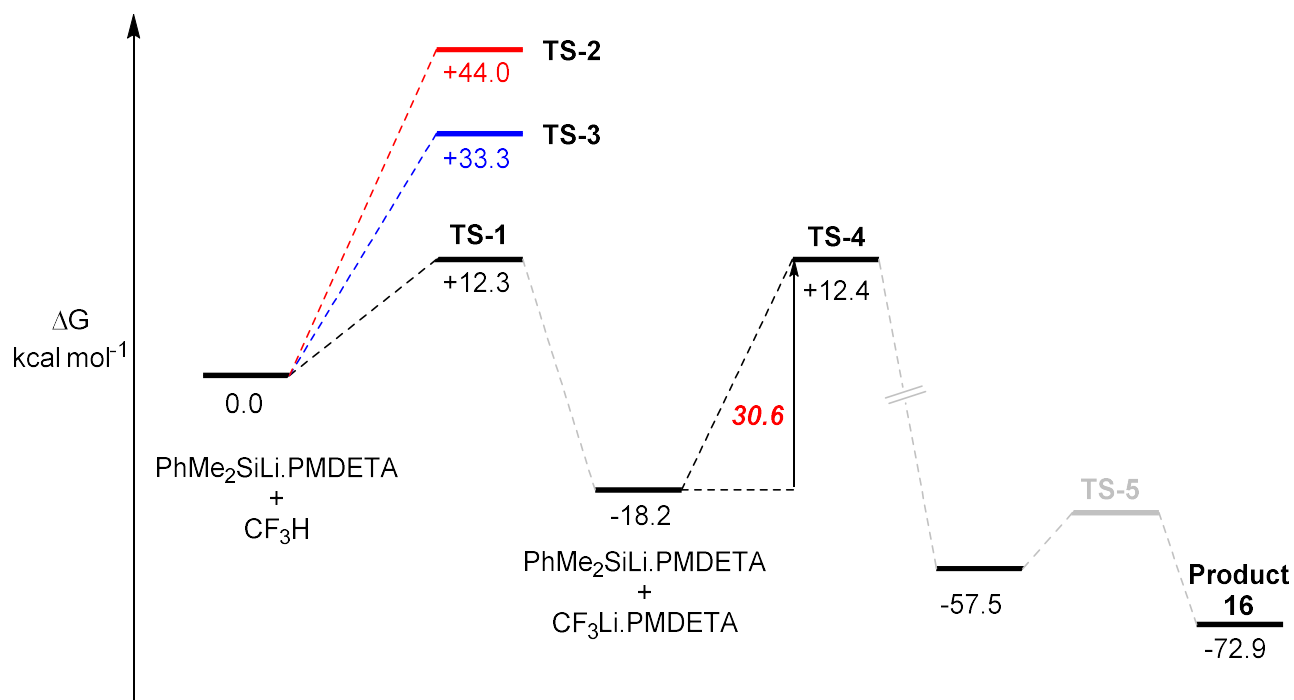


Figure 4.4 Preliminary potential energy surface for the reaction of trifluoromethane with PhMe<sub>2</sub>SiLi.PMDETA (**11.PMDETA**). Transition states not connected to intermediates through IRC calculations, values based on thermodynamic calculations (figure 4.19). B3PW91/6-31G

### 4.3 Experimental

Standard Schlenk line and glovebox techniques were used for all manipulations under an inert atmosphere of dinitrogen or argon unless otherwise stated. NMR scale reactions were performed in J. Young's tap NMR tubes equipped with internal standard capillaries of ferrocene ( $^1\text{H}$  NMR spectroscopy) or 1-trifluoromethylnaphthalene ( $^{19}\text{F}$  NMR spectroscopy) and prepared in a glovebox. An MBraun Labmaster glovebox was utilised, operating at  $<0.1$  ppm  $\text{H}_2\text{O}$  and  $<0.1$  ppm  $\text{O}_2$ .  $^1\text{H}$ ,  $^{13}\text{C}$ ,  $^{29}\text{Si}$ ,  $^7\text{Li}$  and  $^{19}\text{F}$  NMR spectra were recorded on BRUKER 400 MHz or 500 MHz machines. Data were processed using the MestReNova software package.

Solvents were dried over activated alumina from a solvent purification system (SPS) based upon the Grubbs design and de-gassed before use. Glassware was dried for  $>6$  h prior to use at  $120$  °C. Benzene- $d_6$  and toluene- $d_8$  was de-gassed and stored over  $3\text{Å}$  molecular sieves before use. All heating mentioned was performed using dry-syn heating apparatus.

All reagents were acquired from Sigma Aldrich (Merck), Honeywell or Fluorochem and used without further purification unless specified. Fluorinated gases were acquired from Apollo Scientific and used without further purification. Where liquids at  $25$  °C, reagents were dried over activated  $3\text{Å}$  molecular sieves and freeze-pump-thaw degassed prior to use. Silyl lithium reagents were prepared as reported in Chapter 3.<sup>[40]</sup>

Gas chromatography (GC) analyses were performed using an Agilent Technologies 7820A GC using a HP-5 column with FID detector. The carrier gas was helium (at a flow rate of  $25$  mL/min). CHN analysis was run by Stephen Boyer of London Metropolitan University.

#### 4.3.1 General procedure for NMR scale reactions with fluorinated gases

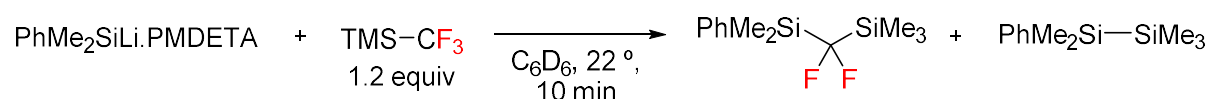
Silyl lithium (x mmol) was dissolved in solvent (0.6 mL) and added to a J. Young NMR tube equipped with a ferrocene capillary internal standard, then a t=0  $^1\text{H}$  NMR spectrum recorded. The solution was degassed once *via* freeze-pump-thaw technique then fluorinated gas (1 bar pressure, approx. 0.1 mmol) was added. The J. Young tube was inverted multiple times then t=1  $^1\text{H}$  and  $^{19}\text{F}$  NMR spectra recorded. The yield was determined *in situ* upon integral comparison in the  $^1\text{H}$  NMR spectrum. Further  $^1\text{H}$  and  $^{19}\text{F}$  NMR spectra were recorded if required.

#### 4.3.2 General procedure for NMR scale reactions with fluorinated liquids

**11.PMDETA** (x mmol) was dissolved in  $\text{C}_6\text{D}_6$  (0.6 mL) and added to a J. Young NMR tube equipped with a ferrocene capillary internal standard, then a t=0  $^1\text{H}$  NMR spectrum recorded. Fluorinated liquid (x mmol) was added and the J. Young tube was inverted multiple times then t=1  $^1\text{H}$  and  $^{19}\text{F}$  NMR spectra recorded. The yield was determined *in situ* upon integral comparison in the  $^1\text{H}$  NMR spectrum. Further  $^1\text{H}$  and  $^{19}\text{F}$  NMR spectra were recorded if required.

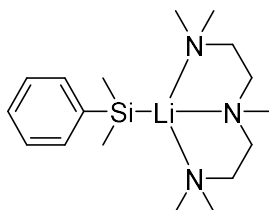
#### 4.3.3 General procedure for large scale reaction with $\text{TMS-CF}_3$

In an ampoule, a solution of  $\text{TMSCF}_3$  (2.0 M in THF) (600  $\mu\text{L}$ , 1.20 mmol) was suspended in toluene (15 mL) and transferred to a glovebox. **11.PMDETA** (315 mg, 1.00 mmol) was dissolved in toluene (15 mL) then added dropwise to the  $\text{TMSCF}_3$  solution. A pale yellow solution was formed upon addition of all **11.PMDETA**. The solution was transferred to a round bottom flask then the solvent removed under reduced pressure. Crude  $^1\text{H}$  and  $^{19}\text{F}$  NMR spectra were recorded. The products were extracted into n-hexane, washing with aqueous 0.1 M HCl (3 x 25 mL) then brine (2 x 25 mL). The organic layers were combined, dried over  $\text{MgSO}_4$  then concentrated *in vacuo*.  $^1\text{H}$  and  $^{19}\text{F}$  NMR spectra were recorded. Analysis of the multinuclear NMR spectra elucidated the presence of two species, one that is fluorinated. Two sets of singlet resonances were observed in the  $^1\text{H}$  NMR spectrum, corresponding to  $\text{Si-CH}_3$  moieties and both sets with approximately 6:9 ratios ( $\delta = 0.38$  and  $-0.8$  ppm,  $\delta = 0.31$  and  $0.06$  ppm).



Consultation of the literature strongly suggested the formation of  $\text{PhMe}_2\text{SiSiMe}_3$  as the minor product.<sup>[36,37]</sup>

#### 4.3.4 Large scale synthesis of silyl lithium reagent



**Synthesis of compound 11. PMDETA on large scale:** Lithium wire (450 mg, 66.8 mmol) was washed with n-hexane and added to a Schlenk flask. The atmosphere was evacuated and backfilled with argon 4 times. THF (50 mL) was added followed by PhMe<sub>2</sub>SiCl (3.00 mL, 17.6 mmol) and the reaction stirred in a room temperature water bath for 24 hours where a colour change to dark red was observed. n-Hexane (80 mL) was added to the reaction and stirred for 15 minutes, then the precipitate allowed to settle. The solution was filtered *via* cannula filtration to a separate Schlenk flask then concentrated *in vacuo*. Toluene (20 mL) was added, then PMDETA (4.4 mL, 20.1 mmol) followed by n-hexane (40 mL). The product was allowed to crystallise over 24 hours at -20 °C. The solution was filtered to a separate Schlenk flask and the product isolated as brown crystals (3.90 g, 70 %, 12.4 mmol)

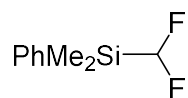
$\delta_{\text{H}}$  (400 MHz, C<sub>6</sub>D<sub>6</sub>, 298K): 7.99 – 7.91 (m, 2H, *o*-CH), 7.44 (apparent t, 2H, <sup>3</sup>J<sub>HH</sub> = 7.5 Hz, *m*-CH), 7.20 (tt, 1H, <sup>3</sup>J<sub>HH</sub> = 7.3 Hz, <sup>4</sup>J<sub>HH</sub> = 1.3 Hz, *p*-CH), 1.79 (s, 18H, N(CH<sub>3</sub>)<sub>6</sub>), 1.73 (s, 6H, N(CH<sub>2</sub>)<sub>3</sub>), 0.87 (s, 6H, CH<sub>3</sub>Si).

$\delta_{\text{C}}$  (100 MHz, C<sub>6</sub>D<sub>6</sub>, 298K): 165.3 (s, 1C, C<sup>V</sup>), 133.9 (s, 2C, *o*-CH), 127.0 (s, 2C, *m*-CH), 123.3 (s, 1C, *p*-CH), 57.0 (s, 2C, NCH<sub>2</sub>), 53.4 (s, 2C, NCH<sub>2</sub>), 45.8 (br s, 4C, N(CH<sub>3</sub>)<sub>2</sub>), 44.8 (s, 1C, N(CH<sub>3</sub>)), 7.7 (s, 2C, Si(CH<sub>3</sub>)<sub>2</sub>)

$\delta_{\text{Li}}$  (100 MHz, C<sub>6</sub>D<sub>6</sub>, 298K): 1.4 (s).

$\delta_{\text{Si}}$  (79.5 MHz, C<sub>6</sub>D<sub>6</sub>, 298K): -27.5 (s).

#### 4.3.5 Preparation of fluorosilicon compounds:



**Compound 16, (difluoromethyl)dimethyl(phenyl)silane:** Toluene (160 mL) was added to a Strauss flask under an argon atmosphere and moved into a glovebox where PhMe<sub>2</sub>SiLi.PMDETA (1.00 g, 3.17 mmol) was added. The solution was degassed once on a Schlenk line *via* freeze-pump-thaw technique then transferred to a room temperature water bath (in case of exotherm). Trifluoromethane (1 bar pressure) was added whilst maintaining manual stirring (swirling of flask) observing a colour change from dark orange to pale yellow. The reaction was left for 10 minutes then the contents transferred to a round bottom flask and the solvent removed under reduced pressure. The product was extracted into n-hexane (50 mL) washing with 0.1 M HCl (2 x 25 mL) then brine (2 x 25 mL) then H<sub>2</sub>O (2 x 25 mL). The organic layers were combined and dried over MgSO<sub>4</sub>, then the solvent removed under reduced pressure yielding a yellow oil. The product was isolated *via* short path distillation (45 °C, 0.1 mbar) and collected into a flask in a cold bath (-78 °C) yielding the desired product (404 mg, 68 %, 2.17 mmol).

$\delta_{\text{H}}$  (400 MHz, C<sub>6</sub>D<sub>6</sub>, 298K): 7.41 – 7.37 (m, 2H, *o*-CH), 7.20 – 7.11 (m, 3H, *m/p*-CH), 5.70 (t, 1H, <sup>2</sup>J<sub>HF</sub> = 46.2 Hz, CHF<sub>2</sub>), 0.20 (s, 6H, Si(CH<sub>3</sub>)<sub>2</sub>).

$\delta_{\text{C}}$  (100 MHz, C<sub>6</sub>D<sub>6</sub>, 298K): 134.5 (s, 2C, *o*-CH), 132.8 (m, 1C, C<sup>IV</sup>Si), 130.5 (s, 1C, *p*-CH), 128.4 (s, 2C, *m*-CH), 123.6 (t, 1C, <sup>1</sup>J<sub>CF</sub> = 255 Hz, CHF<sub>2</sub>), -7.0 (s, 2C, Si(CH<sub>3</sub>)<sub>2</sub>).

$\delta_{\text{F}}$  (376 MHz, C<sub>6</sub>D<sub>6</sub>, 298K): -137.7 (d, 2F, <sup>2</sup>J<sub>HF</sub> = 46.2 Hz, CHF<sub>2</sub>)

$\delta_{\text{Si}}$  (79.5 MHz, C<sub>6</sub>D<sub>6</sub>, 298K): -7.9 (t, <sup>2</sup>J<sub>SIF</sub> = 28.9 Hz).

#### 4.4 References

- [1] G. K. Surya Prakash, P. V. Jog, P. T. D. Batamack, G. A. Olah, *Science*, **2012**, *338*, 1324–1327.
- [2] S. Kyasa, *Synlett* **2015**, *26*, 1911–1912.
- [3] W. Han, Y. Li, H. Tang, H. Liu, *J. Fluor. Chem.* **2012**, *140*, 7–16.
- [4] T. Saito, J. Wang, E. Tokunaga, S. Tsuzuki, N. Shibata, *Sci. Rep.* **2018**, *8*, 11501–11508.
- [5] A. Zanardi, M. A. Novikov, E. Martin, J. Benet-Buchholz, V. V. Grushin, *J. Am. Chem. Soc.*, **2011**, *133*, 20901–20913.
- [6] J. B. Geri, N. K. Szymczak, *J. Am. Chem. Soc.*, **2017**, *139*, 9811–9814.
- [7] N. Punna, T. Saito, M. Kosobokov, E. Tokunaga, Y. Sumii, N. Shibata, *Chem. Commun.*, **2018**, *54*, 4294–4297.
- [8] G. Haufe, *Science*, **2012**, *338*, 1298.
- [9] P. Novák, A. Lishchynskiy, V. V. Grushin, *J. Am. Chem. Soc.*, **2012**, *134*, 16167–16170.
- [10] D. L. S. Brahms, W. P. Dailey, *Chem. Rev.*, **1996**, *96*, 1585–1632.
- [11] C. Ni, J. Hu, *Synthesis* **2014**, *46*, 842–863.
- [12] D. E. Yerien, S. Barata-Vallejo, A. Postigo, *Chem. Eur. J.*, **2017**, *23*, 14676–14701.
- [13] D. O'Hagan, H. S. Rzepa, *Chem. Commun.*, **1997**, 645–652.
- [14] N. A. Meanwell, *J. Med. Chem.* **2018**, *61*, 5822–5880.
- [15] Y. Zafrani, D. Yeffet, G. Sod-Moriah, A. Berliner, D. Amir, D. Marciano, E. Gershonov, S. Saphier, *J. Med. Chem.* **2017**, *60*, 797–804.
- [16] C. S. Thomason, W. R. Dolbier, *J. Org. Chem.* **2013**, *78*, 8904–8908.
- [17] T. G. Miller, J. W. Thanassi, *J. Org. Chem.* **1960**, *25*, 2009–2012.
- [18] T. Iida, R. Hashimoto, K. Aikawa, S. Ito, K. Mikami, *Angew. Chem. Int. Ed.*, **2012**, *51*, 9535–9538.
- [19] B. E. Smart, *The Chemistry of Functional Groups, Supplement D*, Wiley, New York, **1983**.
- [20] K. Honda, T. V. Harris, M. Hatanaka, K. Morokuma, K. Mikami, *Chem. Eur. J.*, **2016**, *22*, 8796–8800.
- [21] K. Aikawa, K. Maruyama, K. Honda, K. Mikami, *Org. Lett.*, **2015**, *17*, 4882–4885.
- [22] K. Aikawa, K. Maruyama, J. Nitta, R. Hashimoto, K. Mikami, *Org. Lett.*, **2016**, *18*, 3354–3357.
- [23] S. Ito, N. Kato, K. Mikami, *Chem. Commun.* **2017**, *53*, 19–21.
- [24] B. Gutmann, M. Köckinger, G. Glotz, T. Ciaglia, E. Slama, M. Zdravec, S. Pfanner, M. C. Maier, H. Gruber-Wölfler, C. Oliver Kappe, *React. Chem. Eng.* **2017**, *2*, 919–927.
- [25] M. Köckinger, T. Ciaglia, M. Bersier, P. Hanselmann, B. Gutmann, C. O. Kappe, *Green Chem.* **2018**, *20*, 108–112.
- [26] M. Köckinger, C. A. Hone, B. Gutmann, P. Hanselmann, M. Bersier, A. Torvisco, C. O. Kappe, *Org. Process Res. Dev.* **2018**, *22*, 1553–1563.
- [27] T. M. Klapötke, J. M. Winfield, *J. Fluor. Chem.* **1998**, *88*, 19–22.

- [28] T. Fuchikami, I. Ojima, *J. Organomet. Chem.* **1981**, 212, 145–153.
- [29] D. A. Braden, E. E. Parrack, D. R. Tyler, *Coord. Chem. Rev.* **2001**, 211, 279–294.
- [30] J. H. Atherton, R. Fields, *J. Chem. Soc.* **1968**, 2276–2278.
- [31] H. Bürger, R. Eujen, P. Moritz, *J. Organomet. Chem.* **1991**, 401, 249–260.
- [32] G. K. S. Prakash, J. Hu, G. A. Olah, *J. Org. Chem.* **2003**, 68, 4457–4463.
- [33] M. Ohashi, R. Kamura, R. Doi, S. Ogoshi, *Chem. Lett.* **2013**, 42, 933–935.
- [34] S. Hyde, J. Veliks, B. Liégault, D. Grassi, M. Taillefer, V. Gouverneur, *Angew. Chem. Int. Ed.*, **2016**, 55, 3785–3789.
- [35] A. K. Yudin, G. K. S. Prakash, D. Deffieux, M. Bradley, R. Bau, G. A. Olah, *J. Am. Chem. Soc.*, **1997**, 119, 1572–1581.
- [36] P. Xiao, Y. Cao, Y. Gui, L. Gao, Z. Song, *Angew. Chem. Int. Ed.*, **2018**, 57, 4769–4773.
- [37] L. Hevesi, M. Dehon, R. Crutzen, A. Lazarescu-Grigore, *J. Org. Chem.* **1997**, 62, 2011–2017.
- [38] T. Hagiwara, T. Fuchikami, *Synlett* **1995**, 1995, 717–718.
- [39] Y. Zhao, W. Huang, J. Zheng, J. Hu, *Org. Lett.*, **2011**, 13, 5342–5345.
- [40] G. Coates, H. Y. Tan, C. Kalff, A. White and M. R. Crimmin, *Angew. Chem. Int. Ed.*, **2019**, 58, 12514–12518.

## Chapter 5. Future Work

This field of fluorocarbon recycling may still be in its infancy, yet over the last three years many exciting advances have been made. I am pleased that the research performed during this PhD programme has culminated with broad scope for future investigations.

This section will be split into three parts, elaborating on the plausible research direction based upon the results from each chapter of this thesis – the  $sp^3C-F$  activation by low oxidation state magnesium reagents, the defluorosilylation of industrially relevant fluoroolefins and similar reactivity with industrial fluorocarbons.

### 5.1 Stereochemistry of $sp^3C-F$ Bond Cleavage

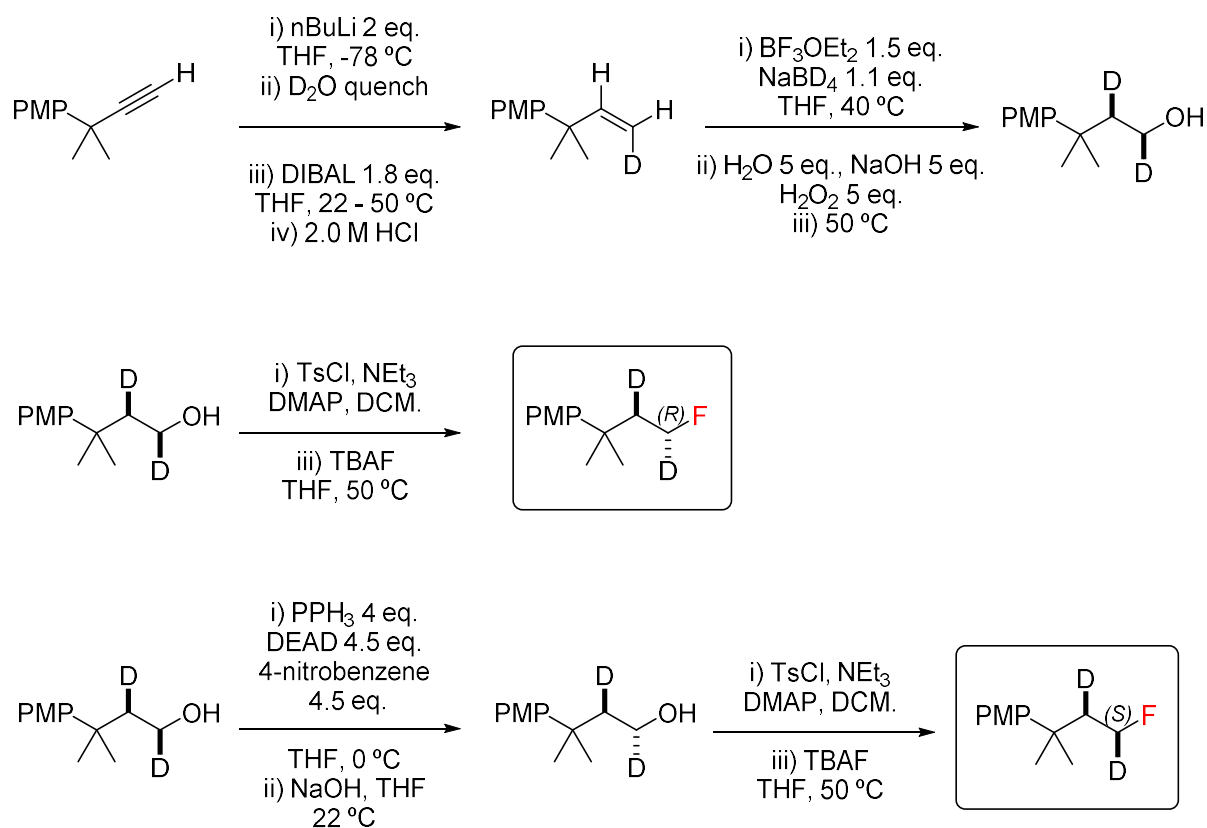
The development of  $sp^3C-F$  bond cleavage reactions at low oxidation state magnesium compounds represented a fundamental step towards further understanding the requirements to activate very strong bonds. However, there were significant limitations to this approach in the context of further synthetic chemistry. The magnesium compounds are highly sensitive to atmospheric conditions and cannot typically be isolated in multi-gram quantities, whilst the substrate scope of  $sp^3C-F$  activation is limited to simple monofluorocarbons.

Despite the limited synthetic utility, an intriguing discovery was made when probing the reaction mechanism using DFT methods. An unusual front-side attack of the fluorocarbon was shown to be the preferred pathway on  $1^\circ$ ,  $2^\circ$  and  $3^\circ$  fluorocarbons. Preliminary experiments to probe the stereospecificity of this reaction using diastereotopic  $2^\circ$  fluorocarbons were unfortunately inconclusive. This could be attributed in part to the significant energy difference between the expected diastereotopic products ( $\Delta\Delta G_{298K} = 5.4 \text{ kcal mol}^{-1}$ ).

Future investigation of this mechanism would require synthesis of enantiomerically pure (or enriched) fluorocarbons. The expected products generated upon C-F activation of chiral fluorocarbons will themselves be chiral. The two product enantiomers would therefore exhibit identical traces in their multinuclear NMR spectra.

An elegant method to achieve this was demonstrated by Martin *et al.* to conclusively confirm an  $S_N2$  inversion process.<sup>[1]</sup> By incorporating diastereotopic deuterium atoms, this method allowed for the identification of each diastereomers by  $^1H$  NMR spectroscopy, alleviating the need for more cumbersome analytical techniques. The route to synthesise the fluorocarbon substrates is a multistep process based on standard organic chemistry techniques.





Scheme 5.1 Multi-step route to synthesise two fluorocarbon enantiomers, described by Martin *et. al.*

Probing the C–F activation of such chiral compounds with Mg–Mg reagents could elucidate whether a stereoinvertive or stereoretentive pathway is dominating and could represent classical  $\text{S}_{\text{N}}2$ -type or unusual  $\text{S}_{\text{N}}\text{X}$  (front-side) reactivity respectively. This method is not guaranteed to conclusively confirm the mechanism, as epimerisation at the Mg–C bond cannot be entirely ruled out.

## 5.2 Scale-Up and Application of Fluorinated Organosilicon Compounds

Excellent progress has been made towards the chemical recycling of 4<sup>th</sup> generation refrigerant gases, transforming them into bottleable organosilicon compounds upon reaction with cheap silicon nucleophiles.

Due to their industrial application (specifically R-1234yf and R-1234ze), one of the next clear challenges would be to increase the scale of these reactions. This would demonstrate that the methodology can be extended beyond academic curiosity.

Continuous flow methods would be appropriate to deal with these fluorinated gases on larger scales. The defluorosilylation reactions are susceptible to exotherms upon the generation of the LiF by-product and performing the reactions under continuous flow conditions would allow for greater temperature dissipation, whilst the pressure of the system is also under greater control. Overall,

continuous flow could represent a safer approach for this chemistry. The efficiency of chemical reactions can also be greatly enhanced through the use of continuous flow, allowing for decreased reaction times (residence time), improved mixing, finer temperature control and enhanced reagent stoichiometry.

Our aim is to optimise a flow reactor to maximise the yield of the fluorinated building blocks. We aim to run the nucleophilic silylation of R-1234yf on a >100 g scale. Ultimately, the goal is to take fluorinated olefins from waste refrigerant sources and generate higher-value fluorinated building blocks. Particular emphasis will be placed on upgrading R-1234yf and R-1234ze to reactive chemical building blocks due to their rapidly growing industrial production and application. Furthermore these products provide access to interesting chemical reagents that can be used in further synthesis, for example to deliver trifluoropropyl or trifluoropropylene groups into organic molecules.

One of the key aspects of this methodology is to recycle fluoroolefins to reduce their emission into the environment. However, to achieve an economical incentive the new recycled products require an application. We believe fluorinated organosilicon compounds exhibit many of the characteristics that are desirable for onward synthesis. They are cheap to produce, bench stable liquids. Organosilicon chemistry is well understood so the transfer of fluoroalkyl group to suitable electrophiles should not require extensive development.

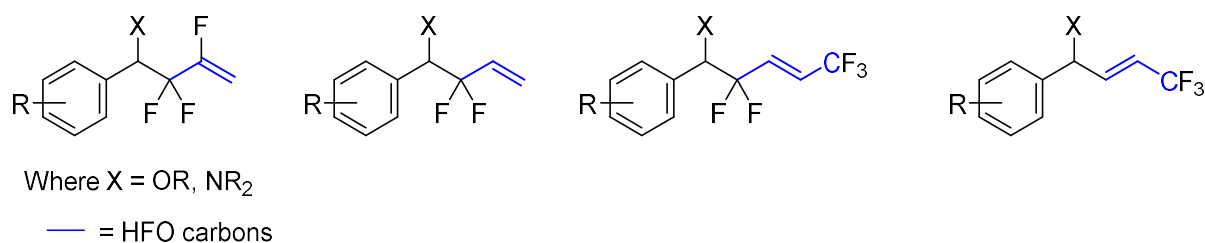


Figure 1 Plausible scaffolds accessible through reaction of fluorinated organosilicon products with electrophiles.

$\alpha,\alpha$ -Difluoromethyl groups are gaining attention as useful modifications to increase the efficacy of agrochemicals and pharmaceuticals, whilst  $\alpha$ -difluoroketones have been shown to be isosteres of the amide group.<sup>[2]</sup> We have demonstrated that the addition of organosilicon compound derived from R-1234yf to a carbonyl electrophile will generate a new difluoromethyl containing compound. We would like to extend the scope of this investigation to include other electrophiles (for example C=O, C=NR based) in conjunction with the library of fluorinated building blocks. Collaboration with other research groups or industrial partners would be desirable, guiding our targets and probing their potential pharmaceutical or agrochemical application.

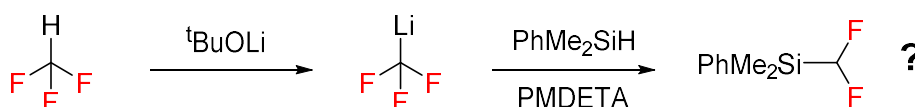
### 5.3 Development of $sp^3C-F$ Activation of HFCs and Mechanistic Understanding

Excellent progress was made during the final months of this PhD thesis towards the C-F functionalisation of industrially significant fluorocarbons, in particular, trifluoromethane (R-23). Conditions were developed for the synthesis and isolation of a silylated difluoromethyl compound ( $\text{PhMe}_2\text{SiCF}_2\text{H}$ ) in good yields from gram scale reactions.

Precedent for selective C-F functionalisation of trifluoromethane is limited and no concrete mechanism has been proven. In all examples, lithium atoms are shown to play an important role.

Preliminary computational investigation into the mechanism has been undertaken. Transition states have been located for the initial deprotonation of  $\text{HCF}_3$  by a silyl-lithium species as well as a transition state for the unusual  $S_N2$  attack on a lithium-carbenoid species ( $\text{LiCF}_3$ ), by another equivalent of silyl-lithium. A similar process has been described by Mikami.<sup>[5]</sup> Our initial studies strongly suggest deprotonation of trifluoromethane occurs as the first step due to the low energy barrier ( $\Delta G^\ddagger_{298\text{K}} = \sim 12 \text{ kcal mol}^{-1}$ ). To gain a deeper insight, all plausible pathways need to be modelled and compared. Another potential mechanism begins with deprotonation of  $\text{HCF}_3$  followed by  $\alpha$ -fluorine elimination and subsequent insertion into the Si-H bond.

To complement the DFT analysis, mechanistic probe experiments should also be undertaken. For example, the lithiation of trifluoromethane (by  $^t\text{BuOLi}$  or similar) and addition to a solution of  $\text{PhMe}_2\text{SiH}$  may give insight into the carbene insertion pathway. This reaction would potentially imitate the second step in the proposed pathway.



*Scheme 2 Outline of mechanism probe experiment*

Finally, the aim would be to extend this methodology to other HFCs with particular interest in 1,1,1,2-tetrafluoroethane (R-134a) due to its widespread application in the refrigeration and air conditioning industries. Elucidating the reaction mechanism with trifluoromethane would allow for more informed development of activation methods for other similar substrates, for example, do we target the C-H bond or C-F bond in the initial step.

The eventual application to continuous flow, as with HFOs is also a feasible ambition.

## 5.4 References

- [1] X. W. Liu, C. Zarate, R. Martin, *Angew. Chem. Int. Ed.*, **2019**, *58*, 2064–2068.
- [2] N. A. Meanwell, *J. Med. Chem.* **2018**, *61*, 5822–5880.
- [3] H. Sakaguchi, M. Ohashi, S. Ogoshi, *Angew. Chem. Int. Ed.*, **2018**, *57*, 328–332.
- [4] P. Gao, G. Wang, L. Xi, M. Wang, S. Li, Z. Shi, *Chin. J. Chem.* **2019**, *37*, 1009–1014.
- [5] K. Honda, T. V. Harris, M. Hatanaka, K. Morokuma, K. Mikami, *Chem. Eur. J.*, **2016**, *22*, 8796–8800.

## 6. Appendix

### 6.1 X-Ray Diffraction Data

| Data  | Compound 1a   | Compound 1a·THF                                    | Compound 1d·THF                                    |
|---|---|--|--|
| formula   | C <sub>70</sub> H <sub>108</sub> Mg <sub>2</sub> N <sub>4</sub> | C <sub>39</sub> H <sub>62</sub> MgN <sub>2</sub> O | C <sub>39</sub> H <sub>60</sub> MgN <sub>2</sub> O |
| solvent   | –   | –  | –  |
| formula weight  | 1054.22   | 599.21   | 597.20   |
| colour, habit   | colourless tablets  | colourless blocky needles                          | colourless blocks                                  |
| temperature / K   | 173   | 173  | 173  |
| crystal system  | monoclinic  | triclinic  | monoclinic   |
| space group   | <i>C</i> 2/ <i>c</i>  | <i>P</i> -1  | <i>P</i> 2 <sub>1</sub> / <i>c</i>                 |
| <i>a</i> / Å  | 22.2035(5)  | 9.4890(5)  | 18.2466(3)   |
| <i>b</i> / Å  | 13.9688(2)  | 12.9255(7)   | 12.7352(2)   |
| <i>c</i> / Å  | 22.6003(4)  | 15.5404(5)   | 16.0810(3)   |
| $\alpha$ / deg  |   | 87.459(4)  |  |
| $\beta$ / deg   | 112.401(2) <sup>o</sup>   | 79.698(4)  | 99.2892(15)  |
| $\gamma$ / deg  |   | 84.082(4)  |  |
| <i>V</i> / Å <sup>3</sup>   | 6480.7(2)   | 1864.65(15)  | 3687.81(10)  |
| <i>Z</i>  | 4 [ <i>C</i> <sub>i</sub> symmetry]                             | 2  | 4  |
| <i>D</i> <sub>c</sub> / g cm <sup>-3</sup>                              | 1.080   | 1.067  | 1.076  |
| radiation used  | Cu-K $\alpha$   | Cu-K $\alpha$                                      | Cu-K $\alpha$                                      |
| $\mu$ / mm <sup>-1</sup>  | 0.634   | 0.623  | 0.630  |
| 2 $\theta$ max / deg  | 135   | 135  | 135  |
| no. of unique reflns  | 6242  | 7103   | 7116   |
| measured ( <i>R</i> <sub>int</sub> )                                    | (0.0203)  | (0.0274)   | (0.0342)   |
| obs,   <i>F</i> <sub>o</sub>   > 4 $\sigma$ (  <i>F</i> <sub>o</sub>  ) | 5118  | 5595   | 5535   |
| no. of variables  | 362   | 435  | 403  |
| <i>R</i> <sub>1</sub> (obs), <i>wR</i> <sub>2</sub> (all) [a]           | 0.0508, 0.1497  | 0.0487, 0.1370                                     | 0.0492, 0.1376                                     |
| CCDC identifier   | 1831354   | 1831355  | 1831356  |

Table 6.1 Crystal Data, Data Collection and Refinement Parameters for the structures of compounds **1a**, **1a·THF** and **1d·THF**

[a]  $R_1 = \sum ||F_o| - |F_c|| / \sum |F_o|$ ;  $wR_2 = \{\sum [w(F_o^2 - F_c^2)^2] / \sum [w(F_o^2)^2]\}^{1/2}$ ;  $w^{-1} = \sigma^2(F_o^2) + (aP)^2 + bP$ .

| Data  | Compound 4/5 <sup>[a]</sup>  | Compound 6   |
|---|--|--|
| formula   | C <sub>47</sub> H <sub>78</sub> B <sub>2</sub> MgN <sub>2</sub> O <sub>4</sub> ·<br>C <sub>47</sub> H <sub>77</sub> B <sub>3</sub> MgN <sub>2</sub> O <sub>6</sub> | C <sub>45</sub> H <sub>74</sub> B <sub>2</sub> MgN <sub>2</sub> O <sub>4</sub> |
| solvent   |  |  |
| formula weight  | 1603.88  | 752.99   |
| colour, habit   | colourless tablets   | colourless tablets   |
| temperature / K   |  | 173  |
| crystal system  | triclinic  | triclinic  |
| space group   | <i>P</i> -1  | <i>P</i> -1  |
| <i>a</i> / Å  | 13.4629(4)   | 11.8426(5)   |
| <i>b</i> / Å  | 18.4137(5)   | 12.3227(6)   |
| <i>c</i> / Å  | 20.0690(8)   | 18.4450(8)   |
| $\alpha$ / deg  | 87.175(3)  | 104.086(4)   |
| $\beta$ / deg   | 86.940(3)  | 93.464(4)  |
| $\gamma$ / deg  | 86.935(2)  | 114.893(5)   |
| <i>V</i> / Å <sup>3</sup>   | 4955.5(3)  | 2327.3(2)  |
| <i>Z</i>  | 2  | 2  |
| <i>D<sub>c</sub></i> / g cm <sup>-3</sup>                               | 1.075  | 1.075  |
| radiation used  | Cu-K $\alpha$  | Mo-K $\alpha$  |
| $\mu$ / mm <sup>-1</sup>  | 0.634  | 0.078  |
| 2 $\theta$ max / deg  | 135  | 135  |
| no. of unique reflns  | 18987  | 9125   |
| measured ( <i>R</i> <sub>int</sub> )                                    | 0.0282   | 0.0192   |
| obs,   <i>F</i> <sub>o</sub>   > 4 $\sigma$ (  <i>F</i> <sub>o</sub>  ) | 14138  | 5883   |
| no. of variables  | 1093   | 549  |
| <i>R</i> <sub>1</sub> (obs), <i>wR</i> <sub>2</sub> (all) [a]           | 0.0486, 0.1399   | 0.0663, 0.1751   |
| CCDC identifier   | 1831357  | 1831358  |

Table 6.2 Crystal Data, Data Collection and Refinement Parameters for the structures of compounds 4/5 and 6

<sup>[a]</sup> Two molecules has co-crystallised

$$[a] R_1 = \Sigma ||F_o| - |F_c| | / \Sigma |F_o|; wR_2 = \{\Sigma[w(F_o^2 - F_c^2)^2] / \Sigma[w(F_o^2)]\}^{1/2}; w^{-1} = \sigma^2(F_o^2) + (aP)^2 + bP.$$

| Data  | [ <sup>Dipp</sup> (L)MgC <sub>4</sub> H <sub>9</sub> ]         | 9a·THF   | 9b  | 11·TMEDA   |
|---|--|--|---|--|
| formula   | C <sub>70</sub> H <sub>96</sub> Mg <sub>2</sub> N <sub>4</sub> | C <sub>43</sub> H <sub>58</sub> MgN <sub>2</sub> OSi | C <sub>37</sub> H <sub>54</sub> MgN <sub>2</sub> Si | C <sub>34</sub> H <sub>70</sub> Li <sub>2</sub> N <sub>6</sub> Si <sub>2</sub> |
| solvent   | 2(C <sub>7</sub> H <sub>8</sub> )                              | —  | —   | —  |
| formula weight  | 1226.39  | 671.31   | 579.22  | 633.02   |
| colour, habit   | yellow blocky needles  | yellow plates  | yellow blocks                                       | yellow blocky needles  |
| temperature / K   | 173  | 173  | 173   | 173  |
| crystal system  | triclinic  | monoclinic   | monoclinic  | monoclinic   |
| space group   | <i>P</i> -1 (no. 2)  | <i>P</i> 2 <sub>1</sub> / <i>c</i> (no. 14)          | <i>P</i> 2 <sub>1</sub> / <i>n</i> (no. 11)         | <i>C</i> 2/ <i>c</i> (no. 15)  |
| <i>a</i> / Å  | 11.5131(5)   | 20.6982(8)   | 11.6602(3)  | 17.5874(4)   |
| <i>b</i> / Å  | 13.1696(5)   | 10.0416(3)   | 15.5707(3)  | 9.1612(2)  |
| <i>c</i> / Å  | 13.3789(8)   | 19.9087(6)   | 20.5187(5)  | 26.1440(6)   |
| $\alpha$ / deg  | 87.437(4)  | 90   | 90  | 90   |
| $\beta$ / deg   | 71.198(5)  | 98.147(3)  | 105.019(3)  | 96.096(2)  |
| $\gamma$ / deg  | 78.199(4)  | 90   | 90  | 90   |
| <i>V</i> / Å <sup>3</sup>   | 1879.23(17)  | 4096.1(2)  | 3598.06(15)   | 4188.52(17)  |
| <i>Z</i>  | 1 [c]  | 4  | 4   | 4 [c]  |
| <i>D<sub>c</sub></i> / g cm <sup>-3</sup>                               | 1.084  | 1.089  | 1.069   | 1.004  |
| radiation used  | Cu-K $\alpha$  | Cu-K $\alpha$  | Cu-K $\alpha$                                       | Cu-K $\alpha$  |
| $\mu$ / mm <sup>-1</sup>  | 0.614  | 0.892  | 0.921   | 0.964  |
| 2 $\theta$ max / deg  | 148  | 147  | 147   | 147  |
| no. of unique reflns  | 7141   | 7825   |   |  |
| measured ( <i>R</i> <sub>int</sub> )                                    | (0.0227)   | (0.0483)   | 6913  | 3988 (0.0247)  |
| obs,   <i>F</i> <sub>o</sub>   > 4 $\sigma$ (  <i>F</i> <sub>o</sub>  ) | 5365   | 4890   | 5184  | 3247   |
| no. of variables  | 436  | 475  | 403   | 236  |
| <i>R</i> <sub>1</sub> (obs), <i>wR</i> <sub>2</sub> (all) [a]           | 0.0658, 0.2183   | 0.0634, 0.1907                                       | 0.0454,   | 0.0435, 0.1238   |
| CCDC identifier   | 1915213  | 1915214  | 1915215   | 1915217  |

Table 6.3 Crystal Data, Data Collection and Refinement Parameters for the structures of [<sup>Dipp</sup>(L)MgC<sub>4</sub>H<sub>9</sub>], 9a·THF, 9b and 11·TMEDA.

[a]  $R_1 = \sum ||F_o| - |F_c|| / \sum |F_o|$ ;  $wR_2 = \{\sum [w(F_o^2 - F_c^2)^2] / \sum [w(F_o^2)^2]\}^{1/2}$ ;  $w^{-1} = \sigma^2(F_o^2) + (aP)^2 + bP$ .

## 6.2 Crystal Structures Absent from Main Text

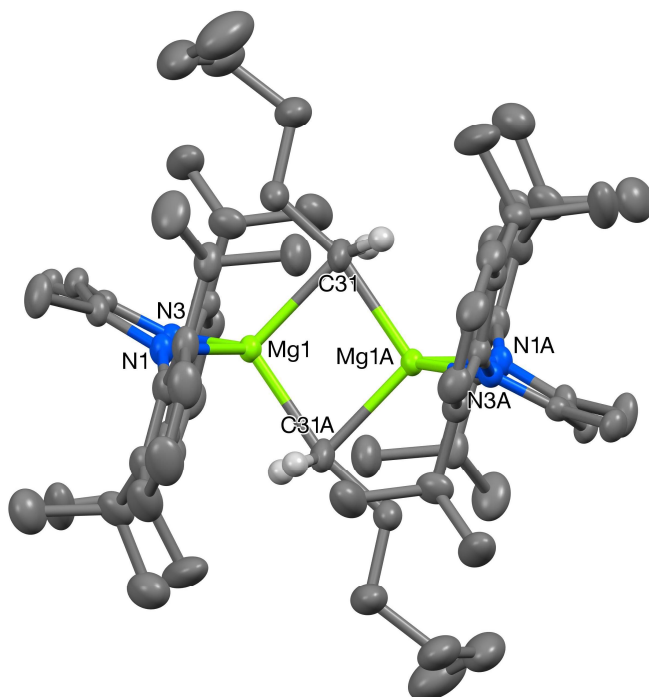


Figure 6.1 The crystal structure of the  $C_i$ -symmetric complex **1a** (50% probability ellipsoids).

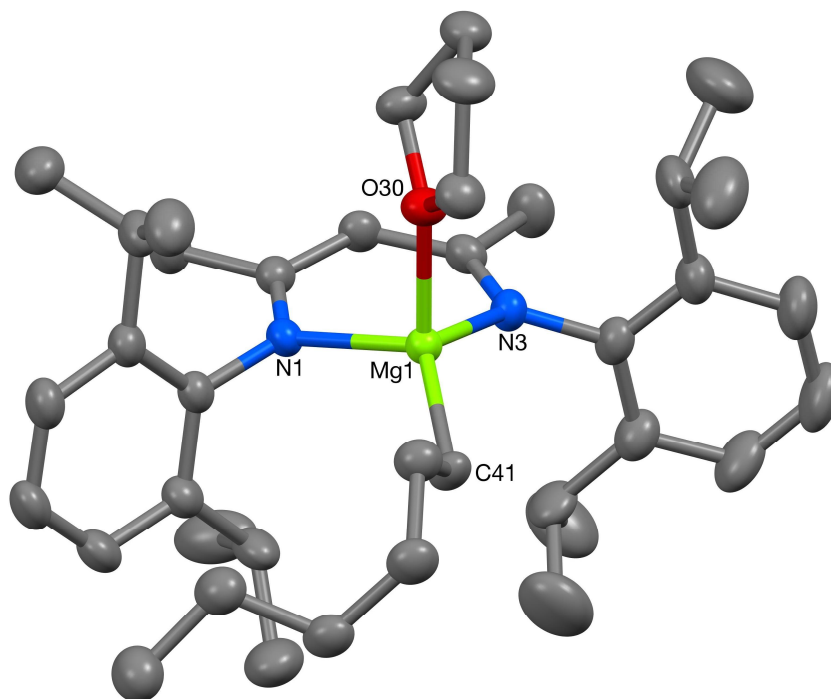


Figure 6.2 The crystal structure of **1a**·THF (50% probability ellipsoids).



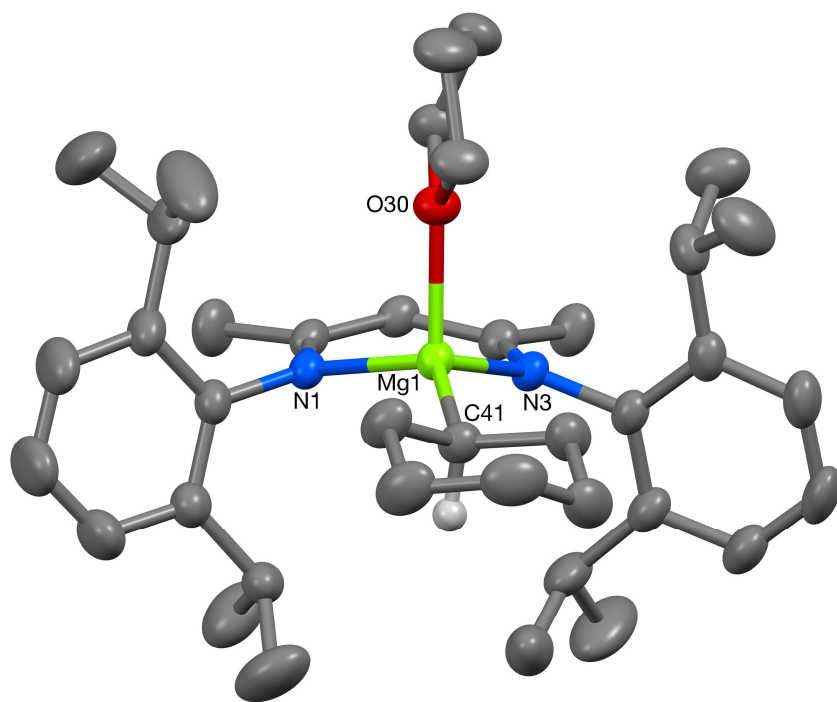


Figure 6.3 The crystal structure of **1d·THF** (50% probability ellipsoids).